KINETIC STUDIES AND MODELING OF NYLON-6 SOLID-STATE POLYCONDENSATION

THÈSE N° 2238 (2000)

PRÉSENTÉE AU DÉPARTEMENT DE CHIMIE

ÉCOLE POLYTECHNIQUE FÉDÉRALE DE LAUSANNE

POUR L'OBTENTION DU GRADE DE DOCTEUR ÈS SCIENCES TECHNIQUES

PAR

Christian SPÜHLER

Ingénieur chimiste diplômé EPF
de nationalité suisse et originaire de Zurich (ZH)

acceptée sur proposition du jury:

Prof. A. Renken, directeur de thèse
Dr W. Loth, rapporteur
Prof. J.-A. E. Manson, rapporteur
Prof. U. Suter, rapporteur

Lausanne, EPFL
2000

Remerciements

Ce travail a été réalisé de novembre 1996 à mai 2000 au Laboratoire de Génie de la Réaction Chimique et Electrochimique de l'Ecole Polytechnique Fédérale de Lausanne.

Je remercie tout particulièrement M. le professeur **Albert Renken** pour m'avoir accueilli dans son groupe de recherche, pour avoir initié ce projet, pour la confiance et la grande liberté de travail qu'il m'a accordées, ainsi que pour sa disponibilité tout au long de ces quatre années.

J'exprime également ma reconnaissance aux professeurs **Jan-Anders Manson** et **Ulrich Suter**, ainsi qu'au Dr. **Wolfgang Loth** pour avoir accepté d'examiner ce travail.

Cette thèse a été effectuée en collaboration avec l'entreprise BASF à Ludwigshafen, Allemagne. Je tiens ici à remercier le Dr. **Klaus-Dieter Hungenberg** et son équipe pour avoir permis le financement de ce projet ainsi que pour l'important soutien analytique. Un merci tout particulier à M. **Gad Kory** pour sa gentillesse et sa disponibilité téléphonique de tous les instants. *Thank you, Gad !*

Merci encore à tous les amis de l'Institut rencontrés pendant ces quatre ans pour leurs compétences professionnelles et pour tous les bons moments partagés : **Laurent Cavin, Jianzhong Yang, Stéphane Porchet, Thomas Zeilmann, Ralf Doepper, Peter Stahl, Völker Höller, Bastien Monnerat, Edi Casali, Sahbi Belkhiria, Wolfgang Zimmerer** ... et tous les autres !

Je m'en voudrais de terminer sans remercier mes **parents** pour leur soutien, leur patience et leurs encouragements.

Berlin, octobre 2000

Christian Spühler

Summary

A kinetic model for solid-state polycondensation of nylon-6 was developed by extrapolation of the melt chemistry to the amorphous phase of the solid polymer. In this way, a phenomenological description of the process was obtained that required examining all possible influences of the semicrystalline structure on the kinetics, equilibrium, and transport phenomena in the polymer granules. Particularly, dramatic apparent kinetics and equilibria changes were postulated due to the confinement of reactive species in a smaller reaction volume upon crystallization. In addition, the dimensional constraint applied by the micro-morphology on the intrinsic kinetics was also assessed. The effect of crystallinity on molecular transport was examined for both the migration of by-products at millimeter scale and the diffusion of reactive functionalities at nanometer scale. In the latter case, the occurrence of a gel effect in step growth polymers was questioned based on the implication of interchange reactions.

A detailed reaction scheme was formulated that incorporated the presence of terminated polymer chains, which can result from the use of chain regulators or from degradation during the melt prepolymerization stage. Predictions were made for the characteristic quantities of the output product, such as molar mass, polydispersity index, concentration of end-groups, water content, extent of remonomerization, and formation of the cyclic dimer.

A single particle model was validated by means of batch experiments carried out in a battery of fixed-bed reactors at laboratory scale. Both the kinetics of polymerization and the evolution of the morphology were tracked, based on techniques including viscometry, titration of functionalities, chromatography, X-ray diffraction, calorimetry, and polarized light microscopy. This led to a refined picture of the complex interplay between reaction and structure. Particularly, implications of the rigid amorphous phase, meso-scale spherulitic structures, polymer skinning, or of the presence of a crystallinity gradient within the polymer were underscored. In addition, the performance of the solid-state model was extensively tested with regard to literature data.

A scale-up of the single particle model was performed to deal with the dynamic operation of an industrial moving-packed bed reactor. Simulations allowed the prediction of reactor start-up and shutdown, possible fluctuation in the feed composition, and on-line grade transition. Potential implications of the developed model as a tool for on-line reactor optimization and process control were discussed, based on a parametric sensitivity analysis.

Version Abrégée

Un modèle cinétique de la polycondensation du nylon-6 en phase solide a été développé par extrapolation de la chimie dans l'état fondu à la phase amorphe du polymère solide. Ainsi, une description phénoménologique du procédé a été obtenue, nécessitant l'examen exhaustif des influences possibles de la structure semi-cristalline sur la cinétique, l'équilibre, et les phénomènes de transfert dans les granulés de polymère. En particulier, d'importantes modifications apparentes de la cinétique et des différents équilibres ont été postulées à cause du confinement des espèces réactives dans un volume de réaction plus petit lors de la cristallisation. De plus, la contrainte dimensionnelle imposée par la micromorphologie sur la cinétique intrinsèque a été aussi estimée. L'effet de la cristallinité sur le transport moléculaire a été examiné à la fois pour la migration des sous-produits à l'échelle du millimètre et la diffusion des fonctionnalités réactives à l'échelle du nanomètre. Dans ce dernier cas, l'existence d'un effet de gel lors de polymérisations par étapes a été mise en doute en se basant sur l'implication des réactions d'interéchange.

Un schéma réactionnel détaillé a été formulé, incorporant la présence de chaînes de polymère terminées pouvant résulter de l'emploi de régulateurs de chaînes ou de réactions de dégradation durant l'étape de prépolymérisation en phase fondue. Ceci a conduit à prédire des caractéristiques du produit final, incluant la masse molaire, l'indice de polydispersité, la concentration en groupes terminaux, la teneur en eau, le degré de remonomérisation, ainsi que la formation du dimère cyclique.

Le modèle à l'échelle d'une particule a été validé au moyen d'expériences discontinues conduites au laboratoire dans une batterie de réacteurs de type lit fixe. La cinétique de polymérisation et l'évolution de la morphologie ont été suivies par viscosimétrie, titration des fonctionnalités, chromatographie, diffraction des rayons X, calorimétrie, et par microscopie optique à lumière polarisée. De la sorte, une image affinée des interactions complexes entre réaction et structure est apparue. En particulier, l'influence de la phase amorphe rigide, des structures sphérulitiques, de phénomènes de peau de polymère, ou la présence d'un gradient de cristallinité à l'intérieur du polymère ont été soulignées. De plus, la performance du modèle a été testée d'une manière étendue sur la base de données de la littérature.

Le modèle à l'échelle d'une particule a été implémenté dans un simulateur permettant de décrire le fonctionnement dynamique d'un réacteur industriel à lit tombant. Des prédictions peuvent être obtenues pour le démarrage et l'arrêt du réacteur, l'influence d'éventuelles fluctuations dans la composition de l'alimentation, et des changements de grade en continu. Le potentiel du modèle développé comme outil pour l'optimalisation et le contrôle en continu du réacteur est discuté, sur la base d'une analyse de sensibilité paramétrique.

Contents

1. Introduction

The name *nylon*, originally the trade name of the first commercially introduced synthetic fiber, is now used as a trivial generic name for all aliphatic linear polyamides. The term *nylon-n* denotes the polyamide made from an ω-amino acid (AB monomer) containing *n* main-chain carbon atoms, whereas the term *nylon-m,n* denotes the polymer created from an aliphatic diamine (AA monomer) with *m* main-chain carbon atoms and an aliphatic diacid (BB monomer) with *n* main-chain carbon atoms.

Nylon is one of the most versatile and long-used polymers. It consists of two major products – nylon-6 and nylon-6,6 – and a host of smaller volume specialty nylons and copolymers.

1.1 The Nylon Industry

The synthesis of polyamides started in 1933 when Carothers [1] reacted hexamethylene diamine and adipic acid to form nylon-6,6. During the same period, many other polyamides were also synthesized, but nylon-6,6 was selected by E.I. Du Pont de Nemours, and its industrial manufacture was begun in 1937. In the following year, the company was making this polymer at a small pilot plant in Wilmington, Delaware. Full-scale production began in December 1939 in Seaford, Delaware, and the first nylon articles were put on sale in May 1940 [2]. The birth of nylon was an epoch-making event in human history. Coming to the world after aluminum, the last arrival (1886) in the metallic age, it was the first fully artificial polymer material and opened the plastics age.

By 1938, Schlack [3] succeeded to polymerize ε-caprolactam in the presence of 6-aminocaproic acid (later replaced by water) and opened the way for the synthesis of nylon-6. The commercial production was undertaken by I.G. Farbenindustrie in Germany in 1941. After 1945, production extended to many countries, especially in Europe (Hoechst, Bayer), the Soviet Union, and Japan [4]. Large-scale operations in the United States (Allied Chemical) commenced only after 1955 [5]. A list of present nylon-6 producers is given in Table 1.1, with the location of their production facilities, common trade names, and number of manufactured grades. These data were collected from recent sources [6-11], however corporate acquisitions, spin-offs, or joint ventures are so frequent in the plastic industry nowadays, that some changes could well have occurred in the meantime.

Nylon found its first wide application as a fiber, when it replaced Asian silk in parachutes during World War II. During the postwar period, conversion of nylon fibers production to civilian uses occurred through hosiery (nylon stockings were a tremendous fashion success), carpeting, tire cords, and automobile upholstery [12]. In

the sixties, cotton and wool usage decreased in the textile industry, while polyester and nylon production boomed [13].

Table 1.1 Nylon-6 producers

Manufacturer	Location	Trade Names	Grades
BASF	Europe, United States	Ultramid	45
Bayer	Europe, United States	Durethan, Triax	33
Cast Nylons	United States	Nycast	10
Custom Resins	United States	Nylene	28
DSM	United States, Canada	Akulon, Ertalon, Nylafil, Plaslube	19
DuPont	United States	Zytel	8
Elf Atochem	Europe	Orgalloy	15
EMS	Europe, United States	Grilon	28
Honeywell *	United States	Capron, Nylast, Nypel, Petra	259
M. A. Hanna	United States	Nymax	10
Mitsubishi	Japan	Novamid	9
Nyltech †	Europe, United States	Nycoa, Sniamid	44
Rhodia ‡	Europe	Technyl	ns
Shinkong	Taiwan	Shinite	ns
The Plastics Group	United States	Polifil	3
Ticona §	Europe, United States	Celanese	13
Toray Industries	Japan	Amilan	7
Ube Industries	Japan	Ube	26
Wellman	United States	Wellamid	11

* AlliedSignal until 1999

† Since 1994, a joint venture between Snia Technopolimeri (part of Fiat) and Rhône-Poulenc

‡ Rhône-Poulenc's specialty chemicals subsidiary, established 1998 after the merger of Hoechst and Rhône-Poulenc into Aventis

§ Hoechst Technical Polymers until 1998

Although most of the nylon is produced in the form of fiber yarns, considerable quantities are applied in many molding, extrusion, and casting operations for the manufacture of injection and blow molded objects with a wide spectrum of applications : appliances, business equipment, consumer products, electrical and electronic devices, furniture, hardware, machinery, packaging, and transportation [14]. The growth rate of nylon production as a thermoplastic resin outmatches the overall growth rate of thermoplastics – mainly PE, PVC, PP and PS – during the last decade, as displayed in Figure 1.1. In 1998, the global production of nylon resins amounted to 583 kt, representing global sales value of 4.5 billions USD [15].

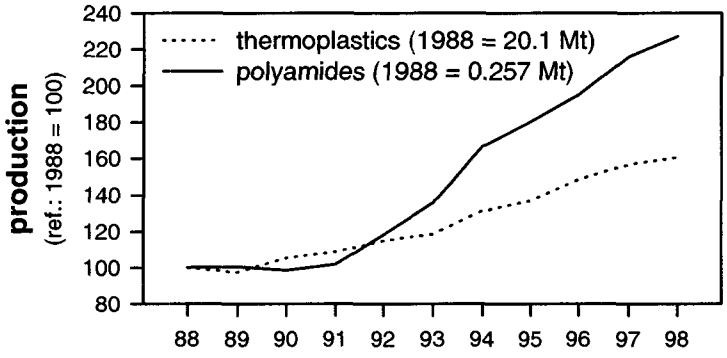

Figure 1.1 Plastics production during the last decade (Source : Chem. Eng. News, June 28, 1999)

The pattern of regional consumption, global end-use, and major global producers for 1998 is shown in Figure 1.2. Although the market outlook in Europe and Japan is for modest growth (2-3% per year), it continues to exhibit strong growth in the United

States (6-8% per year), as it continues to find new uses in automotive applications directed towards weight reduction in motor vehicles [15].

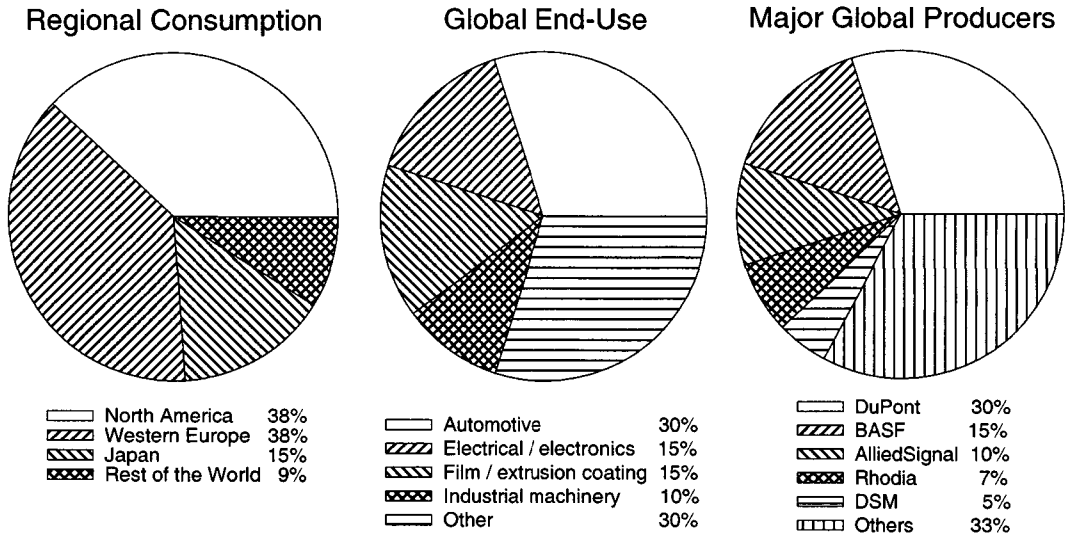

Figure 1.2 Nylon resins market survey, 1998-breakdown [15]

Though there are good growth prospects for the world demand, the competition between major nylon producers is becoming tougher, putting pressure on the prices and the profitability of the companies. Two reasons can be mentioned. First, the price of the monomer is sensitive to the price of crude oil, which was subject to more than a twofold increase during 1999. Second, the capacity in North America increased by 20 % during the last few years, with expansions planned in emerging countries – particularly in China – during the meantime. The result is a risk of global overcapacity, characterized with a supply exceeding the need of the domestic market and difficult to export [16]. Nylon-6 producers are taking action to face this globalizing market. For example, AlliedSignal and Bayer announced in August 1999 an agreement that will provide Bayer in Pittsburgh, Pennsylvania, with nylon-6 resin in North America and AlliedSignal in Rudolstadt, Germany, with caprolactam (nylon-6 monomer) in Europe.

As result of this competition, there is still a need for a better fundamental knowledge of nylon polymerization in order to optimize the production process and decrease manufacturing costs.

1.2 Manufacture Processes

Nylon-6 is commonly produced by the polymerization of ε-caprolactam (C_1), $HN(CH_2)_5CO$. The industrially significant routes for the production of this monomer are based on any of the three raw materials phenol, cyclohexane, and toluene [4]. In a typical synthesis, phenol is hydrogenated to cyclohexanol, which is oxidized to cyclohexanone. Reaction of the latter with hydroxylamine sulfate gives cyclohexanone oxime, which is subjected to the Beckmann rearrangement in 20 % oleum at 100-120°C, and converted to ε-caprolactam [17]. A scheme of the synthetic route to ε-caprolactam is shown in Figure 1.3.

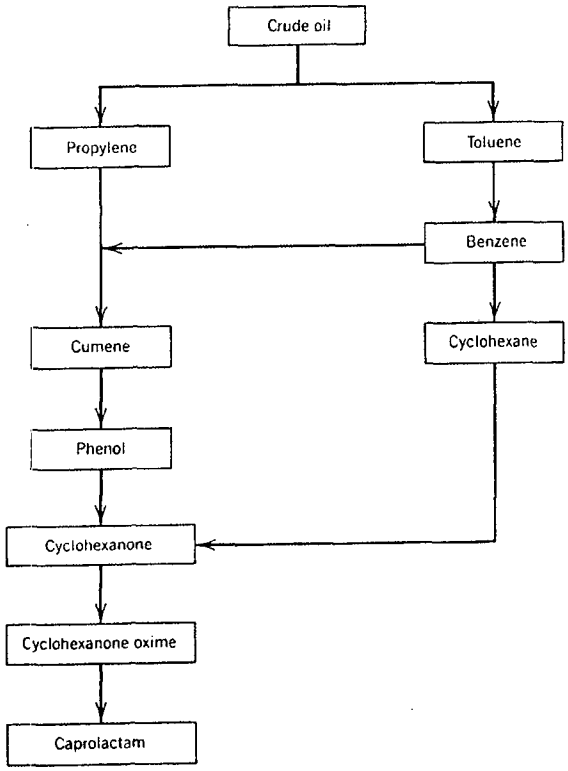

Figure 1.3 Synthesis of ε-caprolactam, nylon-6 monomer [9]

Two routes are employed for the polymerization of ε-caprolactam. The most commonly used process is the hydrolytic polymerization, in which water (W) is used [18, 19] to open the ε-caprolactam ring to give a linear molecule, aminocaproic acid (P_1) $H_2N(CH_2)_5COOH$. Polymerization then proceeds by the step growth mechanism of this bifunctional compound giving linear polymers (P_n) $H(HN(CH_2)_5CO)_nOH$, with water as the condensation by-product. In addition to these reactions, the caprolactam ring can also be directly opened by the amine end-group [20, 21] of any linear polymer molecule. This reaction leads to the growth of the molecule by one monomer unit at a time, and so has characteristics of chain growth polymerization. Thus, the major reactions in the hydrolytic process can be represented schematically by [22] :

$$C_1 + W = P_1 \tag{1.1}$$

$$P_n + P_m = P_{n+m} + W \qquad n,m = 1,2,... \tag{1.2}$$

$$P_n + C_1 = P_{n+1} \qquad n = 1,2,... \tag{1.3}$$

The second route of ε-caprolactam polymerization is by the anionic chain growth mechanism [4, 23], using initiators like sodium hydroxide, lactamates of alkali metals, and pentaalkyl guanidine [24]. The anionic polymerization is of interest because the monomer is converted to polymer in minutes, which not only eliminates the need for costly polymerization facilities but also allows for use of inexpensive molds of complex design. It makes low-volume production feasible but is not economical for mass production of small parts.

Continuous hydrolytic processes are used by the major manufacturers of nylon-6. In the BASF process [14] depicted in Figure 1.4, three main stages can be distinguished : melt polymerization, extraction, and solid-state polymerization.

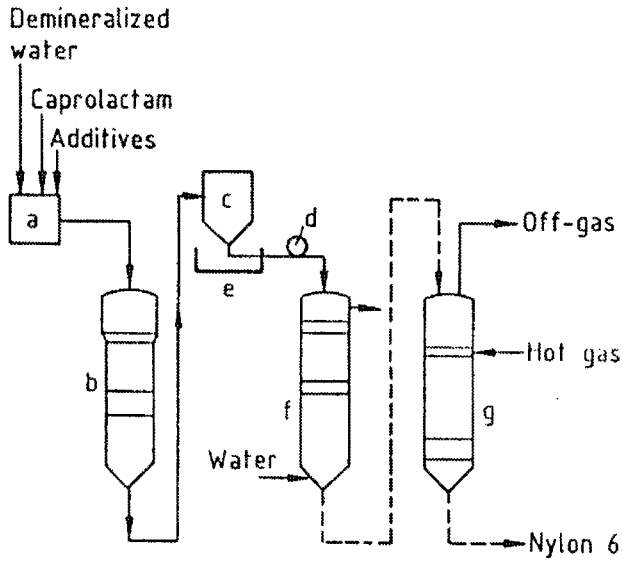

Figure 1.4 Production of nylon-6 by BASF [14]. a) Feed tank ; b) VK tube ; c) Pourer ; d) Pelletizer ; e) Water bath ; f) Extractor ; g) Solid-state reactor

In the *melt polymerization* stage, ε-caprolactam and water are fed into the top of a VK column (Vereinfacht Kontinuierliches Rohr) [25]. This consists of a vertical tube operating at atmospheric pressure. The feed enters the top of the column and is heated up to about 220-270°C [22] using heat exchangers in the form of internal gratings. In this top region, water and ε-caprolactam evaporate continuously. The bubbles of vapor formed in the reaction mass cause intense agitation as they rise up to a reflux condenser, which condenses and returns the monomer to the column. The hydrostatic head some distance downstream and the increase in the boiling point due to the polymerization prevent further vaporization, and so the remainder of the column is a non-vaporizing tubular reactor. Gratings are also used in this section both to facilitate heat removal and to ensure almost plug flow velocity profiles [26].

The polymer leaving the VK tube is quenched in a water bath and granulated. The solid granules are then transferred to the *extraction* stage, where the unreacted monomer and other cyclic species are removed by washing in water at about 100°C [27].

Because of the limited amount of water that can be removed during the melt polymerization stage, the molar mass of the resulting polymer is limited by the polyamidation equilibrium,

$$---COOH + H_2N--- \;=\; ---CONH--- + H_2O \qquad (1.4)$$

In order to remove efficiently the condensate and shift the polyamidation equilibrium to higher molar masses – thus enhancing the polymer properties – a final stage, *solid-state polymerization*, is conducted in a moving packed-bed reactor [28] where the solid granules are further polymerized by heating them below their melting point but above their glass transition temperature, under a counter-current of inert gas.

The basic principle of solid-state polymerization – sometimes also called postcondensation, postpolymerization, finishing stage, or ultrapolymerization [29] – is to maximize the surface area available for mass transfer without the need of powerful mixing equipment used to effect surface renewal in melt polycondensation. Moreover, degradation reactions are disadvantaged due to the low reaction temperature, and the preservation of the geometrical shape allows performing solid-state polymerization on finished objects. The main drawback is the long residence time (typically 10-100h) required because of the low reaction rates.

1.3 An Overview of Patent Literature

The step growth polymers subjected to solid-state polymerization (SSP) in the industry are polyethylene terephthalate (PET), polybutylene terephthalate (PBT), nylon-66 (PA66), and nylon-6 (PA6). As the largest capacity is for the SSP of PET – mainly because of its use in the soda bottle and tire cord industries – most of the patents are related to SSP of polyesters, and the literature dealing with nylon SSP is relatively scarce in comparison. In this section, a brief historical of nylon SSP in the patent literature is reviewed, with the selection of patents that are discussed listed in Table 1.2.

Table 1.2 A selection of patents about solid-state polymerization of nylons*

Author	Year	Patent	Company	Description
Flory	1939	US 2,172,374	DuPont	Discovery of PA66 SSP
Kjellmark.	1962	US 3,015,651	DuPont	Batch PA6 SSP process
Monroe	1962	US 3,031,433	DuPont	Continuous PA66 SSP process
Wiloth	1968	US 3,379,696	Ver. Glanzstoff-Fab.	PA66 SSP from monomers
Silvermann *et al.*	1970	US 3,548,584	Monsanto	SSP of drawn fibers
Brignac *et al.*	1970	US 3,551,548	-	SSP of drawn fibers
Silvermann *et al.*	1971	US 3,562,206	Monsanto	SSP with unbalanced endgroups
Beaton	1974	US 3,821,171	DuPont	Moving-packed bed reactor
Pipper *et al.*	1989	US 4,816,557	BASF	PA6 SSP w/ superheated steam
Knorr	1991	US 5,073,453	Monsanto	SSP of as-spun fibers
Götz	1997	US 5,596,070	BASF	PA SSP process from nitriles
Blanchard *et al.*	1999	WO 99/10408	DuPont	thermal pretreatment of granules

* in chronological order

The possibility to increase the molar mass of nylons by heating a solid prepolymer in a finely divided state below the melting point was discovered by Flory [30] as early as 1939, the year commercial production of nylon-66 was launched by DuPont. The original idea was to raise the molar mass so as to attain fiber-forming properties.

The early designs for the SSP of nylon granules involved configurations where the solid phase is operated discontinuously, using fixed-bed, rotary drum, or fluidized-bed reactors. An example of an intermittent (batch) process is the two-stage reactor designed by Kjellmark [27] for the SSP of nylon-6 granules, where hollow double-trough screws are converted from a mixing to a conveying cycle once the prescribed molar mass is attained (Figure 1.5).

The first continuous process was designed by Monroe [31] for SSP of nylon-66, in which high molar masses are obtained in a moving stirred bed with a gas velocity insufficient to achieve fluidization. Such a method reduces the need for large volumes

of fluidizing gas. In order to avoid an unfavorable imbalance of end-groups resulting from hexamethylene diamine being more volatile than adipic acid, Monroe started the polymerization with the nylon salt. An alternative was proposed by Wiloth [32] who patented a process in which the diamine and diacid monomers are first reacted below their melting points in a closed precondensation reactor up to 15 bar until full conversion of the diamine ; at this point, the pressure is released and a nitrogen stream passed through the reaction mass to initiate SSP. However, it is still possible to increase the molar mass of an unbalanced nylon by means of SSP, as demonstrated by Silvermann *et al.* [33] for a ratio of amine to carboxyl ends between 1.1 and 2.0, making use of phosphorus-based catalysts.

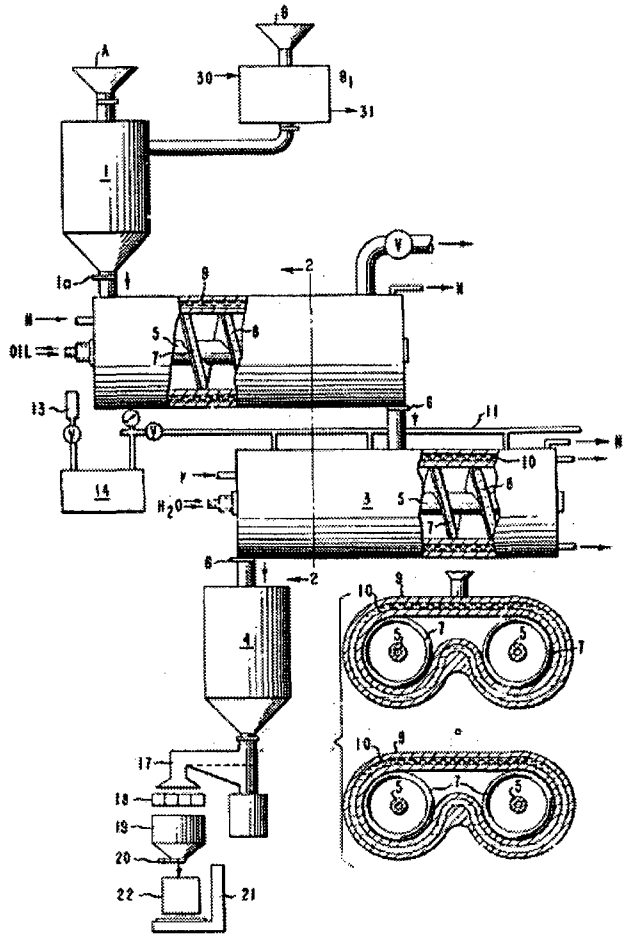

Figure 1.5 Solid-state polycondensation of nylon-6 granules by DuPont [27]. B1) Extraction unit ; 1) Hold-up tank ; 2) Polymerizing vessel ; 3) Quenching vessel ; 4) Canning hopper ; 5) Mixer-conveyors

In 1970, Silvermann *et al.* [34] and Brignac *et al.* [35] undertook SSP of nylon-66 oriented fibers. For this purpose, drawn yarns of nylon were wound onto bobbins and heated in a vacuum oven. As a result of this treatment, the toughness and the dimensional stability of the fibers improved, which eliminated the tendency of tires made with such nylon tire cords to flatspot. By subjecting drawn fibers to SSP, it was thus possible to avoid the major problems occurring when attempts are made to melt-spin fibers directly from a highly polymerized material [34]. More recently (1991), Knorr [36] disclosed a process for the production of nylon yarns of even higher tenacity by subjecting the as-spun (unoriented) yarn to SSP *prior* to drawing.

A simple configuration for continuous SSP is the gravity-conveyed moving packed-bed reactor, in which a quasi plug flow velocity profile of granules is flowing downward, counter-currently to a stream of inert gas (Figure 1.6). The plug flow profile is best achieved using chevron-shaped baffles. The advantage of the moving packed-bed over other continuous reactors in which agitation is provided by mechanical means or fluidization is its narrow residence time distribution, resulting in a product with a smaller polydispersity.

Unfortunately, the granules in a compact bed tend to stick to each other even at temperatures well below the crystalline melting point, causing polymer agglomeration and wall sticking problems. For this reason, moving packed-bed reactors had to be operated at low temperature, hence requiring very large residence times. In 1974, Beaton [37] observed that the softening point of the particles could be raised by preheating them in an uncompacted state before SSP. This enabled him to perform SSP at industrial scale within 20°C of the crystalline melting point of the polymer. Nowadays, the moving packed-bed reactor is the most popular configuration to operate SSP industrially.

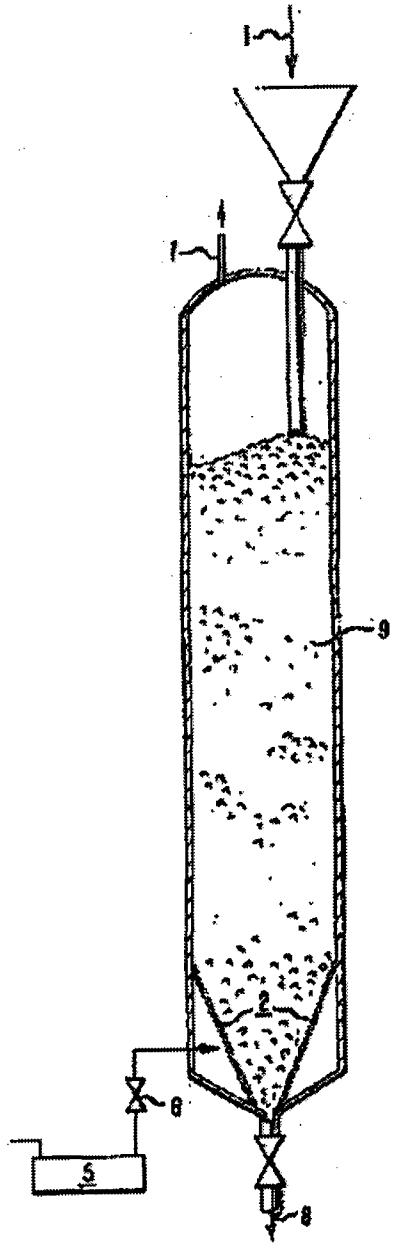

Figure 1.6 A moving packed-bed reactor for nylon solid-state polymerization [37]

Using the preheating step described above, the moving packed-bed reactor is also suitable to remove the ε-caprolactam left unreacted after the VK column (as well as other cyclic oligomers), as disclosed by a BASF patent [38]. In this process, the hot water extraction stage is suppressed, and the preheated nylon-6 granules containing typically from 8 to 12 % ε-caprolactam are directly fed into the reactor, operated under a counter-current of superheated steam. The process has the advantage that the proportion of extractables in the product is reduced in a simple manner to the desired level. Furthermore, monomer recovery from the gas phase is easier than from the dilute aqueous solution arising from the customary hot water extraction stage.

In addition to a narrow residence time distribution, chain regulators may be added to control the dispersion of the molar mass distribution of the product. A BASF patent [39] reports that monoacids (propionic acid, benzoic acid) or monoamines (methylamine, ethylamine, propylamine) in an amount of 0.01 to 0.5 % can be used for this purpose.

Today, more than half a century after the invention of nylon, investigations are still under way to improve manufacture processes in order to gain an economical advantage in the present competition between producers. An example of a recent achievement is the nylon-6 process patented in 1999 by DuPont [40], sketched in Figure 1.7. In this process, the molten prepolymer is subjected to a controlled temperature-time profile before solidification and granulation, on the contrary to classical processes where the product strand exiting the melt polymerization stage is normally quenched. This thermal pretreatment allows operating the SSP reactor at significant higher temperature without agglomeration and wall sticking due to particle softening. This improves the performance of the solid-state reactor by both reducing the required residence time to reach a specified molar mass and enhancing the removal of extractables. The authors related this beneficial effect of the annealing step to an increase of the softening point of the prepolymer – defined as the temperature at which the DSC curve begins to indicate an endotherm associated with polymer melting.

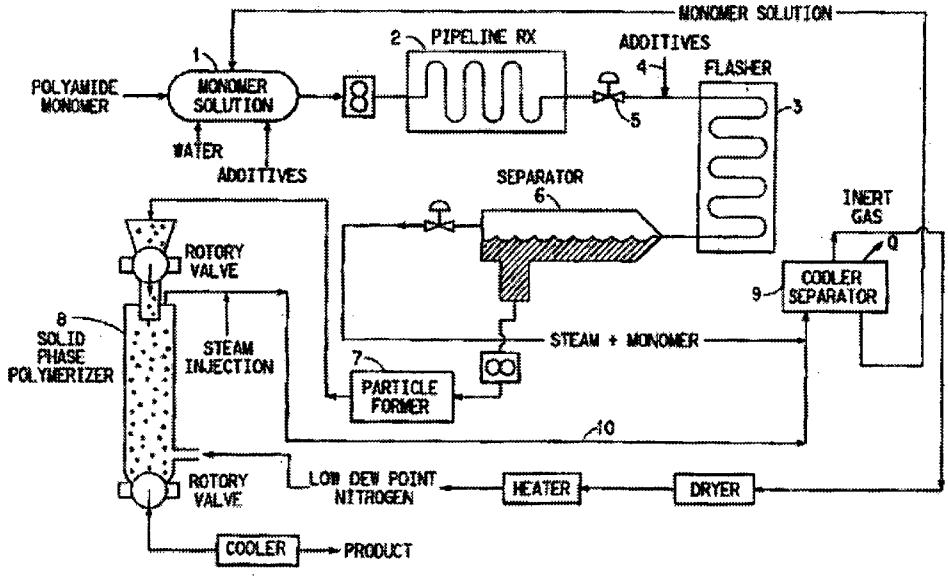

Figure 1.7 Solid-state polymerization of nylon-6 by DuPont [40]. Control of the crystallization rate during the particle-forming step enhances the performance of the SSP reactor

In this work, we shall demonstrate that the influence of the morphology of the solid polymer on the SSP process is generally underestimated. In fact, it could well be that the ability to control the crystallization stage is the key idea to achieve further solid phase advantages such as shorter residence times and impurity removal during SSP. In this perspective, the data disclosed in the DuPont patent [40], will be reexamined based on a phenomenological model for nylon solid-state polymerization.

1.4 Context and Objective of this Work

This thesis gives account of a project on nylon-6 solid-state polycondensation in collaboration with an industrial partner, BASF, in Ludwigshafen, Germany.

The field of polymer reaction engineering of nylon-6 has matured considerably since Flory [41] first postulated the equal-reactivity hypothesis (now associated with his name) in 1936. In the early studies, the equilibrium and rate constants of the main reactions were evaluated using data obtained in small glass ampoules under isothermal conditions [19-21, 42]. In the seventies, the emphasis shifted and the rate constants of important side reactions – formation of cyclic oligomers [43-45], degradation reactions [46] – were evaluated using newly developed chromatographic and spectroscopic techniques [47]. In addition, several chemical engineers entered the field and reported work on various aspects of heat and mass transfer [48, 49]. Studies on the optimization of ideal reactors started to appear in the open literature to obtain interesting qualitative justifications of existing industrial reactors. For example, it was found that one should use high concentrations of water in the feed of ε-caprolactam, followed by removal of water to very low level, in order to minimize the reaction/residence time [50, 51] while producing nylon-6 of number-average chain length of around 150. Only in the late eighties and early nineties were studies reported in the open literature on the simulation and optimization of industrial polymerization reactors with plant data appearing in slightly disguised forms [52, 53]. This paved the way for the development of industrially relevant software packages for the design of step growth polymerization reactors such as POLYRED [54, 55], as well as new concepts for optimal control of nylon-6 polymerization systems [56].

Still, a major limitation to the understanding of nylon-6 manufacture process is that the formidable amount of knowledge described above is restricted to the hydrolytic polymerization of ε-caprolactam, i.e. the melt polymerization part of the process. Studies on the postcondensation stage are strikingly scarce in comparison (on the contrary to PET). In fact, there are only five reports on PA6 SSP in the open literature that include useable experimental data, as listed in Table 1.3. This emphasizes the need for a considerable amount of research in this area, which is all the more relevant since production engineers tend to prefer to modify a desired grade by changing the operating parameters of the solid-state reactor rather than the melt polymerizer, due to the stability of the VK column.

Table 1.3 Experimental data on nylon-6 SSP in the open literature*

Author	Year	Source	Comment
Cawthon *et al.* [57]	1960	journal	Determination of ε-caprolactam at equilibrium
Kjellmark [27]	1962	patent	Influence of extraction step
Fakirov *et al.* [58]	1982	journal	SSP of oriented nylon-6 fibers
Gaymans *et al.* [59]	1982	journal	Kinetic studies in a fluidized bed
Blanchard *et al.* [40]	1999	patent	Influence of a thermal pretreatment

* in chronological order

Detailed modeling of PA6 SSP is consequently also in its infancy. In fact, only two phenomenological models were proposed, by Gupta and coworkers [60, 61] that were unable to predict Gaymans' data correctly. Moreover there exists up to now no published studies in which experiments and modeling were performed simultaneously.

Based on these observations, the objectives of this project on nylon-6 SSP were formulated as follows :

- Undertake a critical literature survey and develop theoretical arguments,
- perform a kinetic study and a structural investigation at laboratory scale,
- develop a phenomenological kinetic model at particle scale, based on both our own experimental data and the data available in the literature,
- and scale-up the single particle model in order to simulate the behavior of an industrial solid-state reactor.

The present report is structured in different parts. A literature review and some new theoretical ideas are developed in Chapter 2. The battery of fixed-bed reactors set up to perform the experimental study and the analytical procedures are presented in Chapter 3. The results of the kinetic studies and the morphological investigation are disclosed in Chapter 4 and Chapter 5, respectively. The development and performance of the single particle model are presented in Chapter 6, whereas modeling of an industrial moving packed-bed reactor is developed in Chapter 7. Concluding remarks and an outlook are given in Chapter 8.

1.5 References

[1] Carothers W.H. (1940). Collected papers of Wallace Hume Carothers on high polymeric substances. *High Polymers*, 1, Mark H. and Whitby G.S. eds., Interscience pub., New York.

[2] Sekiguchi H. and Coutin B. (1992). Polyamides. In : Handbook of polymer synthesis, A, Kricheldorf H.R. ed., Marcel Dekker pub.

[3] Schlack P. (1938). *German patent 748,253 to I.G. Farbenindustrie.*

[4] Reimschuessel H.K. (1977). Nylon 6, chemistry and mechanisms. *J. Polym. Sci. : Macromol. Revs.*, 12, 65.

[5] Kohan M.I. (1973). Introduction. In : Nylon plastics, Kohan M.I. ed., Wiley pub., 1.

[6] Spanoudis S. (2000). Guide to polymer tradenames. *www.geocities.com/ ~spanoudi/tradname.html*

[7] The Plaspec materials selection database (2000). *www.plaspec.com*, Plast. Tech. Inc. pub.

[8] Matweb, the online materials information resource (2000). *www.matls.com*, Automation Creations Inc. pub.

[9] Welgos R.J. (1988). Polyamides, plastics. In : Encyclopedia of polymer science and engineering, 11, Mark H.F. *et al.* eds., Wiley pub., 445.

[10] Guérin B. (1993). Polyamides. In : Monographies des thermoplastiques, Techniques de l'ingénieur, M2, 1.

[11] Chrétien G. and Hatat D. (1990). Initiation aux plastiques et aux composites, Tec. et Doc. Pub., Paris, 62.

[12] A short history of manufactured fibers (1999). *www.fibersource.com*, The Fiber Economics Bureau Inc. pub., Washington D.C.

[13] Rodriguez F. (1996). Principles of polymer systems. Taylor&Francis pub., Washington D.C., 1.

[14] Kohan M.I. (1985). Polyamides. In : Ullmann's encyclopedia of industrial chemistry, VCH pub., A21, 179.

[15] Davenport R. (1999). Supply/demand and market outlook for ETPs. *Proceedings,* AIChE Spring Meeting, March 14-18, Houston TE, 556.

[16] Kuhlke W.C. (1999). World polymer market review – 1999 edition. *Proceedings,* AIChE Spring Meeting, March 14-18, Houston TE, 547.

[17] Zimmermann J. (1988). Polyamides. In : Encyclopedia of polymer science and engineering, 11, Mark H.F. *et al.* eds., Wiley pub., 315.

[18] Carothers W.H. and Berchet G.T. (1930). Studies on polymerization and ring formation. VIII. Amides from ε-aminocaproic acid. *J. Am. Chem. Soc.*, 52, 5289.

[19] Hermans P.H., Heikens D. and van Velden P.F. (1958). On the mechanism of the polymerization of ε-caprolactam. II. The polymerization in the presence of water. *J. Polym. Sci.*, 30, 81.

[20] Kruissink C.A., van der Want G.M. and Staverman A.J. (1958). On the mechanism of the polymerization of ε-caprolactam. I. The polymerization initiated by ε-aminocaproic acid. *J. Polym. Sci.*, 30, 67.

[21] Heikens D., Hermans P.H. and van der Want G.M. (1960). On the mechanism of the polymerization of ε-caprolactam. IV. Polymerization in the presence of water and either an amine or a carboxylic acid. *J. Polym. Sci.*, 44, 437.

[22] Gupta S.K. and Kumar A. (1987). Reaction engineering of step growth polymerization. Plenum Press pub., New York.

[23] Reimschuessel H.K. (1969). Lactams. In : Ring-opening polymerization, Frisch K.C. and Reegen S.L. eds., Dekker pub., New York.

[24] Sebenda J. (1978). Recent progress in the polymerization of lactams. *Prog. Polym. Sci.*, 6, 123.

[25] Gupta S.K. (1988). Nylon polymerization. In : Encyclopedia of engineering materials, A 1, Cheremisinoff N.P. ed., Marcel Dekker pub., 211.

[26] Tang Z.-L., Wang X.-Q., Hung N.-X. and Gerking L. (1999). Polyamide-6 polymerization and its melt flow in the VK tube reactor with optimized baffle structure. *Angew. Makromol. Chem.*, 266, 7.

[27] Kjellmark E.W. (1962). Increasing viscosity of polycaprolactam by removing extractables with solvents and further solid phase polymerizing the polymer. *US patent 3,015,651 to DuPont.*

[28] Mallon F.K. (1997). Solid state polycondensation : modelling and productivity enhancements. Thesis, University of Wisconsin-Madison.

[29] Pilati F. (1986). Solid-state polymerization. In : Comprehensive polymer science, Allen G. and Bevington J.C. eds., Pergamon Press pub., 5, 201.

[30] Flory P.J. (1939). Polymerization process. *U.S. patent 2,172,374 to DuPont.*

[31] Monroe G.C. (1962). Solid phase polymerization of polyamides. *U.S. patent 3,031,433 to DuPont.*

[32] Wiloth F. (1968). Solid state preparation of polyamides. *U.S. patent 3,379,696 to Vereinigte Glanzstoff-Fabriken.*

[33] Silvermann B., Raleigh N.C. and Stewart L.E. (1971). Process for producing ultrahigh molecular weight polyamides. *U.S. patent 3,562,206 to Monsanto.*

[34] Silvermann B., Raleigh N.C. and Stewart L.E. (1970). High molecular weight oriented polyamide textile yarn. *U.S. patent 3,548,584 to Monsanto.*

[35] Brignac E.P., Bascum H.D., Nunning W.J. and Snooks R.J. (1970). Method for spinning polyamide yarn of increased relative viscosity. *U.S. patent 3,551,548.*

[36] Knorr R.S. (1991). High tenacity nylon yarn. *U.S. patent 5,073,453 to Monsanto.*

[37] Beaton D.H. (1974). Continuous, solid-phase polymerization of polyamide granules. *U.S. patent 3,821,171 to DuPont.*

[38] Pipper G. and Cordes C. (1989). Removal of caprolactam and oligomers thereof from nylon granules containing same. *U.S. patent 4,816,557 to BASF.*

[39] Götz W. (1997). High molecular weight polyamides obtained from nitriles. *U.S. patent 5,596,070 to BASF.*

[40] Blanchard E.N., Cohen J.D., Iwasyk J.M., Marks D.N., Stouffer J.M., Aslop A.W. and Lin C. (1999). Process for preparing polyamides. *World patent 99/10408 to DuPont.*

[41] Flory P.J. (1936). Molecular size distribution in linear condensation polymers. *J. Am. Chem. Soc.*, 58, 1877.

[42] Giori C. and Hayes B.T. (1970). Hydrolytic polymerization of caprolactam. I. Hydrolysis – polycondensation kinetics. *J. Polym. Sci. : Part A-1*, 8, 335.

[43] Heikens D. (1956). Determination of the individual cyclic oligomers in equilibrium systems from ε-caprolactam and water. *Rec. trav. chim.*, 75, 1199.

[44] Arai Y., Tai K., Teranishi H. and Tagawa T. (1981). Kinetics of hydrolytic polymerization of ε-caprolactam. III. Formation of cyclic dimer. *Polymer*, 22, 273.

[45] Tai K. and Tagawa T. (1982). The kinetics of hydrolytic polymerization of ε-caprolactam. V. Equilibrium data on cyclic oligomers. *J. Appl. Polym. Sci.*, 27, 2791.

[46] Reimschuessel H.K. and Dege G.J. (1970). Polyamides : decarboxylation and desamination in nylon 6 equilibrium polymer. *J. Polym. Sci. : Part A-1*, 8, 3265.

[47] Tai K., Teranishi H., Arai Y. and Tagawa T. (1979). The kinetics of hydrolytic polymerization of ε-caprolactam. *J. Appl. Polym. Sci.*, 24, 211.

[48] Ahn Y.-C. (1997). Effects of diffusional water removal and heat transfer in nylon 6 reactors. *Polym. Eng. Sci.*, 37, 484.

[49] Nagasubramanian K. and Reimschuessel H.K. (1973). Diffusion of water and caprolactam in nylon 6 melts. *J. Appl. Polym. Sci.*, 17, 1663.

[50] Reimschuessel H.K. and Nagasubramanian K. (1972). On the optimization of caprolactam polymerization. *Chem. Eng. Sci.*, 27, 1119.

[51] Tai K. and Tagawa T. (1983). Simulation of hydrolytic polymerization of ε-caprolactam in various reactors. A review on recent advances in reaction engineering of polymerization. *Ind. Eng. Chem. Prod. Res. Dev.*, 22, 192.

[52] Gupta A., Gupta S.K., Gandhi K.S., Mehta M.H., Padh M.R., Soni A.V. and Ankleswaria B.V. (1992). Modeling of hydrolytic polymerization in a semibatch nylon 6 reactor. *Chem. Eng. Comm.*, 113, 63.

[53] Wajge R.M., Rao S.S. and Gupta S.K. (1994). Simulation of an industrial semibatch nylon 6 reactor : optimal parameter estimation. *Polymer*, 35, 3722.

[54] Appert T., Jacobsen L. and Ray W.H. (1992). A general framework for modelling polycondensation processes. *DECHEMA Monographs*, 127, 189.

[55] Jacobsen L.L. and Ray W.H. (1992). Unified modeling for polycondensation kinetics. *J. Macromol. Sci. - Rev. Macromol. Chem. Phys.*, C32, 407.

[56] Gupta A. and Gupta S.K. (1998). Simulation and optimization of an industrial nylon 6 reactor : a review. *Polym.-Plast. Technol. Eng.*, 37, 201.

[57] Cawthon T.M. and Smith E.C. (1960). Polymerization and depolymerization of nylon 6 above and below its melting point. *Polymer Preprints*, 1, 98.

[58] Fakirov S. and Avramova N. (1982). Influence of thermal treatment, molecular weight and orientation on the mechanical properties of polyamide-6. *Acta Polymerica*, 33, 271.

[59] Gaymans R.J., Amirtharaj J. and Kamp H. (1982). Nylon 6 polymerization in the solid state. *J. Appl. Polym. Sci.*, 27, 2513.

[60] Kaushik A. and Gupta S.K. (1992). A molecular model for solid-state polymerization of nylon-6. *J. Appl. Polym. Sci.*, 45, 507.

[61] Kulkarni M.R. and Gupta S.K. (1994). Molecular model for solid-state polymerization of nylon 6. II. An improved model. *J. Appl. Polym. Sci.*, 53, 85.

2. Solid-State Polymerization

2.1 Literature Review

The early studies on solid-state polymerization of nylons date back to the sixties and concentrated on the *equilibrium* in the solid phase, in comparison with the melt equilibrium of the polymer. Cawthon and Smith [1] determined the caprolactam content in equilibrated PA6 samples below and above the melting point, performing experiments in sealed glass tubes. They observed a sudden decrease of caprolactam after solidification, and attributed this equilibrium shift to the concentration of the monomer exclusively in the amorphous part of the semicrystalline polymer. Andrews *et al.* [2] observed the same behavior for higher PA6 cyclic oligomers, of order 2 to 6, indicating that even large macrocycles cannot be incorporated into the crystalline structure.

Zimmermann [3] reached a similar conclusion for the polyamidation equilibrium. By studying PA6, PA66, and PA6/66 samples equilibrated under some fixed water vapor pressure, this author observed that the polycondensation equilibrium was shifted to higher molar masses in the solid state, and related this phenomenon to the exclusion of water and reactive end-groups from the crystalline domains. Zimmermann also noted a broadening of the chain length distribution (CLD) comparatively to the Flory-Schulz [4, 5] most probable CLD expected in melt polycondensation. Zimmermann's explanation for this was that it is not likely that each polymer chain – passing through crystalline and intervening amorphous regions a number of times – has the same amorphous length.

However, a decade later, Meyer [6] theoretically derived the equilibrium CLD for postcondensed nylons. His conclusion was that the CLD was still of the Flory-Schulz type, in spite of the fact that the calculation yielded a higher average molar mass for the partially crystalline material compared to the amorphous one. In this work, we shall point out other possible causes of a CLD broadening, such as the existence of a non-uniform spatial distribution of crystallites within the amorphous matrix, or radial concentration gradients arising from the diffusion of volatile species under transient conditions.

Since the volatile species are continuously removed from the reaction zone in the SSP process, equilibrium is in principle never reached, and the reaction is kinetically controlled. The authors who first dealt with the *kinetics* of SSP of nylons were the groups of Griskey [7, 8] in the late sixties, who investigated SSP of PA66 and PA6-10, and Gaymans in the seventies, who focused their research on PA46 [9, 10] and PA6 [11]. Their major goal was to identify whether one of the kinetic steps involved could be rate-limiting : diffusion of the reactive end-groups toward each other, at nanometer scale ; chemical reaction ; molecular diffusion of the condensate

by-product, at millimeter scale ; or mass transfer by convection at the polymer particle/gas interface (Figure 2.1).

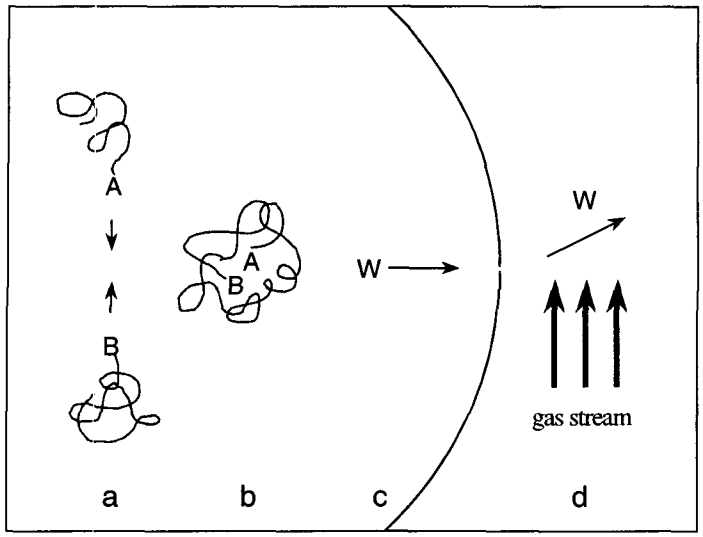

Figure 2.1 The kinetic steps in solid-state polycondensation. a) Diffusion of end-groups ; b) Chemical reaction ; c) Transport of condensate by diffusion ; d) Transport of condensate by convection

As the SSP principle is in essence to maximize the surface area available for mass transfer, we can expect that the convective external transport is not rate controlling, provided sufficient stripping or flashing conditions are applied. This was borne out by Griskey and Lee [7] who obtained the same final number-average molar mass, when PA66 particles were subjected to SSP in a fixed-bed reactor under different nitrogen velocities. A further demonstration was brought by Gaymans and Schuijer [10], who solid-state polymerized a powdered PA46 prepolymer in a fluidized bed under nitrogen, and in a rotary vacuum evaporator. Again, the same final molar mass was attained in both cases.

Surprisingly, Hsu [12] found an influence of the type of purge gas : he observed an enhancement of the SSP of PET with the type of gas in the order $N_2 < CO_2 < He$, which seems to indicate that the gas does not only remove the condensation by-product, but also interacts with the polymer to change some microscopic features, such as crystallinity or the mobility of the chain-ends. This report is nonetheless questionable since Mallon *et al.* [13] were unsuccessful to reproduce the effect described by Hsu.

Whether end-group diffusion, reaction, or condensate diffusion limits the overall kinetics of the SSP of nylons has been the subject of considerable controversy. Chen *et al.* [8] performed experiments with different particle sizes around 1 mm, in the temperature range 90-180°C. By fitting their data to some predefined rate functions, they concluded that chemical reaction is the rate-controlling step for PA66 and PET, whereas SSP of PA6-10 at high temperature is limited by the diffusion of water. However, other mechanisms could also explain their experimental results, as pointed out by Pilati [14].

A closer examination of Chen's polymerization profiles, shown in Figure 2.2, illustrates some interesting points that are generally underestimated when attempts are made to understand SSP process by comparing the behavior of different polymers.

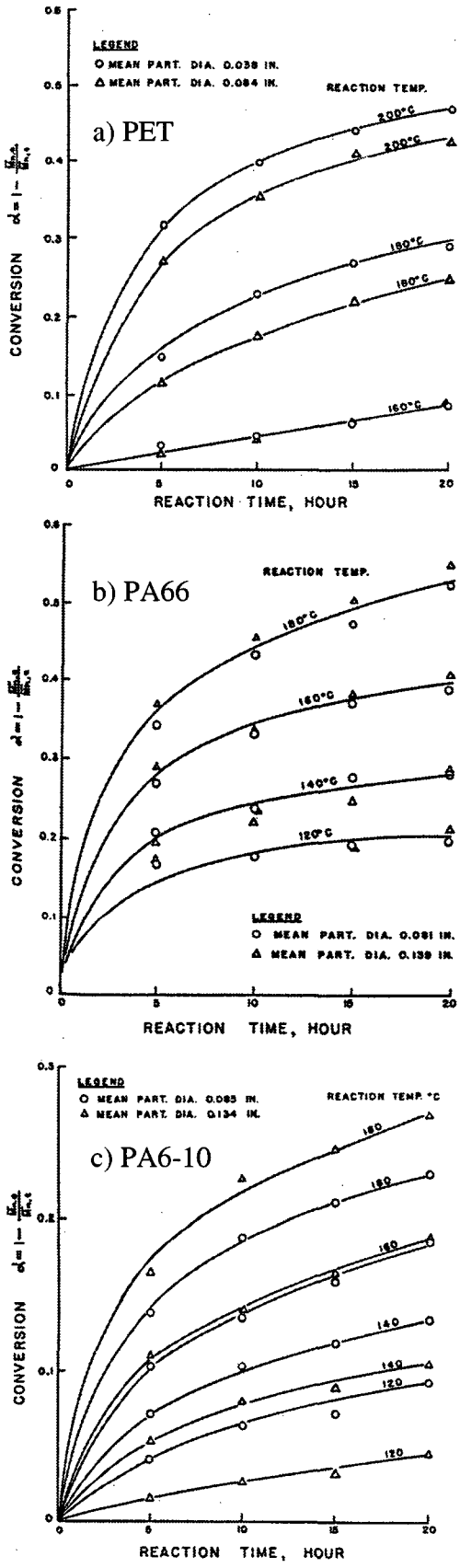

Figure 2.2 Solid-state polymerization profiles measured by Chen *et al.* [8]. a) Polyethylene terephthalate ; b) Nylon-66 ; c) Nylon-6,10

First, a puzzling observation is that SSP of PET (Fig. 2.2.a) is affected by particle size whereas SSP of PA66, carried out under similar conditions, (Fig. 2.2.b) is not ; small PET particles polymerize faster, revealing a kinetic limitation by the diffusion of the condensate out of the granules.

To explain this behavior, we need to recall that the equilibrium constant for the chain-building reaction is very low for polyesters, typically between zero and two for both direct esterification and transesterification [15], whilst it reaches at least several hundreds for polyamidation, depending on temperature and water content [16, 17]. In addition, we can expect the condensate to diffuse faster in polyamides than in polyesters because water has a smaller size than ethylene glycol. For these reasons, it is not surprising that SSP of PET is more sensitive to the rate at which the condensate molecules are removed – and consequently to particle size – than is SSP of PA66. This exemplifies the necessity to be careful when conclusions about SSP of nylons are drawn based on the wealth of PET SSP studies in the literature.

The presence of a diffusion limitation in the SSP of polyesters was confirmed in another way by Buxbaum [18] and Gostoli *et al.* [19] for PBT, who were able to measure a radial profile of intrinsic viscosity, decreasing from the surface to the center of the granule.

Chen's data for PA6-10 (Fig. 2.2.c) exhibit a somewhat curious behavior : the reaction rate decreases with particle size at low reaction temperature, whereas at higher temperatures larger particles actually polymerize faster.

Because water has a lower diffusion coefficient in PA6-10 than PA66 [20], a water diffusion limitation in 6-10 and not in 66 is not surprising (the low temperature curves in Fig. 2.2). The reversal particle size effect can be understood by observing that initially the polymer has relatively high concentrations of the monomer hexamethylene diamine (HMDA). Because HMDA has a low boiling point (205°C), at higher temperatures, the generated HMDA can diffuse to the surface and vaporize. Loss of HMDA leads to an imbalance of functional groups that limits the molar mass [21]. Then, because diffusion distances are shorter in smaller particles, the loss rate per unit volume is higher, and the molar mass limit is more noticeable as the temperature increases.

The imbalance of end-groups occurring when the diamine monomer is more volatile than the diacid monomer is a well known phenomenon, which is sometimes overcome by starting the reaction with the salt instead of the two monomers separately [22, 23]. Of course, this limitation does not hold for *n*-nylons, where both moieties are present on each molecule. Again, this emphasizes how cautious one must be when comparing SSP of different polymers – here *n*-nylons with *n,m*-nylons.

In the limit of a very small diffusion length, irreversible polycondensation is expected to take place. Indeed, Srinivasan *et al.* [24] could fit their data on SSP of thin PA66 fibers with a third-order kinetics, typical for the forward polyamidation reaction [25]. Another study on SSP of fibers was carried out by Fakirov and Avramova [26], who annealed undrawn and drawn PA6 bristles in vacuum in the temperature range 30-240°C.

Unlike Srinivasan, the group of Gaymans [9-11] found much higher apparent orders of reaction – between 3.5 and 5.0 depending on the temperature – for PA46 and PA6 in a fluidized-bed, and therefore suggested that SSP kinetics is limited by the diffusion of end-groups. The idea seemed to be corroborated by their observation that the initial molar mass has a profound influence on the course of reaction, as previously reported by Monroe for PA66 [27]. This was the basis for the development of the "gel effect" model (by analogy with the gel effect in chain radical polymerization), which found a large number of proponents.

A serious criticism of the gel effect model appeared in 1997 when Mallon and Ray [28, 29] presented a non-dimensional analysis based on the polymer-polymer diffusivity data in semicrystalline poly(aryl ether ketone ketone) (PAEKK) [30]. They concluded that the polymer diffusion coefficient should be at least five orders of magnitude lower in order that the gel effect could take place in a polycondensation system. This conclusion was supported in a somewhat different way in 1998 by Srinivasan *et al.* [31], who pointed out that diffusion of the amine functionality in nylons occurs through a "chemical diffusion" mechanism because of the amine-amide interchange reaction, independently of the diffusion of the entire polymer chain. As this leads to an effective diffusion coefficient still higher than the chain diffusion coefficient discussed in Mallon's analysis, the gel effect theory does not seem to describe SSP correctly.

Given the lack of knowledge and the controversy about the rate-limiting step, it is not surprising that most modeling of nylon SSP is practically limited to studies where the authors have correlated their data with empirical functions, which mostly have reaction rates that are non-linear in time [8, 10, 11]. Because of the non-autonomous

properties of this method and the difficulty in applying fitted constants to other work, this type of model has limited value. On the other hand, the two existing attempts to derive a phenomenological model for PA6 SSP are both based on the questionable idea of the gel effect [32, 33]. The sole exception is the model proposed by Mallon and Ray, but they concentrated their efforts on PA66 and PET [29].

Following this literature survey on solid-state polycondensation of polyamides, we shall examine some of the concepts presented above in a more fundamental manner, and develop new theoretical arguments. Particularly, the interaction between solid-state reaction and particle morphology, and the question of the gel effect will be addressed in more details in the next sections.

2.2 Semicrystallinity and Its Potential Implications

As many polymers, nylon-6 forms a semicrystalline structure between its glass transition (T_g = 61°C for a dry and extracted sample [34]) and melting point (T_m = 220°C, measured on moldings [20]), the exact temperature range inside which SSP reactors are operated. In fact, semicrystallinity – the crystalline phase is dispersed into an amorphous continuum – plays a key role with regard to the end-use properties of the polymer in a way analogous to composite materials, combining the hardness of the crystal with the rubbery behavior of the amorphous phase. For this reason, material science engineers have investigated the morphology of polymers extensively for a long time, in order to establish structure-property relationships [35]. However, polymer chemists have somewhat neglected this aspect when attempting to understand reaction in the solid phase. In addition, the interest of production engineers has been usually restricted to the achievement of a polymer of sufficient crystalline content to give a high sticking point, so that necessary temperatures can be achieved without forming a chunk of polymer in the reactor [36].

This section is aimed at clarifying the implication of morphology on the SSP process, which is a prerequisite to develop a phenomenological model. In fact, there is no conceptual difference between the rubbery amorphous phase in the solid polymer and the melt, since melting affects only the crystalline fraction (whereas the glass transition affects only the amorphous phase) [37]. Considering, as we shall see, that reaction in the solid material occurs exclusively in the amorphous phase, we believe that SSP can be understood by extrapolating the nylon melt chemistry to the amorphous phase, taking into account all possible effects caused by the presence of the crystalline structure. In this way, a versatile, phenomenological, and predictive model will be developed based on the well-established melt kinetic and equilibrium parameters [38, 39]. In comparison, most SSP models – even recently published ones [24, 31-33, 40, 41] – use their own data-fitted set of kinetic and equilibrium parameters.

2.2.1 Morphology of Solid Nylon-6

Upon cooling nylon-6 from the melt, a semicrystalline structure is obtained, which is characterized by polymorphism. This means that different crystalline structures can coexist, as determined by X-ray experiments [42]. Two major phases are the α and γ

modifications, in which the chains are organized in sheets where hydrogen bonds are formed. In this context, nylon-6 chains with the –CONH– bonds directed towards a positive or a negative chain axis direction are conventionally called *up* or *down* chains, respectively (note that this distinction exists for *n*-nylons but not for *n,m*-nylons). As shown in Figure 2.3, hydrogen bonds are between antiparallel chains in the α form and between parallel chains in the γ form. In the γ form, sheets of all up or all down chains alternate. In both of the crystalline polymorphs, chains are 50 % up and 50 % down. Both structures were described in terms of monoclinic cells assuming *b* as the unique axis, parallel to the chain axis. Also, in both forms the chain symmetry corresponds to the *s*(2/1) line repetition group, and the period of the chain includes two monomer units [43, 44].

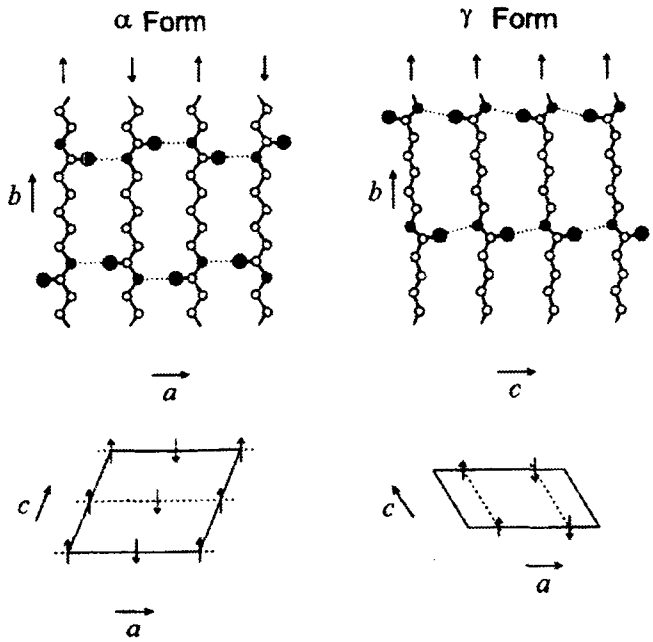

Figure 2.3 Ordered model structures for the α and γ forms of nylon-6 [45]. The unit cells are monoclinic, and *b* is the unique axis coinciding with the chain axes. Projections are shown in the *ab* plane of a sheet of chains where the hydrogen bonds are formed. The unit cells are shown in the *ca* projection (a = 0.956 nm, b = 1.724 nm, c = 0.801 nm, and β = 67.5° for the α form ; a = 0.933 nm, b = 1.688 nm, c = 0.478 nm, and β = 121° for the γ form). The arrows distinguish between up and down chains, and the dashed lines are traces of sheets of hydrogen bonds

According to Holmes *et al.* [43], the chains in the α form are in a all-*trans* planar conformation corresponding to a periodicity of 1.72 nm ; according to Arimoto *et al.* [44] in the γ form the backbone dihedral angles are still in a *trans* conformation, but those adjacent to the amide bonds are around 120° and the periodicity of the chains – lower than in the α form – corresponds to 1.688 nm (see Fig. 2.3).

The α structure is thermodynamically more stable than the γ structure, although both modifications retain their identities up to their melting points upon reasonably rapid heating [34]. During crystallization in the bulk, the γ form appears exclusively at low crystallization temperatures. As these increase, increasing amounts of the α modification appear and only at temperatures very close to T_m pure α crystals of nylon-6 are obtained, as observed by Illers and Haberkorn [46]. The majority of the γ-to-α transformation takes place above the Brill transition temperature, which occurs at

about 187°C [34]. Upon cooling from the melt, kinetics appears to dominate thermodynamics. When the melt is quenched, only the γ-modification crystals appear. As the cooling rates slow down, increasing amounts of the α form appear at the expense of the γ form and at cooling rates lower than about 20 K/min only the α-modification crystals appear. When the α-form crystals are annealed in the solid state, which corresponds to SSP conditions, it has been observed that their crystal perfection and melting point both increase with the duration and temperature of the solid-state annealing process [47].

The reason why the α modification is more stable than the γ modification lies in the slightly twisted configuration adopted by the chains in the γ form, which is necessary to fully satisfy all possible hydrogen bonds. In fact, full consumption of hydrogen bonds seems to be the dominant factor controlling the crystal structure of nylons [48, 49]. Even in the melt, a substantial fraction – up to 30 % – of the hydrogen bonds remains satisfied [50]. Thus, some kind of network subsists in the molten polymer, which could explain the memory effects that are sometimes observed after a melting-recrystallization stage [51].

The ordered phase, dispersed in the amorphous continuum, is constituted of small entities of lamellar shape called crystallites. Nylon-6 crystallites are typically 10 nm thick with the macromolecules perpendicular to the lamellae [52]. As the length of an extended chain (about 100 nm for M_n = 17,000 g/mol) would exceed the thickness of the crystallite, two pictures of the micromorphology can be postulated (Figure 2.4).

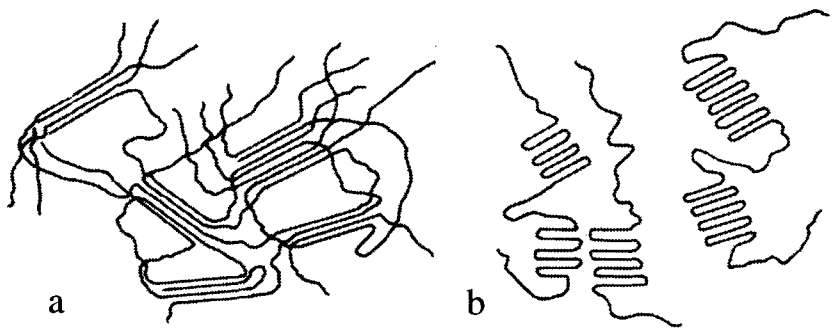

Figure 2.4 Crystallite arrangements. a) Fringed micelles ; b) Folded chains with adjacent reentry

The first description arises from the traditional viewpoint that long-chain molecules form a statistical assemblage of chain units in constant random motion which give rise to no crystal entity other than that caused by short-range aggregation of neighboring chain segments. Here, any individual chain would remain in its overall random configuration, except for parts of it becoming incorporated into a crystalline region. This extended-chain picture is referred to as the *fringed micelles model* (Fig. 2.4.a) [53].

The second picture shows crystallites formed by folding of the chains (Fig. 2.4.b). Both thermodynamic and kinetic arguments have been propounded to explain this *chain-folding model* [54]. The kinetic theory currently favored by some workers views the folding as a means of increasing the crystallization rate, even though crystals with completely extended chains might be more stable under equilibrium conditions. There are numerous experimental evidences that support this latter picture

to the detriment of the fringed micelles model. Examples are the multiple peak structure of the chain length distribution in selectively degraded preparations, corresponding to single-double and multiple traverses in the chain-folded structure [53], or the detection of chain-folds in PA66 by means of infrared spectroscopy [55].

The crystallites grow on their thin faces – called *growth surfaces* – while their two large flat surfaces – called *basal surfaces* – are the ones where chains fold. The morphology of the basal surface is probably more complex than the idealized picture in Fig. 2.4.b with adjacent reentry of the chains. More realistically, some chains also reenter the crystallite at random, creating varying sizes of loops in the amorphous phase. In addition, some chains may meander in the disordered amorphous phase and pass from one crystallite to another. Such interlamellar bonding, which increases as the molar mass increases, is of critical importance for the technological properties of the polymer : the tie molecules form bridges between lamellae and are responsible for the cohesion between them ; they are also responsible for the transfer of stress through the material [56]. Besides *loops* and *bridges*, other possible topological species are *cilia* – i.e. chain-ends to short to be incorporated in the crystallites – and *free chains* that are not incorporated wholly or partly in the crystal phase.

A consequence of the above description of the two-phase model (crystalline/ amorphous) is that the boundary between the two phases should be rough and not extremely well delimited. In fact, recent advances in measurement technologies, including thermal analysis and calorimetry, have led to observations of deviations from the two-phase model [57]. One such deviation is that there is not always a one-to-one correspondence between crystallinity and the jump in heat capacity in the glass transition interval. It has been suggested that such deviations are caused by those bridges, loops, and anchored chains described above whose mobility is hindered. This originated the term *rigid amorphous phase*, first coined by Wunderlich [58], and has led to proposals for a three-phase model of the semicrystalline polymer morphology [59] that includes crystalline, rubbery amorphous and rigid amorphous phases, the latter retaining a glassy behavior above T_g.

The existence of the rigid amorphous interphase has been initially reported for PET, PBT, PEN, PPS, POM, and PE [57]. However, Murthy and Orts [60] demonstrated its occurrence in PA6 using D_2O as a probe in their small-angle neutron scattering (SANS) experiments. They found typical values for the thickness of the interphase ranging from 0.5 to 1.0 nm, depending on the drawing and annealing conditions applied.

The ordered structures discussed so far are sometimes incorporated into superstructures, mainly formed upon crystallization from the melt. For example, the crystallites may be assembled into large spherical entities called *spherulites*, in which lamellae grow from a central nucleus and emanate in all directions, such that when averaged, the crystal orientation within each spherulite and throughout the unoriented specimen turns to be completely random (Figure 2.5). Spherulites range in size from submicroscopic dimensions to millimeters in diameter, and can be recognized in the polarized light microscope because of their birefringence [51, 61]. Depending on the crystallization conditions, spherulites can grow to completion, that is, until their coming into contact with an adjacent spherulite. The intermediate and final stages of this growth mechanism are depicted in Fig. 2.5.a and Fig. 2.5.b, respectively. In the former case, two types of amorphous phases can be distinguished, depending on their

location : the *interlamellar* amorphous phase between the lamellae, and the *bulk* amorphous phase outside the spherulites.

Spherulitic structure is characteristic of crystallization in an environment free from stress on the melt, including both mechanical stress from agitation of the melt and thermal stress from strong temperature gradients. This is why most nylons form spherulites in the carefully controlled environment of slow crystallization on a microscope slide [51]. On the other hand, in commercial processing such as extrusion and molding, considerable stresses of both types are present that somewhat hinder the growth of spherulites [62].

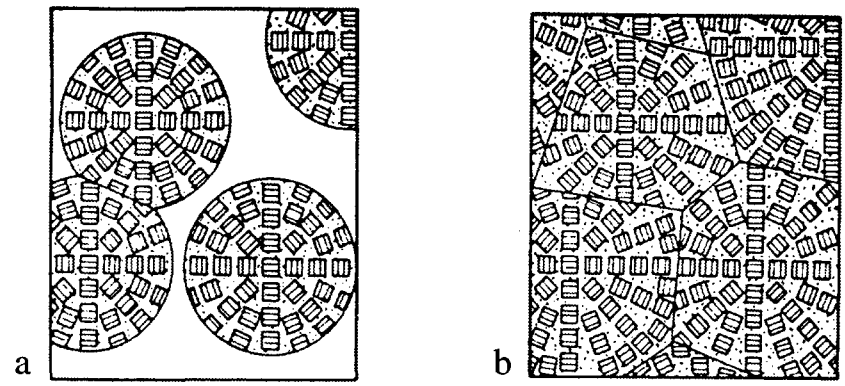

Figure 2.5 Ordering of lamellae in spherulites. a) Situation during crystallization, the amorphous phase is partitioned between bulk and interlamellar fractions ; b) Situation after completion of crystallization

Upon drawing of nylon fibers, the spherulitic structure is lost, but other ribbon-like superstructures are likely to develop that are often referred to as *fibrils*. Although the situation in the oriented polymer is more complex because of its anisotropy, two types of amorphous phases can again be distinguished, as shown by Murthy and associates for PA6 [63, 64] : the *interlamellar* amorphous phase, and the *interfibrillar* amorphous phase in the longitudinal channels between the fibrils.

To conclude this description of the morphology of solid nylon-6, we feel it important to recall that the semicrystalline structure is in essence not an equilibrium one. The following three considerations illustrate this important point.

First, partially crystalline polymers violate the phase rule, $\varphi + v = \kappa + 2$, where φ, v, and κ stand respectively for the number of phases, the variance of the system (number of degrees of freedom), and the number of components. Treating the homopolymer as a one-component system ($\kappa = 1$), the number of possible phases in equilibrium is three at the triple point (constant temperature and pressure, $v = 2$) and two along the melting curve (constant temperature or pressure, $v = 1$). At constant pressure, the normal analysis condition $\varphi + v = \kappa + 1$ applies, and only one phase can exist at different temperatures ($v = 1$). Therefore, semicrystalline polymers below T_m cannot be in equilibrium, even when multiple crystalline modifications and the rigid amorphous phase are not considered.

The second argument is related to the dispersed nature and the size of the ordered phase. As discussed above, tiny crystallites divide a large sample rather than forming a single crystal. These lamellar crystals are small enough that surface effects need to be considered. In other words, the total surface free energy is not at a minimum and

the sample is not in equilibrium. In addition, the lamellar shape itself is metastable because the large basal planes have a higher surface energy than the thin lateral growth planes. In fact, the thickening of the lamellae sometimes observed upon annealing may be explained by the decrease of their surface free energy, as theorized by Sanchez [65]. However, the high-energy lamellar shape is usually retained due to the restrictions imposed by the hydrogen bonds when the fold length is increased.

Third, it is well known that nylons exhibit a large extent of supercooling, that is, the onset of crystallization takes place at T_{cc} far below T_m when the polymer is cooled from the melt. Aharoni [34] mentions T_{cc} values for nylon-6 ranging from 160 to 200°C, depending on the cooling rate and the thermal treatment applied to the melt (some nuclei can survive in the melt giving rise to memory effects). This again emphasizes the metastable nature of the solid state between T_g and T_m.

Consequently, the solid nylon-6 granules processed in the solid state are never in equilibrium, and equilibrium thermodynamics should not be applied to such systems. Of course, we consider here equilibrium as a whole, including thermal, mechanical, and chemical equilibria. However, as we shall see in the next section, chemical equilibrium – the most important to describe polymerization in the solid state – is also affected by the semicrystalline structure.

2.2.2 Effect on Kinetics and Equilibrium

An obvious consequence of semicrystallinity is that polymer chains are so densely packed in the crystallites that one can hardly imagine small molecules being incorporated into them. For instance, upon moisture pick-up in PA6, the unit-cell dimensions and angles of the crystalline phase do not change, while T_g is depressed and may fall far below room temperature, changing the amorphous phase from brittle to ductile [34]. This clearly indicates that the absorbed water is retained exclusively in the amorphous phase. In addition, it is well known that humidity absorption in nylons is a function of crystallinity. For example, Starkweather *et al.* [66] observed for PA66 and PA6-10 a decrease of the equilibrium amount of water absorbed at 100 % relative humidity with increasing crystallinity ; in fact, absorption appeared to be proportional to the amorphous fraction.

Similar conclusions were drawn by Cawthon and Smith [1] for caprolactam, by Andrews *et al.* [2] for cyclic oligomers, and by Zimmermann [3] for the amine and carboxylic polymer chain-ends. In all of those studies, the authors observed a chemical equilibrium shift upon crystallization from the melt that was related to the exclusion of the aforementioned species from the crystalline domains.

Therefore, all reactive groups involved in SSP are concentrated in the amorphous regions – with the sole exception of the amide bonds. This *concentration effect* arising from the semicrystalline morphology is schematized in Figure 2.6, with the corollary of this being that the ordered phase is made of pure polymer repeat units, from which end-groups accidentally embedded during crystallization would diffuse as crystal defects to the amorphous regions. Hence, we conclude that reaction occurs exclusively in the amorphous fraction of the polymer.

The local concentration of non-crystallizing components in the amorphous phase is then given by

$$c_{amorphous} = \frac{c_{overall}}{1 - v_c} \tag{2.1}$$

where v_c denotes the volume fraction of crystalline phase. Since kinetics and equilibrium depend on local concentrations, not overall values, we expect the concentration effect to have a profound influence on the SSP process.

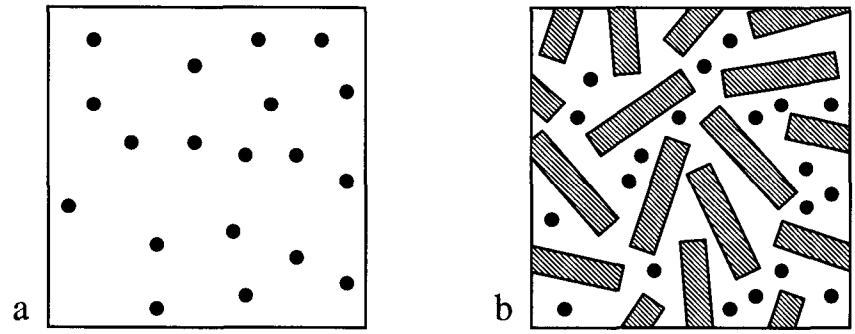

Figure 2.6 Confinement of species in the amorphous phase upon crystallization. a) Situation in the melt ; b) Situation in the solid state. Dots represent functional groups, water, and cyclic molecules ; rectangles represent crystallites

We shall first consider the influence on the *kinetics*. For this purpose, we define a kinetic effectiveness factor as

$$\eta_{kin} = \frac{SSP\ rate\ in\ the\ semicrystalline\ polymer}{SSP\ rate\ in\ a\ (hypothetical)\ wholly\ amorphous\ polymer} \tag{2.2}$$

Note that η_{kin} accounts only for the effect of structure on reaction rates, not for a possible kinetic limitation by the diffusion of by-product molecules. This point will be treated separately in section 2.2.4. By expressing the reaction rates in Eq. (2.2) as a function of the concentrations calculated with Eq. (2.1), we obtain

$$\eta_{kin} = \frac{1}{(1 - v_c)^n} \tag{2.3}$$

where n is the order of reaction. Considering a third-order acid-catalyzed kinetics ($n = 3$) – for polycondensation, polyaddition, and ring opening [39] – and a crystalline content of $v_c = 0.5$ typical for commercial PA6 [67], the calculation of the effectiveness factor gives $\eta_{kin} = 8$, i.e. a dramatic eightfold enhancement of the reaction ! As we shall see, the experimental means to determine the crystallinity usually yield the mass fraction w_c rather than the volume fraction v_c of crystalline phase. Thus, it is more convenient to use the former variable. The relationship between volume and mass fraction is given by

$$v_c = \frac{w_c}{P(1 - w_c) + w_c} \tag{2.4}$$

where $P = \rho_c / \rho_a$ stands for the ratio of crystalline-to-amorphous polymer densities. Substituting Eq. (2.4) into Eq. (2.3) leads to

$$\eta_{kin} = \left[\frac{P(1 - w_c) + w_c}{P(1 - w_c)} \right]^n \tag{2.5}$$

Equation (2.5) reduces to Eq. (2.3) when $P = 1$. By adopting Pflüger's data for the densities of the α crystal modification and amorphous phase [20], a value of $P = 1.138$ is obtained, which can be assumed independent of temperature. This decreases in our example the effectiveness factor from $\eta_{kin} = 8$ to 6.63, if mass and volume fractions are mistaken. This exemplifies the necessity to take the density difference between amorphous and ordered phases into account.

Equation (2.5) is strictly valid provided the concentration of small molecules – monomer or condensate, for instance – in the polymer is close to zero, more precisely $w_s << 1$, where w_s denotes the mass fraction of such *solute* molecules. Should this condition not be fulfilled, then the dilution effect in the amorphous phase cannot be neglected. More precisely, the amorphous density decreases upon concentration of the solute molecules in the amorphous phase, thus somewhat reducing the acceleration effect. Assuming no volume of mixing, we can easily derive the effectiveness factor

$$\eta_{kin} = \left[\frac{(P(1 - w_c) + w_c)(S(1 - w_s) + w_s)}{P S (1 - w_c - w_s + w_c w_s) + P w_s (1 - w_c) + (1 - S) w_c w_s} \right]^n \tag{2.6}$$

where $S = \rho_s / \rho_a$ stands for the ratio of solute-to-polymer densities. By considering the unreacted monomer (caprolactam) as the solute, a value of $S = 0.908$ is obtained based on Giori and Hayes' density data [68]. Again, we can assume S to be roughly independent of temperature. Equation (2.6) reduces to Eq. (2.5) when either $w_s << 1$, the polymer is dry and extracted, or $S = 1$, amorphous polymer and solute have the same densities.

In order to illustrate the effect provoked by the presence of a diluent, we may consider the molten PA6 exiting the prepolymerization stage, which contains about 10 % extractables (mainly unreacted caprolactam), and approximately the same amount of water [38]. Then, introducing $w_s = 0.2$ and $S = 0.908$ into Eq. (2.6), and using the aforementioned values for the other parameters, the calculation of the effectiveness factor yields $\eta_{kin} = 6.30$. Hence, a moderate (5 %) reduction of the kinetic enhancement effect is predicted, in comparison to $\eta_{kin} = 6.63$ obtained from Eq. (2.5). Though the dilution effect appears to be small, it could explain the lowest performance of SSP reactors fed with an unextracted prepolymer, in comparison to the classical process in which the prepolymer is subjected to hot water extraction prior to SSP [69].

We believe that the dramatic enhancement of the reaction rates predicted above, by confining the functional groups in a smaller reaction zone, could explain the rapid SSP kinetics that puzzled many researchers [7-11], considering the low reaction temperatures involved – typically 100 K below the temperature at which polymerization in the melt is usually carried out.

Contrary to its influence on kinetics, which has not been brought to the fore so far, the consequence of the concentration effect on chemical *equilibrium* is well documented [1-3]. We recall from Chapter 1 the major reactions, all reversible, involved in the chemistry of nylon-6 :

$$C_1 + W = P_1 \tag{1.1}$$

$$P_n + P_m = P_{n+m} + W \qquad n,m = 1,2,... \tag{1.2}$$

$$P_n + C_1 = P_{n+1} \qquad n = 1,2,... \tag{1.3}$$

Similarly to kinetics, equilibrium occurs locally and equilibrium constants must be calculated accordingly, based on the concentrations in the amorphous phase given by Eq. (2.1). This leads to the following expressions for K_1, K_2, and K_3, the respective equilibrium constants for ring opening, Eq. (1.1), polycondensation, Eq. (1.2), and polyaddition Eq. (1.3) :

$$K_1 = \frac{\dfrac{[P_1]_{eq}}{1-v_c}}{\left(\dfrac{[C_1]_{eq}}{1-v_c}\right)\left(\dfrac{[W]_{eq}}{1-v_c}\right)} = \frac{[P_1]_{eq}}{[C_1]_{eq}\,[W]_{eq}}(1-v_c) = K_1^*\,(1-v_c) \tag{2.7}$$

$$K_2 = \frac{[-NHCO-]_{eq}\left(\dfrac{[W]_{eq}}{1-v_c}\right)}{\left(\dfrac{[-NH_2]_{eq}}{1-v_c}\right)\left(\dfrac{[-COOH]_{eq}}{1-v_c}\right)} = \frac{[-NHCO-]_{eq}\,[W]_{eq}}{[-NH_2]_{eq}\,[-COOH]_{eq}}(1-v_c) \tag{2.8}$$

$$= K_2^*\,(1-v_c)$$

$$K_3 = \frac{\dfrac{[-NH_2]_{eq} - [P_1]_{eq}}{1-v_c}}{\left(\dfrac{[-NH_2]_{eq}}{1-v_c}\right)\left(\dfrac{[C_1]_{eq}}{1-v_c}\right)} = \frac{[-NH_2]_{eq} - [P_1]_{eq}}{[-NH_2]_{eq}\,[C_1]_{eq}}(1-v_c) = K_3^*\,(1-v_c) \tag{2.9}$$

where equilibrium concentrations are *overall* variables, and the K_i^* denote *apparent* equilibrium constants. For a hypothetical wholly amorphous polymer, or in the case of molten nylon-6, K_i^* reduces to the intrinsic constant K_i. The term $[\text{-}NH_2]_{eq}$-$[P_1]_{eq}$ in the expression for K_3 deserves some explanation : the addition of caprolactam molecules takes place onto the amine ends of the polymer chains [70], so that the forward reaction is proportional to $[\text{-}NH_2]$. The reverse reaction consists in an amine end backbiting the last amide group of its own chain, and thus is also proportional to $[\text{-}NH_2]$ excepted the amine ends located on linear monomers, P_1, which do not contain any amide group.

Equations (2.7-9) predict that all chemical equilibria are shifted by a factor proportional to the amorphous fraction, but the reason why the $(1-\nu_c)$ terms do not vanish is not identical for the three cases. For ring opening and polyaddition, this occurs because the forward reactions are bimolecular whilst the reverse reactions are unimolecular. For polycondensation, in which forward and reverse reactions have the same molecularity, the explanation is that the concentration effect does not apply to the amide bonds because they exist both in the amorphous and crystalline domains. This analysis nevertheless neglects the small discrepancy in amide concentration between amorphous and crystalline phases associated with the density difference.

The predicted equilibrium shift for polycondensation was quantitatively demonstrated by Zimmermann [3], who determined the apparent polyamidation equilibrium constant K_2^* for solid nylon samples equilibrated under some fixed water pressure. Zimmermann successfully related K_2^* to K_2 in Eq. (2.8) by means of a densitometry measurement of the crystallinity. The demonstration for the polyaddition reaction, though only qualitative, was achieved by Cawthon and Smith [1]. Although both studies date back to the early sixties, these results were often ignored. For example, the recent molecular PA6 SSP models proposed by Gupta and his colleagues [32, 33] lack to take this effect into account.

It is noteworthy that the apparent equilibrium shift – as the kinetic effect – produces a beneficial aspect for SSP. First, the polycondensation equilibrium is driven toward higher molar masses. Second, the ring opening and polyaddition equilibria are both driven toward smaller caprolactam concentrations, which is positive because cyclic species are undesired as they cause problems in the spinning and molding of the final polymer. Naturally, equilibrium constants depend on the temperature too. The low reaction temperatures at which SSP reactors are operated are also advantageous for chemical equilibria – contrary to kinetics – since both polycondensation and polyaddition reactions are exothermic [15].

Another type of equilibrium that is modified by semicrystallinity is the vapor-liquid equilibrium (VLE) at the particle/gas interface. For instance, the concentration of condensate molecules into the amorphous regions means that if the nylon granule is in equilibrium with the gas phase, the condensate will flow to the gas upon crystallization of the polymer. This phenomenon is expected to favorably affect the performance of industrial reactors by increasing the driving force for mass transfer. Indeed, we shall see that industrial reactors operate in an integral regime due to their large dimensions. In other words, loading of the gas phase by volatile molecules takes place, and the VLE controls the overall rate of the process.

In conclusion, an analysis of nylon-6 semicrystalline morphology has led us to postulate dramatic *apparent* kinetics and equilibria changes in solid-state polycondensation, due to the confinement of reactive species in a smaller reaction volume upon crystallization. These effects, as stated above, will be core assumptions of the solid-state model developed in Chapter 6, where we shall reexamine the PA6 SSP data in the literature. This will turn out not to be necessarily easy, because most researchers were unaware of the importance of the morphology, and crystallinity was usually not determined. In the next section, we will address the important question about whether the micromorphology could also affect the *intrinsic* kinetics.

2.2.3 Examination of the Kinetics Dimensionality

An underlying assumption in the derivation of the kinetic effectiveness factor η_{kin} is that semicrystallinity affects only concentrations, not rate constants. But is this necessarily true ? Normally, rate constants depend only on the temperature and on the nature of the reactive entities. This holds when the size of the reaction zone is much larger than the reaction distance, that is, when border effects can be neglected. We examine here whether this condition is fulfilled in solid-state polymerization, an interesting question that has not been addressed in the literature so far.

The issue is schematically depicted in Figure 2.7, which shows the distribution of the reactive species (like amine and acid functional groups) throughout the interlamellar amorphous domains, for two limiting cases.

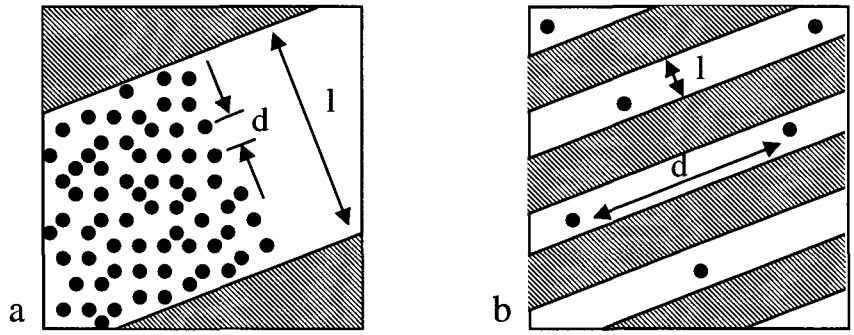

Figure 2.7 Dimensional constraint imposed by the semicrystalline structure on the kinetics. a) Situation at low molar mass or coarse polymer structure, $l/d >> 1$: normal kinetics applies ; b) Situation at high molar mass or fine polymer structure, $l/d << 1$: constrained kinetics applies. Dots represent reactive species ; rectangles represent crystalline lamellae

We consider first a situation where the characteristic distance between chain-ends d is much smaller than the interlamellar spacing l (Fig. 2.7.a). Here the reactive species do not experience the presence of the crystal walls, and the rate constant remains unchanged. Second, a very different situation arises when the interlamellar spacing is much smaller than the reaction distance (Fig. 2.7.b). In this case, the reaction mass is segregated by the presence of the crystallites, and the rate constant is reduced. This can be easily understood by considering two reactive groups located on each side of a particular crystalline lamella. Even though they are within reaction distance of each other, they cannot meet and react because of the impossibility for them to cross the crystalline barrier.

The Brownian motions responsible for the collisions between functional groups occur in three dimensions in the former situation (Fig. 2.7.a), whereas there are restricted inside the planes delimited by the crystalline layers in the latter case (Fig. 2.7.b), so that reaction virtually takes place in two dimensions. This is somewhat analogous to the Knudsen diffusion regime in porous catalysts in which the mean free path of the gaseous molecules is much larger than the pore size.

Obviously, the critical parameter to assess this *dimensional constraint* is the ratio l/d. Even though the effect on the rate constant cannot be quantitatively established, because of the complexity of the molecular geometry involved in the reaction, we can safely assume normal kinetics to apply when $l/d >> 1$, whereas the rate constant would be depleted when l/d approaches unity. In fact, the single case where the

constrained rate constants can be calculated is for perfect gases in the limit $l/d << 1$. This would require re-deriving the classical expression based on the kinetic theory of gases, but in two dimensions.

Such a constrained kinetics is not common. For instance, even microreactors satisfy the condition $l/d >> 1$, with l/d values ranging from 10^3 to 10^5. But the size of the amorphous domains in the semicrystalline polymer is still orders of magnitude lower. For example, Murthy *et al.* [42] determined typical values of 10-20 nm for the interlamellar spacing in solid nylon-6, in their SANS experiments. In addition, it is conceivable that the dimensional constraint appears only during the course of SSP. Two reasons can be mentioned for that. First, the distance between end-groups increases as they are consumed by the polymerization. Second, the annealing process associated with SSP could refine the structure, i.e. decrease the interlamellar spacing.

The above considerations lead us to derive an expression for l/d. First, the characteristic distance between end-groups is expressed as

$$d = \left(c^* N_{Av}\right)^{-\frac{1}{3}} \tag{2.10}$$

where c^* denotes the concentration of end-groups in the amorphous phase, and N_{Av} is the Avogadro number. The local concentration c^* is related to the overall concentration c by means of Eqs. (2.1) and (2.4) :

$$c^* = c\,\frac{P\left(1-w_c\right)+w_c}{P\left(1-w_c\right)} \tag{2.11}$$

Next, it can be easily demonstrated that the number-average molar mass M_n is related to the concentration c by

$$M_n = \left(\frac{\rho_a}{c}\right)\frac{PS\left(1-w_s\right)}{PS\left(1-w_c-w_s\right)+S\,w_c+P\,w_s} \tag{2.12}$$

After appropriate substitutions based on Eqs. (2.11) and (2.12), d in Eq. (2.10) is expressed as a function of M_n :

$$d = \left(\frac{M_n\left(1-w_c\right)\left(PS\left(1-w_c-w_s\right)+S\,w_c+P\,w_s\right)}{N_{Av}\,\rho_a\,S\left(1-w_s\right)\left(P\left(1-w_c\right)+w_c\right)}\right)^{\frac{1}{3}} \tag{2.13}$$

Based on the simplified picture of the semicrystalline structure made of regularly alternating sheets of amorphous and crystalline zones (Fig. 2.7.b), the expression for the interlamellar spacing is readily expressed as

$$l = \frac{\Lambda\alpha_{200}\,P\left(1-w_c\right)}{w_c} \tag{2.14}$$

where the lateral size of the lamellae has been expressed as the length of the coherently scattering crystallite domains in the α-modification, $\Lambda\alpha_{200}$, obtained from

wide-angle X-ray diffraction (WAXD) analysis. For a pure polymer ($w_s << 1$) we finally obtain, from Eqs (2.13) and (2.14),

$$l/d = \frac{\Lambda\alpha_{200} P (1-w_c)^{\frac{2}{3}}}{w_c} \left(\frac{N_{Av} \rho_a}{M_n} \right)^{\frac{1}{3}} \tag{2.15}$$

in which l/d is expressed as a function of observable quantities. To assess the kinetics dimensionality for our SSP experiments presented in the next chapters, we calculate l/d from Eq. (2.15) with typical parameter values listed in Table 2.1. This yields a value decreasing from $l/d = 6.7$ to 4.7 as SSP proceeds. It is difficult to say whether border effects are already felt at this stage. However, we do not expect the kinetics to be strongly constrained given that our l/d values are greater than one. Anyway, such an effect would remain approximately constant during our SSP experiments since l/d does not vary significantly. This is because $\Lambda\alpha_{200}$ remains unchanged, as we shall see in Chapter 5, and the $M_n^{-1/3}$ dependence predicted by Eq. (2.15) seems too low to switch from an unconstrained to a constrained regime during SSP.

Table 2.1 Parameter values for the calculation of the dimensional constraint

Parameter	Symbol	Typical value	Source
Initial number-average molar mass	$M_{n,i}$	17,000 g mol^{-1}	Viscometry measurement
Final number-average molar mass	$M_{n,f}$	51,000 g mol^{-1}	Viscometry measurement
Crystallinity	w_c	0.45	DSC measurement
Lateral size of crystallite	$\Lambda\alpha_{200}$	12 nm	WAXD measurement
Density of amorphous phase (at 165°C)	ρ_a	1,014 kg m^{-3}	Pflüger [20]
Ratio of crystal-to-amorphous densities	P	1.138	Pflüger [20]
Avogadro number	N_{Av}	6.022 10^{23} mol^{-1}	-

A striking conclusion is that the nylon granule behaves like a nanoreactor due to the segregation of the reaction mass by the semicrystalline structure. This point should be borne in mind when SSP kinetics at extremely high molar masses is examined. In particular, we believe that some experimental deviations of SSP profiles observed in the literature, explained on the basis of mass transfer limitations [29], could also arise from a constrained kinetics.

2.2.4 Effect on Transport Phenomena

Two types of transport phenomena are involved in solid-state polymerization : the diffusion of reactive functional groups located on the polymer chains, and the diffusion of volatile by-products like condensate (water) or monomer (caprolactam). The two processes are fundamentally different in terms of both the nature of the diffusing species and the diffusion distance. In the former case, transport involving macromolecules occurs at nanometer scale, whereas in the latter situation small solute molecules diffuse at millimeter scale within the polymer matrix to the surface of the granule.

Diffusion of end-groups pertains to the problematic of the gel effect that will be treated in Section 2.3. Should this step be rate-controlling, then the influence of semicrystallinity is expected to be similar to the one discussed in the previous section for the kinetics, given that diffusion distance and interlamellar spacing are of the same

order of magnitude. Here, we restrict our discussion to the latter case of diffusion of solute molecules. We shall first recall some basic concepts about diffusion in the wholly amorphous phase. Then, we shall review the potential implications of semicrystallinity.

Considerable knowledge has been gained in the field of diffusion in polymer-solvent systems since the early sixties, and some good reviews are available in the literature [71-74]. Non-Fickian diffusion is sometimes observed in the concentrated regime, arising from the sluggish relaxation of large macromolecules. In classical diffusion theory, it is implicitly assumed that an equilibrium liquid structure exists at all points in the diffusion field. This assumption is valid only if the local relaxation in the system is fast compared to the diffusion process, a situation that is not necessarily achieved in a polymeric medium. To assess the magnitude of such anomalous effects, Vrentas *et al.* [75] introduced a diffusion Deborah number defined by

$$De = \frac{\lambda_m}{t_d} \tag{2.16}$$

where λ_m is the mean relaxation time, and t_d is the characteristic time for conductive transport. The value of the Deborah number for a given set of conditions identifies the type of diffusional transport that can be expected. To illustrate this point, a Deborah number diagram is displayed in Figure 2.8 for the system polystyrene-ethylbenzene [71]. At high temperature or large amount of solute, $De << 1$ and conformational changes in the polymer take place essentially instantaneously. The system behaves like a purely viscous fluid and the classical (Fickian) theory of diffusion applies. In the other extreme, $De >> 1$, there is virtually no time variation of the structure of the polymer during the diffusion process. Under these conditions, a solute molecule migrates in a material that appears to have the properties of an elastic solid. These different modes of transport can be observed in samples of different sizes since t_d scales as the square of the sample dimension, while λ_m is obviously independent of it.

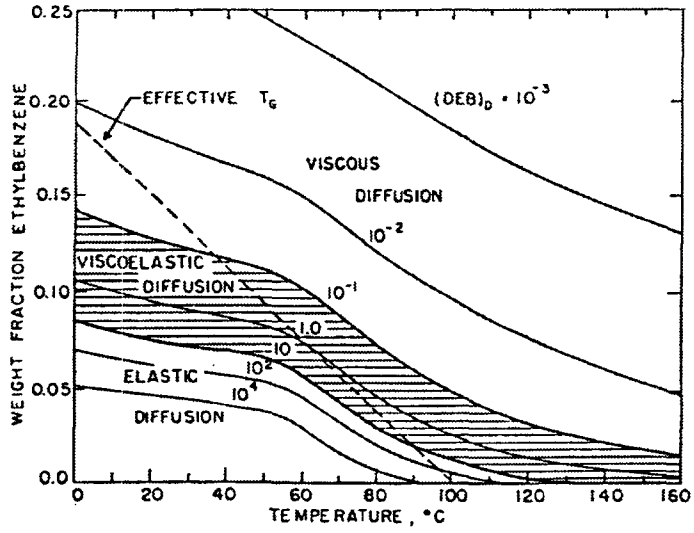

Figure 2.8 Deborah number diagram for the system polystyrene-ethylbenzene (molar mass $M_n = 3 \cdot 10^5$ g/mol, film thickness $R = 10^{-2}$ mm) [71]. Construction of such concentration-temperature diagrams for a particular process helps anticipating anomalous diffusion

Since relaxation of polymer chains is hindered mainly in the glassy state, most non-Fickian effects occur below the glass transition temperature. Then, because SSP reactors operate typically 100 K above T_g, anomalous diffusion is in principle not expected in the systems of interest. However, one should be cautious with semicrystalline PA6, given that a fraction of the disordered phase remains glassy even far above T_g (see the discussion about the rigid amorphous phase in Section 2.2.1).

At present, no general theory exists that describes classical diffusion in polymer-solvent systems over the complete concentration range. For the concentrated regime, however, the theories based on *free volume* have been the most successful in calculating diffusion coefficients [76-78]. Use of the free volume concept avoids the statistical mechanical description of the liquid state in terms of intermolecular force fields, which can be convincingly done for simple liquids but remains a tremendous task for polymers. As a result, the free volume theory (FVT) is rather correlative than predictive.

In the FVT, the specific volume of the amorphous polymer is viewed to consist of two parts : the volume occupied by the molecules themselves, and the empty space between the molecules (Figure 2.9). The empty space is commonly referred to as the free volume, of which only the portion that is continuously redistributed by thermal fluctuations is available for molecular transport. This part of the free volume is denoted the *hole* free volume, while the remainder is termed the *interstitial* free volume. Molecular transport, as perceived by FVT, is consequently governed by the probable occurrence of two events : 1) a hole of sufficient size appears adjacent to a molecule ; and 2) the molecule possesses enough energy to jump into the void.

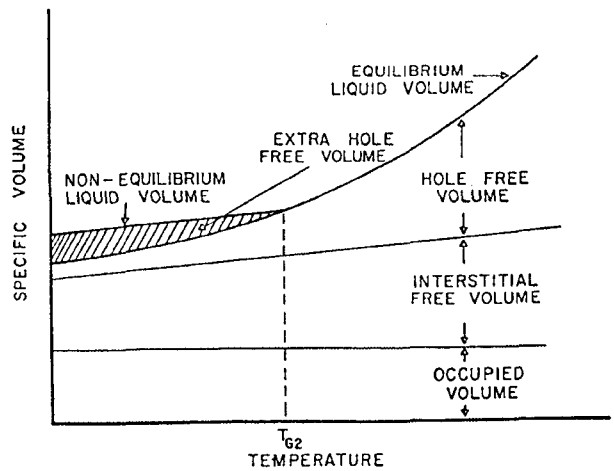

Figure 2.9 Illustration of the division of the specific volume of an amorphous polymer [71]

These simple notions lead directly to expressions for self- and mutual-diffusion coefficients of the polymer and solute. In the limit of zero solute concentration, Ju *et al.* [79] derived the following expression for the solute diffusivity :

$$D = D_\infty \exp\left(\frac{\gamma V_2^* \xi}{K_{12}\left(C_2^g + T - T_g\right)}\right) \tag{2.17}$$

where D_∞ is a constant pre-exponential term, V_2^* is the smallest specific hole free volume that need to form before a polymer can take a diffusive step, and γ is an

overlap factor (between 0.5 and 1), which is introduced because the same free volume is available to more than one molecule. The glass transition temperature of the pure polymer is denoted by T_g, and K_{12} and C_2^g are Williams-Landel-Ferry (WLF) constants, which can be determined from the temperature dependence of the polymer viscosity [80]. Finally, ξ is the ratio of molar volumes for the solute and polymer units involved in discrete diffusive jumps.

Equation (2.17) reduces to an Arrhenius form at high temperature or for a small solute, i.e. when the amount of free volume is large enough so that diffusion is activation-controlled. Conversely, when the diffusion process is dominated by the scarcity of the available free volume, the apparent activation energy for diffusion

$$E_d = RT^2 \left(\frac{\partial \ln D}{\partial T} \right)_p \tag{2.18}$$

becomes a strong function of temperature and solute concentration. Particularly, E_d increases when the polymer approaches its glass transition temperature. According to Zielinski and Duda [74], this deviation from an Arrhenius behavior is expected typically up to T_g + 100 K, approximately the operating temperature of SSP reactors.

Consequently, we expect the diffusivities of volatile species in an (hypothetically) wholly amorphous nylon granule to have the following functionality :

$$D_{amorphous} = f\left(T, c, M_n\right) \tag{2.19}$$

In the FVT framework, the diffusion coefficient increases with *temperature* because of the supplementary hole free volume generated by the thermal expansion. The *concentration* dependence of D arises because the free volume associated with the solute is significantly greater than the free volume of the pure polymer. Thus, diffusivity will increase upon addition of solute, which could be of importance for SSP of unextracted or wet PA6 compared with SSP performed on an extracted and dry material. In addition, a dependence on the *molar mass* of the polymer can be envisaged since the free volume associated with the end-groups of the macromolecules is greater than that associated with interior chain segments. Such an effect should nonetheless be restricted to the beginning of polymerization, when the chain-ends decrease significantly. Under SSP conditions, the fraction of end segments is low (typically smaller than 1 %), and diffusion should be independent of M_n. This was substantiated by Namikawa *et al.* [81] who showed that the diffusivity of glycine in dextran gels is independent of the molar mass of dextran. Similar observations were reported by Bagdonaite *et al.* [82] for diffusion of 2,2-methylene-bis(4-methyl-6-*tert*-butylphenol) in polystyrene-ethylbenzene media.

One limitation of free volume theory is that molecular interactions between the polymer chains and the solute molecules are not explicitly included in the model, since all parameters in the theory can be estimated from pure components properties. To account for strong interactions like hydrogen bonding, Vieth and Howell [83] proposed a *dual mode* theory in which the solute is assumed to exist in two states : adsorbed on the polymer chains, or free. The model assumes that Langmuir-type *ad*sorption occurs onto a limited number of sites, whereas the *ab*sorption of free molecules obeys Henry's law and is linear with pressure. Local adsorption

equilibrium is always maintained, and only the free molecules can diffuse under a concentration gradient. The dual mode theory predicts that diffusion coefficients should decrease greatly at low temperatures and low concentrations, when the Langmuir mode is far from saturation. Because water binds so strongly to carbonyl groups in nylon, it is tempting to describe water diffusion in this way.

Vieth's theory is consistent with the structure postulated by Puffr *et al.* [67] for the states of water in nylons. In this standpoint, the adsorption centers are formed by pairs of amide groups. Such a double center can accommodate only a few water molecules that can be differentiated by the way of their hydrogen bond formation, as depicted in Figure 2.10. First, water can form a bridge-bonded species (Fig. 2.10.a) HNCO···HOH···OCNH by donating both protons to a pair of amide groups that preserve their original interamide hydrogen bonds. Second, a loosely bound species (Fig. 2.10.b) H_2O···HNCO may be formed by water interacting as a proton acceptor. This picture is coherent with a 3 H_2O/2 NHCO stoichiometry at saturation. Third, free water (Fig. 2.10.c) may also exist, condensed in volume defects or pores.

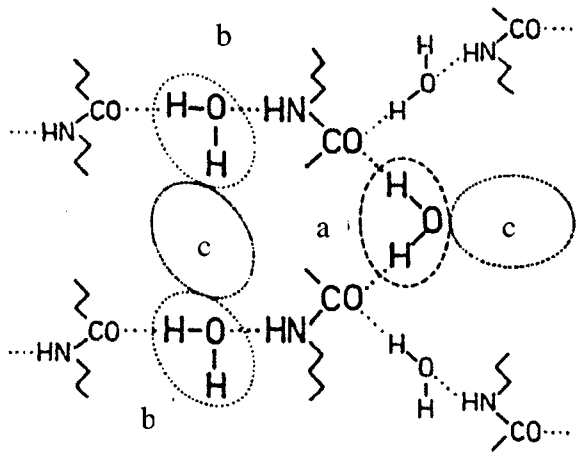

Figure 2.10 Model of water-amide complexes in nylons at saturation [67]. a) Bridge-bound water ; b) Loosely bound water ; c) Free water

The three-state model of Puffr is not unanimously accepted. Le Huy and Rault [84], for instance, propose that all water molecules are bound in the same way to the amide groups, based on their study of glass transition and secondary transition in polyamides swollen by water, alcohol, and acid.

Anyway, literature reports provide ample evidence that water can disrupt interamide hydrogen bonds, as indicated, for instance, by the strong humidity dependence of T_g. Upon moisture pick-up, T_g in PA6 drops off greatly [85-87], because water plasticizes the matrix by replacing interchain hydrogen bonds that act as cross-links, hence decreasing the activation energy for the relaxation process. Another observation indicative of adsorption is the decrease of equilibrium water with decreasing amide group concentration in the *n*-nylon series [88].

These considerations led Mallon and Ray [29] to adopt a two-state model for water (bound/free) in their model for PA66 SSP. Indeed, the existence of free water seems to be corroborated by Hutchinson *et al.* [64], who observed a large central peak in their ^{2}H-NMR studies on oriented PA6 fibers. We nevertheless question this report and shall instead develop a SSP model with a single state for water, seen as diffusing

in discrete jumps from one amide site to another. We put forward two arguments supporting this picture. First, recent relaxation and solid echo ^{2}H-NMR experiments by Loo *et al.* [89] on unoriented PA6 rods indicated no free water. Loo suggested that Hutchinson did not carefully wipe the excess water from the surface of the fibers, and consequently misinterpreted his results. Second, acceptance of dual mode theory would imply a smaller diffusivity for water than for caprolactam, despite their difference in size, because of the strong water-amide interactions. This behavior was predicted by Roos [90]. However, the single literature study in which the diffusivity of caprolactam has been determined reports $D_W = 2.5 \cdot 10^{-8}\ m^2 s^{-1}$ and $D_{Cl} = 8 \cdot 10^{-12}\ m^2 s^{-1}$, in PA6 melt at 265°C [91]. In addition, the single-state assumption avoids introducing an extra model parameter – the adsorption equilibrium constant – and is more consistent with all classical simulation and optimization studies on the melt hydrolytic polymerization of caprolactam [15, 38].

We come now to the effect of semicrystallinity on diffusion. Because crystalline regions are impermeable to solute molecules and therefore allow no diffusion, Kulkarni and Mashelkar [92] extended the free volume theory to this situation by considering that only the amorphous phase contributes to the free volume. This gives the following relation for the diffusion coefficients

$$ln\left(\frac{D_{semicrystalline}}{D_{amorphous}}\right) = -\frac{V_1^*}{V_{FH}}\left(\frac{v_c}{1-v_c}\right) \tag{2.20}$$

where V_1^* is the smallest hole free volume required for a solute molecule to take a diffusive step, and V_{FH} is the total hole free volume. However, this approach is questionable since it recognizes the heterogeneity of the medium only at local (microscopic) level. This is a crude oversimplification because the size of the non-crystalline domains between the radial lamellae and at boundaries of spherulites is not negligibly small compared to the length scale relevant for macro-diffusion. In other words, Eq. (2.20) lacks to account for the lengthening of the diffusion path provoked by the presence of crystallites, as pictured in Figure 2.11.

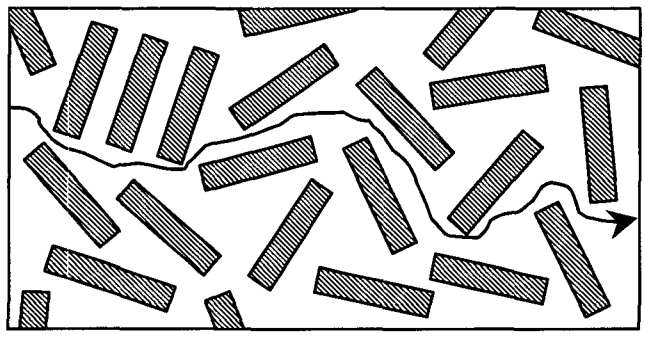

Figure 2.11 The diffusion path of volatile molecules is lengthened because impermeable crystallites must be by-passed

The geometrical constraint imposed by the semicrystalline structure on the diffusion path was described by Michaels and Bixler [93] using a two-parameter model,

$$D_{semicrystalline} = \frac{D_{amorphous}}{\tau\ \beta} \tag{2.21}$$

where τ is a tortuosity ratio independent of the diffusant size, accounting for the necessity of the solute molecules to by-pass crystallites, and β is a size-dependent immobilization factor reflecting the reduction in chain segment mobility brought about through the proximity of crystallites. Obviously, $\beta = 1$ for simple gases while $\beta > 1$ for large molecules – such as the seven-member caprolactam ring in PA6. Equation (2.21) predicts a decrease of the diffusivity with increasing crystallinity, which does not hold for long linear molecules beyond the entanglement threshold. For this latter case, Klein and Briscoe [94] demonstrated both theoretically and experimentally that D actually *increases* upon crystallization. Other models dealing with the functional dependence of D on the polymer structure are based on the concept of transmission function [95], or modification of Maxwell's equation for electrical conductivity of composite systems [96].

The above models may however not be necessary to follow diffusion in the systems of interest, since many experimental studies conclude that the effective diffusivity is simply proportional to the amorphous fraction [97-100] :

$$D_{semicrystalline} = D_{amorphous}\left(1 - v_c\right) \tag{2.22}$$

The empirical functionality in Eq. (2.22) is consistent with a common assumption in heterogeneous catalysis that the diffusivity is proportional to the porosity [101], and we shall use it in our SSP model. This has the advantage that structural parameters that are difficult, if not impossible to measure will not be needed. Note that Eq. (2.22) does not necessarily predict a decrease of the diffusion coefficient upon crystallization, since the obstruction effect of v_c may be counterbalanced by the increase of $D_{amorphous}$ caused by the concentration of solute molecules in the amorphous phase, in accordance with Eq. (2.1) and the free volume viewpoint.

A further structural resistance to diffusion arises sometimes from a dense and impermeable skin – crystalline or glassy – present at the surface of the granule. This *polymer skinning* effect slows down or even impedes diffusion. A theoretical description of this unusual phenomenon can be found in a recent paper by Edwards [102]. The critical point to form a polymer skin is the thermal and mechanical history applied during the granulation of the polymer, and we shall see in Chapter 6 that some puzzling PA6 SSP data in the literature can be reexamined from this angle.

Hence, a complex picture emerges for the diffusion phenomena in solid nylon. Particularly, the expected diffusion field is non-uniform because of the existence of concentration and structural gradients within the polymer particle undergoing SSP. The situation is even worse in oriented fibers, where the diffusion coefficient cannot be represented by a simple scalar field, since the anisotropy of the material leads to rates of transport changing with the direction of diffusion.

Given the above considerations, it seems not reasonable to assume *a priori* a certain functionality for the amorphous diffusion coefficient implemented in the solid-state model. Instead, we shall rather ascertain the kinetic and equilibrium parameters by testing the model for conditions without any diffusion limitation – i.e. for SSP in a closed reactor or under conditions where irreversible polymerization takes place. Then, we shall curve-fit the model to experimental data in the diffusion-limited

regime and analyze *a posteriori* the extracted values for the diffusion coefficients, in terms of the theories discussed in this section. In this way, valuable knowledge may be gained, especially concerning the diffusion characteristics of caprolactam, which are of the utmost importance regarding the optimization of any industrial PA6 solid-state reactor. Curiously, one single report in the open literature discloses a value for the diffusivity of caprolactam [91], and only at one temperature (265°C) far above the melting point. In fact, most theories presented above were developed to deal with devolatilization of chain growth polymers, because of the escalating emphasis on reducing the residual monomer that is often a potential carcinogen – like vinyl chloride in PVC. An illustration of this point is that free volume parameters have been determined for a large number of polyolefins [103], whereas no values are yet available for step growth polymers as common as PA6 or PET.

In summary, the semicrystalline morphology of nylon-6 in the solid state is expected to influence greatly the kinetics, equilibria, and transport phenomena involved in solid-state polymerization. Understanding this complex interplay is a prerequisite to develop a phenomenological model based on the extrapolation of the melt chemistry.

2.3 The Gel Effect – Does it Exist in Polycondensation ?

The diffusion of the polymer reactive end-groups is the least understood step in solid-state polymerization. As mentioned in the literature review (Section 2.1), there is a considerable controversy about whether end-group diffusion controls the overall kinetics of the process. This is mainly because a polymer diffusion limitation cannot be easily revealed by changing some operating condition. For instance, the two different modes for the removal of the condensate scale differently with the sample dimension, R (if the resistance to convection in the gas phase is controlling, then the mass transfer rate scales as R^{-1} because the surface area per unit volume is inversely proportional to the particle radius, whereas a control regime by molecular diffusion in the bulk of the polymer yields a R^{-2} dependence). But neither end-group diffusion nor chemical reaction are affected by particle size because the length scales involved are order of magnitudes smaller ($d << R$).

In this section, we gain a deeper insight into this problematic, which is crucial for the development of any relevant kinetic model for SSP. First, we shall review the literature reports dealing with end-group diffusion in polycondensation and make some comparisons between chain and step growth polymerizations. Next, some arguments about the mechanism and rate of end-group diffusion will be developed, based on the implication of interchange reactions. Finally, we shall derive an expression for the distribution of the diffusion distance, on the basis of which Gaymans' [11] gel effect model for SSP of nylon-6 will be rejected.

2.3.1 Chain vs. Step Growth Polymerization

A sudden increase in the rate of free-radical polymerization as the reaction proceeds was first observed more than fifty years ago [104]. This high-conversion auto-acceleration effect, termed the *gel effect*, was ascertained by Trommsdorff *et al.* [105] to be due to a decrease in the termination rate constant k_t between two growing polymer radicals, because of diffusion limitations arising from the high viscosity of

the reaction medium. By contrast, the propagation rate constant k_p does not change because diffusion of the small monomer is not affected to such an extent that propagation would become diffusion-controlled. The result is a decrease of the ratio k_t/k_p, leading to an enhancement of the overall rate of polymerization.

Kumar *et al.* [106] extended this approach to the description of irreversible polycondensation at high conversion. Here, the chain-building step is analogous to the termination step of free radical polymerization because in both cases long chains are reacting with each other. Hence, a gel effect in step growth polymerization would produce a result opposite to its counterpart in free radical polymerization, i.e. a fall of the overall rate of polymerization. The model of Kumar assumes that two functional groups react only when they lie within a minimum distance x_m of each other (Figure 2.12). If $k_{2,0}$ is the intrinsic forward polycondensation rate constant, this implies that whenever another polymer molecule sweeps within the spherical domain of radius x_m of a given molecule, the collision processes are described by $k_{2,0}$. The model further assumes that at some large distance x_d, the concentration of polymer approaches the value in the bulk, c_b, whereas the effective concentration within the sphere of radius x_m is assumed to be c_m. This nano-gradient then drives the migration of the *B* group at x_d towards *A*, and only then is there chemical reaction.

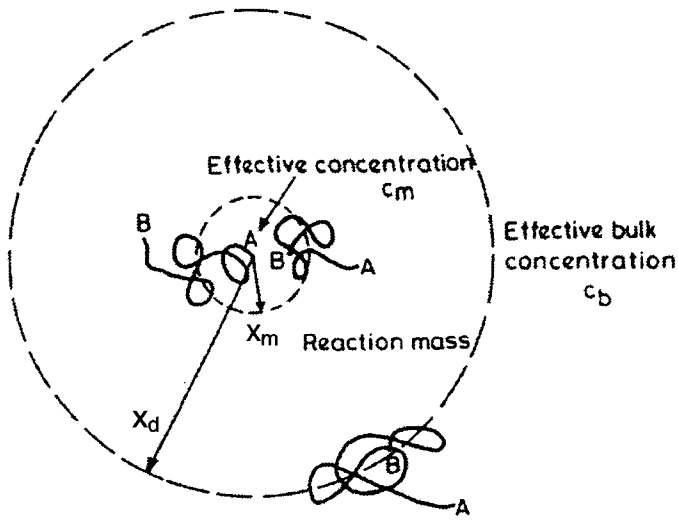

Figure 2.12 Illustration of the gel effect model of Kumar *et al.* [106] for high-conversion irreversible step growth polymerization

Assuming steady state and taking $x_d \to +\infty$, Kumar derived the following expression for the apparent polycondensation rate constant, k_2, by analogy with the model of Chiu *et al.* [107] for free radical polymerization

$$\frac{1}{k_2} = \frac{1}{k_{2,0}} + \frac{x_m^2 c_b}{3D} \tag{2.23}$$

where the concentration and temperature dependence of the polymer diffusivity *D* may be expressed by means of the free volume theories discussed in Section 2.2.4. For instance, Kaushik and Gupta [32] made use of Fujita-Doolittle FVT theory [108] in their gel effect model for PA6 SSP, whereas Kulkarni and Gupta [33] preferred to implement the FVT framework of Vrentas and Duda [71] for the same purpose.

Contrarily to the forward polycondensation, there should be no diffusion resistance for the reverse reaction because a *small* condensate molecule is involved, similarly to propagation in free radical polymerization. Hence, the fall of k_t/k_p in chain radical polymerization corresponds to a decrease of $k_2/k_2' = K_2$, the equilibrium constant, in polycondensation. Consequently, a gel effect in reversible step growth polymerization would not only influence the kinetics, as in free radical reactions, but it would also shift the equilibrium. Mallon [28] argues that this introduces a flaw in the concept because at equilibrium there should be no gradients in the melt, so the calculated shift in the equilibrium constant is incorrect. It is also noteworthy that a gel effect results in a breakdown of Flory equal-reactivity hypothesis [4] because short molecules are expected to diffuse – and react – faster than long ones, leading to a reduced polydispersity.

The origin of the gel effect idea in step growth polymerization dates back to 1982, when Gaymans *et al.* [11] reported puzzling observations in their PA6 SSP experiments carried out in a fluidized-bed, leading them to postulate the conceptual model depicted in Figure 2.13.

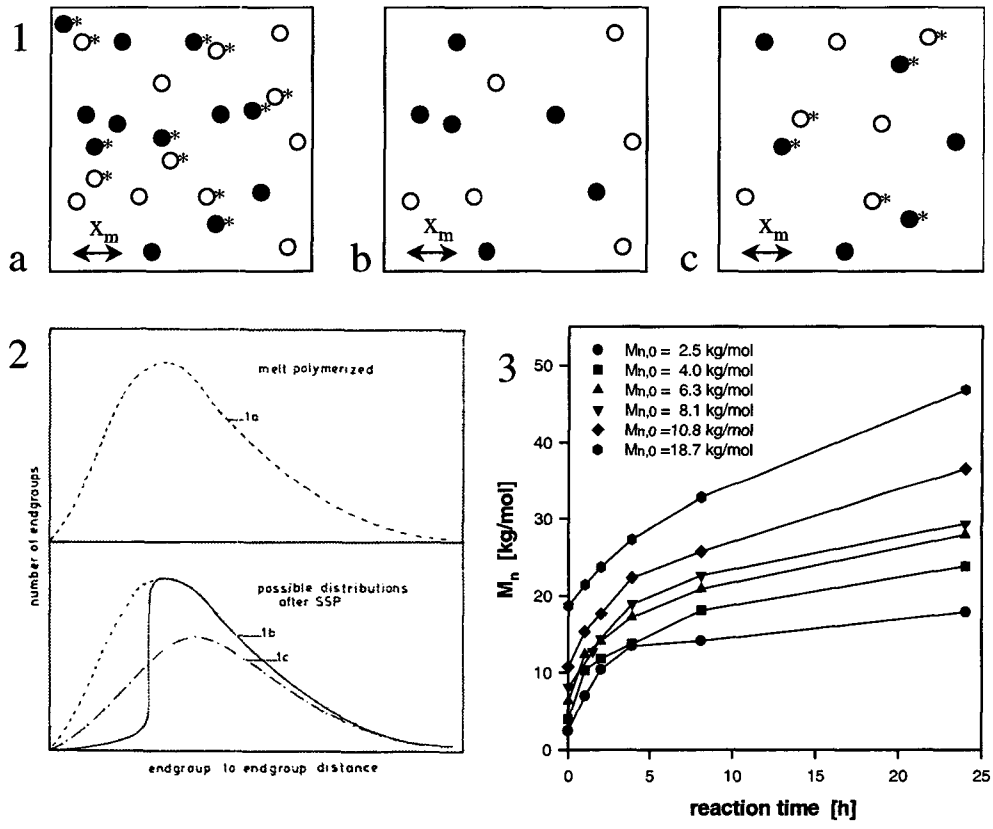

Figure 2.13 The gel effect model of Gaymans *et al.* [11] for solid state polycondensation of nylon-6. 1) Spatial distribution of reactive species ; filled and empty symbols represent acid and amine end-groups, which are labeled with an asterisk when they lie within reaction distance x_m of each other, a) Starting material cooled from the melt, b) Polymer after SSP with limiting diffusivity, c) Polymer after SSP and re-melting ; 2) Distribution of the minimum end-group-to-end-group distance for the cases (1a) to (1c) ; 3) The effect of initial molar mass $M_{n,0}$ on SSP profiles observed by Gaymans led him to postulate the existence of the gel effect (SSP of PA6 particles of size R = 0.2-0.5 mm in a fluidized-bed under N_2 at T = 190°C)

Gaymans' data reveal a strong influence of the initial molar mass on the polymerization profile (Fig. 2.13.3). Actually, the reaction rate at some *definite* molar mass (i.e. polymer concentration) seems to depend on the *initial* molar mass

(concentration). Because a deterministic viewpoint forces the present rate to depend solely on present conditions, not on the past, it follows that the SSP profiles in Fig. 2.13.3 are not a function of end-group concentration only, but that some hidden parameter must also intervene. Gaymans' idea is that this parameter should be the *spatial distribution* of end-groups, changing from random to non-random as polymerization proceeds. In a sample just cooled from the melt, all chain-ends are randomly distributed throughout the material (Fig.2.13.1.a). Then, because of severe diffusion limitations, only the end-groups that lie within critical distance x_m of each other have enough segmental mobility to meet and react (those marked with an asterisk in Fig. 2.13.1). Others are kept virtually frozen in, so that polymerization stops before complete conversion (Fig. 2.13.1.b). By contrast, a fresh sample with an identical concentration would still have some reactive groups within reaction distance, resulting in a non-zero reaction rate (Fig. 2.13.1.c). This idea seems to be corroborated by the observation that an intermediate re-melting of the granules results in an enhancement of the SSP rate [11]. Indeed, re-melting would re-homogenize the end-groups, changing their spatial distribution from the situation depicted in Fig. 2.13.1.b to the one in Fig. 2.13.1.c.

To characterize this spatial distribution, Gaymans ascribed to every functional group the distance to its closest reaction partner, and considered the resulting distribution of minimum end-group-to-end-group distance. The frequency functions corresponding to the situations in Fig. 2.13.1, qualitatively drawn by Gaymans, are shown in Fig. 2.13.2, with the gel effect resulting in a distribution after SSP truncated at x_m.

From the above considerations, it can be seen that Gaymans' model is a special case of the Kumar model in the limit where the polymer chain diffusivity goes to zero, which could occur in the solid state when the macromolecules are anchored in crystalline lamellae.

At this point, it should be emphasized that any comprehensive gel effect theory must account for the *mechanism* of polymer chain diffusion. Kumar *et al.* [106] distinguish between the different steps pictured in Figure 2.14. Two molecules first migrate by *bulk diffusion* to within close proximity of each other in the reaction mass. Chemical reaction between the functional groups A and B cannot occur yet because these groups are buried inside the coiled macromolecules. However, *segmental diffusion* (intramolecular motion) brings these groups together, finally enabling them to react.

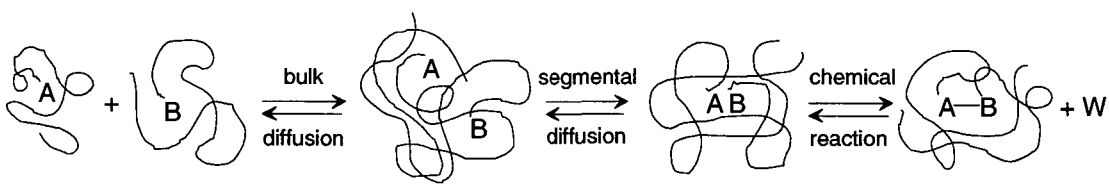

Figure 2.14 The diffusive steps in ARB step growth polymerization, according to Kumar *et al.* [106]

Beyond a critical molar mass M_e, the molecules get entangled and their movement cannot be described as simply in terms of bulk and segmental motions. Instead, polymer chains move by a snake-like wriggling motion along their length termed *reptation*. This phenomenon – due to the long chain nature of the polymer molecules which can slip onto each other, but cannot cross each other – was investigated by de Gennes [109, 110] and led to a completely new theoretical framework. The topological constraint imposed by entanglements may be represented by a network of

fixed obstacles, or by the chain diffusing in a one-dimensional tube defined by the locus of interactions with adjacent molecules (Figure 2.15).

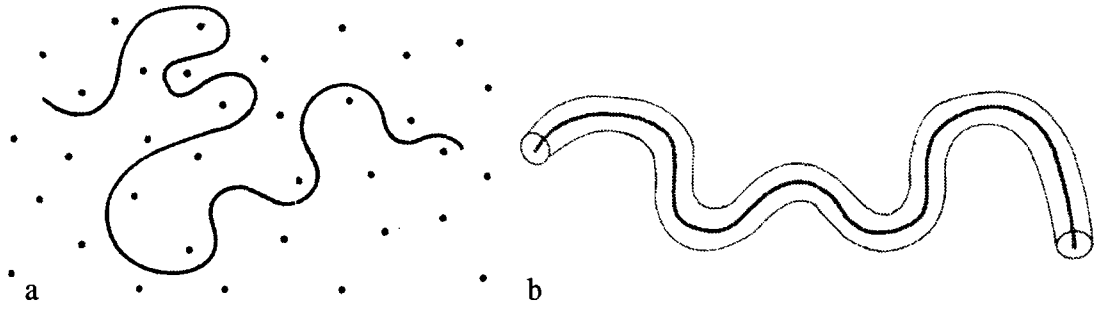

Figure 2.15 Effect of entanglements on the reptation dynamics of a polymer chain [109]. a) The chain in a network of fixed obstacles ; b) The chain trapped in a tube

Several theories of the gel effect in free radical polymerization were developed based on the reptation concept, which are equally successful in explaining experimental data on PMMA and PS systems as are free volume-based theories. For instance, O'Driscoll *et al.* [111] simply assumed that molecules beyond M_e react with a lower rate constant. Gupta and Kumar [15] adapted this approach to polycondensation, suggesting the following reaction scheme

$$P_{n,e} + P_{m,e} \xrightarrow{k_{2,e}} P_{(n+m),e} \tag{2.24}$$

$$P_{n,e} + P_m \xrightarrow{(k_2 k_{2,e})^{0.5}} P_{(n+m),e} \tag{2.25}$$

$$P_n + P_m \xrightarrow{k_2} P_{(n+m)} \tag{2.26}$$

where the molecule $P_{(n+m)}$ is entangled if its molar mass is greater than M_e. The rate constant $k_{2,e}$ can be modeled as inversely proportional to the number-average molar mass. Tirrell *et al.* [112], on the other hand, argue that there are two critical molar masses, $M_{1,c}$ and $M_{2,c}$. Above $M_{1,c}$ but below $M_{2,c}$, polymer chains begin to entangle to the extent that segmental diffusion is the slowest step. However, for polymer chains beyond $M_{2,c}$, polymer chains are highly entangled and the only mechanism by which they can move from one place to another is by reptation. Aharoni [113] determined a value for the characteristic molar mass between entanglements of M_e = 5,020 g/mol for PA6. By comparison, a typical value for the number-average molar mass of the prepolymer before SSP is $M_{n,i}$ = 17,000 g/mol. Consequently, the major part of the chain length distribution is entangled during SSP of PA6.

In 1997, Mallon and Ray [28, 29] first questioned the whole concept of the gel effect in step growth polymerization. They put forward two arguments to support their viewpoint that polymer diffusion cannot be rate limiting. First, they claimed that polymer and condensate diffusion cannot simultaneously control the overall kinetics, that is, experimentally observed radial profiles in SSP-processed granules [18, 19], or influence of sample size on the polymerization time profiles [8, 99], are incompatible with the gel effect. Second, they presented a non-dimensional analysis of the gel effect by defining the following group

$$K = \frac{k_2 \, c^* \, d^2}{D} \tag{2.27}$$

which is the ratio of the characteristic time for diffusion, d^2/D, to the characteristic time for chemical reaction, $1/k_2c^*$. By analyzing experimental data for PMMA and PS, Mallon and Ray showed that the critical step switches from reaction to diffusion when K becomes greater than ~ 1. Thus, K seems to describe the gel effect for free radical polymerization. Then, extrapolating the polymer diffusivity D from PAEKK data to PET and nylons, they concluded that D should be at least five orders of magnitude lower to provoke a diffusion limitation. Therefore, the gel effect theory does not seem to describe polycondensation systems.

It is our belief that Mallon and Ray were rightly inspired to reject the gel effect model, although we think that they presented the wrong arguments. Indeed, simultaneous polymer and condensate diffusion limitations are not incompatible since their relevant length scales differ by orders of magnitude. Consider for instance a situation in which the condensate is removed from the granule at some finite rate. Then, a radial concentration gradient arises, with chemical equilibrium limiting the net rate of chain building near the center of the granule (where the condensate concentration is high). In the meantime, the concentration in the outer shell may fall to near zero provided sufficient stripping is applied in the gas phase, thus making it possible for a gel effect to take place in this local reaction zone. In other words, the concept of the single rate-limiting step is exclusively valid in the steady state [114], which is in essence never achieved in batch SSP.

Moreover, Mallon and Ray assume in their analysis that migration of a functional group requires diffusion of the polymer chain to which it is attached – or at least segmental diffusion. But we shall see in the next section that end-groups can move independently of the chains, by means of a chemical diffusion mechanism due to interchange reactions. This will definitively make the gel effect concept irrelevant to describe polycondensation systems.

2.3.2 Implication of the Redistribution Reaction

The development of a reaction scheme for polycondensation requires distinguishing between *functional* and *chemical* species. Functional species are the entities directly involved in chemical reaction – like carboxyl end-group, amine end-group, or amide bond, in the case of nylons. Chemical species, on the other hand, denote the molecules bearing those moieties. Examples are monomer, oligomers, polymer chains, chain regulators, or macro-cycles. Note that the condensation molecule (water in nylons) belongs to both categories. Because numerous properties of the end-product depend on parameters such as the chain length distribution, the residual monomer content, or the amount of cyclic species, any relevant kinetic model should incorporate a reaction scheme based on chemical species.

Only two major reactions of functional groups, both reversible, need to be considered to describe the chemistry of nylon-6, namely

$$--COOH \; + \; H_2N-- \; = \; --CONH-- \; + \; H_2O \tag{1.4}$$

representing *amidation* and *hydrolysis*, and

$$--CONH-- + \{H_2N--\} = --CO\{NH--\} + \{H\}HN-- \qquad (2.28)$$

standing for the *amine-amide interchange*. In the formulation of a reaction scheme based on chemical species, the amidation reaction leads to either *polycondensation* or *cyclization* (the reverse ring opening), depending on whether it is inter- or intramolecular, respectively. The interchange reaction, in turn, is necessary to explain the occurrence of *polyaddition* of caprolactam,

$$P_n + C_1 = P_{n+1} \qquad n = 1,2,... \qquad (1.3)$$

which is responsible for chain building in the early stage of the hydrolytic route [15]. Indeed, addition of the monomer proceeds by the nucleophilic attack of the amine group of P_n onto the carbonyl group of the amide linkage of C_1 [115, 116]. Also, the reverse reaction, *remonomerization*, requires interchange to occur intramolecularly, that is, it consists of an amine end backbiting the last amide group of its own chain. As reaction involves solely functional species – in other words, reactive moieties cannot see on which molecules they are located – then the amine-amide interchange *must* also occur between two linear chains, leading to *redistribution*,

$$P_n + P_m = P_{n+r} + P_{m-r} \qquad n, m = 1, 2, ... \qquad r = 1, ..., m-1 \qquad (2.29)$$

whose equilibrium constant obviously is $K_r = 1$. Since the number of end-groups (and consequently also M_n) remains unchanged, the redistribution reaction is difficult to detect experimentally. Nevertheless, its existence is evidenced by the production of block copolymers and the subsequent formation of the random copolymer upon blending two different polyamides in the absence of water [117]. Note that possible acid-amide or amide-amide interchanges could also lead to redistribution. While the latter case was dismissed by Miller [118], who could not observe any reaction between *N*-ethylcaproamide and *N*-hexylacetamide in a dry environment, there is some controversy about the former possibility of amide acidolysis [117, 119]. Anyway, the dominant redistribution mechanism in PA6 is the amine-amide interchange.

The only effect of Eq. (2.29) is to statistically redistribute the CLD, leading to Flory-Schulz [4, 5] most probable distribution. Because step growth polymerization itself is also a statistical process (providing all functional groups have the same reactivity), redistribution does not impact the course of polycondensation carried out in a batch or a continuous plug-flow reactor. However, in case of a non-Flory-Schulz CLD, arising for instance upon blending two different polymers (initial bimodal distribution), or from *irreversible* step growth polymerization in a reactor with a broad residence time distribution (RTD), then redistribution relaxes the CLD towards the most probable distribution, as demonstrated by Beers [120]. Note that the same effect is obtained if *reversible* polycondensation is considered. Indeed, forward polycondensation followed by the reverse reaction – hydrolysis in nylons – is equivalent to redistribution.

Because redistribution neither changes conversion nor builds polymer but only returns the CLD to the most probable distribution, it has usually not been incorporated in kinetic models, which is perhaps the reason why its implication on the mechanism of diffusion of functionality in SSP has been somewhat neglected. Indeed, this question was first addressed in 1998 by Srinivasan *et al.* [31], who showed that the likely mechanism allowing the required migration of functional groups in SSP of polyamides and polyesters are interchange reactions. This viewpoint is pictured in Figure 2.16, representing an amine-amide redistribution reaction leading to the migration of the amine moiety by a chemical diffusion mechanism, independent of the diffusion of polymer chains.

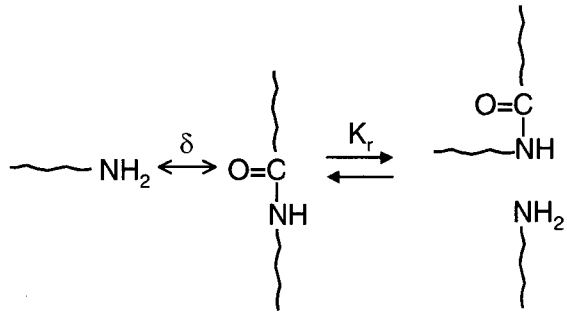

Figure 2.16 The amine-amide redistribution reaction in nylons provides a chemical diffusion mechanism for the migration of amine end-groups, which is independent of the diffusion of chains. The critical reaction distance δ is the distance over which the functionality jumps with each interchange reaction

Srinivasan and his colleagues assumed that each interchange reaction occurs within a critical distance δ, with the functionality hopping over this distance as a consequence. Then, the frequency of reaction of an chain-end, together with this hop distance, determines an *effective* diffusion coefficient of the amine end-group, in a way similar to diffusion-controlled bimolecular reactions of small molecules :

$$D_{eff} = \frac{1}{6} \delta^2 \, k_r \, [-NHCO-] \tag{2.30}$$

Consequently, migration of the functionality is facilitated, provided the redistribution rate constant k_r is large enough. In order to assess the relative influences of end-group diffusion and chemical reaction on the overall rate of SSP, we rewrite Mallon and Ray's gel effect number by substituting Eq. (2.30) into Eq. (2.27), yielding

$$K = \left(\frac{k_2}{k_r} \right) \frac{6 \, c^* \, d^2}{\delta^2 \, [-NHCO-]} \tag{2.31}$$

By assuming no volume of mixing and neglecting the contribution of end-groups to the polymer specific volume, it can be easily shown that the amide bond concentration is given by

$$[-NHCO-] = \left(\frac{\rho_a}{M_{C1}} \right) \frac{S(1-w_c-w_s)}{(S(1-w_c-w_s)+w_s)} \tag{2.32}$$

where M_{Cl} stands for the molar mass of caprolactam (i.e. also the molar mass of a chain repeat unit). Equation (2.32) reduces to [-*NHCO*-] = ρ_a/M_{Cl} for a pure polymer ($w_s << 1$). After appropriate substitutions based on Eqs. (2.11-13) and (2.32), we finally obtain, for $w_s << 1$,

$$K = \left(\frac{k_2}{k_r}\right)\frac{6\,M_{Cl}}{\delta^2}\left(N_{Av}^2\,\rho_a^2\,M_n\,(1-w_c)\right)^{\frac{1}{3}} \tag{2.33}$$

where K is expressed as a function of observable quantities. The gel effect number is plotted as a function of M_n and w_c in Figure 2.17, using the parameter values listed in Table 2.2. Because the characteristic time for diffusion is proportional to $d^2 \sim c^{-2/3}$ while the characteristic reaction time is inversely proportional to the concentration, K scales with $c^{1/3}$. The effect of molar mass and crystallinity displayed in Fig. 2.17 can then be understood by examining their respective influences on c (c decreases upon polymer build-up, but increases upon crystallization according to the concentration effect discussed in Section 2.2.2).

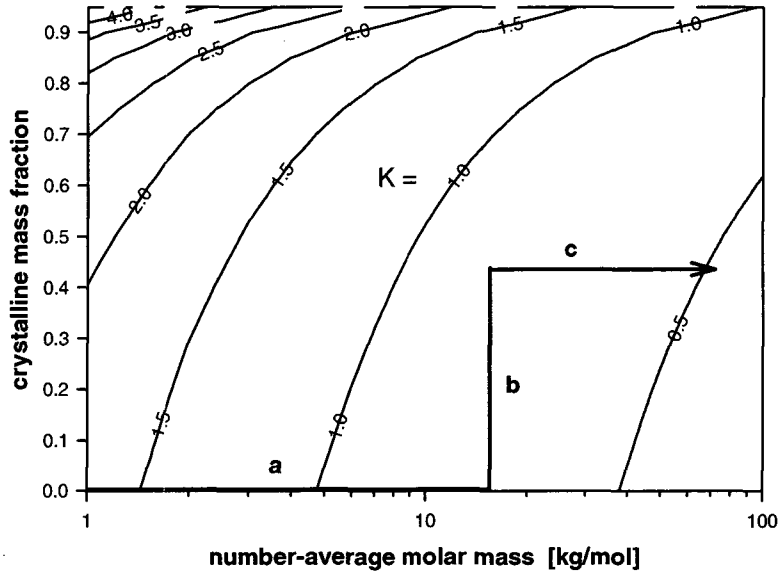

Figure 2.17 Gel effect number diagram for nylon-6. The arrow represents the trajectory during the manufacture process. a) Melt pre-polymerization ; b) Crystallization ; c) Solid-state polymerization. Only in the early stage of the melt reaction does the diffusion of end-groups limit the polycondensation kinetics ($K > 1$). The relation $K < 1$ holds during solid-state polymerization, hence no gel effect is expected to take place

The trajectory of the three-stage manufacture of PA6 in the M_n-w_c plane is represented by an arrow in Fig. 2.17. For typical SSP conditions – M_n values greater than 10,000 g/mol and w_c up to 50 %, the relation $K < 1$ holds. Therefore, end-group diffusion is not rate limiting during SSP and the gel effect concept is not consistent. In fact, Eq. (2.33) predicts a diffusion limitation ($K > 1$) only in the early stage of the melt prepolymerization, which is not necessarily relevant because at low conversion, the dominant mechanism for chain building is polyaddition, not polycondensation. Since the gel effect number diagram was constructed with parameter values at 240°C (a single value of k_r at this temperature is available in the literature), this type of analysis assumes that K is not too sensitive to temperature. This holds approximately

because the activation energies for polycondensation and redistribution should be similar, due to the symmetry of the reaction scheme [116] :

$$\frac{redistribution}{polyaddition} = \frac{reverse\ polycondensation}{ring\ opening} \tag{2.34}$$

Because polycondensation kinetics has been found to be a mix of uncatalyzed (2nd order) and carboxyl catalyzed (3rd order) reactions [38], it could be argued that the amine chemical diffusion mechanism only facilitates the former one. However, the autocatalyzed reaction does not necessarily require a trimolecular collision (or could on that ground be deemed improbable). Rather, formation of complexes between two different end-groups is within possibility, as reported by Van Velden [121] for caprolactam and carboxylic acids.

Table 2.2 Parameter values for the calculation of the gel effect number

Parameter	Symbol	Value	Source
Redistribution rate constant *	k_r	$2\ 10^{-6}$ m^3 mol^{-1} s^{-1}	Srinivasan *et al.* [31]
Polycondensation rate constant †	k_2	$9.34\ 10^{-7}$ m^3 mol^{-1} s^{-1}	Tai and Tagawa [38]
Redistribution reaction distance *	δ	$5.12\ 10^{-10}$ m	Srinivasan *et al.* [31]
Density of amorphous phase *	ρ_a	975.2 kg m^{-3}	Pflüger [20]
Molar mass of caprolactam	M_{Cl}	0.11316 kg mol^{-1}	-
Avogadro number	N_{Av}	$6.022\ 10^{23}$ mol^{-1}	-

* at T = 240°C

† at T = 240°C and M_n = 17 kg mol^{-1}

It is worth noting that redistribution also has morphological implications in semicrystalline nylons regarding the topological species discussed in Section 2.2.1. For instance, Figure 2.18 shows how a bridge molecule – responsible for the cohesion between crystalline lamellae and for the transfer of stress through the material – is transformed into a loop molecule upon amine-amide interchange. This field of investigation has also not received much attention up to now, although it looks promising with regard to the formation of high-performance morphologies in fibers of semi-rigid polymers [31].

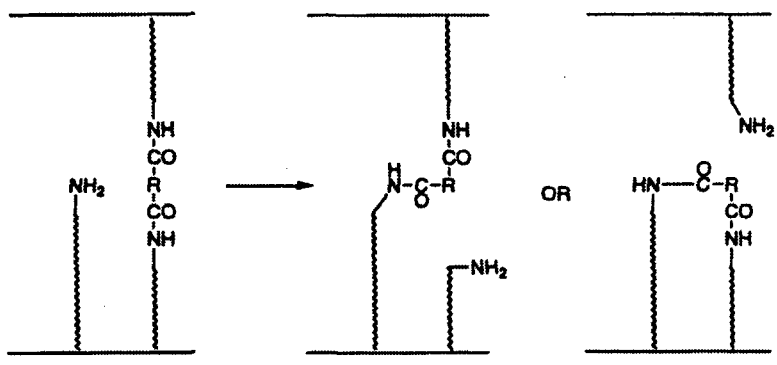

Figure 2.18 Example of the morphological effects of amine-amide interchange reaction in intercrystalline domains of nylons [31]

In summary, migration of functionality via interchange reactions, not molecular or segmental diffusion, is the facilitating mechanism which allows two functional groups to approach each other within the required distance for the chain growth reaction, making the gel effect concept irrelevant in polycondensation. This can be generalized

to other condensation polymers since interchange reactions are not restricted to polyamides. Polyesters, for instance, exhibit significant rates of alcohol-ester and acid-ester interchanges [119, 120, 122].

2.3.3 Rejection of Gaymans' Model

Because the gel effect model in high-conversion polycondensation originates from Gaymans' [11] observation and theoretical concept presented in Section 2.3.1, we intend here to gain more insight into it, particularly because this author only qualitatively drew the distribution of minimum end-group-to-end-group distance (Fig. 2.13.2) and consequently could not put his model to test against his experimental data (Fig. 2.13.3). In the following, we shall formulate the distribution of the diffusion distance on a mathematical basis, which will allow us to reexamine Gaymans' nylon-6 solid-state polymerization data quantitatively. This will give additional credence to our conclusion from the previous section, namely that there is no gel effect in polycondensation.

For deriving the distribution of minimum end-group-to-end-group distance, we consider a three-dimensional spatial distribution of particles – representing acid or amine end-groups. If the distribution is random, the probability for a given particle ι to be located in any volume element ΔV is proportional to ΔV :

$$Prob[\iota \in \Delta V] = \alpha \, \Delta V \tag{2.35}$$

To solve the problem, a finite space is required. Hence, we define a sphere of radius X centered in O, containing N particles. We choose $N >> 1$ so that border effects can be neglected. The proportionality factor in Eq. (2.35) is then obtained by considering that the probability is equal to 1 when $\Delta V = (4/3)\pi X^3$, the volume of the sphere :

$$\alpha = \left(\frac{4}{3} \pi \, X^3 \right)^{-1} \tag{2.36}$$

The probability that the same particle ι is *not* in ΔV is given by

$$Prob[\iota \notin \Delta V] = 1 - \alpha \, \Delta V \tag{2.37}$$

Next, the probability for ΔV to be *empty* is obtained by multiplying N times Eq. (2.37), leading to

$$Prob[N_{\Delta V} = 0] = (1 - \alpha \, \Delta V)^N \tag{2.38}$$

Finally, the probability that *at least* one particle is located in ΔV is expressed by

$$Prob[N_{\Delta V} \geq 1] = 1 - (1 - \alpha \, \Delta V)^N \tag{2.39}$$

Consider now an opposite moiety (i.e. an amine end-group if the N particles represent acid end-groups, and vice versa) at the center O of the sphere. The probability $f(x)dx$

that its nearest reaction partner is situated at a distance between x and $x+dx$ requires the occurrence of two events, as represented in Figure 2.19 : 1) the sphere of radius x centered in O is empty ; and 2) the spherical shell between x and $x+dx$ contains at least one particle. The probability of the former event is obtained by substituting ΔV in Eq. (2.38) by the volume of the sphere, $(4/3)\pi x^3$, and expressing α according to Eq. (2.36). If the sphere of radius x is empty, then all particles are confined in the remaining volume, $(4/3)\pi(X^3-x^3)$, and the *conditional* probability for the shell to contain at least one particle is obtained by substituting ΔV and α in Eq. (2.39) by $4\pi x^2 dx$ (the volume of the shell) and $((4/3)\pi(X^3-x^3))^{-1}$, respectively, yielding

$$f(x)dx = \left(1-\frac{\frac{4}{3}\pi x^3}{\frac{4}{3}\pi X^3}\right)^N \left[1-\left(1-\frac{4\pi x^2 dx}{\frac{4}{3}\pi\left(X^3-x^3\right)}\right)^N\right] \tag{2.40}$$

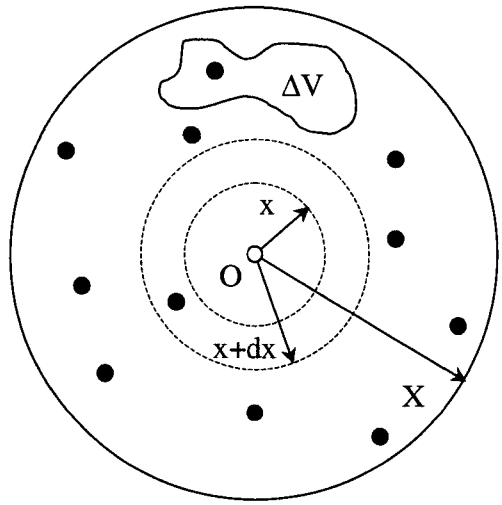

Figure 2.19 Coordinate system for the derivation of the minimum end-group-to-end-group distance distribution. The number of end-groups (represented by dots) is assumed large so that border effects can be neglected

After rearrangement, the frequency function of minimum end-group-to-end-group distance is finally written, to leading order, as

$$f(x) = \frac{3N x^2 \left(X^3-x^3\right)^{N-1}}{X^{3N}} \tag{2.41}$$

in which the number of particles N may be conveniently replaced by the particle density ρ by means of

$$N = \rho\left(\frac{4}{3}\right)\pi X^3 \tag{2.42}$$

A simple way of verifying this result is to check that the total probability is equal to one :

$$\int_0^X f(x)dx = \left[-\frac{\left(X^3 - x^3\right)^N}{X^{3N}} \right]_0^X = 1 \tag{2.43}$$

Plots of $f(x)$ are shown in Figure 2.20 for several values of ρ and X. Increasing the density of particles logically diminishes the distance between them (Fig. 2.20.a). Upon reducing the size of the system, border effects appear in the upper part of the distribution where $x \sim X$ (Fig. 2.20.b). Of course, the asymptotic condition $f(X) = 0$ applies. Furthermore, $f(x)$ tends towards a single symmetrical curve at some large value of X, corresponding to a spatial distribution of moieties in a system of infinite size. Hence, it is always possible to provide an arbitrarily large value for X – say $X = R$, the dimension of the nylon sample – so that no border effects are felt. In other words, X is a pseudo-parameter in the expression for $f(x)$.

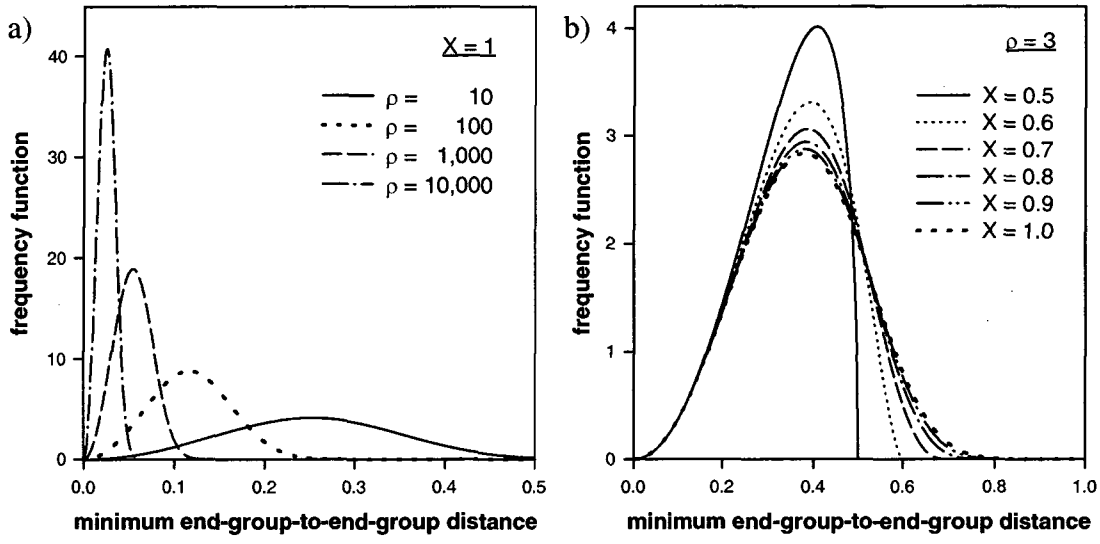

Figure 2.20 Distribution of the minimum end-group-to-end-group distance for different parameter values. a) Effect of ρ for $X = 1$ – the diffusion distance decreases with increasing particle density ; b) Effect of X for $\rho = 3$ – border effects appear in the upper part of the distribution where $x \sim X$

The mean diffusion distance is given by

$$\langle x \rangle = \int_0^X x f(x)dx = N X \frac{\Gamma(N)\Gamma\left(\frac{4}{3}\right)}{\Gamma\left(N + \frac{4}{3}\right)} \tag{2.44}$$

where Γ is Euler gamma function :

$$\Gamma(z) = \int_0^{+\infty} t^{z-1} exp(-t)dt \tag{2.45}$$

Given the strong symmetrical aspect of the distribution, the complicated expression for $\langle x \rangle$ may be approximated by the mode of $f(x)$, obtained by solving $\partial f / \partial x = 0$:

$$\tilde{x} = (2\pi\rho)^{-\frac{1}{3}} \tag{2.46}$$

Thus, given the relation $c^* = \rho / N_{Av}$, the average minimum diffusion distance $\langle x \rangle$ is related to the characteristic distance between end-groups d, defined in Eq. (2.10), by

$$\langle x \rangle \cong \tilde{x} = (2\pi)^{-\frac{1}{3}} d \cong 0.54\, d \tag{2.47}$$

We come now to examine Gaymans' data based on the expression for $f(x)$ derived above. For this purpose, consider the SSP runs performed on PA6 prepolymers of initial molar mass $M_{n,1}$ = 2,500 and $M_{n,2}$ = 18,700 g/mol (the upper and lower curves in Fig. 2.13.3). The corresponding polymerization profiles are displayed again on Figure 2.21.a. Note that the run starting at $M_{n,1}$ plateaus at about $M_{n,2}$, that is, at the initial value for the second run.

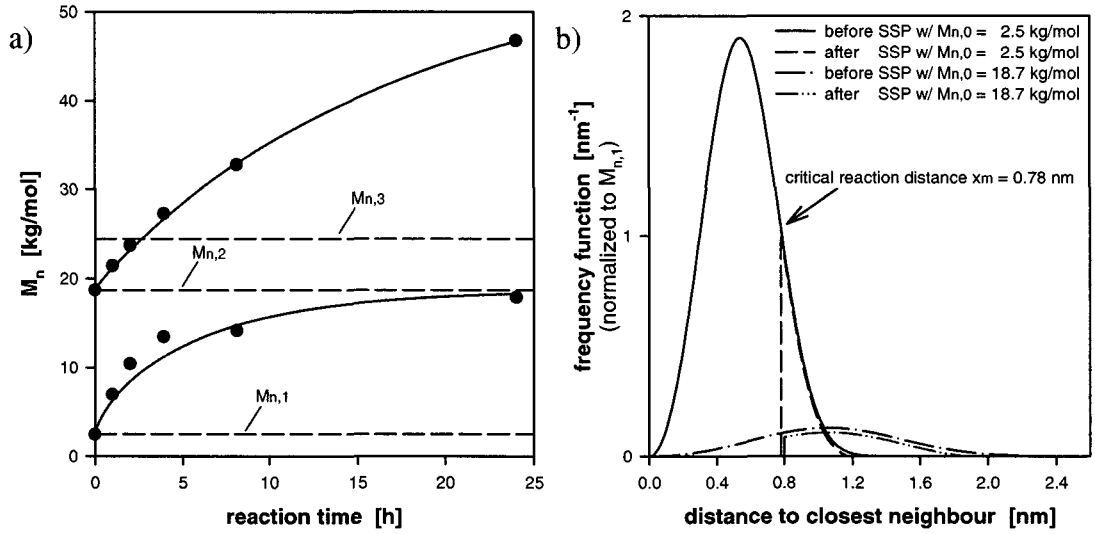

Figure 2.21 Rejection of Gaymans' [11] gel effect model for solid-state polycondensation of nylon-6. a) SSP profiles at 190°C for initial number-average molar masses $M_{n,1}$ = 2.5 and $M_{n,2}$ = 18.7 kg/mol – symbols represent Gaymans' experimental data and lines show the prediction of the model developed in Chapter 6. The molar mass achieved when starting with $M_{n,2}$ exceeds the maximum value $M_{n,3}$ = 24.4 kg/mol predicted by Gaymans' gel effect model ; b) Distribution of the minimum end-group-to-end-group distance before and after completion of the SSP runs shown in a), according to Gaymans' concept

First, we calculate the initial random distributions of minimum end-group-to-end-group distance $f_1(x)$ and $f_2(x)$ (for the two runs starting at $M_{n,1}$ and $M_{n,2}$, respectively) from Eq. (2.41). The number of particles N in Eq. (2.41) is replaced by the number-average molar mass M_n making use of

$$N = \frac{4\pi X^3 \rho_a N_{Av}}{3 M_n (1 - w_c)} \tag{2.48}$$

which has been derived assuming $P = S = 1$. The resulting distributions before SSP are displayed in Fig. 2.21.b, with their area proportional to the concentration of end-groups (that is, only $f_1(x)$ is normalized).

Next, we need to introduce the conversion p of end-groups, which is related to the number-average chain length DP_n as follows (providing the initial state under consideration consists of monomer only) [21]

$$p = \frac{DP_n - 1}{DP_n} \tag{2.49}$$

Introduction of

$$M_n = M_{C1}\, DP_n \tag{2.50}$$

that is, negelecting the contribution of terminal groups, leads to

$$p = \frac{M_n - M_{C1}}{M_n} \tag{2.51}$$

from which the conversion at the beginning of each postcondensation run is calculated as $p_1 = 0.9545$ and $p_2 = 0.9940$, respectively. Reaction during the experiment starting at $M_{n,1}$ reaches completion at $M_{n,2}$, after all chain-ends within critical reaction distance x_m have reacted according to Gaymans' standpoint. Therefore, x_m is obtained by solving

$$\int_0^{x_m} f_1(x)dx = \frac{p_2 - p_1}{1 - p_1} \tag{2.52}$$

which yields $x_m = 0.78$ nm and the corresponding truncated spatial distribution of end-groups after SSP shown in Fig. 2.21.b. With x_m known, the maximum conversion p_3 that can be achieved in the second run starting at $M_{n,2}$ is calculated by solving

$$\int_0^{x_m} f_2(x)dx = \frac{p_3 - p_2}{1 - p_2} \tag{2.53}$$

which gives $p_3 = 0.9954$, corresponding to $M_{n,3} = 24{,}400$ g/mol. Because Gaymans' experimental data after 24 h of reaction exceeds this value by a factor of 2 (Fig. 2.21.a), without even reaching a plateau by that time, we conclude that Gaymans' gel effect model does not describe his own data, and must consequently be rejected. This substantiates our conclusion from the previous section that diffusion of end-groups is not rate limiting.

If the spatial distribution of functional groups remains random during SSP, how can the pronounced influence of the starting molar mass on the course of polymerization be explained ? We shall see that the kinetic model developed in Chapter 6 predicts Gaymans' data accurately if a mass transfer resistance for water is assumed at the particle surface, which may be caused by polymer skinning (see Section 2.2.4). The formation of a polymer skin due to the thermo-mechanical treatment applied to ground the prepolymer to powder is indeed within possibility. The following two points support this idea. First, no particular effect of $M_{n,0}$ is reported when SSP is performed on standard commercial granules of size R ~ 1-2 mm, as we shall see in

Chapter 4. Second, a recent work by Wu *et al.* [123] on SSP of PET discloses an effect similar to the one observed by Gaymans (Figure 2.22). Because Wu grounded prepolymer chips to powder prior to SSP, similarly to the procedure used by Gaymans, the assumption of the formation of a polymer skin seems reasonable.

Furthermore, Fig. 2.22 shows that the change in polymerization rate with initial molar mass observed by Wu seems even more dramatic than the effect reported by Gaymans. Then, for the same reason, such data cannot be explained based on the gel effect concept.

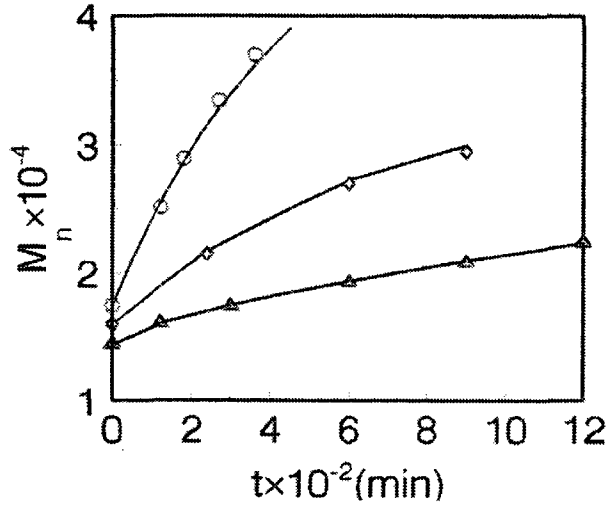

Figure 2.22 Effect of starting molar mass on solid-state polymerization of poly(ethylene terephthalate) in powder form (T = 235°C, R = 0.25 mm) – data from Wu *et al.* [123]. The influence of $M_{n,0}$ is even more pronounced than the one observed by Gaymans *et al.* [11] for nylon-6

In the calculation of $f_1(x)$ and $f_2(x)$, a crystallinity value of w_c = 0.76 was assumed, which had been obtained by curve-fitting Gaymans' data with our SSP model (see Section 6.4.3). This was necessary because Gaymans did not determine the crystalline content of his nylon samples. One might suspect that this diminishes the confidence in the above demonstration, but this is not the case. Indeed, though x_m depends on w_c through the concentration effect, a change in crystallinity would shift the distributions in Fig. 2.21.b by the same factor, with the maximal molar mass achievable $M_{n,3}$ unchanged.

In summary, no gel effect is expected to take place in solid-state polycondensation, because of the implication of interchange reactions on the rate of migration of reactive moieties. A quantitative formulation of Gaymans' [11] gel effect concept is unable to explain his observation of a reduced reaction rate as solid-state polymerization proceeds. Rather, this phenomenon is postulated to be indicative of mass transfer limitations due to polymer skinning, not limited diffusion rates of end-groups. Such a reexamination of Gaymans' data is important because his work paved the way for the development of gel effect theories for high-conversion polycondensation [15, 106] and kinetic models for solid-state polymerization of nylon-6 [32, 33] or poly(ethylene terephthalate) [123].

2.4 A Dimensional Analysis of the Kinetic Steps

In Section 2.3.2, the rates of end-group diffusion and chemical reaction were compared based on the dimensionless number K defined by Mallon and Ray [28, 29], from which it was concluded that the gel effect concept is irrelevant in polycondensation. Here, we extend this type of analysis to all kinetic processes involved in solid-state polymerization of nylon-6, by calculating their characteristic times for typical conditions. In this way, the rate-controlling step may be assessed, and the operating regime of SSP reactors anticipated.

First, the *characteristic time for chemical reaction* is defined as the ratio of the initial concentration to the initial reaction rate,

$$t_r = \frac{c_i}{r_i} \tag{2.54}$$

which leads to the following expressions for forward and reverse polycondensation (indices 2 and 2', respectively) :

$$t_{r,2} = \frac{1}{k_2 c_i^*} = 93h \tag{2.55}$$

$$t_{r,2'} = \frac{K_2}{k_2 [-NHCO-]_i} = 1593h \tag{2.56}$$

The time values in Eqs. (2.55) and (2.56) were obtained for T = 165°C using Eqs. (2.11), (2.12), and (2.32). The parameter values needed to perform the calculations (and further calculations in this section) are listed in Table 2.3.

Next, the *characteristic time for molecular diffusion* over a length scale L_c is given as

$$t_d = \frac{L_c^2}{D} \tag{2.57}$$

By expressing the diffusivity D from Eq. (2.22) and taking the characteristic length as the particle radius R, a value of $t_{d,W}$ = 2.0 h is obtained for the conductive removal of water out of the granules. The characteristic time for end-group diffusion is also calculated with Eq. (2.57) based on the expression for D in Eq. (2.30), and with $L_c = d$, the characteristic distance between chain-ends defined in Eq. (2.10), which yields $t_{d,eg}$ = 73 h.

As forward polycondensation requires the migration of end-groups, while the diffusion of the condensate competes with the reverse reaction (hydrolysis), their respective time scales must be compared accordingly. In the former case, a ratio $t_{d,eg}/t_{r,2} = K = 0.78$ is obtained. Although this value is close to one, a limitation by the rate of migration of functionality is not expected, in accordance with the gel effect number analysis in Section 2.3.2. In the latter case, the ratio $t_{d,W}/t_{r,2'}$ yields a value of 0.0013, indicating that hydrolysis is negligible. In other words, the diffusion of water is so fast that irreversible polycondensation takes place. We conclude that SSP

kinetics must be controlled by the chemical chain-building reaction (providing enough gas stripping is applied).

Also noteworthy is that upon taking L_c = 1 μm, that is, the length scale of crystalline superstructures like spherulites or fibrils, diffusion of water is found to take place instantaneously ($t_{d,W} = 3 \cdot 10^{-3}$ s) with regard to the reaction time, while end-groups cannot escape from such morphological features ($t_{d,eg} = 4 \cdot 10^{10}$ s = 1300 y). Hence, a consequence of the existence of this micrometer length scale, intermediate between molecular dimensions (nm) and particle size (mm), is that a possible partition of the amorphous phase between bulk and interlamellar (or interfibrillar) fractions (see Fig. 2.5) would lead to different rate of SSP in each region because of different local concentration effects. We shall see in Chapter 6 that some SSP literature data on the annealing of drawn PA6 fibers can be reexamined in this way.

Table 2.3 Parameter values for the calculation of time scales in nylon-6 SSP

Parameter	Symbol	Value	Source
Specific heat at constant pressure	$c_{p,p}$	3,175 J kg^{-1} K^{-1}	Ramesh [124]
Diffusivity of water in amorphous phase *	$D_{W,0}$	4.96 10^{-10} m^2 s^{-1}	Pflüger [20]
Polycondensation rate constant †	k_2	2.90 10^{-8} m^3 mol^{-1} s^{-1}	Tai and Tagawa [38]
Redistribution rate constant ‡	k_r	6.25 10^{-8} m^3 mol^{-1} s^{-1}	Srinivasan *et al.* [31]
Polycondensation equilibrium constant *	K_2	1,492	Tai and Tagawa [38]
Avogadro number	N_{Av}	6.022 10^{23} mol^{-1}	-
Molar mass of caprolactam	M_{Cl}	113.16 g mol^{-1}	-
Initial number-average molar mass	$M_{n,i}$	17,000 g mol^{-1}	viscometry analysis
Ratio of crystal-to-amorphous densities	P	1.138	Pflüger [20]
Particle radius §	R	1.44 mm	measurement
Mass fraction of crystalline phase	w_c	0.45	DSC analysis
Mass fraction of solutes	w_s	0	assumption
Redistribution reaction distance	δ	5.12 10^{-10} m	Srinivasan *et al.* [31]
Enthalpy of polycondensation	ΔH_2	-24,883 J mol^{-1}	Tai and Tagawa [38]
Thermal conductivity amorphous phase	λ_a	0.36 W m^{-1} K^{-1}	Aharoni [34]
Density of amorphous phase *	ρ_a	1,014 kg m^{-3}	Pflüger [20]

* at T = 165°C

† at T = 165°C and M_n = 17 kg mol^{-1}

‡ from the reported value at T = 240°C and the activation energy for polycondensation [38]

§ granulate assumed spherical

It may seem surprising that SSP is limited by the rate of polycondensation reaction, not chemical equilibrium, given that the principle of SSP is to speed up the volatilization of the condensate by-product. In fact, it is worth noting that even without any removal of the condensate by-product (i.e., $D_W = 0$), a substantial increase in molar mass may be achieved from the dry prepolymer. This is because the value of the polycondensation equilibrium constant is large, so that water build-up in the polymer is to some extent inconsequential. In order to clarify this point, we calculate the equilibrium conversion p_{eq} that is achieved in a closed system, starting from a dry prepolymer, $[W]_i = 0$, of initial conversion p_i. The polyamidation equilibrium is expressed by

$$K_2^* = \frac{[-NHCO-]_{eq}[W]_{eq}}{c_{eq}^2} \tag{2.58}$$

where $c_{eq} = [\text{-}NH_2]_{eq} = [\text{-}COOH]_{eq}$. The conversion is routinely defined regarding a feed of pure monomer (concentration c_0). Therefore, p_i and p_{eq} are expressed as :

$$p_i = \frac{c_0 - c_i}{c_0} \tag{2.59}$$

$$p_{eq} = \frac{c_0 - c_{eq}}{c_0} \tag{2.60}$$

A mole balance based on the stoichiometry of polycondensation leads to the following expressions for the concentrations of water and amide bonds at equilibrium :

$$[W]_{eq} = c_i - c_{eq} \tag{2.61}$$

$$[-NHCO-]_{eq} = [-NHCO-]_i + c_i - c_{eq} = c_0 - c_i + c_i - c_{eq} = c_0 - c_{eq} \tag{2.62}$$

After appropriate substitutions into Eq. (2.58), based on Eqs. (2.59-62), the equilibrium constant is obtained as

$$K_2^* = \frac{p_{eq}\left(p_{eq} - p_i\right)}{\left(1 - p_{eq}\right)^2} \tag{2.63}$$

which can be solved for p_{eq} to give

$$p_{eq} = 1 - \frac{1}{DP_{n,eq}} = \frac{2K_2^* - p_i - \left(p_i^2 - 4K_2^* p_i + 4K_2^*\right)^{0.5}}{2\left(K_2^* - 1\right)} \tag{2.64}$$

For a prepolymer conversion $p_i = 0.9933$ (obtained from Eq. (2.51) and $M_{n,i}$ = 17,000 g/mol) and an apparent equilibrium constant K_2^* = 3,569 (obtained from Eq. (2.8) and K_2 = 1,492 at 165°C [38]), Eq. (2.64) predicts p_{eq} = 0.9988, which, in turn, corresponds to $M_{n,eq}$ = 91,500 g/mol. Hence, a significant progress of SSP can be achieved without withdrawing water, before an equilibrium limitation is felt. Indeed, typical molar masses of PA6 after SSP are usually far below 100,000 g/mol. Gaymans *et al.* [11], for instance, obtained M_n = 46,800 g/mol after 25 h of reaction at 190°C in a fluidized-bed, starting with $M_{n,i}$ = 18,700 g/mol (see Fig. 2.21.a). For a feed of pure monomer (p_i = 0), Eq. (2.64) reduces to

$$p_{eq} = 1 - \frac{1}{DP_{n,eq}} = \frac{K_2^* - \left(K_2^*\right)^{0.5}}{K_2^* - 1} \tag{2.65}$$

which has been derived by Gupta and Kumar [125], and yields $M_{n,eq}$ = 4,500 g/mol ($DP_{n,eq}$ = 40) for the hydrolytic polymerization of caprolactam in a closed vessel. Note that such a large equilibrium constant is peculiar to polyamides. For instance, the polymerization of PET from bis-hydroxyethyl terephthalate has an extremely unfavorable K_2 of about 0.5, independent of temperature [126]. For this value of the equilibrium constant, Eq. (2.65) predicts the equilibrium chain length as $DP_{n,eq}$ = 1.71, which is too low a value for the product to be of any interest, and Eq. (2.64) predicts a maximal increase of the chain length during SSP without removal of ethylene glycol

of ΔDP_n = 1.07. Therefore, SSP of PET is much more susceptible to be limited by chemical equilibrium than is SSP of PA6.

Another quantity of interest is the *characteristic time for heat transfer* by conduction,

$$t_h = \frac{L_c^2}{\alpha} \tag{2.66}$$

where the thermal diffusivity α is expressed by

$$\alpha = \frac{\lambda_a}{\rho_a \, c_{p,p}} \tag{2.67}$$

Taking $L_c = R$, and the values for the thermal conductivity λ_a, the density ρ_a, and the specific heat $c_{p,p}$ from Table 2.3, a thermal diffusion time of t_h = 19 s is obtained. This is negligibly small compared to reaction times of several hours, so the nylon granules can be considered isothermal. It can be further emphasized that the maximal amount of heat produced by polycondensation is in any case inconsequential, as shown by the calculation of the adiabatic temperature rise

$$\Delta T_{ad} = \frac{-\Delta H_2}{M_{C1} \, c_{p,p}} (1 - p_i) = 0.46 \ K \tag{2.68}$$

where ΔH_2 is the enthalpy of polycondensation. A negligibly small value of ΔT_{ad} is obtained despite polycondensation being strongly exothermic because of the very high initial conversion (p_i = 0.9933). Indeed, Eq. (2.68) predicts a much larger temperature increase, ΔT_{ad} = 69 K, when a feed of pure monomer (p_i = 0) is considered. For the same reason, the amount of water released during SSP is also excessively small. This implies that microgravimetric methods, such as the one developed by us for the determination of the kinetics of low-conversion polycondensations [127], are not suitable to follow SSP because the mass loss is of the order of the experimental noise. Therefore, we shall perform SSP at laboratory scale in small reactors with discontinuous analysis of the nylon granules, as presented in the next chapter.

Finally, the polymer micromorphology is not expected to change during the course of SSP because the *characteristic time for isothermal crystallization* has been reported as t_c ~ 10 min [66, 128], that is, much smaller than common reaction or reactor residence times (~ 50 h). This is important for the modeling, regarding the profound influence of the semicrystalline structure on SSP (see Section 2.2). Here again, PET exhibits a different behavior since its secondary crystallization lasts for several hours [129].

In summary, we expect the kinetics of chain building during solid-state polymerization of nylon-6 to be controlled by the intrinsic rate of polycondensation, not by chemical equilibrium. Of course, this holds only if there is no significant resistance to mass transfer in the gas phase (good stripping conditions), and if loading of the purge gas by condensate molecules is negligible, that is, for a single particle or a reactor operating in the *differential mode*. For packed-beds of several meters in height, this assumption can break down, corresponding to operation in an *integral*

mode. In this case, a gradient of condensate concentration in the gas phase exists along the reactor axis, and the molar mass achieved is governed by the vapor-liquid equilibrium conditions at the interface, which in turn, are determined by the pressure and temperature applied.

2.5 References

[1] Cawthon T.M. and Smith E.C. (1960). Polymerization and depolymerization of nylon 6 above and below its melting point. *Polymer Preprints*, 1, 98-105.

[2] Andrews J.M., Jones F.R. and Semlyen J.A. (1974). Equilibrium ring concentrations and the statistical conformations of polymer chains : Part 12. Cyclics in the molten and solid nylon-6. *Polymer*, 15, 424.

[3] Zimmermann J. (1964). Equilibria in solid-phase polyamidation. *Polym. Letters*, 2, 955.

[4] Flory P.J. (1936). Molecular size distribution in linear condensation polymers. *J. Am. Chem. Soc.*, 58, 1877.

[5] Flory P.J. (1946). Fundamental principles of condensation polymerization. *Chem. Rev.*, 39, 137.

[6] Meyer K. (1973). Zur Nachkondensation von Polyamiden im teilkristallinen Zustand. *Angew. Makromol. Chem.*, 34, 165.

[7] Griskey R.G. and Lee B.I. (1966). Thermally induced solid-state polymerization in nylon 66. *J. Appl. Polym. Sci.*, 10, 105.

[8] Chen F.C., Griskey R.G. and Beyer G.H. (1969). Thermally induced solid state polycondensation of nylon 66, nylon 6-10 and polyethylene terephtalate. *AIChE J.*, 15, 680.

[9] Gaymans R.J., Van Utteren T.E.C. and Van den Berg J.W.A. (1977). Preparation and some properties of nylon 46. *J. Polym. Sci.*, 15, 537.

[10] Gaymans R.J. and Schuijer J. (1978). Polyamidation in the solid phase. In : Polymerization reactors and processes, Henderson J.N. and Barton T.C. eds., 137.

[11] Gaymans R.J., Amirtharaj J. and Kamp H. (1982). Nylon 6 polymerization in the solid state. *J. Appl. Polym. Sci.*, 27, 2513.

[12] Hsu L.C. (1967). Synthesis of ultrahigh molecular weight poly(ethylene terephtalate). *J. Macromol. Sci.-Phys.*, B1, 801.

[13] Mallon F.K., Beers K., Ives A. and Ray W.H. (1998). The effect of the type of purge gas on the solid-state polymerization of polyethylene terephthalate. *J. Appl. Polym. Sci.*, 69, 1789.

[14] Pilati F. (1986). Solid-state polymerization. In : Comprehensive polymer science, Allen G. and Bevington J.C. eds., Pergamon Press pub., 5, 201.

[15] Gupta S.K. and Kumar A. (1987). Reaction engineering of step growth polymerization. Plenum Press pub., New York.

[16] Wiloth F. (1955). Ueber den Mechanismus und die Kinetik der ε-Caprolactam Polymerisation in Gegenwart von Wasser. 4. Mitteilung. *Z. Phys. Chem. (Münich)*, N.F. 4, 66.

[17] Giori C. and Hayes B.T. (1970). Hydrolytic polymerization of caprolactam. II. Vapor-liquid equilibria. *J. Polym. Sci. Part A-1*, 8, 351.

[18] Buxbaum L.H. (1979). Solid-state polycondensation of poly(butylene terephtalate). *J. Appl. Polym. Sci.*, 35, 59.

[19] Gostoli C., Pilati F., Sarti G.C. and Di Giacomo B. (1984). Chemical kinetics and diffusion in poly(butylene terephtalate) solid-state polycondensation: experiments and theory. *J. Appl. Polym. Sci.*, 29, 2873.

[20] Pflüger R. (1975). Physical constants of poly(imino(1-oxohexamethylene) (polyamide 6) and poly(iminohexamethyleneiminoadipoyl) (polyamide 66). In: Polymer handbook, Brandrup J. and Immergut E.H. eds., Wiley pub.

[21] Flory P.J. (1953). Principles of polymer chemistry. Cornell University Press pub., Ithaca, New York.

[22] Ogata N. (1960). Studies on polycondensation reactions of nylon salt. I. The equilibrium in the system of polyhexamethylene adipamide and water. *Makromol. Chem.*, 42, 52.

[23] Ogata N. (1961). Studies on polycondensation reactions of nylon salt. II. The rate of polycondensation reaction of nylon 66 salt in the presence of water. *Makromol. Chem.*, 43, 117.

[24] Srinivasan R., Desai P., Abhiraman A.S. and Knorr R.S. (1994). Solid-state polymerization vis-à-vis fiber formation of step-growth polymers. I. Results from a study of nylon 66. *J. Appl. Polym. Sci.*, 53, 1731.

[25] Steppan D.D., Doherty M.F. and Malone M.F. (1987). A kinetic and equilibrium model for nylon 6,6 polymerization. *J. Appl. Polym. Sci.*, 33, 2333.

[26] Fakirov S. and Avramova N. (1982). Influence of thermal treatment, molecular weight and orientation on the mechanical properties of polyamide-6. *Acta Polymerica*, 33, 271.

[27] Monroe G.C. (1962). Solid phase polymerization of polyamides. *U.S. patent 3,031,433 to DuPont.*

[28] Mallon F.K. (1997). Solid state polycondensation : modelling and productivity enhancements. Thesis, University of Wisconsin-Madison.

[29] Mallon F.K. and Ray W.H. (1998). Modeling of solid-state polycondensation. I. Particle models. *J. Appl. Polym. Sci.*, 69, 1233.

[30] Lustig S.R., Van Alsten J.G. and Hsiao B. (1993). Polymer diffusion in semicrystalline polymers. 1. Poly(ether imide)/Poly(aryl ether ketone ketone). *Macromol.*, 26, 3885.

[31] Srinivasan R., Almonacil C., Narayan S., Desai P. and Abhiraman A.S. (1998). Mechanism, kinetics and potential morphological consequences of solid-state polymerization. *Macromol.*, 31, 6813.

[32] Kaushik A. and Gupta S.K. (1992). A molecular model for solid-state polymerization of nylon-6. *J. Appl. Polym. Sci.*, 45, 507.

[33] Kulkarni M.R. and Gupta S.K. (1994). Molecular model for solid-state polymerization of nylon 6. II. An improved model. *J. Appl. Polym. Sci.*, 53, 85.

[34] Aharoni S.M. (1997). *n*-nylons: their synthesis, structure and properties. Wiley pub.

[35] Rodriguez F. (1996). Principles of polymer systems. Taylor&Francis pub., Washington D.C.

[36] Blanchard E.N., Cohen J.D., Iwasyk J.M., Marks D.N., Stouffer J.M., Aslop A.W. and Lin C. (1999). Process for preparing polyamides. *World patent 99/10408 to DuPont.*

[37] Fried J.R. (1995). Polymer science and technology. Prentice Hall pub., Englewood Cliffs, New Jersey.

[38] Tai K. and Tagawa T. (1983). Simulation of hydrolytic polymerization of ε-caprolactam in various reactors. A review on recent advances in reaction engineering of polymerization. *Ind. Eng. Chem. Prod. Res. Dev.*, 22, 192.

[39] Mallon F.K. and Ray W.H. (1998). A comprehensive model for nylon melt equilibria and kinetics. *J. Appl. Polym. Sci.*, 69, 1213.

[40] Hagen R. (1995). Ein Reaktormodell für die Festphasenpolykondensation von Polyethylenterephthalat. *Chem.-Ing.-Tech.*, 67, 770.

[41] Gantillon B., McKenna T. and Spitz R. (1999). Advances in post-condensation polymerization of ethylene terephthalate. Proceedings of the AIChE Spring Meeting, March 14-18, Houston, Texas, 54.

[42] Murthy N.S., Akkapeddi M.K. and Orts W.J. (1998). Analysis of lamellar structure in semicrystalline polymers by studying the absorption of water and ethylene glycol in nylons using small-angle neutron scattering. *Macromol.*, 31, 142.

[43] Holmes D.R., Bunn C.W. and Smith D.J. (1955). The crystal structure of polycaproamide : nylon 6. *J. Polym. Sci.*, 17, 159.

[44] Arimoto H. (1964). α–γ transition of nylon 6. *J. Polym. Sci. Part A*, 2, 2283.

[45] Auriemma F., Petraccone V., Parravicini L. and Corradini P. (1997). Mesomorphic form (β) of nylon 6. *Macromol.*, 30, 7554.

[46] Illers K.-H. and Haberkorn H. (1971). Schmelzverhalten, Struktur und Kristallinität von 6-Polyamid. *Makromol. Chem.*, 142, 31.

[47] Arakawa T. and Nagatoshi F. (1970). Melting of paracrystals. *J. Polym Sci. Polym. Lett. Ed.*, 8, 41.

[48] Sandeman I. and Keller A. (1956). Crystallinity studies of polyamides by infrared, specific volume and X-ray methods. *J. Polym. Sci.*, 19, 401.

[49] Roberts M.F. and Jenekhe S.A. (1991). Site-specific reversible scission of hydrogen bonds in polymers. An investigation of polyamides and their Lewis acid-base complexes by infrared spectroscopy. *Macromol.*, 24, 3142.

[50] Coleman M.M., Lee K.H., Skrovanek D.J. and Painter P.C. (1986). Hydrogen bonding in polymers. 4. Infrared temperature studies of a simple polyurethane. *Macromol.*, 19, 2149.

[51] Ramesh C., Keller A. and Eltink S.J.E.A. (1994). Studies on the crystallization and melting of nylon 66 : 2. Crystallization behavior and spherulitic morphology by optical microscopy. *Polymer*, 35, 5293.

[52] Reimschuessel H.K. (1977). Nylon 6, chemistry and mechanisms. *J. Polym. Sci.: Macromol. Revs.*, 12, 65.

[53] Keller A. (1977). Polymer crystallization: a survey and salient current issues. *J. Polym. Sci.: Polymer Symposium 59*, 1.

[54] Iguchi M., Kanetsuna H. and Kawai T. (1971). Formation of polymer crystals during polymerisation. *Br. Polym. J.*, 3, 177.

[55] Koenig J.L. and Agboatwalla M.C. (1968). Infrared studies of chain folding in polymers. V. Polyhexamethylene adipamide. *J. Macromol. Sci.-Phys.*, B2, 391.

[56] Eisele U. (1990). Introduction to polymer physics. Springer pub., Berlin.

[57] Seyler R.J. (1997). Semi-crystalline polymers : Two phases or three ? An overview and perspectives. *J. Therm. Anal.*, 49, 491.

[58] Wunderlich B. (1997). Detection of multiple nanophases by DSC. *J. Therm. Anal.*, 49, 513.

[59] Mathot V. (1994). Calorimetry and thermal analysis of polymers. Mathot V.B.F. ed., Hanser pub.

[60] Murthy N.S. and Orts W.J. (1994). D_2O as a probe for studying the noncrystalline regions in nylon 6 using small-angle neutron scattering. *Proc. ACS Div. Polym. Mater. : Sci. Eng.*, 71 (Fall), 293.

[61] Franco L., Subirana J.A. and Puiggali J. (1998). Structure and morphology of odd polyoxamides [nylon 9,2]. A new example of hydrogen-bonding interactions in two different directions. *Macromol.*, 31, 3912.

[62] Clark E.S. and Wilson F.C. (1973). Physical structure of nylons. In : Nylon plastics, Kohan M.I. ed., Wiley pub., 271.

[63] Murthy N.S. and Orts W.J. (1994). Hydration in semicrystalline polymers: small-angle neutron scattering studies of the effect of drawing in nylon-6 fibers. *J. Polym. Sci. Part B : Polym. Phys.*, 32, 2695.

[64] Hutchinson J.L., Murthy N.S. and Samulski E.T. (1996). Deuterium NMR studies of water in oriented nylon 6 fibers. *Macromol.*, 29, 5551.

[65] Sanchez I.C. (1977). Problems and theories of polymer crystallization. *J. Polym. Sci.: Polymer Symposium 59*, 109.

[66] Starkweather H.W., Moore G.E., Hansen J.E., Roder T.M. and Brooks R.E. (1956). Effect of crystallinity on the properties of nylons. *J. Polym. Sci.*, 21, 189.

[67] Puffr R., Raab M. and Dolezel B. (1991). Lactam-based polyamides, 1, Polymerization, stucture, and properties, §6, properties. Puffr R. and Kubanek V. eds., CRC Press.

[68] Giori C. and Hayes B.T. (1970). Hydrolytic polymerization of caprolactam. I. Hydrolysis – polycondensation kinetics. *J. Polym. Sci. Part A-1*, 8, 335.

[69] Kjellmark E.W. (1962). Increasing viscosity of polycaprolactam by removing extractables with solvents and further solid phase polymerizing the polymer. *US patent 3,015,651 to DuPont.*

[70] Heikens D., Hermans P.H. and van der Want G.M. (1960). On the mechanism of the polymerization of ε-caprolactam. IV. Polymerization in the presence of water and either an amine or a carboxylic acid. *J. Polym. Sci.*, 44, 437.

[71] Vrentas J.S. and Duda J.L. (1979). Molecular diffusion in polymer solutions. *AIChE J.*, 25, 1.

[72] Mashelkar R.A. (1984). Diffusional phenomena in reacting macromolecular media. In : Recent advances in the engineering analysis of chemically reacting systems, Doraiswamy L.K. ed., Wiley Eastern pub., NewDelhi, 497.

[73] Astarita G. (1989). Heat and mass transfer in solid polymeric systems. In : Transport phenomena in polymeric systems, Mashelkar R.A., Mujumdar A.S. and Kamal R. eds., Ellis Horwood pub., Chichester, 339.

[74] Zielinski J.M. and Duda J.L. (1996). Solvent diffusion in polymeric systems. In : Polymer devolatilization, Albalak R.J. ed., Marcel Dekker pub., 35.

[75] Vrentas J.S., Jarzebski C.M. and Duda J.L. (1975). A Deborah number for diffusion in polymer-solvent systems. *AIChE J.*, 21, 894.

[76] Fujita H. (1961). Diffusion in polymer-diluent systems. *Fortschr. Hochpol.-Forsch.*, 3, 1.

[77] Vrentas J.S. and Duda J.L. (1977). Diffusion in polymer-solvent systems. I. Reexamination of the free-volume theory. *J. Polym. Sci., Polym. Phys. Ed.*, 15, 403.

[78] Ju S.T., Duda J.L. and Vrentas J.S. (1981). Influence of temperature on the diffusion of solvents in polymers above the glass transition temperature. *Ind. Eng. Chem. Prod. Res. Dev.*, 20, 330.

[79] Ju S.T., Liu H.T., Duda J.L. and Vrentas J.S. (1981). Solvent diffusion in amorphous polymers. *J. Appl. Polym. Sci.*, 26, 3735.

[80] Williams M.L., Landel R.F. and Ferry J.D. (1955). The temperature dependence of relaxation mechanisms in amorphous polymers and other glass-forming liquids. *J. Am. Chem. Soc.*, 77, 3701.

[81] Namikawa R., Okazaki H., Nakanishi K., Matsuno R. and Kamikubo T. (1977). Diffusion of amino acids and saccharides in solutions of dextran and its derivatives. *Agric. Biol. Chem.*, 41, 1003.

[82] Bagdonaite V.A., Juskeviciute S.S. and Shlyapnikov Y.A (1981). On macro- and microviscosity of high polymer solutions. *Polym. Comm.*, 22, 145.

[83] Vieth W.R. and Howell J. M. (1976). Dual sorption theory. *J. Membr. Sci.*, 1, 177.

[84] Le Huy H.M. and Rault J. (1994). Remarks on the α and β transitions in swollen polyamides. *Polymer*, 35, 136.

[85] Papir Y.S., Kapur S. and Rogers C.E. (1972). Effect of orientation, anisotropy and water on the relaxation behavior of nylon 6 from 4.2 to 300 K. *J. Polym. Sci. Part A-2*, 10, 1305.

[86] Kettle G.J. (1977). Variation of the glass transition temperature of nylon 6 with changing water content. *Polymer*, 18, 742.

[87] Müller F.H. and Hellmuth E. (1962). Permeation, swelling, diffusion and relaxation in polymers. 2. Diffusion in nylon 6. *Kolloid Z. Z. Polym.*, 181, 97.

[88] Razumovskii L.P., Markin V.S. and Zaikov G.Y. (1986). Sorption of water by aliphatic polyamides. Review. *Acta Polym.*, 37, 146.

[89] Loo L.S., Cohen R.E. and Gleason K.K. (1998). Correlation times of motion of deuterium oxide in polyamide 6 rods. *Macromol.*, 31, 8907.

[90] Roos J.P. (1974). Mathematical modeling of the sorption of volatile components in Newtonian-high-viscous liquids with the aid of bubbling. *Adv. Chem. Ser.*, 133, 303.

[91] Nagasubramanian K. and Reimschuessel H.K. (1973). Diffusion of water and caprolactam in nylon 6 melts. *J. Appl. Polym. Sci.*, 17, 1663.

[92] Kulkarni M.G. and Mashelkar R.A. (1983). A unified approach to transport phenomena in polymeric media – II. Diffusion in solid structured polymers. *Chem. Eng. Sci.*, 38, 941.

[93] Michaels A.S. and Bixler H.J. (1961). Flow of gases through polyethylene. *J. Polym. Sci.*, 50, 413.

[94] Klein J. and Briscoe B.J. (1977). Diffusion of long molecules through solid polyethylene. II. Measurements and results. *J. Polym. Sci. Polym. Phys. Ed.*, 15, 2065.

[95] Klute C.H. (1959). Diffusion of small molecules in semicrystalline polymers : water in polyethylene. *J. Appl. Polym. Sci.*, 1, 340.

[96] Connelly T.M. and Turner J.C.R. (1979). Two-phase diffusion : diffusion through polymers and polymer blends. *Chem. Eng. Sci.*, 34, 319.

[97] Lasoki S.W. and Cobbs W.H. (1959). Moisture permeability of polymers. I. Role of crystallinity and orientation. *J. polym. Sci.*, 36, 21.

[98] Michaels A.S., Vieth W.R. and Barrie J.A. (1963). Diffusion of gases in polyethylene terephthalate. *J. Appl. Phys.*, 1, 13.

[99] Chang T.M. (1970). Kinetics of thermally induced solid state polycondensation of poly(ethylene terephthalate). *Polym. Eng. Sci.*, 10, 364.

[100] Yoon K.H., Kwon M.H., Jeon M.H. and Park O.O. (1993). Diffusion of ethylene glycol in solid state poly(ethylene terephthalate). *Polym. J.*, 25, 219.

[101] Hill C.G. (1977). An introduction of chemical engineering kinetics and reactor design. Wiley pub., New York.

[102] Edwards D.A. (1999). An asymptotic analysis of polymer desorption and skinning. *Macromol. Theory Simul.*, 8, 10.

[103] Ferry J.D. (1970). Viscoelastic properties of polymers. Wiley pub., New York.

[104] Norrish R.G.W. and Smith R.R. (1942). Catalysed polymerisation of methyl methacrylate in the liquid phase. *Nature*, 150, 336.

[105] Trommsdorff E., Kohle H. and Lagally P. (1948). Über den Mechanismus des explosiven Polymerisationsverlaufes des Methacrylsäuremethylesters. *Makromol. Chem.*, 1, 169.

[106] Kumar A., Saksena K., Foryt J.P. and Gupta S.K. (1987). Effect of segmental diffusion on irreversible, step growth polymerizations of ARB monomers. *Polym. Eng. Sci.*, 27, 753.

[107] Chiu W.Y., Carratt G.M. and Soong D.S. (1983). A computer model for the gel effect in free-radical polymerization. *Macromol.*, 16, 348.

[108] Turner D.T. (1977). Autoacceleration of free-radical polymerization. 1. The critical concentration. *Macromol.*, 10, 221.

[109] De Gennes P.G. (1979). Scaling concepts in polymer physics. Cornell University Press pub., Ithaca, New York.

[110] De Gennes P.G. (1982). Kinetics of diffusion-controlled processes in dense polymer systems. II. Effects of entanglements. *J. Chem. Phys.*, 76, 3322.

[111] O'Driscoll K.F., Dionisio J.M. and Mahabadi H.K. (1979). Polymerization reactors and processes. Henderson J.N. et Bouton T.C. eds., ACS pub., Washington D.C., 361.

[112] Hanley B. and Tirrell M. (1985). An empirical correlation for polymer self-diffusion data in the dilute and semidilute concentration regimes. *Polym. Eng. Sci.*, 25, 947.

[113] Aharoni S. M. (1986). Correlations between chain parameters and the plateau modulus of polymers. *Macromol.*, 19, 426.

[114] Pekar M. and Koubek J. (1997). Rate-limiting step. Does it exist in the non-steady state ? *Chem. Eng. Sci.*, 52, 2291.

[115] Carothers W.H. and Berchet G.T. (1930). Studies on polymerization and ring formation. VIII. Amides from ε-aminocaproic acid. *J. Am. Chem. Soc.*, 52, 5289.

[116] Hermans P.H., Heikens D. and van Velden P.F. (1958). On the mechanism of the polymerization of ε-caprolactam. II. The polymerization in the presence of water. *J. Polym. Sci.*, 30, 81.

[117] Jacobs D.B. and Zimmermann J. (1977). Preparation of 6,6-nylon and related polyamides. In: Polymerization processes, Schildknecht C.E. and Skeist I. eds., Wiley pub., New York.

[118] Miller I.K. (1976). Amide-exchange reactions in mixtures of *N*-alkylamides and in polyamide melt blends. *J. Polym. Sci.*, 14, 1403.

[119] Fakirov S. (1990). Solid state reactions in linear polycondensates. In : Solid state behaviour of linear polyesters and polyamides, Schultz J.M. and Fakirov S. eds., Prentice Hall pub.

[120] Beers K.J. (1997). General kinetic modeling of compositional microstructure in condensation polymers. Proceedings of the Engineering Foundation Conference, March 20, Palm Coast, Florida.

[121] Van Velden P.F. (1956). Freezing-point curves for binary systems of ε-caprolactam with carboxylic acids. *Rec. Trav. Chim.*, 75, 58.

[122] Kotliar A.M. (1981). Interchange reactions involving condensation polymers. *J. Polym. Sci. Macromol. Rev.*, 16, 367.

[123] Wu D., Chen F., Li R. and Shi Y. (1997). Reaction kinetics and simulations for solid-state polymerization of poly(ethylene terephthalate). *Macromol.*, 30, 6737.

[124] Ramesh G.M. and Gupta S.K. (1993). Modelling of an industrial autothermal nylon-6 flow reactor. *Polymer*, 34, 1716.

[125] Gupta S.K. and Kumar A. (1983). Simulation of step-growth polymerizations. *Chem. Eng. Commun.*, 20, 1.

[126] Ravindranath K. and Mashelkar R.A. (1982). Modeling of poly(ethylene terephthalate) reactors : 5. A continuous prepolymerization process. *Polym. Eng. Sci.*, 22, 619.

[127] Spühler C., Zimmerer W. and Renken A. (1998). Microgravimetric determination of polycondensation kinetics. DECHEMA Monographs, 134, Wiley-VCH pub., 587.

[128] Albano C., Sciamanna R., González R., Navarro O. and González E. (1999). Study and modelling of the nylon solidification process. Proceedings of the 2nd European Congress of Chemical Engineering, Montpellier, France.

[129] Jabarin S.A. (1987). Crystallization kinetics of polyethylene terephthalate. I. Isothermal crystallization from the melt. *J. Appl. Polym. Sci.*, 34, 85.

3. Experimental Set-Up and Analytical Tools

In order to model the kinetics of nylon-6 solid-state polymerization on a phenomenological basis, we shall make use of the theoretical arguments discussed in Chapter 2, but we also need experimental data. Because literature reports are scarce (see Table 1.3), with operating conditions often underreported, we have decided to carry out PA6 SSP experiments at laboratory scale. In this chapter, the equipment set up to perform this task is presented. First, the construction of a battery of fixed-bed reactors in an oil bath is described, and the experimental procedure used is detailed. Next, the consistency and reliability of the system are checked by means of some preliminary experiments. Finally, we present the analytic methods employed to characterize the polymer, for both the kinetic studies and the structural investigation.

3.1 A Battery of Fixed-Bed Reactors

Although standard designs used to study SSP at laboratory scale include mainly vacuum rotary evaporators [1] and fluidized-bed reactors [2], we have built a fixed-bed reactor (Figure 3.1) to process nylon granules discontinuously. This configuration is more consistent with the industrial continuous moving packed-bed reactor, which operates under a stream of purge gas below the fluidizing velocity [3].

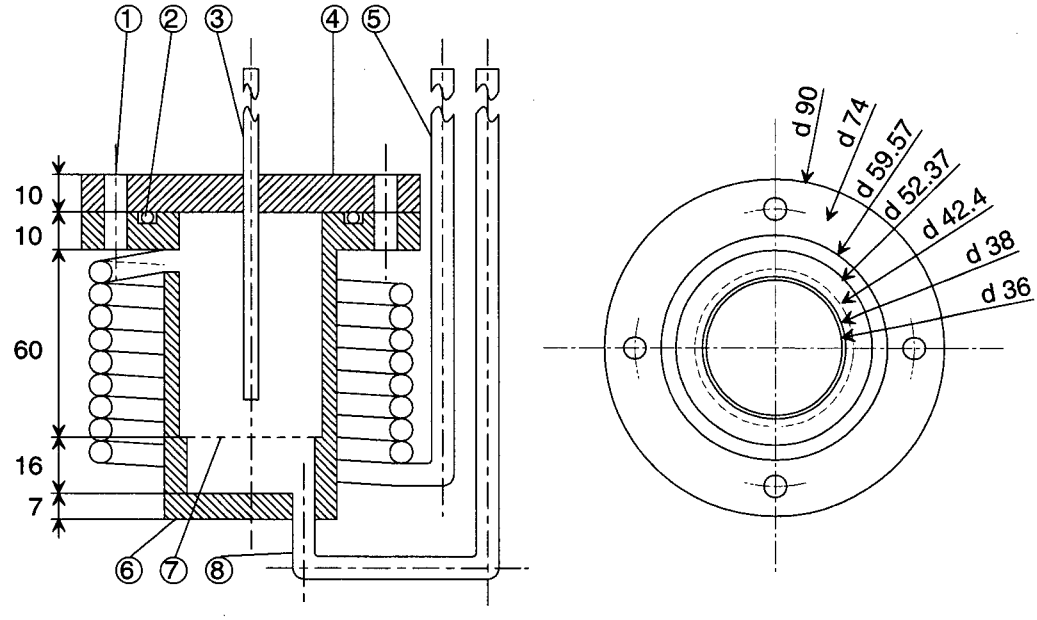

Figure 3.1 A fixed-bed reactor for solid-state polymerization of nylon-6 (distances in mm). 1) Screw (4x) ; 2) O-ring gasket ; 3) Thermocouple ; 4) Reactor top ; 5) Gas preheat coil ; 6) Reactor body ; 7) Sample support ; 8) Gas exit

A small reactor inner diameter, ϕ = 38 mm, is chosen to minimize any mass or heat transfer limitations, while still being ~ 20 times larger than the size of a polymer granule to avoid gas maldistribution at the wall. A punched plate support retains the bed of polymer particles. Nitrogen as the purge gas is fed through a preheat coil into the upper part of the reactor and flows downward through the fixed-bed. Purge exhaust exits the system via a tubing connected to the bottom of the reactor. The apparatus is operated under atmospheric pressure and the top of the reactor is sealed to its body with a PTFE O-ring gasket covered with Viton®. A K-type thermocouple is employed to measure the resin bed temperature. The reactor is manufactured in stainless steel and its total immersed volume is 295 cm^3.

Because polymer analysis are discontinuous and long reaction times are involved, we developed a battery of five fixed-bed reactors working simultaneously in parallel (Figure 3.2). This is also required because a single reactor cannot be easily opened for sampling during a SSP run due to the rapid thermo-oxidative degradation of PA6 in the presence of air [4].

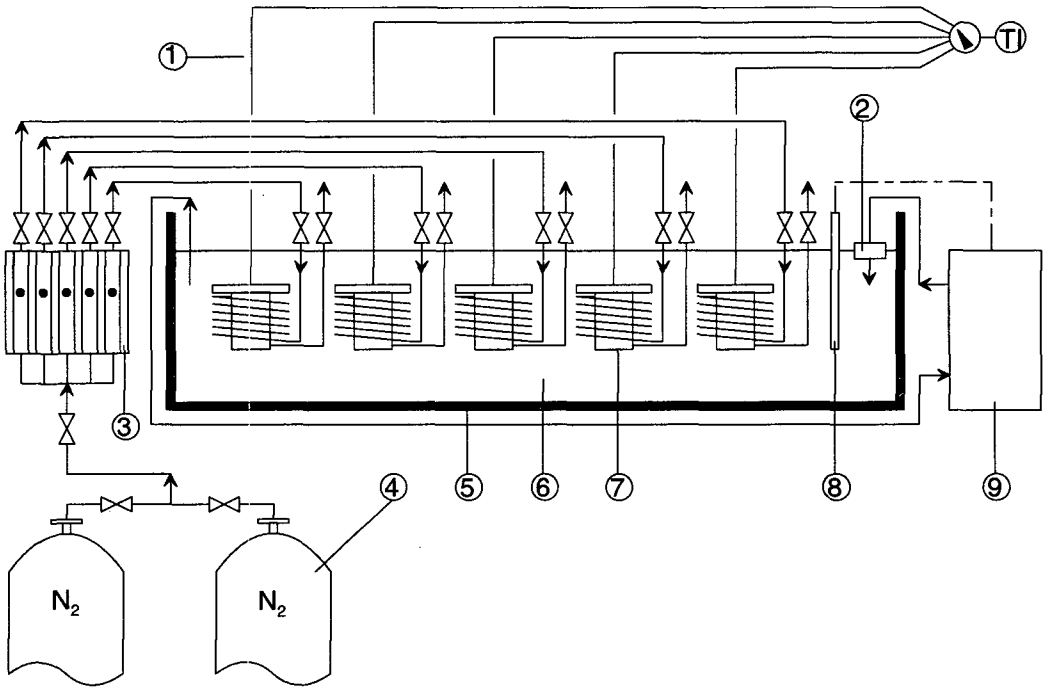

Figure 3.2 Set-up of the battery of fixed-bed reactors. 1) Thermocouples ; 2) Level control ; 3) Flow meters ; 4) Purge gas cylinders ; 5) Insulated vessel ; 6) Oil bath ; 7) Fixed-bed reactors ; 8) Temperature control ; 9) Circulating thermostat

The reactors are immersed in an oil bath to heat and keep the polymer at reaction temperature, and preheat the nitrogen stream. The oil (Marlotherm SH, Hüls Inc., Marl, Germany) is contained in a vessel insulated with polyurethane and connected to an external circulating thermostat (Polystat 12HP, Bioblock Scientic Inc., Frenkendorf, Switzerland). The oil temperature is controlled with a PID algorithm via a Pt100 sensor tube (Julabo Inc., Allentown, PA) immersed in the bath. In order to equilibrate the flow rates of the suction and force pumps and ensure a constant level in the bath, a floater is used, which acts on a metallic disk inserted inside the inlet bath tubing. A deviation of the liquid level from the specified position provokes the rotation of the disc, thus mechanically controlling the flow rate of the force pump by adjusting the pressure drop. A technical grade of nitrogen (Carbagas Inc., Lausanne,

Switzerland) is drawn from feed cylinders (50 L, 200 bar) and passed through rotameters (Aalborg Inc., Orangeburg, NY) prior to entering the reactors. The gas volumetric flow rate Q_g is measured at ambient temperature by means of a 1000 mL bubble flow meter (Supelco Inc., Bellefonte, PA), which can be connected at the reactor outlet. Assuming an ideal gas phase and neglecting the pressure drop, the superficial gas velocity inside the polymer bed is given as

$$u = \frac{4Q_g}{\pi \phi^2 \varepsilon}\left(\frac{T}{T_{amb}}\right) \tag{3.1}$$

where ε stands for the bed porosity. A value of ε = 0.43 has been determined for the bed of nylon granules (mostly short right cylinders with a slightly elliptical cross-section, obtained upon extrusion of the prepolymer). This is in good agreement with values of ε = 0.36-0.41 reported by Tsotsas [5] for a fixed-bed of spheres that are monodisperse in size.

In a standard procedure, PA6 granules graciously provided by BASF are first dried overnight at 60°C under vacuum (final pressure p ~ 50 mbar) in an electrical oven (Vacucenter, Renggli Inc., Renens, Switzerland). Next, each reactor is charged with ~ 20 g of pellets and purged with nitrogen at room temperature for 1 min, before being immersed in the oil bath previously brought to reaction temperature. Both the position in the bath and the reaction time (t = 3.62, 7.25, 22.75, 31.25 and 50 h) for each reactor are assigned using a chance procedure. The resin bed temperature is controlled to less than ± 0.3°C during a run. The reaction is terminated by sealing the reactor, removing it from the bath, and then air-cooling it to room temperature. Finally, polymers removed from the reactors are stored in plastic containers and kept in a fridge at –24°C, protected from light.

3.2 Preliminary Experiments

An empty reactor was first run at the largest gas velocity under consideration (u = 12.08 cm/s) to check that the preheat coil is long enough to heat the purge gas to reaction temperature. Next, the thermal inertia of the polymer bed was characterized by recording the heat-up and cool-down times in a typical experiment (u = 3.48 cm/s, T = 165°C). Figure 3.3 shows that ~1 h is required to bring the polymer to the desired temperature, which then remains constant throughout the experiment. Because heat-up and cool-down times are similar (Fig. 3.3) and thus tend to compensate for each other (furthermore the reaction rate is negligibly small below ~ 120°C), the resulting error is estimated as ± 15 min, i.e. ± 0.5 % of the largest reaction time (t = 50 h). Hence, the fixed-bed reactor is considered isothermal, in agreement with the calculation in Section 2.4.

Second, a reference set of parameters (Table 3.1) was chosen to match typical operating conditions of an industrial moving packed-bed reactor [6]. Using these base case parameters, two identical experiments were performed to ascertain the reproducibility of the experimental procedure. The corresponding polymerization profiles are shown in Figure 3.4.a, where the relative viscosity μ_{rel} is plotted against reaction time (see next section for the determination of μ_{rel}). The two runs yield

identical results. Moreover, the efficiency of the experimental set-up is emphasized by the fact that no equilibrium limitation appears within 50 h of reaction.

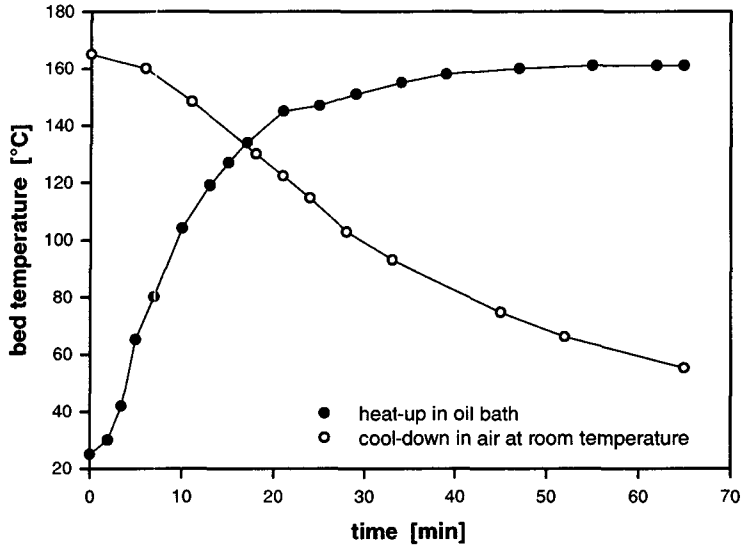

Figure 3.3 Heat-up and cool-down times of the bed of polymer granules (T = 165°C, u = 3.48 cm/s). The lines are drawn for visualization purposes

Third, a base case run was conducted with the same reaction time (t = 50 h) assigned to all five reactors in order to gain a quantitative estimate for the precision of the data. In this way, possible differences between reactors or any effect of their respective position in the oil bath would also be taken into account. The increase in relative viscosity $\Delta\mu_{rel}$ of the processed granules is displayed in Fig. 3.4.b for each reactor. Assuming a randomly distributed experimental error (i.e. obeying Gaussian statistics), the relative error at a 95 % confidence level is calculated from the mean and the standard deviation as

$$\Delta(\Delta\mu_{rel}) = \pm 2\sigma / \Delta\mu_{rel} = \pm 1.97\ \% \tag{3.2}$$

including all contributions of the experimental procedure : prepolymer variability, solid-state polymerization, sampling, and polymer analysis. The validity of any model fitted to the data can thus be established by checking that its prediction goes through the error bars defined by Eq. (3.2).

Table 3.1 Reference set of operating parameters

Reactor parameter	Symbol	Value
Temperature	T	165°C
Gas superficial velocity	u	3.48 cm s^{-1}
Bed height	h	3 cm
Prepolymer characteristics	**Symbol**	**Value**
Particle radius *	R	1.44 mm
Number-average chain length	$DP_{n,0}$	151
Caprolactam mass fraction	$w_{C1,0}$	0.00029
Cyclic dimer mass fraction	$w_{C2,0}$	0.00045
Water mass fraction	$w_{W,0}$	0.00172
Crystallinity	w_c	0.456

* granulate assumed spherical

Finally, to verify that the batch laboratory-scale experiments are consistent with SSP at industrial scale, a run was carried out with parameters from Table 3.1 and compared with the steady-state data of a continuous moving packed-bed operated under similar conditions. For this purpose, reaction time (discontinuous reactor) and residence time (continuous reactor) were superimposed. This can be done because baffles ensure a plug flow profile of granules in the moving bed. Also, the difference in bed height – 3 cm for the fixed bed vs. ~ 10 m for the moving bed – is unimportant here because the initial prepolymer is dry, which implies that water removal cannot be rate limiting (see calculation in Section 2.4). In other words, whether the reactors operate in a differential or an integral mode does not influence the polymerization profile in this case.

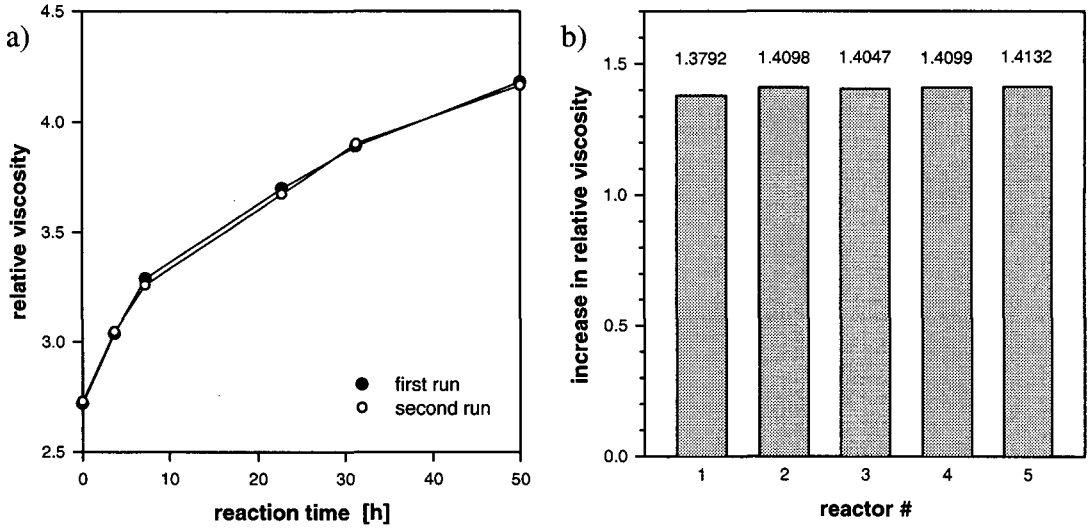

Figure 3.4 Reproducibility. a) Two runs performed under identical conditions (base case); b) Experimental error for the longest reaction time (t = 50 h for all reactors)

A good agreement was found between laboratory- and industrial-scale data. Hence, the battery of fixed-bed reactors appears to be a reliable tool to study solid-state polymerization of nylon-6, formulate a kinetic model at particle scale, then scale-up this model to simulate the industrial reactor.

3.3 Determination of Chain Length and Chemical Species

The analytical techniques set up to determine the chain length and the chemical species of the nylon-6 samples polymerized in the solid state are listed in Table 3.2. We gratefully acknowledge the BASF company for the help with an important part of the analytical work (see Table 3.2).

Table 3.2 Analytical methods for the kinetic studies of nylon-6 SSP

Technique	Abbreviation	Determination of	Performed at
Solution viscometry	-	μ_{rel}, DP_n	EPFL / BASF
Titration (amine & carboxyl groups)	-	DP_n, end-group imbalance	BASF
Liquid adsorption chromatography	HPLC	C_1 to C_6	BASF
Thermogravimetry	TG	W	EPFL

Dilute *solution viscometry* is the most commonly used technique to estimate the chain length. The basic quantity of interest is the relative viscosity μ_{rel}, which is the dynamic viscosity of the polymer solution, μ, divided by that of the solvent, μ_s. We made use of a procedure routinely employed in industry [4], which consists in measuring the relative viscosity of a solution containing 1 g PA6 in 100 mL of 96 % sulfuric acid at 20°C. For this purpose, an Ubbelohde capillary viscometer (Viscologic TI.1, SEMATech Inc., Nice, France) of 1.36 mm inner diameter was employed (Figure 3.5.a). The capillary tube is protected by an external glass jacket connected to a water-circulating thermostat (Julabo F25, Julabo Inc., Allentown, PA), which controls the temperature to within 0.1°C of the set value.

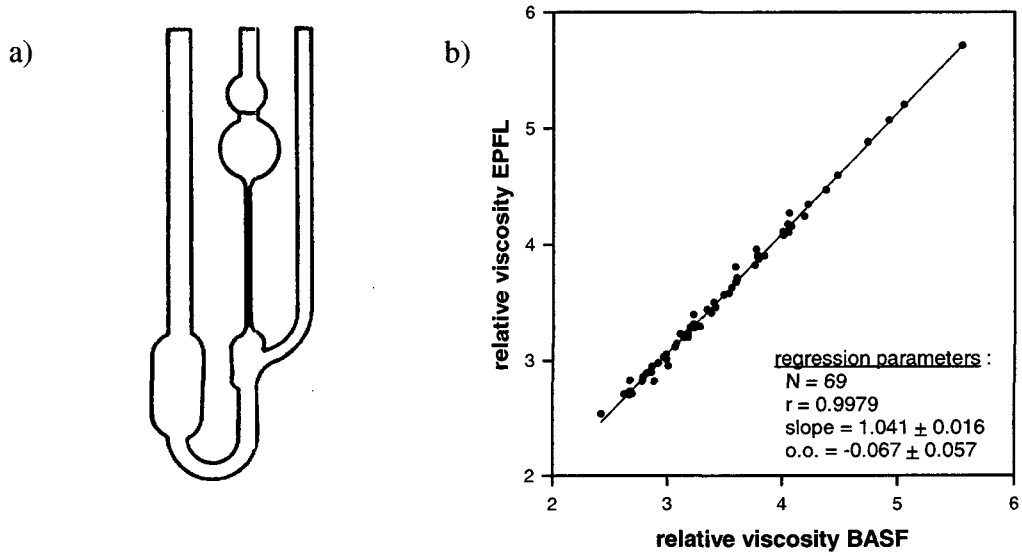

Figure 3.5 Determination of the relative viscosity. a) Sketch of an Ubbelohde viscometer; b) Consistency of our analysis with standard industrial practice

The solutions were prepared by dissolving approximately 400 mg of dry polymer in the appropriate volume of 96 % sulfuric acid (Fluka Inc., Hauppauge, NY) in stirred Erlenmeyers overnight. This corresponds to 20-30 granules that are randomly sampled in the fixed-bed. In this way, possible discrepancies due to differences in shape and size of the granules are statistically averaged.

The time t required for the solution to fall from one fiducial mark to another in the glass capillary is determined by means of an incorporated photocell device (average of 7 measurements). Because the density difference between solution and solvent is negligible, and with a capillary diameter properly selected to avoid a kinetic-energy correction, the dynamic viscosity is proportional to the efflux time [7]. Consequently, the relative viscosity is obtained as

$$\mu_{rel} = \frac{\mu}{\mu_s} = \frac{t}{t_s} \tag{3.3}$$

where t_s stands for the drainage time of the pure solvent (t_s = 45.23 s). By repeating the measurement of t a large number of times, a value of σ= 0.17 s was found for the standard deviation. This implies a ~ 1 % relative error on μ_{rel}, for typical values of t ranging from 100 to 200 s. Thus, rather accurate viscosity data may be obtained. Note

that care must be taken to have the solvent time sufficiently long while keeping the solution efflux time from being inordinately long, to prevent both the evaporation of the solvent and adsorption of the polymer solute to the capillary walls.

In order to check that our viscometric analysis is consistent with BASF industrial practice, a selection of 69 solid-state polymerized PA6 samples were analyzed in both laboratories. The two sets of data compare well, as seen in Fig. 3.5.b. The slope slightly higher than one (1.041 ± 0.016) obtained upon linear regression of the data in Fig. 3.5.b may be caused by tiny differences between capillary tubes or due to some variability in the solvent quality. Anyway, an excellent correlation is obtained, which is a prerequisite if one wants to develop a model capable of simulating an industrial BASF reactor based on the results of our laboratory-scale experiments.

The number-average chain length has been reported to depend linearly on the relative viscosity. For instance, Zimmermann [4] mentions

$$DP_n = 92.79\left(\mu_{rel} - 1\right) \tag{3.4}$$

whereas another study by Crotti *et al.* [8] suggests a slightly different form :

$$DP_n = 101.63\left(\mu_{rel} - 1\right) \tag{3.5}$$

In fact, solution viscometry provides only an indirect characterization of the chain length. More precisely, straightforward application of the empirical correlations (3.4) or (3.5) is questionable, since the presence of even minute amounts of cyclic oligomers [9], use of chain regulators [8], or a changing polydispersity index, all greatly influence the viscosity. Moreover, Eqs. (3.4) and (3.5) were developed to follow polymerization in the melt, where the viscosity does not reach values as high as the ones obtained during SSP. Therefore, calibration of the viscometric analysis was undertaken based on an absolute method for the determination of the number-average chain length, namely analysis of end-groups.

End-group analysis was carried out by *titration* of both carboxyl and amine moieties, using methods similar to the ones originally proposed by Waltz and Taylor [10]. The terminal carboxyl groups were analyzed by hot titration of a solution of 0.5 g PA6 in 30 mL benzyl alcohol with 0.02 M potassium hydroxide in *n*-propanol. The end point is obtained visually with cresol red as the indicator. A parallel blank must be run to account for the possible oxidation of benzyl alcohol to benzoic acid. The determination of amine groups was performed by dissolving 0.5 g PA6 in 25 ml of a mixture of phenol and methanol at 145°C, then titrating with dilute hydrochloric acid at ambient temperature. The end point is obtained potentiometrically. More details about the procedures used can be found in a BASF patent [11].

End-group concentrations are commonly expressed in mmol/kg, and the accuracy of the titrations is estimated as ± 3 mmol/kg for both end-groups [4]. By analyzing solid-state polymerized samples obtained in the absence of any chain regulator, we found a concentration of amine ends systematically higher than the concentration of acid ends. This imbalance remains constant during SSP, as shown in Figure 3.6.a, in which no effect of the viscosity is seen. The mean value is $[\text{-}NH_2]\text{-}[COOH]$ = 3.56 mmol/kg with a large scatter of the data (σ = 2.22 mmol/kg) indicative of the poor accuracy of

the titrations. This somewhat surprising result does not originate in our experimental set-up, since a similar observation was made on an industrial moving-bed reactor.

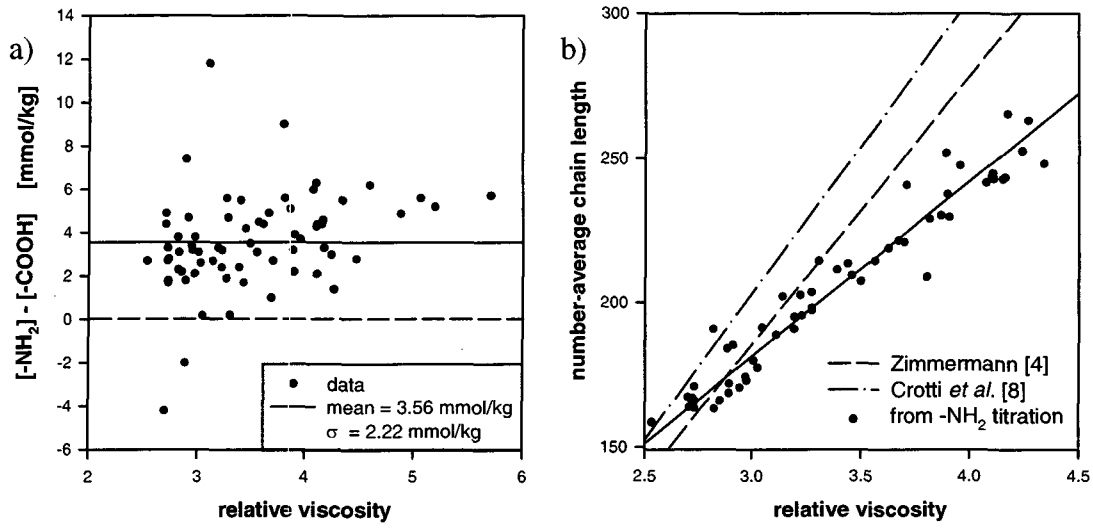

Figure 3.6 Analysis of end-groups for a selection of nylon-6 samples after solid-state polymerization. a) Imbalance of ends is assumed to result from decarboxylation during the melt prepolymerization ; b) Calibration of the viscometric analysis by means of titration for the amine groups

Given that viscosity data show no sign of either branching or cross-linking, the observed difference between end-groups is postulated to result from the degradation of some carboxyl terminal moieties during the melt prepolymerization stage. This is in agreement with Reimschuessel and Dege's [12] finding that equilibrium PA6 melts undergo significant decarboxylation – characterized by the liberation of carbon dioxide – above 250°C, i.e. the approximate operating temperature of the VK column. Then, no further degradation is expected during SSP due to the much lower temperature involved, which is consistent with an invariant imbalance since there is always a one-to-one ratio of end-groups that will react to form longer chains. A constant difference of end-groups during SSP has been reported in a Monsanto patent [13] for PA66 yarns, thus giving additional credence to this viewpoint.

For a typical prepolymer (Table 3.1), the observed excess of 3.56 mmol/kg amine ends means that 5.64 % of all polymer chains before SSP bear only one reactive (amine) group. These monofunctional molecules are expected to influence the course of polymerization by acting as do chain regulators. Hence, we shall need to formulate a kinetic SSP model that takes into account decarboxylation in the prepolymerization stage.

If one assumes that degradation reactions in the melt are restricted to decarboxylation (no desamination), then there is exactly one amine moiety per polymer molecule. Consequently, the number-average chain length is inversely proportional to the concentration of amine groups and is given by ([-NH_2] in mmol/kg)

$$DP_n = \frac{1000\,(1 - w_s)}{M_{CL}\,[-NH_2]} \tag{3.6}$$

When the polymer is wet or unextracted, $w_s > 0$ and care must be taken to determine its humidity content or the amount of extractables before titration. The result of the

calibration of the viscometric analysis is displayed in Fig. 3.6.b, where DP_n calculated from Eq. (3.6) is plotted versus μ_{rel}. A linear correlation passing through the origin,

$$DP_n = 60.53\,\mu_{rel} \tag{3.7}$$

fits the data much better than do Eqs. (3.4) and (3.5) (see Fig. 3.6.b). In particular, the linear correlations by Zimmermann (3.4) and Crotti (3.5) overestimate the chain length at large viscosities. The data with $\mu_{rel} > 4.5$ were discarded for the calibration because end-group analysis was too inaccurate in this case. Indeed, as the chain length increases, the number of chain-ends decreases, thus making the noise in the measurement more significant. On the contrary, the viscometric analysis becomes more precise with increasing chain length because of longer drainage times in the capillary. Consequently, combining viscometry (a sensitive but indirect method to ascertain DP_n) with end-group analysis (an absolute technique, but with poor accuracy), the number-average chain length can be reliably determined.

The residual caprolactam and the cyclic oligomers were separated from the polymer granules by extraction with first methanol, then cyclohexane. Next, *high-performance liquid chromatography* (HPLC) was used to analyze the cyclic species up to the hexamer C_6. A detailed description of an HPLC procedure for the determination of cyclics in PA6 is described by Tai and Tagawa [14].

Finally, the water content was assessed by *thermogravimetry*. For this purpose, a single granule (~ 12 mg) was dried in a microbalance (STA1500, Rheometric Scientific Inc., Piscataway, NJ) at 95°C for 4 h under a stream of nitrogen, and the mass loss was recorded. The cited temperature and time avoid complications due to polymerization and hydrolysis. The possibility of mass loss due to the volatilization of caprolactam is taken into account.

3.4 Methods to Characterize the Morphology

The analytical techniques used to investigate the solid-state structure of the nylon granules are compiled in Table 3.3. Here again, we are greatly indebted to the BASF company for the help with an important part of the analytical work.

Table 3.3 Analytical methods for the structural studies of nylon-6 SSP

Technique	Abbreviation	Determination of	Performed at
Differential scanning calorimetry	DSC	w_c, T_g, T_m, T_{cc}, T_c, T_s	EPFL / BASF
Wide-angle X-ray diffraction	WAXD	w_c, α/γ, $\Lambda\alpha_{200}$, $\Delta 2\theta_\alpha$	BASF
Polarized light microscopy	PLM	Meso-scale structures	EPFL / BASF

Differential scanning calorimetry (DSC) data were recorded on a TC 11 instrument (Mettler-Toledo Inc., Greifensee, Switzerland), which was calibrated using indium as a standard. One dry nylon granule (~ 12 mg) was cut in 10 pieces to achieve a good thermal contact with the sample aluminum pan, which was ramped up to 280°C at 20°C/min. This heating rate is a trade-off to prevent both superheating and recrystallization [15]. The equipment was operated in nitrogen to avoid oxidative degradation of the polymer. Typical thermograms are shown in Figure 3.7.

Upon heating, a broad interval of melting is observed (Fig. 3.7.a) because of the distribution of sizes and defects of crystallites. This interval is extended to lower temperature also by melting of metastable surface layers formed from chain loops, ends of chains, and bridge molecules. The melting point T_m is taken at the peak value of the endotherm. The softening point T_s, an important property with regard to the operation of a solid-state reactor, is defined as the temperature at which the DSC trace begins to indicate the endotherm. The extent of supercooling, a characteristic of the metastable nature of the semicrystalline polymer, is expressed by $\Delta T = T_m - T_{cc}$, where T_{cc} is the temperature at which the onset of crystallization takes place, as determined on the thermogram obtained upon cooling the nylon sample from the melt (Fig. 3.7.b). In addition, the temperature T_c at which the crystallization rate is maximal is obtained from the peak value of the exotherm in Fig. 3.7.b. Note that PA6 crystallizes in the very temperature range inside which SSP reactors are operated.

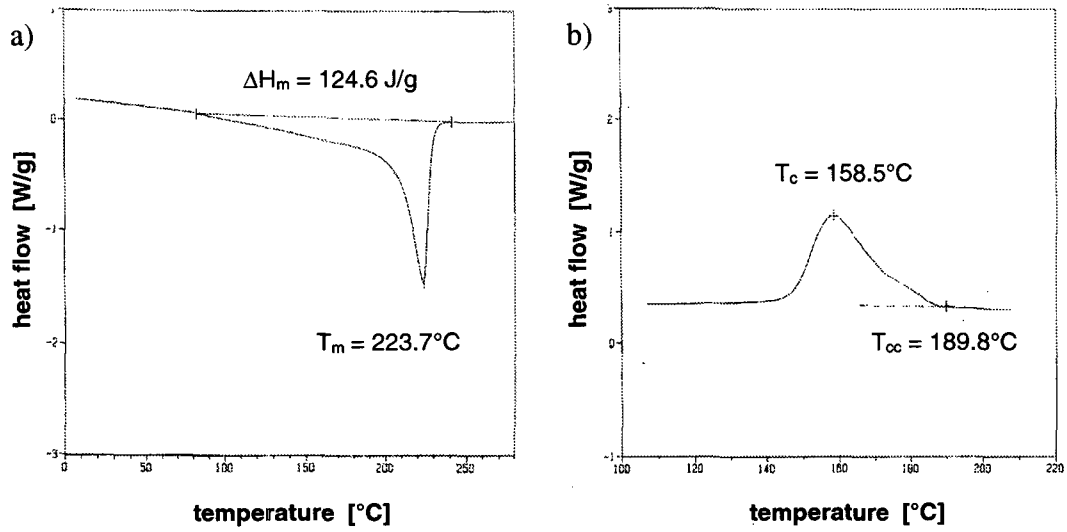

Figure 3.7 DSC thermograms of a nylon-6 sample recorded upon a) heating from room temperature ; b) cooling from the melt at 280°C

A further structural information contained in the DSC curve is the melting enthalpy, ΔH_m, obtained upon integration of the melting endotherm. Indeed, ΔH_m is a valuable quantitative measure of the crystalline content since fusion affects only the crystalline phase. Consequently, the crystallinity is readily assessed as

$$w_c = \frac{\Delta H_m}{\Delta H_m^0} \tag{3.8}$$

where ΔH_m^0 denotes the melting enthalpy at 100 % crystallinity. Two complications arise here. First, a wholly crystalline sample cannot be obtained, so that calibration by means of an independent technique is required. Second, the different crystalline modifications in a PA6 sample have different heats of fusion, so that ΔH_m also depends on the polymorphic composition of the ordered phase. Based on values of the melting enthalpies of the pure α and γ modifications obtained in a BASF laboratory [16] by coupling DSC and densitometry, and on X-ray diffraction results (see below) showing that the α/γ ratio is constant during SSP, an average value of $\Delta H_m^0 = 230$ J/g was derived. Note that this type of analysis assumes an invariant size of the crystallites, because the lamellae are so small that surface effects need to be

considered. In other words, the contribution of the free energy of fold surfaces to the heat of fusion cannot be neglected. As we shall see in Chapter 5, the size of crystallites remains constant during SSP, so this is not a problem here.

Wide-angle X-ray diffraction (WAXD) data were collected in transmission on a D500 diffractometer (Siemens Inc., Munich, Germany) using a Cu-Kα incident beam of wavelength $\lambda = 0.15405$ nm. An example of a diffractogram obtained on an extracted PA6 sample is displayed in Figure 3.8. The background pattern is due to scattering from amorphous regions (the amorphous halo), while the peaks represent scattering from the crystalline regions having regular spacing. The crystalline peaks at the angles $2\theta \sim 20°$ and 24° are due to the α crystalline form (corresponding to the (200) and (020) interferences, respectively) whereas the peak of the γ crystalline form occurs at $2\theta \sim 21°$, and appears here only as a shoulder. The index of crystal density, $\Delta 2\theta_\alpha$, obtained from the 2θ separation between the two intense reflections at ~ 20° and 24° yields a measure of the degree of perfection within the α crystals. An increase of $\Delta 2\theta_\alpha$ corresponds to a decrease in the unit cell volume, that is, an increased crystalline density. The procedure for the determination of the lateral size of the α-crystallite, $\Lambda\alpha_{200}$, is described by Murthy and Minor [17].

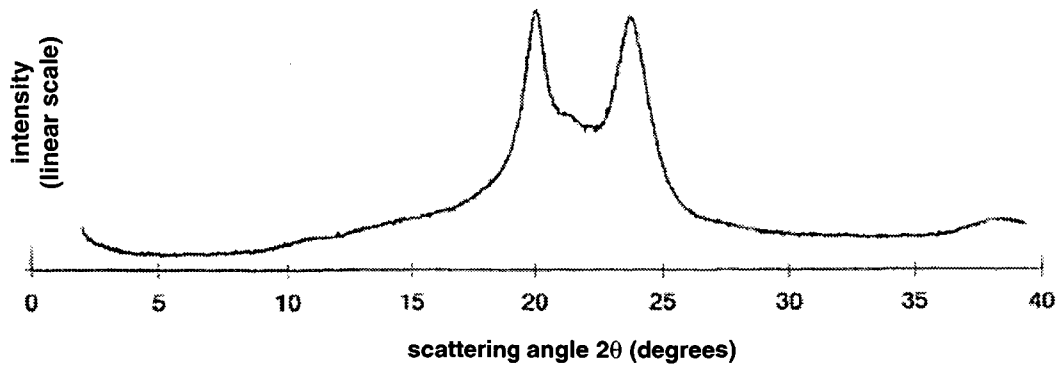

Figure 3.8 Wide-angle X-ray diffraction pattern of a nylon-6 sample

A standard way to resolve the diffraction pattern between the crystalline and amorphous regions is to take the ratio of the area under the crystalline peaks to the total scattered intensity between the 2θ values of 10 and 35° [18]. In this way, an estimation of the crystallinity is obtained, which was compared to the value determined by DSC for three PA6 samples. Both techniques agree well (Figure 3.9), although their sensitivities appear to be rather poor. Crystallinity values disclosed in Fig. 3.9 range from $w_c = 0.45$ to 0.55, with an experimental error of ± 0.05. Because w_c is expected to influence the rate of SSP so much (see Section 2.2.2), it could be that the accuracy of its measurement will be a limiting factor for the discrimination of kinetic models.

In a study on annealed PA6 fibers, Fakirov and Avramova [19] measured w_c by means of DSC, WAXD, and densitometry. They observed a dispersion of the data similar to the results in Fig. 3.9. We believe that such discrepancies between analytical techniques arise from the nature of the semicrystalline morphology rather than from the precision of the method itself. Indeed, the two-phase model (crystalline/ amorphous) is an oversimplification of the reality because there is no obvious demarcation between crystalline and amorphous regions, as discussed in Section

2.2.1. Consequently, analytical techniques based on the measure of different quantities (heat of melting, regular spacing, density) can yield slightly different estimates of the crystalline content.

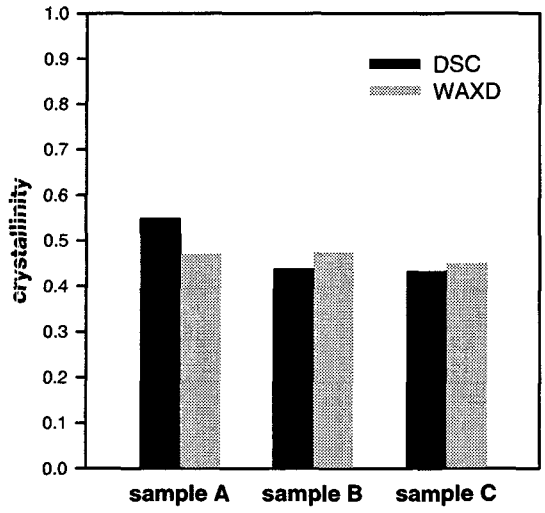

Figure 3.9 Comparison of DSC and WAXD methods for the assessment of the crystallinity

Finally, *polarized light microscopy* was set up to investigate micrometer-scale morphological features like spherulites, making use of their birefringent properties. For this purpose, nylon granules were embedded in a low viscosity epoxy resin that was left to cure at room temperature. Then, 30 μm sections were prepared using a Reichert-Jung sliding microtome (Leica Microsystems Inc., Wetzlar, Germany) with a glass knife, and observed under a BH-2 optical microscope (Olympus Inc., Melville, NY) between crossed polarizers.

3.5 References

[1] Gaymans R.J. and Schuijer J. (1978). Polyamidation in the solid phase. In : Polymerization reactors and processes, Henderson J.N. and Barton T.C. eds., 137.

[2] Gaymans R.J., Amirtharaj J. and Kamp H. (1982). Nylon 6 polymerization in the solid state. *J. Appl. Polym. Sci.*, 27, 2513.

[3] Beaton D.H. (1974). Continuous, solid-phase polymerization of polyamide granules. *U.S. patent 3,821,171 to DuPont.*

[4] Zimmermann J. (1988). Polyamides. In : Encyclopedia of polymer science and engineering, 11, Mark H.F. ed., Wiley pub., 315.

[5] Tsotsas E. (1990). Über die Wärme- und Stoffübertragung in durchströmten Festbetten. VDI pub., Düsseldorf.

[6] Pipper G. and Cordes C. (1989). Removal of caprolactam and oligomers thereof from nylon granules containing same. *U.S. patent 4,816,557 to BASF.*

[7] Lacey E.M. (1973). Characterization of nylons. In : Nylon plastics, 83, Kohan M.I. ed., Wiley pub., 102.

[8] Crotti S., Filippini-Fantoni R. and Tang Z.-L. (1997). A theoretical model for ε-caprolactam polymerization : comparison with practical results on continuous plants. Proceedings of the 1st European Congress of Chemical Engineering, Florence, Italy, 1, 155.

[9] Aharoni S.M. (1997). *n*-nylons: their synthesis, structure and properties. Wiley pub.

[10] Waltz J.E. and Taylor G.B. (1947). Determination of the molecular weight of nylon. *Anal. Chem.*, 19, 448.

[11] Götz W. (1997). High molecular weight polyamides obtained from nitriles. *U.S. patent 5,596,070 to BASF.*

[12] Reimschuessel H.K. and Dege G.J. (1970). Polyamides: decarboxylation and desamination in nylon 6 equilibrium polymer. *J. Polym. Sci. : Part A-1*, 8, 3265.

[13] Silvermann B., Raleigh N.C. and Stewart L.E. (1970). High molecular weight oriented polyamide textile yarn. *U.S. patent 3,548,584 to Monsanto.*

[14] Tai K. and Tagawa T. (1982). The kinetics of hydrolytic polymerization of ε-caprolactam. V. Equilibrium data on cyclic oligomers. *J. Appl. Polym. Sci.*, 27, 2791.

[15] Puffr R., Raab M. and Dolezel B. (1991). Lactam-based polyamides, 1, Polymerization, stucture, and properties, §6, properties. Puffr R. and Kubanek V. eds., CRC Press.

[16] Illers K.-H. (1978). Polymorphie, Kristallinität und Schmelzwärme von Poly(ε-caprolactam). 2. Kalorimetrische Untersuchungen. *Makromol. Chem.*, 179, 497.

[17] Murthy N.S. and Minor H. (1990). General procedure for evaluating amorphous scattering and crystallinity from X-ray diffraction scans of semicrystalline polymers. *Polymer*, 31, 996.

[18] Murthy N.S., Akkapeddi M.K. and Orts W.J. (1998). Analysis of lamellar structure in semicrystalline polymers by studying the absorption of water and ethylene glycol in nylons using small-angle neutron scattering. *Macromol.*, 31, 142.

[19] Fakirov S. and Avramova N. (1982). Influence of thermal treatment, molecular weight and orientation on the mechanical properties of polyamide-6. *Acta Polymerica*, 33, 271.

4. Kinetic Studies

The kinetics of nylon-6 solid-state polymerization was studied batchwise at laboratory scale in the battery of fixed-bed reactors described in the previous chapter. For the sake of identifying the respective influences of all operating conditions, experiments were performed using the reference set of parameters defined in Table 3.1, by variating one parameter at a time around its base case value. Here, the results of these kinetic studies are presented, that will substantiate some of our theoretical arguments derived in Chapter 2. With this knowledge, as well as with the results of the structural investigation disclosed in Chapter 5, we shall assess the basic assumptions that are needed to formulate the mathematical model in Chapter 6.

4.1 Effect of Bed Height and Gas Velocity

In order to gain experimental data that can be compared with the prediction of a single particle model, the fixed-bed reactors must operate in a differential mode. This means that no concentration gradient in the gas phase should exist along the reactor axis, so that each granule in the packed-bed is subjected to the same conditions and is solid-state polymerized to the same extent. To verify that this condition is fulfilled, two runs were performed with different bed heights, $h = 1$ and 3 cm. The resulting polymerization time profiles are displayed in Figure 4.1.a.

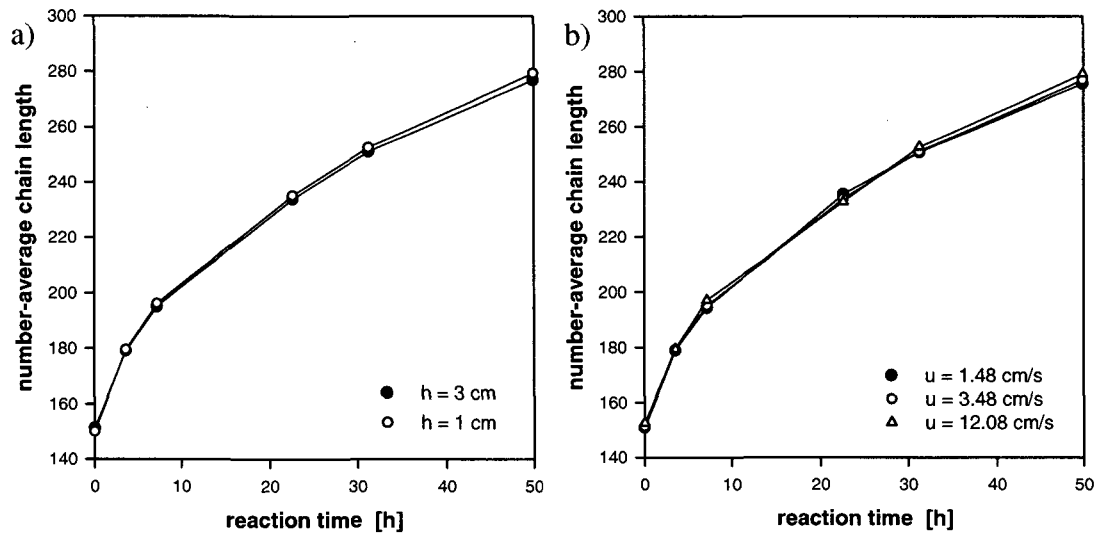

Figure 4.1 Solid-state polymerization profiles. a) Effect of bed height ; b) Effect of gas velocity. Other experimental conditions from base case (Table 3.1). The lines are drawn for visualization purposes

Since the granules for the viscometric analysis were sampled at random, the data in Fig. 4.1.a represent a spatial average over the whole bed. Therefore, a limitation by the vapor-liquid equilibrium due to a possible gradient of water in the gas – obviously

different for the two values of h – would be revealed. As the polymerization profiles are identical, we conclude that the fixed-bed reactors operate in a differential regime. Note that this behavior breaks down for industrial reactors because of their much larger dimensions. Indeed, columns of typical height $h \sim 10$ m [1] operate in an integral regime because loading of the gas phase by volatile by-product molecules is not negligible in this case [2].

Upon pelletizing the prepolymer, a large surface area is generated that allow mass transfer of volatile molecules to the gas phase. This surface area is maintained during SSP as the granules remain separate from each other in the reactor and allow gas to flow between them. Hence, if good stripping is applied, the main resistance to mass transfer must be the diffusion within the polymer, not convection at the polymer/gas interface. This assumption was put to test by using different values of the gas superficial velocity, u = 1.48, 3.48, and 12.08 cm/s. As shown in Fig. 4.1.b, there is no difference between the resulting polymerization profiles. Because a reduced rate of water vaporization does not necessarily affect the build-up of polymer (see Section 2.4), this information is not sufficient to exclude the possibility of a mass transfer resistance in the gas phase. Consequently, polymer samples were also analyzed for caprolactam and cyclic dimer, as these species are volatile (see Section 4.4). The resulting curves are displayed in Figure 4.2.

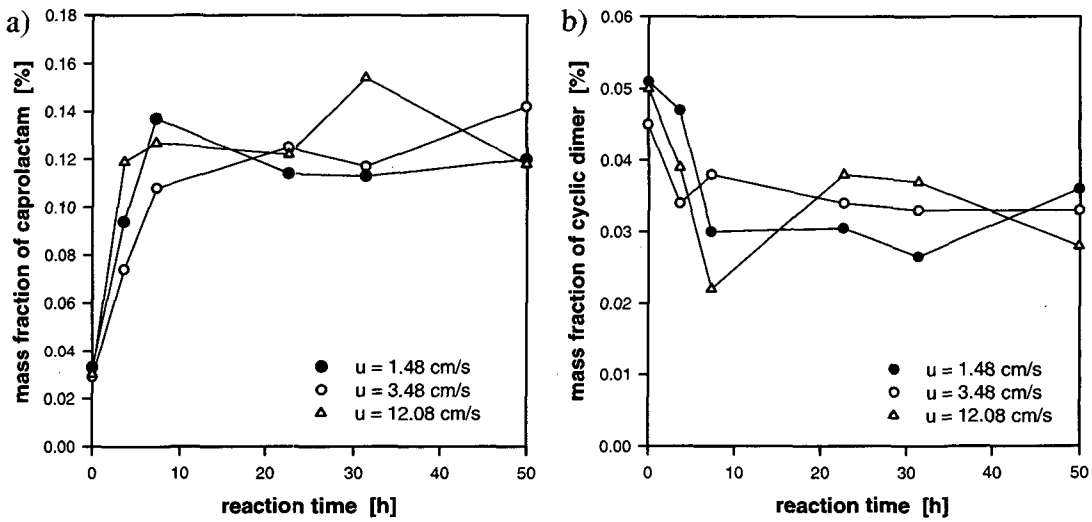

Figure 4.2 Effect of gas velocity on : a) Remonomerization ; b) Formation of cyclic dimer. Other experimental conditions from base case (Table 3.1)

The observed remonomerization (Fig. 4.2.a) takes place through the cyclization reaction, that is, the reversal of the polyaddition of caprolactam. This occurs because the monomer was depleted to below its equilibrium value (of several percents) by the hot water extraction stage. The formation of caprolactam during SSP is undesirable since it creates problems in the spinning and molding of the final polymer. Therefore, controlling the extent of re-equilibration must be of prime concern during the manufacture process, to avoid a second energy-intensive extraction step. The value of $w_{Cl} \sim 0.14$ % obtained in the fixed-bed reactors is below common specifications – for instance, a BASF patent [3] reports a critical value of $w_{Cl} \sim 0.5$ % for the end-product. By contrast, the amount of cyclic dimer, also undesirable, decreases slightly during SSP (Fig. 4.2.b). This is in agreement with a cyclization equilibrium constant much smaller for the cyclic dimer than for caprolactam [4].

Figure 4.2 does not reveal, within experimental accuracy, any influence of the nitrogen velocity. Therefore, we conclude that no significant resistance to mass transfer exists in the gas phase for the velocity range under consideration. Note that many SSP studies in the literature were performed with much higher flow rates of nitrogen. For instance, Beaton [1] used $u = 74$ cm/s to conduct SSP of PA66 in a fixed-bed of 5.5 cm diameter. Also, fluidized-bed designs requiring even larger amount of purge gas (typically, $u = 240$ cm/s [5]) seem not necessary. Of course, in industrial (integral) reactors, the vapor-liquid equilibrium must also be considered to optimize the flow rate of purge gas. In a recent DuPont patent [2], a value of $u = 27$ cm/s is disclosed for a PA6 SSP reactor.

4.2 Effect of Particle Size, Initial Chain Length, and Crystallinity

In a series of solid-state polymerization experiments, a nylon-6 prepolymer was used that had been pelletized to different particle sizes, $R = 1.16$, 1.44, and 1.53 mm. These values represent an average over 50 granules sampled at random, with a standard deviation of $\sigma = 0.06$ mm in each case. The resulting polymerization profiles, displayed in Fig. 4.3.a, do not differ significantly, given the small discrepancy between the starting values of the chain length. Therefore, the rate of polymer build-up is not controlled by the amidation equilibrium. This is consistent with the calculation in Section 2.4, where the diffusional transport of water out of the particles was found to occur much faster than hydrolysis of the amide bonds. Indeed, a kinetic limitation by the withdrawal of condensate would scale with R^{-2}, because the diffusion length per unit volume is inversely proportional to the square of the sample dimension. This implies that the smaller granules in Fig. 4.3.a should polymerize $1.16^{-2}/1.53^{-2} = 1.74$ times faster than the larger ones. As this is obviously not the case, we conclude that the polymer chips are small enough that irreversible polycondensation takes place.

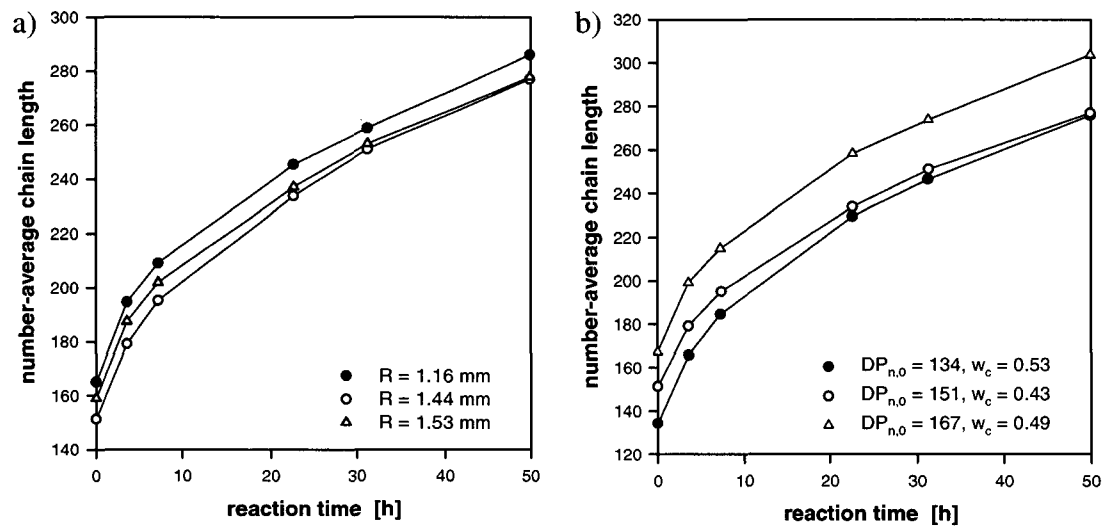

Figure 4.3 Solid-state polymerization profiles. a) Effect of particle size ; b) Effect of initial chain length and crystallinity. Other experimental conditions from base case (Table 3.1)

Note that in the presence of a diffusion limitation at particle scale, radial concentration gradients would arise. In this case, the value for the number-average chain length determined by viscometry is the spatial average over the whole granule.

Solid-state polymerization runs were also conducted with prepolymers of different chain lengths, $DP_{n,0}$ = 134, 151, and 167. For some reason, these samples also had different crystallinities, w_c = 0.53, 0.43, and 0.49, respectively. So, the influences of both parameters must be considered when analyzing the resulting polymerization profiles (Fig. 4.3.b).

First, there is obviously no such dramatic effect of the initial chain length on the rate of SSP as was reported by Gaymans *et al.* [6] for PA6 and Wu *et al.* [7] for PET (see Fig. 2.13 and 2.22, respectively). This adds credence to our assumption of a polymer skin arising upon grounding the prepolymer chips to powder, not a gel effect, to explain Gaymans and Wu's data (see Section 2.3.3).

Second, Fig. 4.3.b also clearly shows that samples of higher crystallinity polymerize faster, in accordance with our postulate of an increased reaction rate due to the confinement of the reactive species in the amorphous volume (see Section 2.2.2). To our knowledge, this is the first experimental evidence of the influence of crystallinity on the kinetics of solid-state polymerization in polyamides. This underscores the potential for process optimization lying in a better control of the morphology during the manufacture of nylon-6.

4.3 Effect of Temperature

The influence of reaction temperature on the course of solid-state polymerization of nylon-6 was investigated for T = 125, 145, 165, 180, and 190°C. An enhancement of polymer build-up with increasing temperature was observed, as shown in Figure 4.4.a.

After cool-down, all polymer particles flowed easily out of the reactors, except for the highest temperature – T = 190°C, that is, ~ 30°C below T_m – where there were some minor signs of polymer agglomeration and wall sticking. Though a slight extent of surface softening does not affect the performance of a small fixed-bed reactor, this is not the case for large moving-beds, where it can cause pluggage or disturb the residence time distribution. This is why industrial reactors operate well below the crystalline melting point – see the reference value of T = 165°C (Table 3.1). Also, a DuPont patent [2] discloses a maximal value of T = 170°C for SSP of PA6 in a continuous reactor to avoid agglomeration of particles. Therefore, an important processing advantage could be gained by increasing the softening temperature. This is especially visible in Fig. 4.4.a : the extent of polymerization after 50 h at T = 165°C (base case) could be achieved in only 10 h at T = 190°C. Some recent efforts in industry give prominence to this viewpoint [2].

In several studies on the SSP of nylons, a kinetic analysis of the data was carried out empirically using non-autonomous rate functions [6, 8, 9]. Walas [10] and Harrison [11], for instance, pointed out that the rate of reaction in solid materials usually varies as some power of the time, that is,

$$rate = k\,t^{n} \tag{4.1}$$

Assuming such a relation to hold gives us for the case at hand

$$\frac{dDP_n}{dt} = k\,t^{n} \tag{4.2}$$

By fitting Eq. (4.2) to the polymerization profiles at different temperatures, an excellent description of the data is obtained with the following optimal values of n (in increasing order of T) : n = -0.55, -0.45, -0.44, -0.47, and -0.51. Thus, an average value of n = -1/2 was taken, which is appropriate to describe the experimental data (Fig. 4.4.a). Interestingly, Griskey and Lee [8] also found n = -1/2, but for SSP of PA66. The empirical rate constant k obeys an Arrhenius relationship, as displayed in Fig. 4.4.b, with an apparent activation energy E_a = 54.7 kJ/mol.

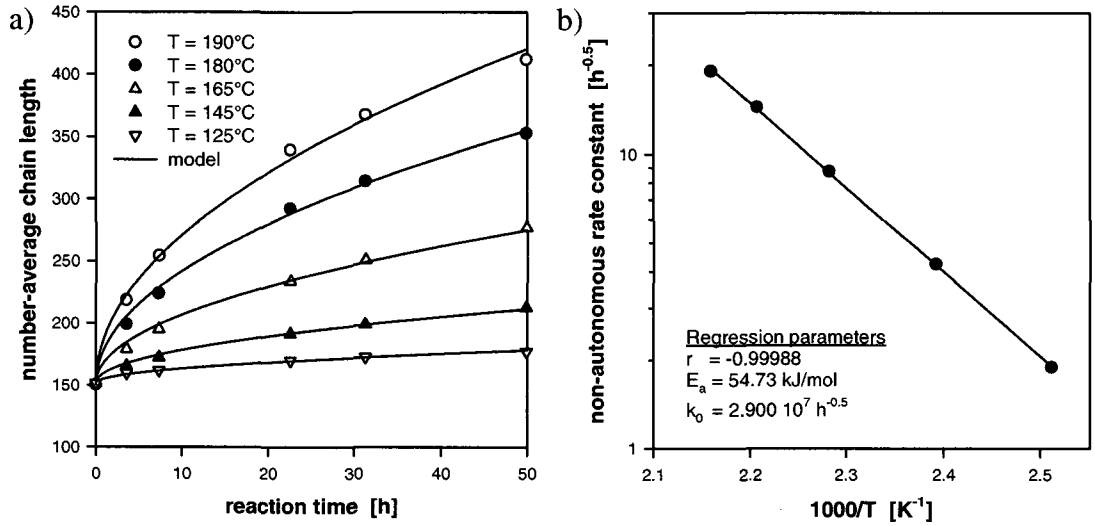

Figure 4.4 Effect of temperature and application of a non-autonomous model $dDP_n/dt = kt^n$. a) Polymerization profiles for different values of T with other experimental conditions from base case (Table 3.1) ; b) Arrhenius diagram for the empirical rate constant k

It is instructive to make a comparison with apparent energies of activation found elsewhere (Table 4.1). Quite surprisingly, an excellent agreement is observed between our data and the values of E_a reported by Matsuda *et al.* [12] for PA6, Griskey and Lee [8] for PA66, and Chen *et al.* [9] for PA6-10, although the solid state data from two of these sources [9, 12] were obtained by using rate functions different than the one of the present work. The fact that E_a is not sensitive to the type of nylon is consistent with chemical reaction being the controlling step, since the same amidation reaction is involved in the chain building of all polyamides. In addition, the single data out of range in Table 4.1 is the one by Gaymans *et al.* [6] for SSP of PA6 in powder form. This, again, bears out our assumption of a diffusion limitation due to polymer skinning in Gaymans' data (Section 2.3.3).

Table 4.1 Apparent activation energies for SSP of nylons

Polymer	E_a [J/mol]	Source
Polyamide-6	54,700	This work
Polyamide-6	53,100	Matsuda *et al.* [12]
Polyamide-6	105,000	Gaymans *et al.* [6]
Polyamide-6,6	54,300	Griskey and Lee [8]
Polyamide-6,10	55,300	Chen *et al.* [9]

Empirical rate functions like Eq. (4.2) reflect no theoretical understanding of the process. Therefore, such non-autonomous models are suitable for interpolation, but cannot be used to make predictions outside the range of experiments. Furthermore, an empirical model is difficult to scale up and implement in a simulator. For these reasons, a phenomenological approach based on the analysis of the reaction scheme is preferred (Chapter 6).

High reaction temperatures are also beneficial with regard to the formation of caprolactam and cyclic dimer (Figure 4.5). The remonomerization profiles (Fig. 4.5.a) pass through a maximum, with a peak value that seems to be higher and located earlier with increasing temperature. This must arise from a complex interplay between reaction and diffusion. Indeed, the rate of cyclization is proportional to the concentration of amine groups [13], which are consumed upon polymerization. Hence, remonomerization dominates diffusion in the early stage of SSP, and caprolactam is regenerated. Then, the end-groups are depleted to such an extent by polycondensation that cyclization is slowed down, and the diffusional removal of caprolactam becomes the dominant mechanism. Because the rates of cyclization, polycondensation, and diffusion all increase with temperature, the effect is more pronounced for high values of T, leading to sharper concentration profiles.

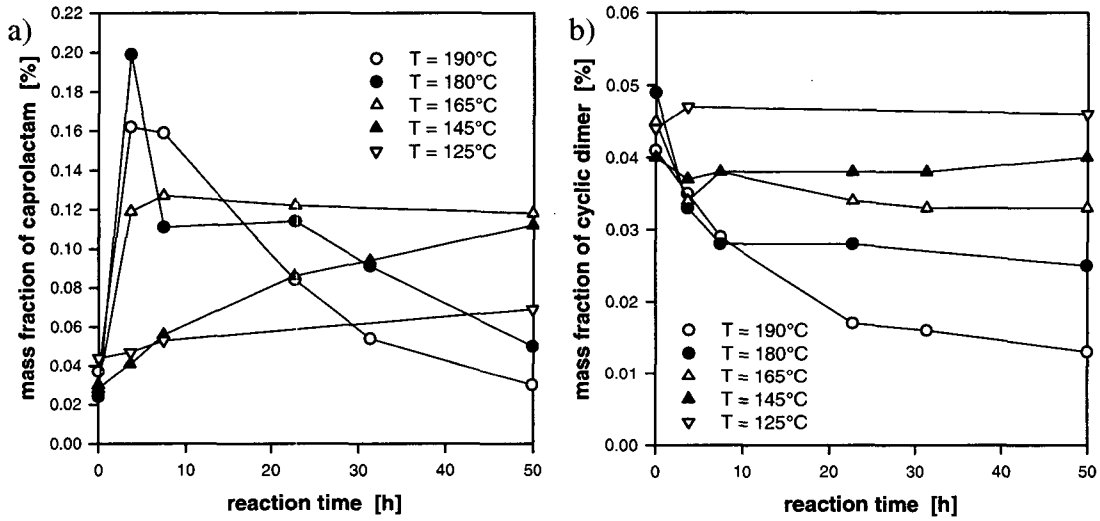

Figure 4.5 Effect of reaction temperature on : a) Remonomerization profile ; b) Cyclic dimer profile. Other experimental conditions from base case (Table 3.1)

The concentration profiles of the cyclic dimer C_2 (Fig. 4.5.b) do not exhibit such abrupt changes as for caprolactam. Three reasons can be mentioned for that. First, the cyclic dimer is close to equilibrium [4], whereas the equilibrium value of caprolactam is about 1-2 % [14], i.e. far above the curves in Fig. 4.5.a. Hence, the driving force for chemical reaction is reduced in the former case. Second, the intramolecular interchange reaction has a higher probability to yield a small cyclic molecule than a large one, so the rate constant is smaller in the case of the dimer [4]. Third, diffusion is also expected to be slower because of the larger size of the dimer molecule. In fact, Fig. 4.5.b indicates that diffusion dominates reaction, particularly at high temperature.

It is worth noting that the concentration profiles in Fig. 4.5 are controlled by the kinetics (of reaction and diffusion), not by equilibrium. This is evidenced by the fact

that the smallest values of C_1 and C_2 after 50 h of SSP are obtained for the highest temperature (190°C), although both cyclization reactions are endothermic [15].

The above observations are consistent with disclosures in patents that a higher operating temperature enhances the removal of extractables from solid nylon-6 granules [2, 3]. However, the effect of temperature on the vapor-liquid equilibrium must also be considered for integral reactors.

4.4 Effect of Extraction Step

In order to assess the influence of the extraction step on solid-state polymerization, an experiment was conducted with an unextracted nylon-6 prepolymer. This is of interest because the hot water leaching of the granules is energy intensive, and any economical optimization of the manufacture process should consider it. In particular, the determination of optimal temperature and residence time in the extractor cannot be treated independently of the postcondensation stage, because of remonomerization taking place during SSP.

The unextracted sample had initial equilibrium values of $w_{C1,0} = 10.1$ % and $w_{C2,0} = 0.46$ %, compared to $w_{C1,0} = 0.029$ % and $w_{C2,0} = 0.045$ % for the extracted material (base case). As shown in Figure 4.6.a, the granules that were not subjected to extraction polymerize at a slower rate, which is in accord with Kjellmark's [16] results on an industrial solid-phase polymerizer.

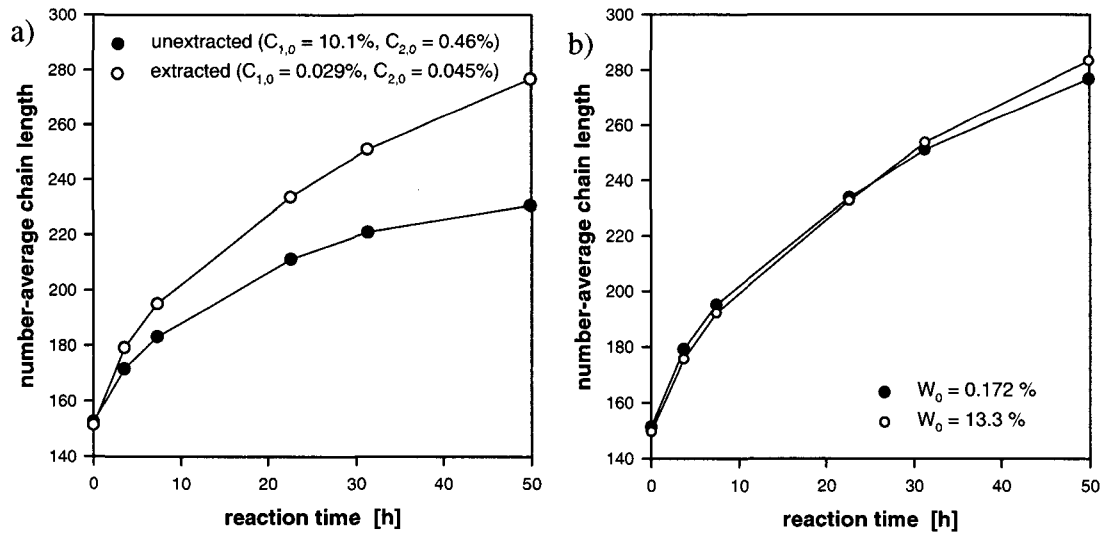

Figure 4.6 Solid-state polymerization profiles. a) Effect of extraction step ; b) Effect of initial water content. Other experimental conditions from base case (Table 3.1)

Hence, the extraction step is found to favorably affect SSP – in addition to removing the undesired cyclic species – by increasing the rate of polymer build-up. This could arise from a lower initial crystallinity due to the disturbing effect of large amounts of caprolactam on the crystal structure (we shall see in Chapter 5 that some crystallization takes place during extraction), or to the decrease of the amorphous density upon concentration of the monomer into the amorphous phase – see Eq. (2.6). Note that the polymerization profile for the unextracted polymer in Fig. 4.6.a was calculated directly from the titration of amine groups, not via the viscometric

measurement. This is because the cyclic species strongly influence the rheological solution properties [17], so that the correlation for the relative viscosity, Eq. (3.7), is untrustworthy in this case.

In the experimental procedure used so far, the prepolymer was dried before SSP. In a typical industrial process, on the contrary, the granules leaving the extractor and fed into the finisher are saturated with water [18]. Therefore, some nylon granules were soaked in distilled water for five days at ambient temperature before being subjected to SSP. The initial water content was $w_{W0} = 13.3$ %, comparatively to $w_{W0} = 0.172$ % in the base case. The pretreatment did not change the crystallinity. As a result, no influence of the initial water content on the polymerization profile was observed (Fig. 4.6.b), in agreement with the calculation in Section 2.4 of a much larger time scale for hydrolysis than for the diffusion of water. Again, this emphasizes that polycondensation in a differential SSP reactor is virtually irreversible. In an industrial column, however, there can be a substantial loading of the gas phase with water, so that the extent of reaction is governed by the vapor-liquid equilibrium. For this reason, the upper part of the solid-state reactor, sometimes referred to as the *dryer*, is usually operated under a higher flow rate of purge gas by means of a recycle loop.

In the experiment with an unextracted prepolymer, a white substance was found to crystallize in the outlet tubing of the reactors, that yielded a sharp endothermic peak at 69°C upon DSC analysis, characteristic for the melting of caprolactam. It was not possible to check for the presence of the cyclic dimer ($T_m = 347$°C [19]) due to the boiling of caprolactam at 270°C. Nonetheless, both caprolactam and the cyclic dimer will be treated as volatile species in the kinetic model.

The influence of the extraction step on the evolution of caprolactam and the cyclic dimer during postcondensation are reported in Figure 4.7. Clearly, the feasibility of a process without intermediate removal of extractables depends on the specification for the quality of the end-product. In case of an integral reactor, an economical balance between the cost of extraction and the additional need for purge gas should also be considered.

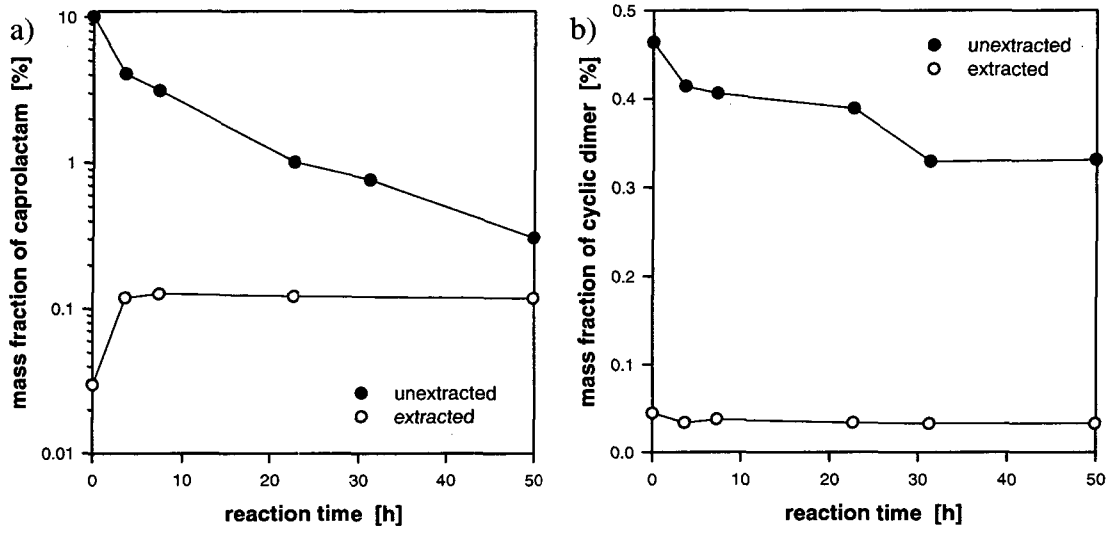

Figure 4.7 Effect of extraction step on : a) Caprolactam profile ; b) Cyclic dimer profile. Other experimental conditions from base case (Table 3.1)

4.6 References

[1] Beaton D.H. (1974). Continuous, solid-phase polymerization of polyamide granules. *U.S. patent 3,821,171 to DuPont.*

[2] Blanchard E.N., Cohen J.D., Iwasyk J.M., Marks D.N., Stouffer J.M., Aslop A.W. and Lin C. (1999). Process for preparing polyamides. *World patent 99/10408 to DuPont.*

[3] Pipper G. and Cordes C. (1989). Removal of caprolactam and oligomers thereof from nylon granules containing same. *U.S. patent 4,816,557 to BASF.*

[4] Arai Y., Tai K., Teranishi H. and Tagawa T. (1981). Kinetics of hydrolytic polymerization of ε-caprolactam. III. Formation of cyclic dimer. *Polymer*, 22, 273.

[5] Mallon F.K. (1997). Solid state polycondensation : modelling and productivity enhancements. Thesis, University of Wisconsin-Madison.

[6] Gaymans R.J., Amirtharaj J. and Kamp H. (1982). Nylon 6 polymerization in the solid state. *J. Appl. Polym. Sci.*, 27, 2513.

[7] Wu D., Chen F., Li R. and Shi Y. (1997). Reaction kinetics and simulations for solid-state polymerization of poly(ethylene terephthalate). *Macromol.*, 30, 6737.

[8] Griskey R.G. and Lee B.I. (1966). Thermally induced solid-state polymerization in nylon 66. *J. Appl. Polym. Sci.*, 10, 105.

[9] Chen F.C., Griskey R.G. and Beyer G.H. (1969). Thermally induced solid state polycondensation of nylon 66, nylon 6-10 and polyethylene terephtalate. *AIChE J.*, 15, 680.

[10] Walas S.M. (1959). Reaction kinetics for chemical engineers. McGraw-Hill pub., New York, 127.

[11] Harrison L.G. (1969). The theory of solid phase kinetics. In: Chemical kinetics, 2, Bamford C.H. and Tipper C.F.H. eds., Elsevier pub., 377.

[12] Matsuda Y., Marusawa H., Cyuayo K. and Sakakibara K. (1960). *Kobunshi Kagaku*, 17, 413.

[13] Reimschuessel H.K. and Nagasubramanian K. (1972). On the re-equilibration of nylon 6. *Polym. Eng. Sci.*, 12, 179.

[14] Cawthon T.M. and Smith E.C. (1960). Polymerization and depolymerization of nylon 6 above and below its melting point. *Polymer Preprints*, 1, 98.

[15] Tai K. and Tagawa T. (1983). Simulation of hydrolytic polymerization of ε-caprolactam in various reactors. A review on recent advances in reaction engineering of polymerization. *Ind. Eng. Chem. Prod. Res. Dev.*, 22, 192.

[16] Kjellmark E.W. (1962). Increasing viscosity of polycaprolactam by removing extractables with solvents and further solid phase polymerizing the polymer. *US patent 3,015,651 to DuPont.*

[17] Aharoni S.M. (1997). *n*-nylons: their synthesis, structure and properties. Wiley pub.

[18] Kohan M.I. (1986). The history and development of nylon-66. In : High performance polymers : their origin and development, Seymour R.B. and Kirshenbaum G.S. eds., Elsevier pub., New York.

[19] Hermans P.H. (1956). Constitution of the cyclic polyamides isolated from nylon 6 polymers. *Nature*, 177, 126.

5. Structural Investigation

This chapter reports on the experimental characterization of the morphology of the solid nylon-6 granules subjected to solid-state polymerization. The techniques used were wide-angle X-ray diffraction, differential scanning calorimetry, and polarized light microscopy. A detailed description of the analytical procedures is in Section 3.4.

5.1 Determination of the Crystallinity

Given the expected effect of semicrystallinity on SSP (Section 2.2), the crystalline mass fraction w_c appears as the major structural parameter of interest in the formulation of a kinetic model. Values of w_c have been determined by DSC for the SSP runs performed at different temperatures in the battery of fixed-bed reactors (Figure 5.1). The crystallinity was assessed for each reaction time at $T = 165$ and 190°C, whereas data were recorded for $t = 0$, 3.62 and 50 h only for the other reaction temperatures.

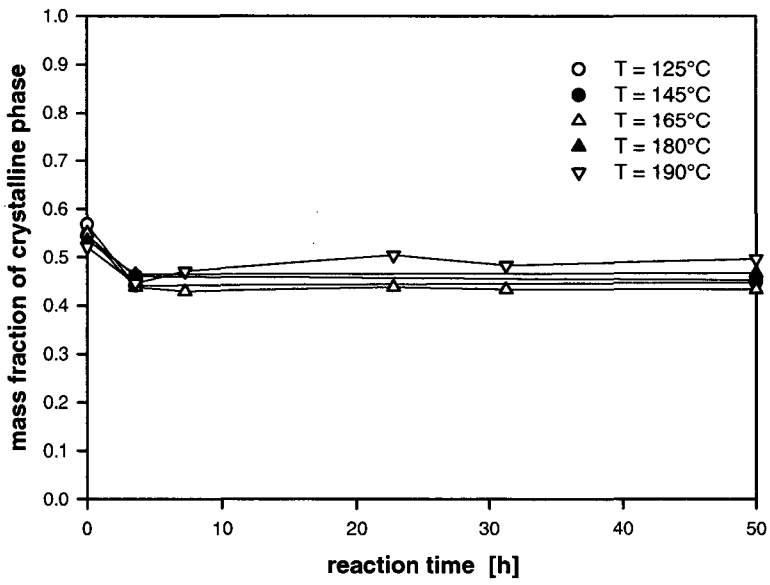

Figure 5.1 Evolution of crystallinity during solid-state polymerization of nylon-6 (DSC measurement)

The crystallinity does not vary during SSP (except for $t = 0$, which will be discussed in the next paragraph). This agrees with the observation of Starkweather *et al.* [1] that rapidly quenched PA66 films subjected to isothermal annealing reach a constant crystallinity after about 10 minutes. Moreover, Srinivasan *et al.* [2] observed the crystallinity of PA66 fibers to remain approximately unchanged during SSP. Therefore, w_c will be treated as a constant parameter in the kinetic model. By contrast, PET exhibits a much slower secondary crystallization [3, 4] and any realistic SSP

model requires coupling an equation for the crystallization (e.g. Avrami) to the set of population-balance equations [5]. Although the values of w_c are systematically higher for $T = 190°C$ than for 165°C, no definite influence of the reaction temperature can be ascertained from Fig. 5.1. The crystallinity is similar for all temperatures given the experimental accuracy of ± 0.05 (Section 3.4). The average value of $w_c = 0.456$ is taken as the reference value for the modeling.

The observed reduction in crystallinity from $w_c \sim 0.55$ to 0.45 between $t = 0$ and 3.62 h is puzzling, since it also occurs for the lowest temperature (125°C). Indeed, it seems unconceivable that small metastable crystallites already melt at this temperature since the onset of the DSC endotherm (the softening point) is at about 165°C. To clarify this point, a prepolymer granule was brought to reaction temperature (165°C) in the calorimeter and then immediately cooled to room temperature, with heat-up and cool-down times similar to those in the fixed-bed reactor. A subsequent ramp to 280°C at 20°C/min then yielded the normal value of w_c. In addition, the effect did not show up when w_c was estimated by WAXD. Consequently, the higher initial values in Fig. 5.1 were considered as an artifact and disregarded.

5.2 Morphology during Solid-State Polymerization

The values of some structural parameters during solid-state polymerization of PA6 are compiled in Table 5.1. The morphology appears to be frozen during SSP since all parameters, not only w_c, remain practically unchanged. Therefore, a potential improvement of the polymer structure with regard to SSP performance should infer from an optimization of the prior steps : solidification, granulation, and extraction. Particularly interesting would be an increased crystallinity, given the enhancement effect theorized in Section 2.2.2 and experimentally evidenced in Section 4.2 (by contrast, a high w_c slows down the SSP of PET [3] because the diffusion effect dominates due to the low equilibrium constant).

Table 5.1 Evolution of solid structure during PA6 solid-state polymerization*

Reaction time [h]	w_c [%]	$\Lambda\alpha_{200}$ [nm]	$\Delta 2\theta_\alpha$ [°]	γ/α [-]	T_m [°C]	T_{cc} [°C]	T_c [°C]
0	47	11.9	3.78	0.08	224	190	158
3.62	48	11.9	3.74	0.10	223	188	156
50.0	45	12.2	3.76	0.08	221	188	154

* see Section 2.4 for the definition of all the variables

The polymer strand exiting the VK column is quenched in a water bath (Fig. 1.4), which should result in a rather low crystallinity. For example, Srinivasan *et al.* [2] found $w_c = 0.25$ for as-extruded PA66 fibers. As the crystalline phase is the thermodynamically stable form below T_m, it would make sense to cool the molten prepolymer at a slower pace to attempt to reach a higher w_c. This suggestion is borne out by a recent DuPont patent [6], which claims to achieve SSP operating advantages when the solidification step is carefully controlled. The authors ascribed this benefit to a higher softening point, but their treatment might increase w_c as well, as we shall see in Section 6.4.4. An additional indication of the metastable nature of the morphology obtained upon quenching is the significant amount of the less stable γ crystalline modification [7]. By contrast, the ratio γ/α is rather low during SSP, so a γ-

to-α transformation must have taken place during the extraction step. This may be due to a facilitating reorganization mechanism provided by the water molecules, which are able to disrupt interchain hydrogen bonds. It would be consistent with Starkweather's [1] observation that moisture effects a further increase in crystallinity of a PA66 sample over that produced by dry heat. Certainly, the structural changes that are expected to take place upon extraction are also linked to the removal of the ~ 10 % of equilibrium caprolactam. This is evidenced by the shift of T_m during SSP of unextracted granules (Figure 5.2), which parallels the decrease of caprolactam (Fig. 4.7.a). Nevertheless, the expected influence of the extraction step may offer some new prospect to improve the polymer structure.

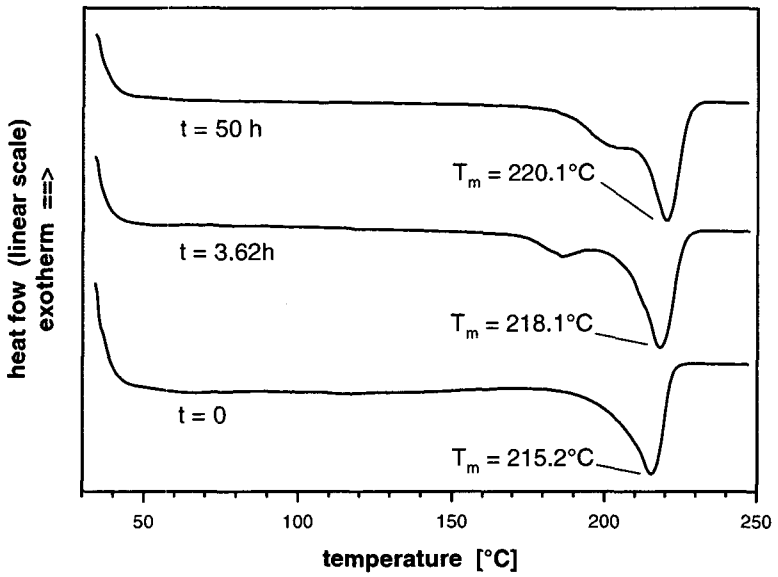

Figure 5.2 DSC melting endotherms during solid-state polymerization of unextracted nylon-6 granules. The position of the peak value is shifted to a higher temperature as the caprolactam content decreases

The lateral size of the α crystallite is approximately constant during solid-state polymerization ($\Lambda\alpha_{200}$ ~ 12 nm). This is of interest for the assessment of the kinetics dimensionality (Section 2.2.3), and for a refined SSP model that will be formulated in Section 6.3.1.

5.3 Polarized Light Microscopy

In Figure 5.3 are shown four sequences of photomicrographs taken at various stages of the process : before and after extraction, and after t = 3.62 and 50 h of solid-state polymerization of an extracted sample. In all cases, the largest part of the polymer is finely crystallized, giving rise to no superstructure. The orientations of the lamellae are random and there is no contrast in the PLM picture (dark background). The absence of a spherulitic texture backs up the idea of a frozen microstructure formed upon quenching the molten prepolymer. This blocked morphology would then hinder a subsequent growth of crystalline superstructures. Indeed, the operating SSP temperatures correspond to spherulite growth rates of typically 10 to 500 μm/min [8]. In other words, the granules should be entirely filled with large spherulites if the thermal and mechanical histories were not so drastic. This can be achieved in the carefully controlled environment of slow crystallization on a microscope slide (hot stage PLM) [9].

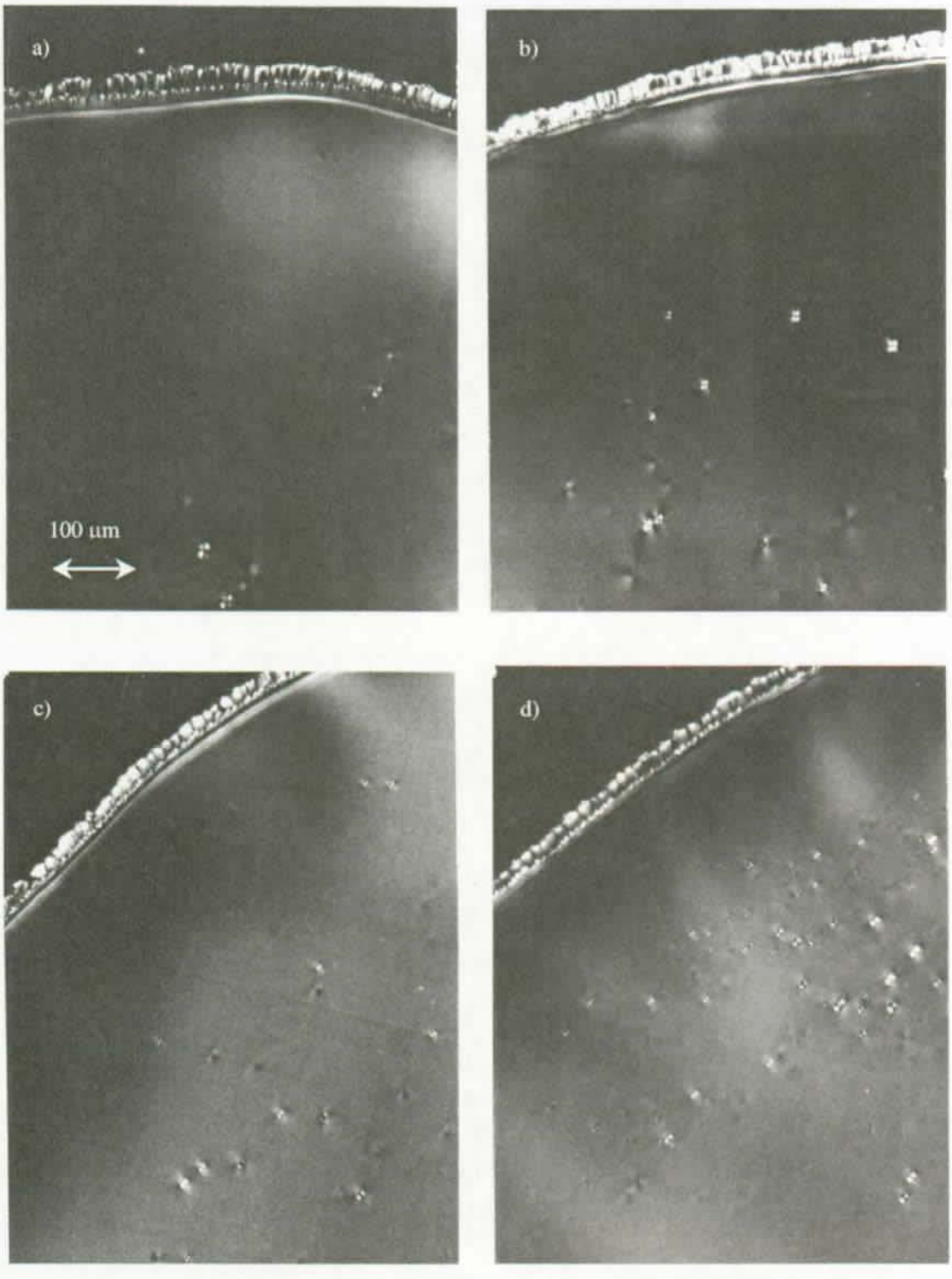

Figure 5.3 Optical micrographs of a nylon-6 granule during solid-state polymerization at 165°C. a) Initial material before extraction ; b) Initial material after extraction ; c) Extracted sample after 3.62 hours of SSP ; d) Extracted sample after 50 hours of SSP

Some isolated spherulites showing simple extinction crosses under the polarizing microscope (Maltese cross) are nonetheless visible within the granule. Their concentration and size both increase during SSP (Table 5.2), although they always fill a negligible portion of the chip volume.

Table 5.2 Estimated average size of the spherulites

Situation after...	Estimated spherulitic diameter [μm]
Extraction	6 - 8
SSP for 3.6 hours at T = 165°C	10 - 14
SSP for 50 hours at T = 190°C	18 - 24

Another interesting feature is the occurrence at the surface of a rough crystalline skin, 40 to 50 μm thick, made of pillar-shape superstructures grown from the outside to the inside. We suggest that this structure is formed by mechanical-induced crystallization in the extruder (because of the shear stress at the extruder wall). This idea is supported by the fact that the skin arises only on the conical surface of the granule, not on the cross sections. In addition, the skin is already present before extraction (Fig. 5.3.a) and is not affected by the subsequent treatments.

In summary, the semicrystalline morphology is essentially constant during solid-state polymerization. Although the crystalline phase is thermodynamically more stable than the amorphous phase (a supercooled melt) in the temperature range inside which solid-state reactors are operated, a maximal crystallinity of about 45 % is observed in commercial nylon-6 granules processed in the solid-state. Therefore, potential possibilities to increase the crystallinity and enhance the reaction should lie in the stages of the manufacture process where the microstructure is formed : cool-down from the melt, granulation, and hot water extraction.

5.4 References

[1] Starkweather H.W., Moore G.E., Hansen J.E., Roder T.M. and Brooks R.E. (1956). Effect of crystallinity on the properties of nylons. *J. Polym. Sci.*, 21, 189.

[2] Srinivasan R., Almonacil C., Narayan S., Desai P. and Abhiraman A.S. (1998). Mechanism, kinetics and potential morphological consequences of solid-state polymerization. *Macromol.*, 31, 6813.

[3] Chang T.M. (1970). Kinetics of thermally induced solid state polycondensation of poly(ethylene terephthalate). *Polym. Eng. Sci.*, 10, 364.

[4] Jabarin S.A. (1987). Crystallization kinetics of polyethylene terephthalate. I. Isothermal crystallization from the melt. *J. Appl. Polym. Sci.*, 34, 85.

[5] Mallon F.K. and Ray W.H. (1998). Modeling of solid-state polycondensation. I. Particle models. *J. Appl. Polym. Sci.*, 69, 1233.

[6] Blanchard E.N., Cohen J.D., Iwasyk J.M., Marks D.N., Stouffer J.M., Aslop A.W. and Lin C. (1999). Process for preparing polyamides. *World patent 99/10408 to DuPont.*

[7] Aharoni S.M. (1997). *n*-nylons: their synthesis, structure and properties. Wiley pub.

[8] Schreiber S. and Philipps P.J. (1997). Crystallization of copolymers based on nylon 66. *Annu. Tech. Conf. – Soc. Plast. Eng.*, 55, 1872.

[9] Ramesh C., Keller A. and Eltink S.J.E.A. (1994). Studies on the crystallization and melting of nylon 66: 2. Crystallization behavior and spherulitic morphology by optical microscopy. *Polymer*, 35, 5293.

6. Single Particle Model

A comprehensive kinetic model is developed here to handle the polymerization of nylon-6 in the solid state at particle scale. First, an overview of the different mathematical techniques that are available to compute the chain length distribution from the reaction scheme are discussed. Second, the solid-state model is formulated, based on both the theoretical arguments presented in Chapter 2 and the experimental results from Chapters 4 and 5. The model versatility is then illustrated by simulating the hydrolytic polymerization of caprolactam in a batch isothermal reactor. Next, literature reports dealing with SSP of PA6 are reexamined in the light of the propounded model. Finally, its performance with regard to the data from the battery of fixed-bed reactors is assessed.

6.1 Kinetic Modeling in Polymer Reaction Engineering

Historically, batch polymerization problems were initially treated using statistical or probabilistic methods, which view chain growth as a stochastic process having possible states resulting from the kinetic mechanism and state transition probabilities dependent on the kinetic parameters. In fact, this was the predominant approach when the concept of polymer reaction engineering started to develop in the forties, with the pioneering works of Kuhn [1], Schulz [2], and Flory [3-5]. Laurence *et al.* [6] classified the statistical methods into three categories: direct, formal Markov chain theory, and recursive approaches. Lowry [7], in an excellent book, showed how it is possible to combine the various probabilities of reaction in a Markov chain transition matrix and then obtain the CLD and its moments by matrix manipulation.

Statistical approaches have the advantages of simplicity and directness in some cases, as well as occasionally revealing certain characteristics of the polymerization process which is marked by a purely deterministic treatment. On the other hand, statistical techniques frequently do not work explicitly in terms of time as a variable, which is a drawback since one usually wishes to make predictions as a function of time. A further disadvantage of statistical methods is that they rely heavily on intuition, making them unworkable for complex reaction schemes. For this reason, a probabilistic approach will not be used in this study.

The deterministic alternative consists in writing the population-balance equations explicitly for the kinetic mechanism under consideration, leading to a set of usually highly non-linear and coupled differential equations governing the evolution of the concentration of polymers with a given chain length : P_1, P_2, ..., P_i, ... In case of depolymerization processes, the equations can be solved directly, usually by numerical means, to yield the entire CLD. Examples include the treatment by Basedow *et al.* [8] of the acid hydrolysis of dextran as well as our own work on the fragmentation kinetics of mannan [9]. However, a difficulty arises for polymerization

processes because the equations form an infinite set in this case. A possibility is to solve an arbitrarily large number, say N, of these equations such that the concentration of P_N is close to zero. Nonetheless, some truncation error is introduced in the repeat count variable because higher chain length species are neglected. This method was used by Gupta *et al.* [10] to track the CLD during the hydrolytic polymerization of caprolactam in a batch isothermal reactor. The technique may be quite burdensome: these authors, by numerical integration of the first 750 equations, needed 5 hours of computing time to simulate 8 hours of polymerization.

A mathematical technique suitable to solve the infinite set of population-balance equations is to make use of the generating function defined as

$$G(s,t)=\sum_{n=1}^{+\infty} s^n P_n \tag{6.1}$$

where s is a dummy variable less than one. Using Eq. (6.1), the infinite set of equations can be collapsed into a single one which can, in turn, be easily solved for $G(s,t)$; then, the inverse transformation determines the entire CLD [11, 12]. An example of the application of the generating function to the polymerization of caprolactam is provided by Tirrell *et al.* [13]. Alternatively, the Z-transform can be applied, which is defined as

$$Z(z,t)=\sum_{n=1}^{+\infty} z^{-n} P_n \tag{6.2}$$

where z is an arbitrary variable whose absolute value is larger than or equal to one [11, 12]. By comparing with Eq. (6.1), it appears that the generating function and the Z-transform techniques are identical if one recognizes the mapping of $s=z^{-1}$. Nonetheless, one possible advantage of Z-transforms over the generating function is the existence of more extensive tables of the Z-transform and inverses. An example of the application of the Z-transform to the hydrolytic polymerization of caprolactam is given by Gupta *et al.* [14] for a three-stage reactor with intermediate removal of water.

Still another transform than the discrete methods cited above is the continuous-variable approximation. Here, an attempt is made to replace the infinite set of population-balance equations (ordinary differential equations for a well-mixed reactor) by a single partial differential equation. This is done by defining a continuous variable, $P(n, t)$, of chain length n as well as time t, whose variation with respect to n and t are governed by the mechanism of polymerization. For instance, for the following simplified mechanism for chain-growth polymerization,

$$P_n + M \rightarrow P_{n+1} \tag{6.3}$$

a $P(n\text{-}1, t)$ term arises from the balance equation, which can be expanded in a Taylor series about $P(n, t)$. The accuracy of the approximation was shown to depend strongly on the number of terms retained in the expansion [11]. The partial differential equation must then be solved to produce $P(n, t)$. Miller *et al.* [15] have solved a number of systems by using Laplace transforms, while Zeman and Amundson

[16, 17] have treated a large number of examples by direct numerical integration of the partial differential equation. Obviously, making the discrete chain length increment $\Delta n = 1$ tending toward the infinitesimal value dn holds only for long chains, and can lead to absurd results such as relaxation of the invariance of mass, when misused in systems comprising large amounts of monomer [18]. From this viewpoint, the continuous variable approximation could look like an appropriate technique to track the CLD in SSP, since the polymer chains are already typically more than 100 units long before reaction. However, step growth polymerization cannot be described by the successive addition of the monomer as postulated in Eq. (6.3), and this method is virtually useless for this mechanism of polymerization.

The mathematical techniques discussed so far become less tractable for complex reaction schemes as the one for PA6. In addition, it may be somewhat awkward to use the full CLD to represent the state of the reacting polymer for on-line quality control purposes, for instance. Therefore, we shall use, in this work, the leading moments of the CLD to represent the state of the polymer, and assume that the CLD is adequately described by these moments. While this representation only uniquely defines average quantities (e.g., average chain length, breadth of the distribution, and degree of asymmetry), the description is usually a good one for most applications. In fact, Ray [11] demonstrated that there are a number of cases where these averages uniquely define the CLD. For example, the living polymerization mechanism of Eq. (6.3) in a batch reactor leads to a Poisson CLD that is uniquely described by only one moment.

The kth unnormalized moment of the CLD is defined by

$$\lambda_k = \sum_{n=1}^{+\infty} n^k P_n \tag{6.4}$$

Some of the moments have a physical significance. For instance, λ_0 is the total polymer concentration, while λ_1 is the concentration of repeat units. A useful relation is the concentration of bonds, expressed as

$$\sum_{n=1}^{+\infty}(n-1)P_n = \sum_{n=1}^{+\infty} n P_n - \sum_{n=1}^{+\infty} P_n = \lambda_1 - \lambda_0 \tag{6.5}$$

because a P_n molecule is made of n repeat units linked by (n-1) bonds. The number-average chain length is written as

$$DP_n = \frac{\lambda_1}{\lambda_0} \tag{6.6}$$

whereas the mass-average chain length is readily obtained as

$$DP_w = \sum_{n=1}^{+\infty} n\, w_n = \sum_{n=1}^{+\infty} n \frac{n P_n}{\lambda_1} = \frac{\lambda_2}{\lambda_1} \tag{6.7}$$

The variance of the CLD is given by the second moment about the mean

$$\sigma_n^2 = \frac{\sum_{n=1}^{+\infty}(n - DP_n)^2 P_n}{\sum_{n=1}^{+\infty} P_n} = \frac{\lambda_2}{\lambda_0} - \left(\frac{\lambda_1}{\lambda_0}\right)^2 \tag{6.8}$$

However, a more commonly employed measure of the breadth of the CLD is the polydispersity index defined as

$$PDI = \frac{DP_w}{DP_n} \tag{6.9}$$

which is related to the variance by

$$PDI = 1 + \frac{\sigma_n^2}{DP_n^2} \tag{6.10}$$

Population-balance equations are then replaced by moment-balance equations. As we shall restrict ourselves to the first three moments (λ_0, λ_1 and λ_2), this means that the concentrations of hundreds of individual chain lengths are condensed to just three equations, from which the most useful properties for the polymer can be calculated. Hence, the method of moments reduces the number of equations to a tractable set, thus leading to substantial savings of computer time. The moment-balance equations may be derived either by multiplying the equation for P_n by n^k and summing over all terms, or by using the generating function formalism and differentiate them using [6]

$$\lambda_k = \left(\frac{\partial^k G(s)}{\partial (ln\ s)^k}\right)_{s \to 1} \tag{6.11}$$

A problem arising from the reversibility of polycondensation is that the set of moment equations is not closed. This means that the rate equation for λ_2 involves λ_3, which implies that λ_2 cannot be determined unless a suitable equation for λ_3 is established. If a similar relation for λ_3 is written, it would be found to involve λ_4, and so on, thus forming a hierarchy of equations to be solved [12]. Hence a moment closure approximation must be made, which consists in assuming the value for the k+1th moment and using that information to calculate the derivatives for the kth moment. In this study, we shall make use of the Schulz-Zimm equation to calculate λ_3 [14, 19] :

$$\lambda_3 \cong \frac{\lambda_2 \left(2\lambda_2 \lambda_0 - \lambda_1^2\right)}{\lambda_1 \lambda_0} \tag{6.12}$$

Gupta and Kumar [20] have shown that the exact assumption for the moment closure has very little impact on the simulation results. This means that any errors introduced through Eq. (6.12) is of little consequence and do not noticeably constraint the applicability of the moment technique.

6.2 Model Formulation

6.2.1 Basic Solid-State Assumptions

Based on the considerations in Chapter 2 and the experimental data in Chapters 4 and 5, the basic assumptions of the solid-state model are formulated as follows :

- Reaction occurs only in the amorphous phase of the semicrystalline polymer (Section 2.2.2).

- The chemistry in the amorphous phase is extrapolated from the melt, without any kinetic limitation due to the diffusion of polymer chains, i.e. no gel effect takes place (Section 2.3). In addition, the intrinsic kinetics is not constrained by the micromorphology (Section 2.2.3).

- The reactive species are concentrated in the amorphous phase (with the exception of the amide bonds) ; chemical equilibria and reaction rates must therefore be expressed as a function of local concentrations (Section 2.2.2) :

$$c^* = c\,\frac{P\left(1-w_c\right)+w_c}{P\left(1-w_c\right)} \tag{2.11}$$

- The crystallinity is constant during solid-state polymerization (Section 5.2).

- Water exists in a single thermodynamic state. No distinction is made between "free" and "adsorbed" water (Section 2.2.4).

- Chemical species are separated between volatile and non-volatile states. The volatile compounds that diffuse within the particle are water, caprolactam, and the cyclic dimer (Section 4.4).

- The diffusion coefficients of volatile species are proportional to the amorphous content (Section 2.2.4) :

$$D_i = D_{i,0}\left(1-v_c\right) \tag{2.22}$$

- The resistance to mass transfer by convection in the gas phase is negligible (Section 4.1).

- In case of a non-zero concentration of volatiles in the gas phase, the vapor-liquid equilibrium at the polymer/gas interface is governed by Flory-Huggins thermodynamics :

$$p_i = p_i^0\, w_i^*\, exp\left(1+\chi_i\right) \tag{6.13}$$

where p_i, p_i^0, and χ_i stand respectively for the partial pressure, the pure vapor pressure, and the interaction parameter of component *i*. For convenience, the

volume fraction has been replaced by the mass fraction w_i^* (local value !) as suggested by Merrill [21].

- The gas phase is ideal and non-reactive.
- Multicomponent effects on diffusion and phase equilibria are neglected.
- The volume of the particle does not change upon SSP. This holds because crystallinity is constant and mass loss due to volatilization is excessively small for an unextracted material (Section 2.4).
- The polymer particle is isothermal (Section 2.4).

6.2.2 A Detailed Reaction Scheme

The major reactions involved in the chemistry of nylon-6 are recalled from Chapter 1,

$$C_1 + W = P_1 \tag{1.1}$$

$$P_n + P_m = P_{n+m} + W \qquad n,m = 1,2,... \tag{1.2}$$

$$P_n + C_1 = P_{n+1} \qquad n = 1,2,... \tag{1.3}$$

where Eq. (1.1) represents ring opening, Eq. (1.2) polycondensation, and Eq. (1.3) polyaddition. Here, we shall extend this kinetic scheme by considering reactions with the cyclic dimer C_2, and the possible existence of monofunctional compounds. Indeed, monofunctional acids may be added to the feed of caprolactam to control the chain length of the polymer formed, or to increase the rate of polymerization. For instance, propionic acid is sometimes employed as a chain regulator in the industrial process [22]. A monoacid chain of length i will be denoted by the symbol Q_i. In addition, polymer chains bearing a single amine moiety as a reactive group are also present due to decarboxylation occurring to some extent in the VK column (see Section 3.3). A monoamine chain of length i will be denoted by the symbol R_i. Finally, the possible existence of polymer chains with no functionality, which can result from the condensation of a monoamine with a monoacid, are also taken into account for sake of completeness. Such a dead chain of length i will be denoted by the symbol S_i. The various chemical species involved in the chemistry of PA6 are listed in Table 6.1.

Table 6.1 Different populations of species in nylon-6 chemistry

Name	Symbol	Formula
Bifunctional chains	P_i	H-[NH-(CH_2)$_5$-CO]$_i$-OH
Monofunctional acid chains *	Q_i	X-[NH-(CH_2)$_5$-CO]$_i$-OH
Monofunctional amine chains *	R_i	H-[NH-(CH_2)$_5$-CO]$_i$-X
Dead chains *	S_i	X-[NH-(CH_2)$_5$-CO]$_i$-X
Cyclic species	C_i	
Condensate	W	H_2O

* X denotes a non-reactive group

We can now write the various elementary reactions taking place in the solid granules, including reactions with the cyclic dimer and the chains with a functionality of less than two. The resulting reaction scheme is disclosed in Table 6.2.

Table 6.2 A detailed reaction scheme for nylon-6 SSP

1.Ring opening

$$C_1 + W \underset{k_1'}{\overset{k_1}{\rightleftarrows}} P_1 \tag{6.14}$$

2. Polycondensation

$$P_n + P_m \underset{2k_2'}{\overset{2k_2}{\rightleftarrows}} P_{n+m} + W \quad n,m = 1,2,... \tag{6.15}$$

$$P_n + Q_m \underset{k_2'}{\overset{k_2}{\rightleftarrows}} Q_{n+m} + W \quad n,m = 1,2,... \tag{6.16}$$

$$P_n + R_m \underset{k_2'}{\overset{k_2}{\rightleftarrows}} R_{n+m} + W \quad n,m = 1,2,... \tag{6.17}$$

$$Q_n + R_m \underset{k_2'}{\overset{k_2}{\rightleftarrows}} S_{n+m} + W \quad n,m = 1,2,... \tag{6.18}$$

3. Polyaddition

$$P_n + C_1 \underset{k_3'}{\overset{k_3}{\rightleftarrows}} P_{n+1} \quad n = 1,2,... \tag{6.19}$$

$$R_n + C_1 \underset{k_3'}{\overset{k_3}{\rightleftarrows}} R_{n+1} \quad n = 1,2,... \tag{6.20}$$

4. Ring opening of cyclic dimer

$$C_2 + W \underset{k_4'}{\overset{2k_4}{\rightleftarrows}} P_2 \tag{6.21}$$

5. Polyaddition of cyclic dimer

$$P_n + C_2 \underset{k_5'}{\overset{2k_5}{\rightleftarrows}} P_{n+2} \quad n = 1,2,... \tag{6.22}$$

$$R_n + C_2 \underset{k_5'}{\overset{2k_5}{\rightleftarrows}} R_{n+2} \quad n = 1,2,... \tag{6.23}$$

For polyaddition, only the P and R species are considered because the opening of a ring molecule occurs through the reaction of an amine end-group [23]. Degradation reactions like decarboxylation [24], desamination [24], and peroxidation of

caprolactam [25] have high activation energies, and thus do not occur significantly at the low temperatures involved in SSP. For this reason, they are not included in Table 6.2.

In the formulation of the reaction scheme, equal reactivity of the functional groups is assumed. In other words, the rate at which a functional group reacts depends neither on the length of the chain to which it is attached, nor on the type of polymer (P, Q, R, or S). This is a generalization of Flory's [3] equal reactivity hypothesis, which holds for long chains [5, 26]. Since low-order oligomers are present in very small amounts during SSP, this assumption can be safely used. For the cyclic species, however, the monomer C_1 is known to behave differently than the oligomers C_i, $i = 2, 3, \ldots$, because the seven-member caprolactam still retains some ring strain [27]. Therefore, different rate constants are assigned for the reactions with C_1 and C_2.

The presence of a multiplicative factor before some of the rate constants in Table 6.2 is a consequence of the definition of the k_i's with regard to the reaction of *functional species*. This factor, which we call the symmetry number s, is the number of distinct ways for the given reaction between *chemical species* to occur. Figure 6.1 illustrates this point with some examples.

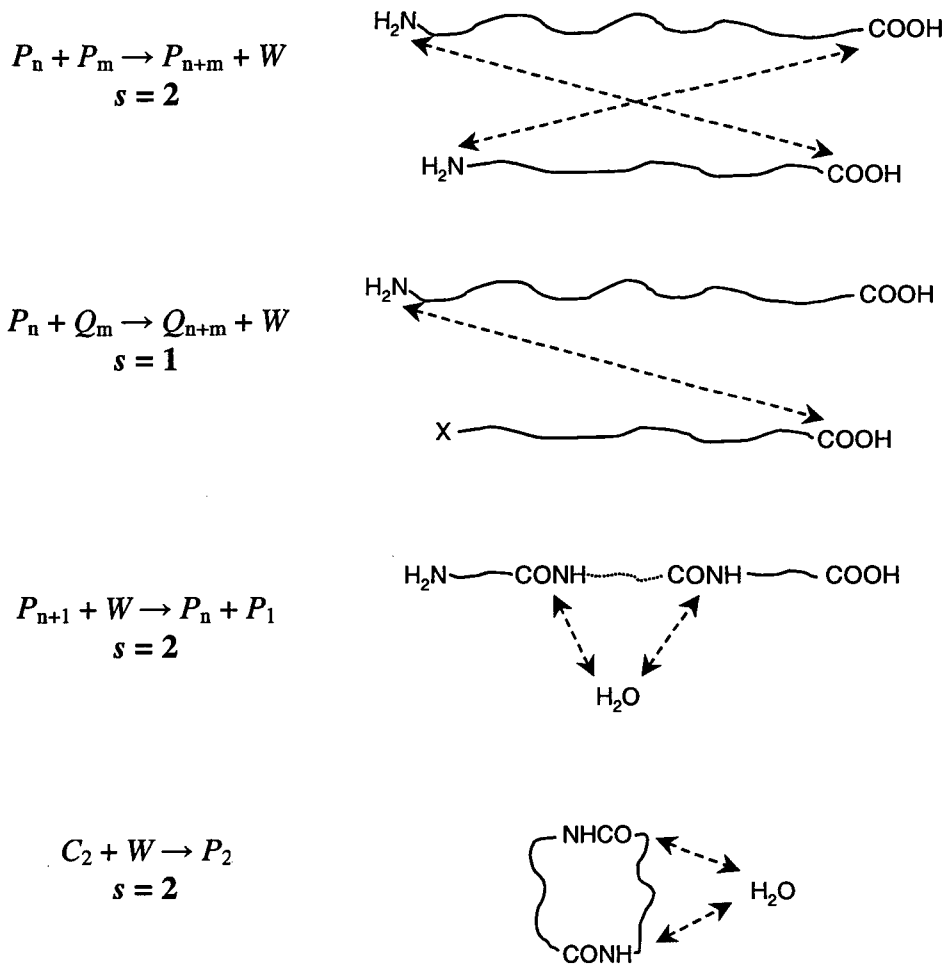

Figure 6.1 Illustration of the different ways in which polymer molecules can react

A peculiarity not mentioned in Table 6.2 arises for Eq. (6.15) when $n = m$ (i.e. $P_n + P_n = P_{2n} + W$). In this case, the symmetry number for the forward reaction is only one to avoid counting twice the reactive collisions. In addition, the reverse reaction is obtained upon hydrolysis of the single central bond, so that again $s = 1$, instead of 2 in the general case $n \neq m$.

Introducing the moments of the CLD for each population of chains,

$$\lambda_{\zeta,k} = \sum_{n=1}^{+\infty} n^k \zeta_n \qquad \zeta = P,Q,R,S\ ;\ k = 0,1,2,... \tag{6.24}$$

we derived the rates of generation by chemical reaction for the various species and moments, based on the reaction scheme in Table 6.2 and the procedure discussed in Section 6.1. The resulting expressions for the 19 species and moments of interest are listed in Table 6.3, in which the concentrations are local concentrations (the asterisk was omitted for sake of clarity), and must be replaced by overall concentrations by means of Eq. (2.11).

The various reactions in Table 6.2 have been found to be catalyzed by the carboxyl groups [28] and the forward rate constants can be represented empirically by

$$k_i = k_i^0 + k_i^c \left[-COOH\right]^* \qquad i = 1,2,3,4,5 \tag{6.25}$$

where the local concentration of acid groups is given by

$$\left[-COOH\right]^* = \lambda_{P,0}^* + \lambda_{Q,0}^* \tag{6.26}$$

The non-catalyzed and catalyzed rate constants, k_i^0 and k_i^c respectively, are assumed to follow the Arrhenius law,

$$k_i^0 = k_{i,\infty}^0 \exp\left(-\frac{E_i^0}{RT}\right) \qquad k_i^c = k_{i,\infty}^c \exp\left(-\frac{E_i^c}{RT}\right) \tag{6.27}$$

where E_i^0 and E_i^c denote the non-catalyzed and catalyzed activation energies, respectively, and $k_{i,\infty}^0$ and $k_{i,\infty}^c$ are the corresponding pre-exponential factors. The reverse rate constants are written as

$$k_i' = k_i / K_i \tag{6.28}$$

in which the equilibrium constants are given by the standard thermodynamic equation,

$$K_i = \exp\left(\frac{\Delta S_i}{R} - \frac{\Delta H_i}{RT}\right) \tag{6.29}$$

where ΔS_i and ΔH_i stand respectively for the entropy and the enthalpy of reaction, which are assumed to be independent of temperature.

Table 6.3 Chemical production rates for the species and moments

1.Caprolactam

$$R_{C_1} = -k_1 C_1 W + k_1' P_1 - k_3 C_1 (\lambda_{P,0} + \lambda_{R,0}) + k_3' (\lambda_{P,0} + \lambda_{R,0} - P_1 - R_1) \tag{6.30}$$

2. Cyclic dimer

$$R_{C_2} = -k_4 C_2 W + k_4' P_2 - k_5 C_2 (\lambda_{P,0} + \lambda_{R,0}) + k_5' (\lambda_{P,0} + \lambda_{R,0} - P_1 - R_1 - P_2 - R_2) \tag{6.31}$$

3. Water

$$R_W = -k_1 C_1 W + k_1' P_1 + k_2 (\lambda_{P,0}^2 + \lambda_{P,0}\lambda_{Q,0} + \lambda_{P,0}\lambda_{R,0} + \lambda_{Q,0}\lambda_{R,0}) \tag{6.32}$$
$$- k_2' W \sum_{\zeta} (\lambda_{\zeta,1} - \lambda_{\zeta,0}) - k_4 C_2 W + k_4' P_2 \qquad \zeta = P, Q, R, S$$

4. Aminocaproic acid

$$R_{P_1} = k_1 C_1 W - k_1' P_1 - k_2 P_1 (2\lambda_{P,0} + \lambda_{Q,0} + \lambda_{R,0}) \tag{6.33}$$
$$+ k_2' W (2\lambda_{P,0} + \lambda_{Q,0} + \lambda_{R,0} - 2P_1 - Q_1 - R_1) - k_3 C_1 P_1 + k_3' P_2$$
$$- k_5 C_2 P_1 + k_5' P_3$$

5. Zeroth moment of bifunctional chains

$$R_{\lambda_{P,0}} = k_1 C_1 W - k_1' P_1 - k_2 \lambda_{P,0} (\lambda_{P,0} + \lambda_{Q,0} + \lambda_{R,0}) \tag{6.34}$$
$$+ k_2' W (\lambda_{P,1} + \lambda_{Q,1} + \lambda_{R,1} - \lambda_{P,0} - \lambda_{Q,0} - \lambda_{R,0}) + k_4 C_2 W - k_4' P_2$$

6. First moment of bifunctional chains

$$R_{\lambda_{P,1}} = k_1 C_1 W - k_1' P_1 - k_2 \lambda_{P,1} (\lambda_{Q,0} + \lambda_{R,0}) + \frac{1}{2} k_2' W (\lambda_{Q,2} + \lambda_{R,2} - \lambda_{Q,1} - \lambda_{R,1}) \tag{6.35}$$
$$+ k_3 C_1 \lambda_{P,0} - k_3' (\lambda_{P,0} - P_1) + 2k_4 C_2 W - 2k_4' P_2$$
$$+ 2k_5 C_2 \lambda_{P,0} - 2k_5' (\lambda_{P,0} - P_1 - P_2)$$

7. Second moment of bifunctional chains

$$R_{\lambda_{P,2}} = k_1 C_1 W - k_1' P_1 + k_2 (2\lambda_{P,1}^2 - \lambda_{P,2}\lambda_{Q,0} - \lambda_{P,2}\lambda_{R,0}) \tag{6.36}$$
$$+ \frac{1}{6} k_2' W (2\lambda_{P,1} - 2\lambda_{P,3} + 2\lambda_{Q,3} - 3\lambda_{Q,2} + \lambda_{Q,1} + 2\lambda_{R,3} - 3\lambda_{R,2} + \lambda_{R,1})$$
$$+ k_3 C_1 (\lambda_{P,0} + 2\lambda_{P,1}) + k_3' (\lambda_{P,0} - 2\lambda_{P,1} + P_1) + 4k_4 C_2 W - 4k_4' P_2$$
$$+ 4k_5 C_2 (\lambda_{P,0} + \lambda_{P,1}) + 4k_5' (\lambda_{P,0} - \lambda_{P,1} + P_2)$$

Table 6.3 (*Continued*)

8. Monoacid chain regulator

$$R_{Q_1} = -k_2 Q_1 \left(\lambda_{P,0} + \lambda_{R,0}\right) + k_2' W \left(\lambda_{Q,0} + \lambda_{S,0} - Q_1 - S_1\right) \tag{6.37}$$

9. Zero moment of monoacid chains

$$R_{\lambda_{Q,0}} = -k_2 \lambda_{Q,0} \lambda_{R,0} + k_2' W \left(\lambda_{S,1} - \lambda_{S,0}\right) \tag{6.38}$$

10. First moment of monoacid chains

$$R_{\lambda_{Q,1}} = k_2 \left(\lambda_{P,1} \lambda_{Q,0} - \lambda_{Q,1} \lambda_{R,0}\right) + \frac{1}{2} k_2' W \left(\lambda_{S,2} - \lambda_{Q,2} - \lambda_{S,1} + \lambda_{Q,1}\right) \tag{6.39}$$

11. Second moment of monoacid chains

$$R_{\lambda_{Q,2}} = k_2 \left(2\lambda_{P,1} \lambda_{Q,1} + \lambda_{P,2} \lambda_{Q,0} - \lambda_{Q,2} \lambda_{R,0}\right) \tag{6.40}$$

$$- \frac{1}{6} k_2' W \left(4\lambda_{Q,3} - 3\lambda_{Q,2} - \lambda_{Q,1} - 2\lambda_{S,3} + 3\lambda_{S,2} + \lambda_{S,1}\right)$$

12. Monoamine chain regulator

$$R_{R_1} = -k_2 R_1 \left(\lambda_{P,0} + \lambda_{Q,0}\right) + k_2' W \left(\lambda_{R,0} + \lambda_{S,0} - R_1 - S_1\right) - k_3 C_1 R_1 + k_3' R_2 \tag{6.41}$$

$$- k_5 C_2 R_1 + k_5' R_3$$

13. Zero moment of monoamine chains

$$R_{\lambda_{R,0}} = -k_2 \lambda_{Q,0} \lambda_{R,0} + k_2' W \left(\lambda_{S,1} - \lambda_{S,0}\right) \tag{6.42}$$

14. First moment of monoamine chains

$$R_{\lambda_{R,1}} = k_2 \left(\lambda_{P,1} \lambda_{R,0} - \lambda_{R,1} \lambda_{Q,0}\right) + \frac{1}{2} k_2' W \left(\lambda_{S,2} - \lambda_{R,2} - \lambda_{S,1} + \lambda_{R,1}\right) \tag{6.43}$$

$$+ k_3 C_1 \lambda_{R,0} - k_3' \left(\lambda_{R,0} - R_1\right) + 2k_5 C_2 \lambda_{R,0} - 2k_5' \left(\lambda_{R,0} - R_1 - R_2\right)$$

15. Second moment of monoamine chains

$$R_{\lambda_{R,2}} = k_2 \left(2\lambda_{P,1} \lambda_{R,1} + \lambda_{P,2} \lambda_{R,0} - \lambda_{R,2} \lambda_{Q,0}\right) \tag{6.44}$$

$$- \frac{1}{6} k_2' W \left(4\lambda_{R,3} - 3\lambda_{R,2} - \lambda_{R,1} - 2\lambda_{S,3} + 3\lambda_{S,2} + \lambda_{S,1}\right) + k_3 C_1 \left(\lambda_{R,0} + 2\lambda_{R,1}\right)$$

$$+ k_3' \left(\lambda_{R,0} - 2\lambda_{R,1} + R_1\right) + 4k_5 C_2 \left(\lambda_{R,0} + \lambda_{R,1}\right) + 4k_5' \left(\lambda_{R,0} - \lambda_{R,1} + R_2\right)$$

Table 6.3 Chemical production rates for the species and moments *(Continued)*

16. Non-reactive monomer

$$R_{S_1} = 0 \tag{6.45}$$

17. Zero moment of dead chains

$$R_{\lambda_{S,0}} = k_2\,\lambda_{Q,0}\,\lambda_{R,0} - k_2^{'} W\left(\lambda_{S,1} - \lambda_{S,0}\right) \tag{6.46}$$

18. First moment of dead chains

$$R_{\lambda_{S,1}} = k_2\left(\lambda_{Q,1}\,\lambda_{R,0} + \lambda_{R,1}\,\lambda_{Q,0}\right) - k_2^{'} W\left(\lambda_{S,2} - \lambda_{S,1}\right) \tag{6.47}$$

19. Second moment of dead chains

$$R_{\lambda_{S,2}} = k_2\left(2\lambda_{Q,1}\,\lambda_{R,1} - \lambda_{Q,2}\,\lambda_{R,0} - \lambda_{R,2}\,\lambda_{Q,0}\right) - k_2^{'} W\left(\lambda_{S,3} - \lambda_{S,2}\right) \tag{6.48}$$

Tai and Tagawa [29] carried out an extensive series of experiments [30, 31] on the hydrolytic polymerization of caprolactam at melt temperatures between 230 and 280°C with different initial water concentrations. They recorded the concentrations of aminocaproic acid, carboxyl and amine end-groups, as well as the cyclic dimer, and obtained a set of values for the rate and equilibrium parameters using a nonlinear regression technique (Table 6.4).

Table 6.4 Rate and equilibrium constants for nylon-6 polymerization [29]

i *	$k_{i,\infty}^{0}$	E_i^0	$k_{i,\infty}^{c}$	E_i^c	ΔH_i	ΔS_i
	kg/(mol s)	J/mol	kg²/(mol² s)	J/mol	J/mol	J/(mol K)
1	$1.6632\cdot 10^{2}$	$8.3198\cdot 10^{4}$	$1.1965\cdot 10^{4}$	$7.8703\cdot 10^{4}$	$8.0268\cdot 10^{4}$	$-3.2997\cdot 10^{1}$
2	$5.2617\cdot 10^{6}$	$9.7389\cdot 10^{4}$	$3.3650\cdot 10^{6}$	$8.6504\cdot 10^{4}$	$-2.4883\cdot 10^{4}$	$3.9496\cdot 10^{0}$
3	$7.9328\cdot 10^{5}$	$9.5606\cdot 10^{4}$	$4.5492\cdot 10^{6}$	$8.4148\cdot 10^{4}$	$-1.6923\cdot 10^{4}$	$-2.9068\cdot 10^{1}$
4	$2.3827\cdot 10^{8}$	$1.7577\cdot 10^{5}$	$6.4742\cdot 10^{8}$	$1.5652\cdot 10^{5}$	$-4.0176\cdot 10^{4}$	$-6.0766\cdot 10^{1}$
5	$7.1392\cdot 10^{4}$	$8.9141\cdot 10^{4}$	$8.3639\cdot 10^{5}$	$8.5374\cdot 10^{4}$	$-1.3263\cdot 10^{4}$	$2.4384\cdot 10^{0}$

* see Table 6.2 for the numbering of the reactions

The rate constants in Table 6.4 were expressed by Tai and Tagawa on a mass basis. As we prefer to use conventional units on a volumetric basis, the values in Table 6.4 have to be corrected for the density of the amorphous phase (chosen at the reference temperature of T = 165°C).

$$k_{i,\infty}^{0} = \frac{k_{i,\infty}^{0}(Table\ 6.4)}{\rho_{a,165°C}} \qquad k_{i,\infty}^{c} = \frac{k_{i,\infty}^{c}(Table\ 6.4)}{\rho_{a,165°C}^{2}} \tag{6.49}$$

where the density of the amorphous polymer is obtained with the correlation in Giori and Hayes [34] :

$$\rho_a\left(kg/m^3\right) = 1{,}100 - 0.52\,T(°C) \tag{6.50}$$

For the same reason, some equilibrium constants calculated from the values of ΔH_i and ΔS_i in Table 6.4 also need a density correction :

$$K_i = \frac{K_i(Table6.4)}{\rho_a} \qquad i = 1,3,4,5 \tag{6.51}$$

Note that the density correction is not required for K_2 because forward and reverse polycondensation have the same molecularity.

Recently, Mallon and Ray [32] questioned the thermodynamic consistency of Tai's set of parameters. These authors formulated an entirely new model for nylon equilibria and kinetics in which water exists in two states (free/bound). By assuming a fast salting pre-equilibrium, they successfully explained the variation in nylon kinetics over a wide range of water content according to a changing mixture dielectric constant.

We nevertheless shall make use of Tai's parameters in this study because they are currently the industry standard in all simulation and optimization studies on PA6 reactors [12]. Furthermore, a model with a single thermodynamic state for water is in agreement with recent ^{2}H-NMR results [33], as discussed in Section 2.2.4.

6.2.3 Population-Balance Equations

Population-balance equations can now be written for the various components and moments of interest. For the non-volatile states, they are readily expressed as

$$\frac{\partial \zeta_1^*}{\partial t} = R_{\zeta_1} \qquad \zeta = P,Q,R,S \tag{6.52}$$

for the monomeric compounds, and

$$\frac{\partial \lambda_{\zeta,k}^*}{\partial t} = R_{\lambda_{\zeta,k}} \qquad \zeta = P,Q,R,S \quad k = 0,1,2 \tag{6.53}$$

for the moments of the CLDs. For the volatile species, diffusion through the immobile polymer matrix is taken into account,

$$\frac{\partial c_i^*}{\partial t} = R_i + D_i \nabla^2 c_i^* \qquad i = C_1, C_2, W \tag{6.54}$$

The effect of crystallinity on the diffusion coefficient D_i is expressed by Eq. (2.22). An Arrhenius form is postulated for the temperature dependence of the amorphous diffusivity of water :

$$D_{W,0} = D_{W,0,373.15K} \exp\left[\frac{E_{d,W}}{R}\left(\frac{1}{373.15\ K} - \frac{1}{T}\right)\right] \tag{6.55}$$

with the values of $D_{W,0,373.15\,K} = 5.5 \cdot 10^{-11}$ m^2/s and $E_{d,W} = 46$ kJ/mol from Pflüger [35].

The Laplacian in Eq. (6.54) is written as

$$\nabla^2 c_i^* = \frac{\partial^2 c_i^*}{\partial r^2} + \frac{\nu}{r}\frac{\partial c_i^*}{\partial r} \tag{6.56}$$

for geometries described by a single spatial coordinate r. The value of ν in Eq. (6.56) is zero for a plane sheet, one for a cylinder of infinite length, and two for a sphere [36]. The granules used for the SSP experiments in the fixed-bed reactors were mostly short right cylinders with a slightly elliptical cross-section. Since the cylinders were of approximately the same length as the particle diameter, the granules are modeled as spheres having an equivalent radius R. In this case, the geometrical parameter is taken as $\nu = 2$, and r represents the radial position.

The generalization of geometry in the model is of interest because SSP of nylon is also performed on flakes ($\nu = 0$), or on fibers ($\nu = 1$) as in the tire cord industry [37]. These types of operations are termed *postextrusion SSP*, compared to *preextrusion SSP* for the reaction of pellets [38].

After replacement of local concentrations by overall concentrations using Eq. (2.11), Eqs. (6.52-54) form a set of 19 coupled partial differential equations (PDEs) that must be solved with appropriate initial, boundary, and closure conditions to yield the time and spatial concentration profiles of the various species and moments.

Initial conditions for C_1, C_2 and W are given by the analysis of the prepolymer. There are no radial concentration profiles before SSP since the solid prepolymer is obtained upon cooling of the melt. As the standard prepolymer was produced without a chain regulator, the values of the Q and S species are identically zero in this case (the polymerization of nylon-6 in the presence of a chain regulator will be discussed in Section 6.3.2). Given the constant volume hypothesis, the total concentration of repeat units in linear molecules is an invariant given by

$$\lambda_{P,1} + \lambda_{R,1} = \lambda_{P,1,0} + \lambda_{R,1,0} = \frac{\rho_a}{M_{C1}} \tag{6.57}$$

For an unextracted material, the volume loss upon volatilization is not negligible and a correction based on Eq. (2.32) must be made. The equal reactivity hypothesis is postulated for the decarboxylation reaction in the VK tube, which implies that the initial fraction of monoamine polymer chains is expressed as

$$\frac{\lambda_{R,1,0}}{\lambda_{P,1,0} + \lambda_{R,1,0}} = \psi \tag{6.58}$$

where $\psi = 0.0564$ is the extent of decarboxylation evidenced by end-group analysis (Section 3.3). The initial first moments are thus obtained by solving simultaneously Eqs. (6.57) and (6.58) to yield

$$\lambda_{P,1,0} = \frac{(1-\psi)\,\rho_a}{M_{C1}} \tag{6.59}$$

$$\lambda_{R,1,0} = \frac{\psi\,\rho_a}{M_{C1}} \tag{6.60}$$

Next, the initial zero moments are derived from the value of the number-average chain length obtained by viscometry, and Eq. (6.6) :

$$\lambda_{P,0,0} = \frac{\lambda_{P,1,0}}{DP_{n,0}} \qquad \lambda_{R,0,0} = \frac{\lambda_{R,1,0}}{DP_{n,0}} \tag{6.61}$$

It is reasonable to assume that the CLD after the melt prepolymerization stage is of the Flory-Schulz type [5, 12]. Therefore, the initial second moments are given by

$$\lambda_{P,2,0} = \lambda_{P,1,0}\ PDI_0 = \lambda_{P,1,0}\left(\frac{1+p_0}{1-p_0}\right) \tag{6.62}$$

$$\lambda_{R,2,0} = \lambda_{R,1,0}\ PDI_0 = \lambda_{R,1,0}\left(\frac{1+p_0}{1-p_0}\right) \tag{6.63}$$

and the initial concentrations of monomers as

$$P_{1,0} = \lambda_{P,0,0}(1-p_0) \qquad R_{1,0} = \lambda_{R,0,0}(1-p_0) \tag{6.64}$$

where the initial conversion p_0 is obtained using Eq. (2.49).

Boundary conditions must be supplied for the volatile species. The first spatial derivatives are zero at the center of the particle due to the symmetry of the system :

$$\left.\frac{\partial c_i}{\partial r}\right|_{r=0} = 0 \qquad \forall t\ ; i = C_1, C_2, W \tag{6.65}$$

Next, a constant concentration is assigned at the surface of the particle. This concentration is zero for the experiments in the fixed-bed since pure nitrogen was used as the purge gas. However, we also consider non-zero concentrations of volatiles in the gas phase to keep the model general. The surface concentration is then fixed by the vapor-liquid equilibrium. The effect of crystallinity on the VLE is evidenced by substituting Eq. (2.11) into Eq. (6.13) to yield a modified Flory-Huggins expression :

$$p_i = p_i^0\, w_i \left(exp(1+\chi_i)\right)\left(\frac{P(1-w_c)+w_c}{P(1-w_c)}\right) \tag{6.66}$$

The mass fraction is expressed as a function of the concentration by

$$w_i = \left(\frac{M_i}{\rho_a}\right) c_i \tag{6.67}$$

whose substitution into Eq. (6.66) leads to

$$\rho_a RT c_{g,i} = M_i p_i^0 c_i \left(exp\left(1+\chi_i\right)\right)\left(\frac{P\left(1-w_c\right)+w_c}{P\left(1-w_c\right)}\right) \tag{6.68}$$

in which the partial pressure p_i has also been replaced by the gas phase concentration $c_{g,i}$, making use of the ideal gas assumption. Finally, solving Eq. (6.68) for c_i leads to the boundary condition at the particle surface :

$$c_i\big|_{r=R} = \left(\frac{\rho_a RT c_{g,i}}{M_i p_i^0 exp\left(1+\chi_i\right)}\right)\left(\frac{P\left(1-w_c\right)}{P\left(1-w_c\right)+w_c}\right) \qquad \forall t \;;\; i = C_1, C_2, W \tag{6.69}$$

The following expression was used for the temperature dependence of the pure vapor pressure,

$$p_i^0 = exp\left(A_i - \frac{B_i}{T - C_i}\right) \qquad i = C_1, C_2, W \tag{6.70}$$

where values of the coefficients A_i, B_i and C_i may be found in [39] for caprolactam and water.

Closure conditions for the moments of the CLDs are supplied by assuming the Schulz-Zimm relation, Eq. (6.12), to hold for every population of chains :

$$\lambda_{\zeta,3} \cong \frac{\lambda_{\zeta,2}\left(2\lambda_{\zeta,2}\lambda_{\zeta,0} - \lambda_{\zeta,1}^2\right)}{\lambda_{\zeta,1}\lambda_{\zeta,0}} \qquad \zeta = P, Q, R, S \tag{6.71}$$

In addition, closure approximations are also needed to break the hierarchy of equations for the chains bearing an amine moiety [12] :

$$\zeta_3 = \zeta_2 = \zeta_1 \qquad \zeta = P, R \tag{6.72}$$

Next, the radial coordinate is discretized using finite elements, in order to transform each PDE into a set of ordinary differential equations (ODEs) that can be integrated by numerical means. For this purpose, the particle radius is divided into a series of $N = 10$ equally spaced nodes, from the center ($j = 1$) to the surface ($j = N$). Then, the second derivative in the diffusion term, Eq. (6.56), is calculated using a three-point finite difference approximation,

$$\frac{\partial^2 c_i(j)}{\partial r^2} = \frac{c_i(j+1) - 2c_i(j) + c_i(j-1)}{(\Delta r)^2} \qquad j = 2, \ldots, N-1 \tag{6.73}$$

where $\Delta r = R/(N\text{-}1)$ is the radial increment. The first derivative is calculated using a central finite difference approximation,

$$\frac{\partial c_i(j)}{\partial r} = \frac{c_i(j+1) - c_i(j-1)}{2\,\Delta r} \qquad j = 2,...,N-1 \tag{6.74}$$

and the radial position is given by

$$r(j) = (j-1)\Delta r \tag{6.75}$$

In a similar vein, the boundary condition at the particle center, Eq. (6.63), is discretized using a forward finite difference approximation,

$$\frac{\partial c_i(1)}{\partial r} = \frac{c_i(2) - c_i(1)}{\Delta r} = 0 \;\Rightarrow\; c_i(1) = c_i(2) \;\Rightarrow\; \frac{dc_i(1)}{dt} = \frac{dc_i(2)}{dt} \tag{6.76}$$

whereas the boundary condition at the particle surface, Eq. (6.67), is readily expressed as :

$$c_i(N) = const. \;\Rightarrow\; \frac{dc_i(N)}{dt} = 0 \tag{6.77}$$

The set of 19 species × 10 grid points = 190 ODEs has been numerically solved using Gear's BDF-LSODE algorithm [40] in the SimuSolv integration package [41], to give the time course of the different species. The computing time for 50 hours of reaction was typically 1 minute on a Sun station.

After integration, the number-average and mass-average chain lengths are computed from Eq. (6.6) and (6.7) by summing over all populations of chains :

$$DP_n = \frac{\sum_{\zeta} \lambda_{\zeta,1}}{\sum_{\zeta} \lambda_{\zeta,0}} \qquad DP_w = \frac{\sum_{\zeta} \lambda_{\zeta,2}}{\sum_{\zeta} \lambda_{\zeta,1}} \qquad \zeta = P,Q,R,S \tag{6.78}$$

The concentrations of end-groups are given by

$$[-COOH] = \lambda_{P,0} + \lambda_{Q,0} \tag{6.79}$$

$$[-NH_2] = \lambda_{P,0} + \lambda_{R,0} \tag{6.80}$$

Spatial averages of the various quantities of interest are defined by

$$\overline{x} = \frac{\iiint_V x\,dV}{\iiint_V dV} = \frac{\nu+1}{R^{\nu+1}} \int_0^R x\,r^{\nu}\,dr \qquad x = C_1, C_2, W, \zeta_1, DP_n, DP_w \tag{6.81}$$

and computed by means of the following discretized form of Eq. (6.81) :

$$\bar{x} = \left(\frac{\Delta r}{R}\right)^{\nu+1} \sum_{j=1}^{N-1} \left(j^{\nu+1} - (j-1)^{\nu+1}\right) x(j) \tag{6.82}$$

Finally, the polydispersity index of the polymer is calculated as

$$PDI = \frac{\overline{DP_w}}{\overline{DP_n}} \tag{6.83}$$

6.3 Simulation of Hydrolytic Polymerization of Caprolactam

One advantage of a kinetic model for solid-state polymerization of nylon-6 based on the extrapolation of the melt chemistry to the amorphous phase of the semicrystalline polymer is that hydrolytic polymerization of caprolactam in the melt appears as a special case of the model. This is of interest for two reasons. First, the correct implementation of the melt rate and equilibrium parameters in the solid-state model may be verified by comparison with literature data. Second, in some instances the state of the prepolymer before SSP cannot be guessed as easily as described in the previous section, for example when chain regulators have been used. In this case, the model can also be used to simulate the melt prepolymerization stage and get an estimate of the initial condition for the SSP process. The next two sections are aimed at illustrating these points.

6.3.1 Comparison with Literature Data

Here, we examine the ability of the model to handle the data of Tai and Tagawa [29], and Arai *et al.* [42], on the melt hydrolytic polymerization of caprolactam. For this purpose, the crystallinity and all diffusion coefficients are set to zero, a temperature above the melting point is assigned, and the initial state is defined as a function of caprolactam and water only. In this way, the nylon granule behaves like an isothermal batch reactor with no volatilization, which is consistent with Tai and Arai's experiments performed in sealed glass ampoules.

The model is compared in Figure 6.2 to the kinetic data obtained at five different temperatures between $T = 230$ and 280°C, for an initial water fraction of $w_{W,0} = 1.33$ %. Results at $T = 259$°C for different initial water contents between $w_{W,0} = 0.68$ and 1.90 % are disclosed in Figure 6.3. Model predictions compare well to the data for caprolactam, cyclic dimer, and end-groups. The shape of the calculated profiles for aminocaproic acid is in agreement with the experimental values, although a quantitative discrepancy is observed. This problem has already been recognized and discussed by Tai *et al.* [30]. Aminocaproic acid is used as an explicit state in the model where moments are calculated because of the ring opening reaction. This reaction plays a fundamental role in the hydrolytic route by initiating the polymerization, but is of marginal importance during SSP. Therefore, the mismatch for P_1 is unimportant for the present study.

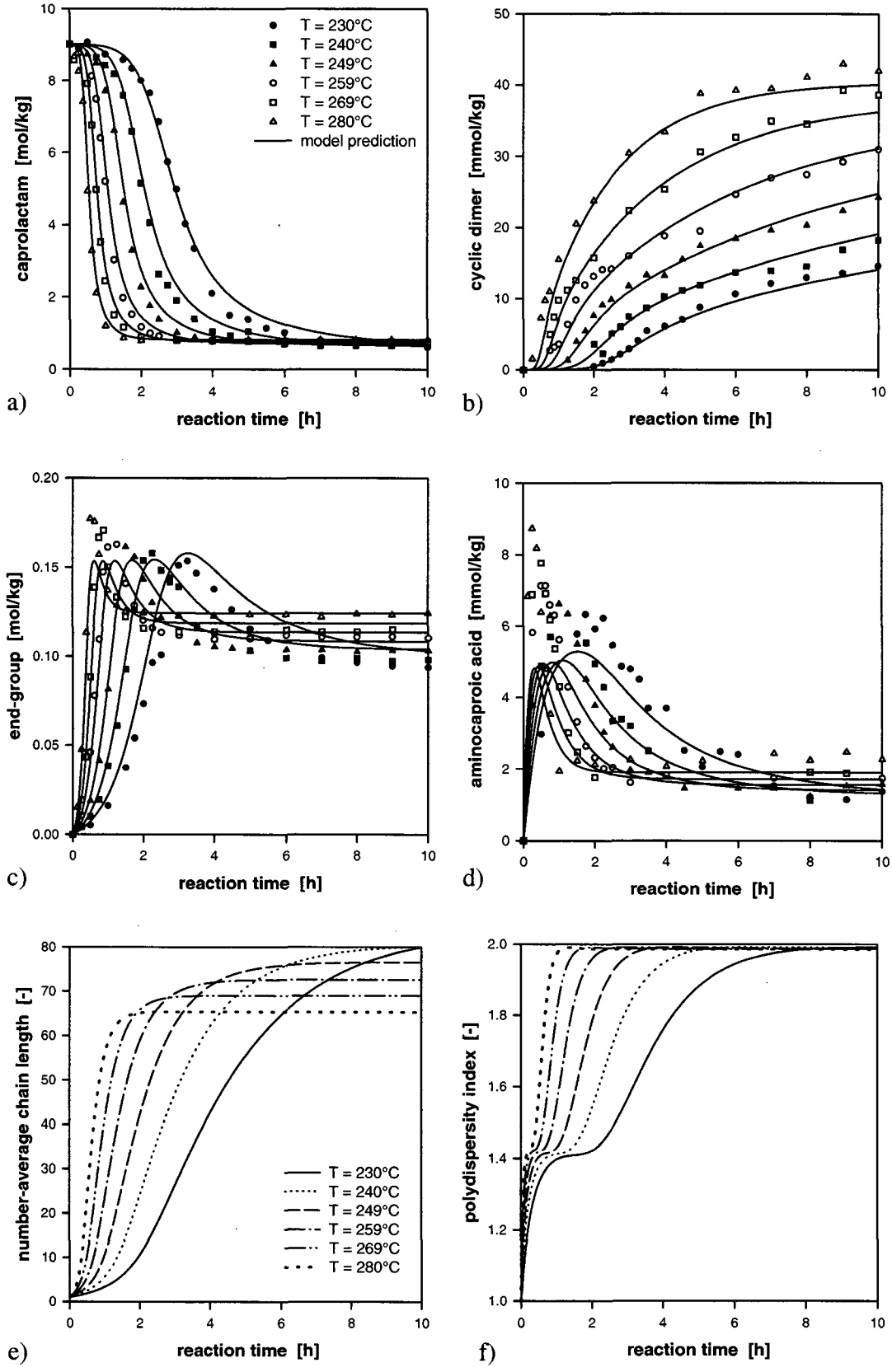

Figure 6.2 Hydrolytic polymerization of caprolactam as a special case of the solid-state model. Simulations for an isothermal batch reactor at different temperatures, T = 230, 240, 249, 259, 269, and 280°C, and initial water content $w_{w,0}$ = 1.33 %. Prediction for : a) Caprolactam ; b) Cyclic dimer ; c) End-group, amine or acid ; d) Aminocaproic acid ; e) Number-average chain length ; f) Polydispersity index. Caprolactam, end-group, and aminocaproic data from Tai and Tagawa [29], cyclic dimer data from Arai *et al.* [42]

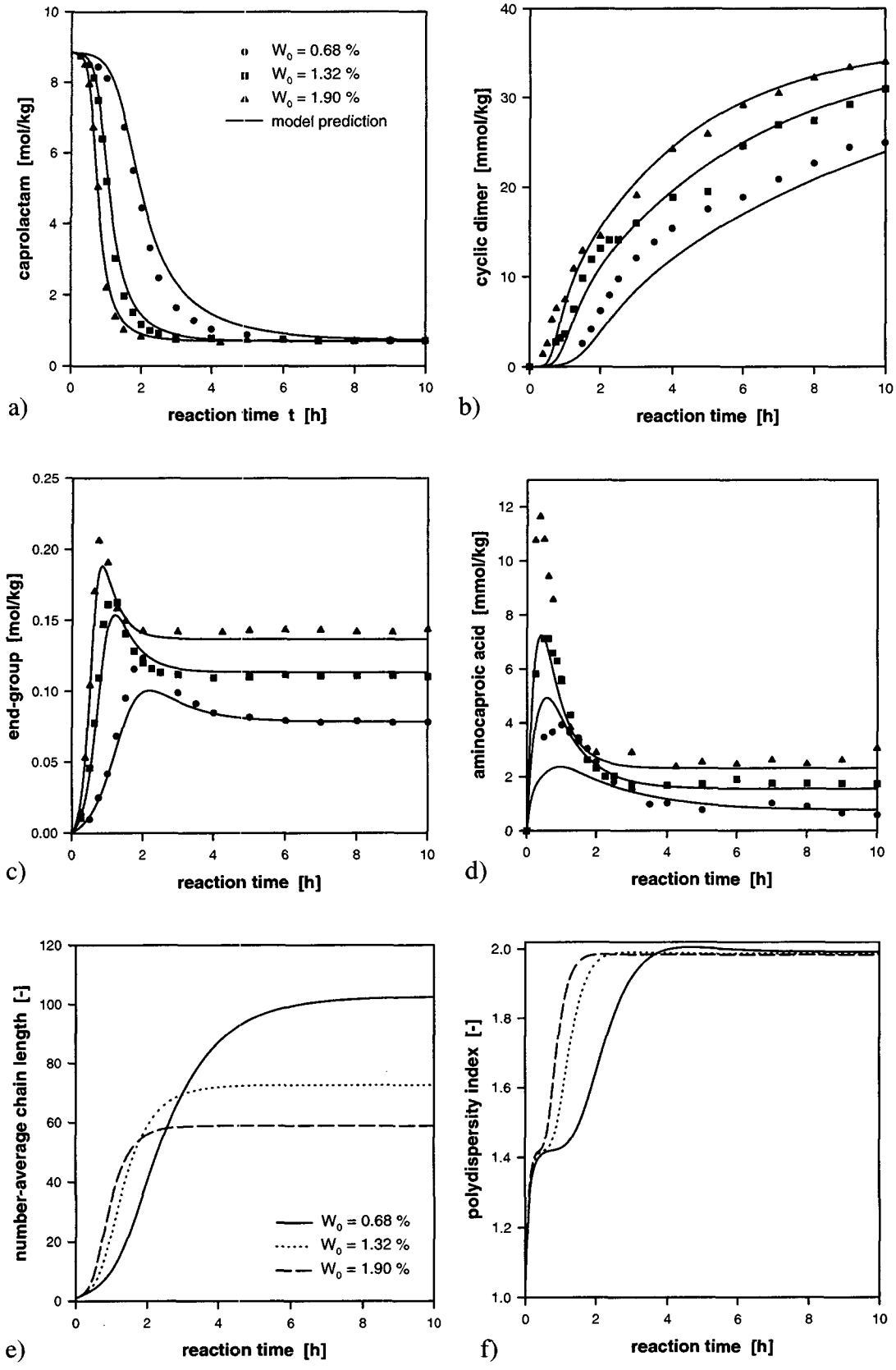

Figure 6.3 Hydrolytic polymerization of caprolactam as a special case of the solid-state model. Simulations for an isothermal batch reactor at different initial water contents, $w_{W,0} = 0.68$, 1.32, and 1.90 %, and $T = 259$°C. Prediction for : a) Caprolactam ; b) Cyclic dimer ; c) End-group, amine or acid ; d) Aminocaproic acid ; e) Number-average chain length ; f) Polydispersity index. Caprolactam, end-group, and aminocaproic data from Tai and Tagawa [29], cyclic dimer data from Arai *et al.* [42]

It is also worth noting that the constant-volume assumption does not hold precisely here, contrary to SSP, because the caprolactam density is about 90 % of the density of polymer [34]. This is not negligible for second or third order reactions, and may account for some of the minor discrepancies between measured and calculated data.

The predictions for the number-average chain length and the polydispersity index are also given in Fig. 6.2 and 6.3. The calculated curves for DP_n illustrate a basic principle for any optimizing strategy dealing with the hydrolytic production of nylon-6. In the early stage where kinetics dominates, high temperatures and water contents are desirable since these lead to higher rate constants and enhance the ring opening initiation step, respectively. By contrast, lower temperatures and water contents are favorable when the reaction becomes limited by the chemical equilibrium. The beneficial effect of a low temperature on the chain-building equilibrium is due to the amidation reaction being exothermic. Hence, optimization studies are generally directed toward the generation of optimal temperature profiles [43-45]. The equilibrium value of the polydispersity index is found to be close to the theoretical limit of $PDI = 2$ for a Flory-Schulz CLD, irrespective of the operating conditions.

The quality of the model prediction is not surprising, given that the rate and equilibrium parameters in Table 6.4 were generated from the very experimental data disclosed in Fig. 6.2 and 6.3. Merely, this proves that the melt nylon chemistry has been correctly implemented in the solid-state model.

6.3.2 Optimizing Strategies

Gupta *et al.* [14] simulated the hydrolytic polymerization of caprolactam in an isothermal batch reactor for different feed conditions, from which they deduced some arguments regarding reactor design and operation. Here, we make use of our kinetic model to extend Gupta's simulations to the entire manufacture process of nylon-6, that is, including the extraction and solid-state polymerization steps. The conditions for the calculations are listed in Table 6.5 and the resulting time courses of number-average chain length, polydispersity index, and cyclic dimer are given in Figure 6.4.

Table 6.5 Simulation conditions for Figure 6.4

1. Melt polymerization of caprolactam	t = 0 to 16 h
Reactor	Batch isothermal (no volatilization)
Temperature	T = 235°C
Feed composition	$w_{W,0}$ = 0.79 % (solid line)
	$w_{W,0}$ = 0.79 % and $w_{Q1,0}$ = 0.53 % (dotted line) *
	$w_{W,0}$ = 0 and $w_{P1,0}$ = 5.77 % (dashed line)
2. Extraction and drying	At t = 16 h
Effect on polymer	C_1, C_2 and W are set to zero
3. Solid-state polymerization	t = 16 to 48 h
Reactor	Fixed-bed, differential
Temperature	T = 165°C
Crystallinity	w_c = 0.456
Size of granules	R = 1.44 mm
Amorphous diffusion coefficients	$D_{C1,0}$ and $D_{C2,0}$: see Section 6.5.3
	$D_{W,0} = 4.96 \cdot 10^{-10}$ m^{2}s^{-1} [35]
Purge gas	Concentrations of volatiles in gas phase = 0

* Q_1 is acetic acid

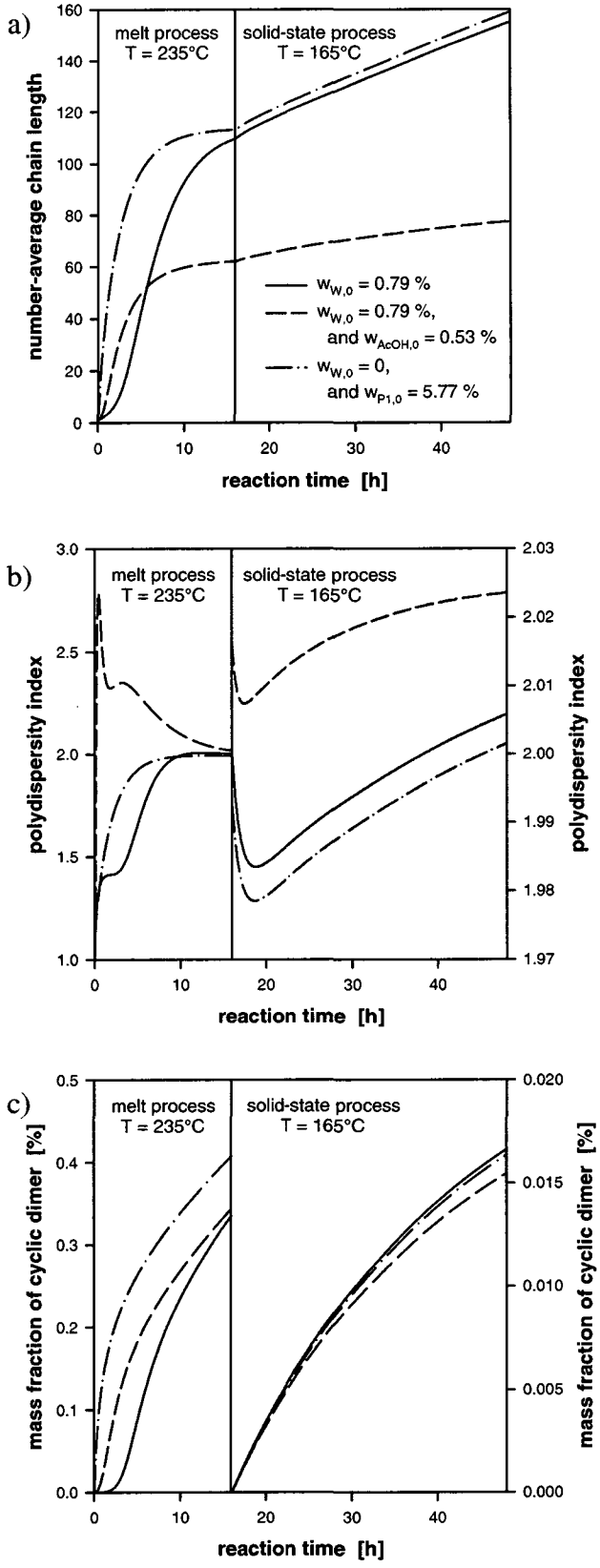

Figure 6.4 Effect of various feed conditions on the product composition during the manufacture of nylon-6

Simulation results for three different cases are disclosed in Fig. 6.4 : first, caprolactam is polymerized in the presence of water only ; second, acetic acid is added as a chain regulator ; and third, water is replaced by an equimolar amount of aminocaproic acid as the ring-opening agent. Fig. 6.4.a shows that the addition of either a monofunctional acid or aminocaproic acid to the feed enhances polymer build-up in the early stage of the melt prepolymerization. In the former case, this is because the reaction of P_n with the monofunctional species produces more water, which speeds up the ring opening reaction. In the latter case, this is because the addition of P_1 to the feed speeds up the polyaddition reaction. The addition of acetic acid, however, reduces substantially the equilibrium chain length and thus does not look attractive here.

The polydispersity index is found to reach the theoretical value of 2 at the end of the melt polymerization stage, irrespective of the feed conditions. The use of a chain regulator leads to higher values of *PDI* only at small reaction times in batch reactors. During SSP, the polydispersity index remains very close to the most probable value of 2. The small deviations observed in Fig. 6.4.b are attributed to the radial concentration profiles within the polymer granules that arise upon diffusion of the volatile species.

The alternative of using P_1 instead of W to initiate the polymerization and cut down the required reaction time in the melt stage has been discussed by Gupta *et al.* [14], based on the first part of the simulations in Fig. 6.4. Although P_1 is not available easily, it can be manufactured by depolymerizing scrap PA6 in a plant by heating it with an excess of hot water at high pressure. Gupta mentioned the increased rate of C_2 formation upon addition of P_1 in the feed (Fig. 6.4.c) as a potential drawback of this strategy. However, extending the simulations to the extraction and SSP stages leads to a final value of C_2 almost identical in all cases. Therefore, the suggestion of using P_1 to reduce the residence time of the complete manufacture process seems to offer attractive advantages. In addition to the method described above, it may be interesting to recycle a fraction of the reaction mass to the feed point since P_1 gets produced in the reactor itself when water is used in the feed. Alternatively, the use of a continuous stirred reactor may be envisaged since the reaction would occur in the presence of P_1 due to the backmixing.

6.4 Reexamination of Literature Reports

Given the paucity of reports in the open literature dealing with solid-state polymerization of nylon-6 (see Table 1.3), an exhaustive comparison between these data and the developed model has been carried out. In this way, the proposed model may be validated and its performance tested over a wide range of conditions. In addition, we shall see that reexamining the literature results within this new framework can bring some interesting features to light.

6.4.1 Data of Cawthon and Smith

In 1960, Cawthon and Smith [46] reported experimental results on isothermal nylon-6 polymerization carried out in sealed glass tubes at temperatures above and below the melting point, in which the concentration of caprolactam was recorded. As shown in Figure 6.5, these authors observed a monotonic decrease of the equilibrium monomer

content with decreasing reaction temperature, due to the exothermicity of the polyaddition reaction, but also noticed a sharp change at the melting transition, which they attributed to the confinement of caprolactam molecules into the amorphous phase upon solidification. As discussed in Section 2.2.2, this was the original postulate of the effect of crystallinity on apparent chemical equilibria in SSP, which was ascertained for the polyamidation reaction four years later by Zimmermann [47].

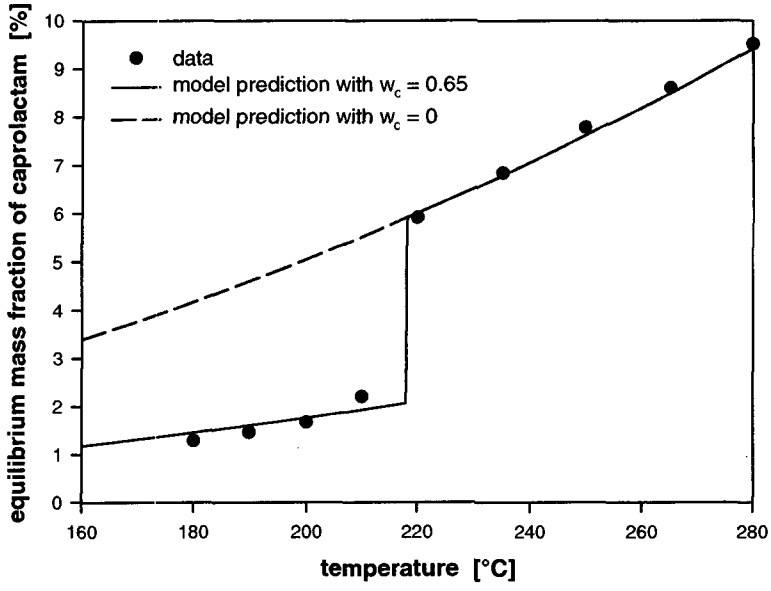

Figure 6.5 Comparison of model to data of Cawton and Smith [46] on residual monomer in equilibrated nylon-6 below and above the melting point

Monomer equilibration is governed by the polyaddition equilibrium constant, expressed in the framework of the developed model by

$$K_3 = \frac{[-NH_2]_{eq} - P_{1,eq}}{[-NH_2]_{eq} C_{1,eq}} \left(\frac{P(1-w_c)}{P(1-w_c)+w_c} \right) = \frac{1}{C_{1,eq}} \left(\frac{P(1-w_c)}{P(1-w_c)+w_c} \right) \tag{6.84}$$

which was obtained by substitution of Eq. (2.4) into Eq. (2.9). The concentration of amine moieties cancels in the above equation because the fraction of end-groups pertaining to aminocaproic acid molecules is negligibly small at high conversion. Precisely, this ratio is given for a most probable CLD from Eq. (6.62) as

$$\frac{P_1}{[-NH_2]} = 1 - p \tag{6.85}$$

and does not exceed 1 % because the conversion p at the beginning of SSP is usually higher than 0.99. Consequently, the equilibrium amount of monomer is independent of the chain length, that is, independent of the extent of polymer build-up during SSP (the same is true for low-order cyclic oligomers). This emphasizes the importance of crystallinity as a potential user-manipulated variable to reduce the extent of remonomerization. The equilibrium mass fraction of caprolactam is finally obtained from Eq. (6.84) as

$$w_{C1,eq} = \frac{M_{C1}}{\rho_a K_3}\left(\frac{P(1-w_c)}{P(1-w_c)+w_c}\right) \tag{6.86}$$

Using the relations for ρ_a and K_3 in Eq. (6.50) and (6.51), respectively, as well as M_{C1} = 0.11316 kg/mol and P = 1.138 [35], the monomer value predicted by Eq. (6.86) is compared to Cawthon and Smith's results. As these authors did not measure the crystallinity, this parameter was fitted to their data. The calculated curve in Fig. 6.5 compares well with the experimental points for an optimized value of w_c = 0.65. This good agreement bears out the description of chemical equilibria in the amorphous phase of the semicrystalline polymer by extrapolation from the melt chemistry. Particularly, the assumption of a constant enthalpy of reaction over a wide temperature range appears to be substantiated. Hence, the model performance regarding Cawthon and Smith's equilibrium data validates the implementation of chemical equilibria in the solid-state model.

The value of the crystallinity affects only the magnitude of the discontinuity at T_m. To underline this point, a calculation, represented by the dashed curve in Fig. 6.5, was also performed for a wholly amorphous polymer (w_c = 0). This emphasizes the error that results when the equilibrium effect of crystallinity is not taken into account, as is the case in the most recent attempts to model SSP of PA6 [48, 49].

The equilibrium data in Fig. 6.5 were determined by Cawthon and Smith by using polymers that contained initial caprolactam concentrations greater than and less than the equilibrium value. In their paper, these authors disclosed the corresponding time profiles of monomer for the two temperatures of 220 and 190°C, as shown in Figure 6.6. Therefore, it is also of interest to compare these data with the kinetic predictions of the solid-state model.

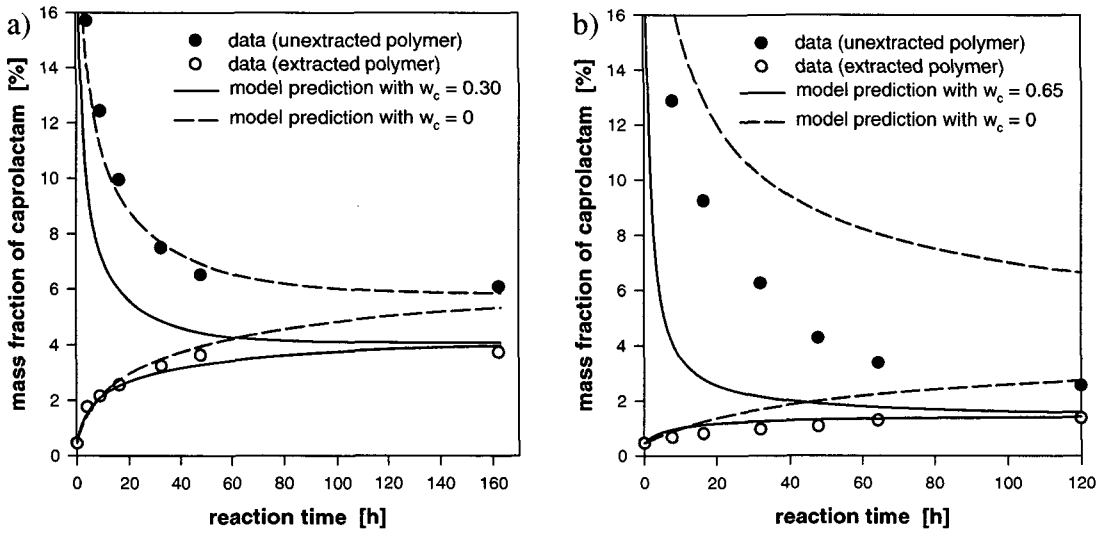

Figure 6.6 Prediction of caprolactam time profile during SSP without volatilization, data from Cawthon and Smith [46]. a) T = 220°C ; b) T = 190°C

Cawthon and Smith prepared the unextracted polymer used in their studies by polymerizing caprolactam in the presence of water at 260°C to 73.5 % monomer conversion [46]. With this information, we can take advantage of the model's ability to simulate the melt prepolymerization stage (section 6.3) to provide the initial

conditions not reported by the authors that are required for the simulation of the SSP stage. Thus, hydrolytic polymerization of caprolactam was simulated (with $T = 260°C$ and $w_{W,0} = 1.5$ %) until the specified monomer conversion was reached to generate the set of values listed in Table 6.6. These values were taken to be the initial conditions for the SSP, except for the concentration of water, which was set to zero to duplicate the experimental drying of the prepolymer. The extracted prepolymer contained $w_{C1,0} = 0.46$ % residual monomer [46], with no other mention except that it consisted of "commercial nylon 6 pellets". Thus, the initial conditions in this case were approximated by assuming $DP_{n,0} = 151$ (from Table 3.1) and applying the procedure described in Section 6.2.3, but disregarding the monofunctional species. Finally, Cawthon and Smith's experimental kinetic data were simulated by setting all diffusion coefficients to zero, since reaction was carried out in closed ampoules.

Table 6.6 Starting values for the simulation of Cawthon and Smith's SSP data

Variable	Symbol	Value [mol/m^3]
Caprolactam	$C_{1,0}$	2,369.1
Cyclic dimer	$C_{2,0}$	7.4590
Water	W_0	685.48
Aminocaproic acid	$P_{1,0}$	3.1460
Zero moment of the CLD *	$\lambda_{P,0,0}$	146.17
First moment of the CLD *	$\lambda_{P,1,0}$	6,578.5
Second moment of the CLD *	$\lambda_{P,2,0}$	543,920

* Monofunctional species were disregarded

The data set at 220°C (Fig. 6.6.a) exhibits an interesting behavior : although reaction times extended to about seven days (162 h), the monomer concentrations in the runs with unextracted and extracted prepolymers did not approach a common value. Cawthon and Smith suggested that the unextracted samples contained sufficient monomer to depress the fusion temperature to a value less than 220°C and remained amorphous throughout the experiment, while the extracted samples were semicrystalline and insufficient monomer was formed to depress T_m to a value less than 220°C. This explanation is clearly borne out by our kinetic model. Indeed, the model prediction for the run with an unextracted material compares perfectly with the data when the crystallinity is set to zero – with no adjusted parameters. By contrast, a crystallinity value of $w_c = 0.30$ is required to fit the run performed with an extracted polymer. Hence, the solid-state model provides conclusive evidence that unextracted and extracted samples approached different equilibrium monomer concentrations because of the difference in crystallinity.

The situation at 190°C also leads to interesting observations (Fig. 6.6.b). The model yields an excellent prediction of the run starting with a low monomer content when the crystallinity is taken as $w_c = 0.65$, that is, the value obtained by the fit in Fig. 6.5. Contrarily, there is no agreement with the data for the unextracted run, whether the crystallinity is set to $w_c = 0.65$ or the polymer is assumed amorphous ($w_c = 0$). Rather, the initial rate of caprolactam consumption appears to be consistent with the upper calculated curve ($w_c = 0$) whereas the experimental profile seems to approach an equilibrium value that is close to the lower calculated curve ($w_c = 0.65$). This suggests that the polymer gradually crystallizes as reaction proceeds, due to an increase of the melting point as the monomer concentration gets depressed. This viewpoint is corroborated by our own SSP experiment on unextracted nylon granules, throughout which the melting point was found to increase from $T_m = 215.2$ to 220.1°C (see Chapter 5).

The ability of the model to describe the time evolution of monomer during SSP validates the extrapolation of the reaction kinetics from the melt to the amorphous phase of the semicrystalline polymer. This means, for instance, that the confinement effect of crystallinity on the kinetics postulated in Section 2.2.2 appears to be ascertained, as is the accuracy of the activation energies derived from experiments conducted at temperatures far above SSP conditions. This is particularly true as there was no need to fit any diffusivity, since the experiments were conducted in closed vessels.

In summary, the performance of the solid-state model with regard to Cawthon and Smith's data is excellent. Furthermore, the implementation of both chemical equilibrium and reaction kinetics into the model is validated – at least for the polyaddition reaction.

6.4.2 Data of Fakirov and Avramova

In 1982, Fakirov and Avramova [50] studied the effect of annealing on the mechanical properties of drawn nylon-6 bristles. Since these authors also determined the molar mass, it is of interest to test the model performance for this set of data on the solid-state polymerization of an oriented (anisotropic) material.

The polymer used was a commercial PA6 bristle taken immediately after polymerization, which was dried then drawn at ambient temperature to a draw ratio of about 3.2, yielding a radius of $R = 0.85$ mm. The oriented samples, with fixed ends, were then annealed isothermally under vacuum for 6 hours, at different temperatures up to $T = 230$°C. The relative viscosity of the initial material measured in the same conditions as in this work was reported to be $\mu_{rel} = 2.50$, which, according to the correlation in Eq. (3.7), corresponds to $DP_{n,0} = 151$. This is the very same value as the one of the commercial prepolymer used by us in the experimental part of this work.

Given that Fakirov and Avramova only reported the viscosity-average chain length, DP_v, of their samples after SSP, a correlation for the number-average chain length, DP_n, is needed. For this purpose, we calculated the ratio of both averages from the reported values for the initial polymer, which yielded $DP_{v,0}/DP_{n,0} = 1.47$, and assumed that it remained constant throughout SSP. Srinivasan *et al.* [38] mentioned that this assumption holds for high-conversion polycondensation following the equal reactivity hypothesis. Furthermore, this value is in close agreement with the value of $DP_v/DP_n = 1.41$ (average of 7 samples) reported by Gaymans *et al.* [51], which bears out this procedure.

A remarkable aspect of this set of PA6 SSP data is that it is the single report in the open literature where the crystallinity was disclosed. This is of interest because *a priori* predictions can be made with the kinetic model, which was not possible for the data of Cawthon and Smith [46] where the crystallinity had to be fitted. Fakirov and Avramova assessed the crystallinity by three different methods (DSC, WAXD, and densitometry) and obtained values increasing from $w_c = 0.24$ to $w_c = 0.49$ with increasing annealing temperature. The average of all three measurements was taken for the simulations. In addition, the initial water concentration was set to zero to account for the drying procedure used, and the geometrical parameter was taken as

$\nu = 1$ since the experiments were performed on fiber-shape samples. The complete set of simulation conditions is given in Table 6.7.

Table 6.7 Parameters for simulation of Fakirov and Avramova's SSP data

Parameter	Value
Polymer geometry	$\nu = 1$ (fiber)
Fiber radius	$R = 0.85$ mm
Annealing duration	$t = 6$ h
Annealing temperature	$T = 20, 100, 120, 140, 160, 180, 200, 210, 220, 230$°C
Crystallinity	$w_c = 0.244, 0.312, 0.343, 0.355, 0.400, 0.423, 0.491, 0.492, 0.481, 0.455$ (in the respective order of the values of T)
Initial chain length *	$DP_{n,0} = 151$
Initial volatiles	$C_{1,0} = C_{2,0} = W_0 = 0$ (prepolymer extracted and dried)
Gas concentrations	$c_{g,C1} = c_{g,C2} = c_{g,W} = 0$ (vacuum)
Diffusion parameters	$D_{C1,0}$ and $D_{C2,0}$: see Section 6.5.3 ; $D_{W,0}$: see Eq. (6.55)

* Monofunctional species were disregarded

The calculated increase in number-average chain length is compared to the experimental data in Figure 6.7.a. The agreement is good considering that no parameters were adjusted. In particular, the kinetic enhancement effect postulated in Section 2.2.2 is clearly demonstrated since much lower values of the chain length would have been obtained if the distinction between local and overall concentrations had not been formulated.

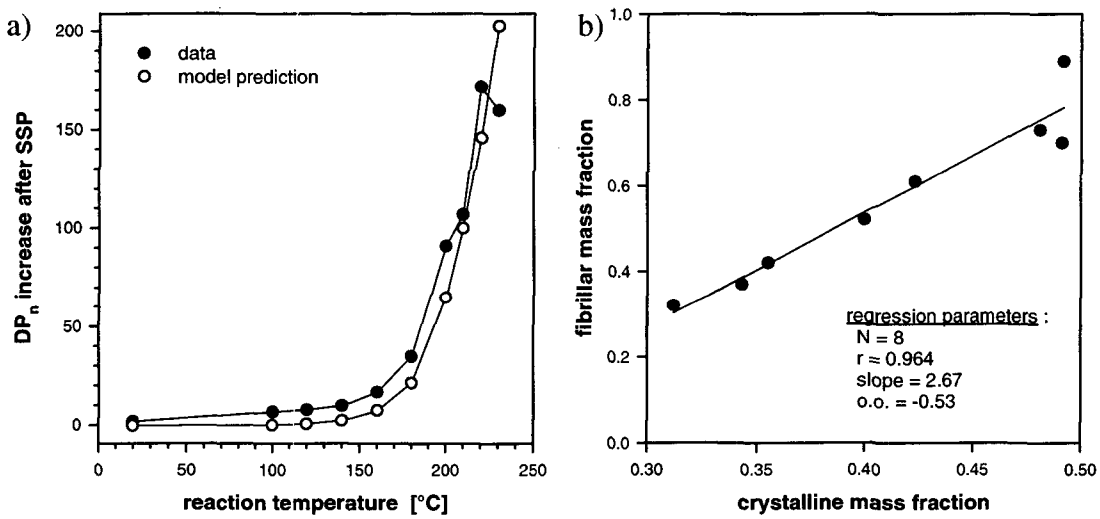

Figure 6.7 Reexamination of annealing data of Fakirov and Avramova [50] on nylon-6 fibers. a) *A priori* prediction of the final number-average chain length (lines are drawn for visualization purposes) ; b) In a refined solid-state model, the fitted fibrillar fraction is found to correlate with the crystallinity

Although the fit in Fig. 6.7.a appears very satisfactory, a closer scrutiny reveals a small but systematic underestimation of the final chain length (except for the data at $T = 230$°C where the occurrence of thermal degradation is probable). This could be easily explained by either a systematic error in the determination of the crystallinity (the three methods used were found by Fakirov and Avramova to yield quite different values), or a value of the ratio DP_v/DP_n not fully accurate. However, the reason for the discrepancy may also lie in the semicrystalline structure peculiar to fibers. Indeed, recent ^{2}H-NMR and SANS studies by Murthy and coworkers [52, 53] suggest that the amorphous phase in oriented PA6 fibers is partitioned between interlamellar and interfibrillar domains. The *interlamellar* amorphous phase is between the folded chain

interfaces of a stacked pair of crystalline lamellae, whereas the *interfibrillar* amorphous phase consists of the longitudinal channels surrounding the fibrils. This situation is analogous to an intermediate stage of spherulitic growth in an unoriented sample (see Fig. 2.5.a). Because fibrils are much larger than molecular dimensions, the functional end-groups cannot migrate from one type of amorphous phase to the other within reasonable time (see Section 2.4) and will be differently confined in the two regions. In other words, reactive species are expected to experience different local crystallinities. While the crystallinity in the interfibrillar spaces is obviously zero, the local crystallinity inside the fibrils is given according to this viewpoint as

$$w_{c,f} = \frac{w_c}{w_f} \tag{6.87}$$

where w_f stands for the fibrillar mass fraction (that is, the sum of the crystalline and amorphous interlamellar mass fractions). It follows that the reaction is expected to take place at different rates in each region, increasing the overall rate of SSP. To put this idea to test, Fakirov and Avramova's data were simulated again using this two-state assumption for all species, except for the volatiles (C_1, C_2, W) for which an instantaneous equilibrium between both amorphous phases was assumed according to the calculation in Section 2.4. In this way, it was possible to fit the value of $w_{c,f}$ for each run, so as to achieve the exact final number-average chain length. The optimization was made with a Nelder-Mead search method incorporated into the SimuSolv integration package [41].

The optimized value of the fibrillar fraction is plotted against the (overall) crystallinity in Fig. 6.7.b. Both parameters are clearly correlated, which gives credence to the above picture of the structure of PA6 fibers. The positive slope in Fig. 6.7.b suggests that orientation-induced crystallization occurs more by crystallization of the material inside the longitudinal voids surrounding the fibrils than by incorporation of the interlamellar domains.

In summary, the performance of the solid-state model with regard to Fakirov and Avramova's data substantiates the postulated effect of crystallinity on the rate of solid-state polymerization. A precise interpretation of the data provides an insight into the complex semicrystalline structure in anisotropic nylon-6 fibers and bears out some results from recent structural investigations that suggest the existence of two different types of amorphous regions.

6.4.3 Data of Gaymans *et al.*

In 1982, Gaymans *et al.* [51] reported experimental results on the solid-state polymerization of nylon-6 on fine powder ($R = 0.175$ mm) in a fluidized-bed reactor in a stream of dry nitrogen. Polymerization time-profiles were recorded for prepolymers of different chain lengths ($DP_{n,0} = 22$ to 165) at $T = 190$°C, and at different reaction temperatures ($T = 115$ to 205°C) with $DP_{n,0} = 56$. This data set is the most comprehensive one in the open literature and has been primarily used to compare model predictions to experiment [48, 49, 54].

The pronounced influence of the initial molar mass on the rate of SSP observed by Gaymans and coworkers led them to postulate the conceptual gel effect model presented in Section 2.3.1 and criticized in Section 2.3.3. Here, we shall examine the ability of the solid-state model to handle Gaymans' data based on the alternative assumption of a diffusion barrier at the particle surface due to polymer skinning. The possibility for an impermeable skin to arise from the thermo-mechanical treatment applied to ground the prepolymer to powder was first suggested by Mallon [55] in 1997, and was discussed in Section 2.3.3.

To obtain samples of variable chain length, Gaymans melt-polymerized caprolactam in sealed glass tubes at $T = 240°C$ with a variable amount of water, as listed in Table 6.8.

Table 6.8 Initial water content used by Gaymans to produce the prepolymers

Initial water mass fraction for melt polymerization $w_{W,0}$ [%]	Number-average chain length of prepolymer DP_n
20	22
10	35
5	56
1.3	95
0.4	165

Using these indications, we first simulated the liquid prepolymerization stage until the specified number-average chain length was attained, to yield the concentration values shown in Table 6.9. This set of parameters is more accurate than the values published by Gupta *et al.* [48, 49] since these authors simulated Gaymans' hydrolytic polymerization of caprolactam taking $w_{W,0} = 1.81$ % for all runs instead of the exact values in Table 6.8. For example, it can be seen from the moments of the CLD in Table 6.9 that the polydispersity index is in all cases very close to 2, that is, the prepolymers are equilibrated. By contrast, the polydispersity index predicted by Gupta is only $PDI = 1.41$ for the sample with $DP_n = 22$, far from equilibrium.

Table 6.9 Starting values for the simulation of Gaymans' SSP data *

	Initial concentrations for the different runs [mol/m^3]				
Variable	$DP_{n,0} = 22$	35	56	95	165
$C_{1,0}$	599.22	609.43	750.30	832.20	1,196.2
$C_{2,0}$	27.913	22.797	14.487	14.547	12.885
W_0	7,663.8	3,380.1	1,296.8	455.45	133.76
$P_{1,0}$	13.326	5.9601	2.6852	1.0162	0.38106
$\lambda_{P,0,0}$	303.06	213.26	140.57	83.560	45.895
$\lambda_{P,1,0}$	6,925.3	7,621.3	7,840.0	7,900.9	7,597.4
$\lambda_{P,2,0}$	309,650	537,340	866,280	1,493,200	2,552,700

* Monofunctional species were disregarded

The solid-state experiments of Gaymans were then modeled assuming no mass transfer to account for the polymer skin. The values in Table 6.9 were taken as the initial conditions, except for caprolactam and the cyclic dimer, which were set to zero to duplicate the washing of the samples in boiling methanol. For each simulation, an initial water content was assumed that is less than the corresponding value after the melt polymerization (Table 6.9). This idea assumes that the processing done prior to SSP does not remove all the water. The mass transfer limitation will turn out only to be significant for the low molar mass cases. For the runs starting with higher molar masses, the reduced end-group concentration is sufficient to cause the polymerization

to be kinetically limited over the observed time scale. In addition, the crystallinity was also tuned since it was not measured by Gaymans. Figure 6.8.a shows that the model compares well to the data for the best-fit values of W_0 and w_c disclosed in Table 6.10. Hence, the solid-state model bears out the idea of a structural diffusion barrier at the particle surface to explain Gaymans' puzzling observation on PA6 powder, not a kinetic limitation by the diffusion of functionalities.

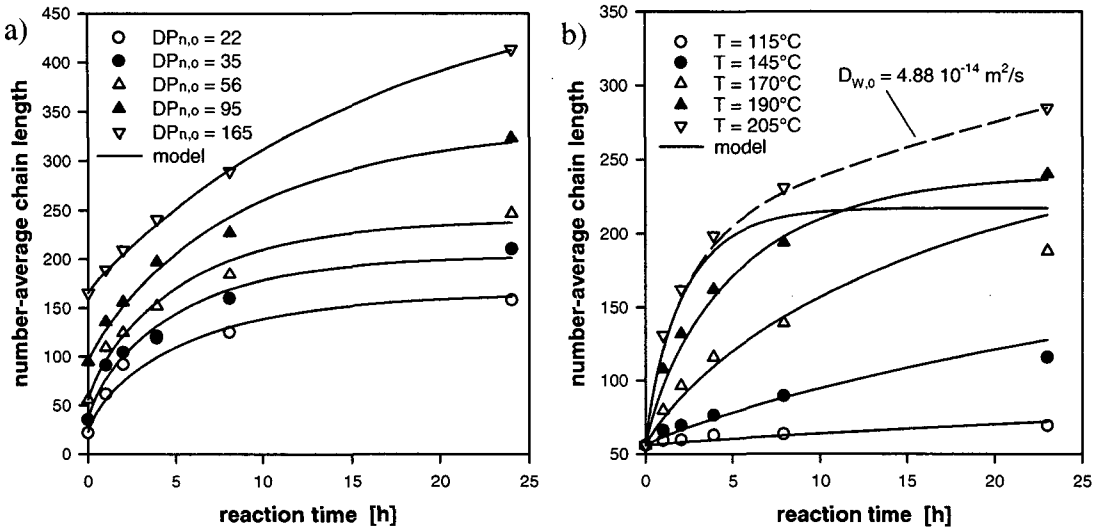

Figure 6.8 Comparison of model to data of Gaymans *et al.* [51] on the solid-state polymerization of nylon-6 in powder form. a) Series with different initial chain lengths ; b) Series with different reaction temperatures

The best-fit values for the initial concentration of water (Table 6.10) are all below the calculated values after the liquid prepolymerization stage (Table 6.9) and decrease with increasing molar mass of the prepolymer – as do the values in Table 6.9. In other words, the limitation by the amidation equilibrium in the lower curves in Fig. 6.8.a appears to arise also because of the higher amount of water that was used by Gaymans to produce samples of lower molar mass.

Table 6.10 Best-fit parameter values for the simulation of Gaymans' SSP data

Initial chain length of experiment $DP_{n,0}$	Initial water concentration W_0 [mol/m^3]	Crystallinity w_c
22	596	0.69
35	589	0.75
56	524	0.77
95	281	0.78
165	108	0.76

The optimization procedure yielded similar best-fit values of the crystallinity for all runs ($w_c = 0.75$ to 0.78), except for the experiment starting with the lowest molar mass where a slightly lower crystallinity ($w_c = 0.69$) was obtained. This may be related to the presence of a particularly large amount of water during the solidification of the corresponding prepolymer. Anyhow, the nylon particles processed by Gaymans seem to be much more crystalline than are the commercial chips used in the experimental part of this study ($w_c = 0.456$). This is consistent with Gaymans cooling the starting material from the melt at a slow rate (5°C/min), whereas the product strand exiting industrial melt prepolymerizer is usually quenched. Therefore, reexamining Gaymans' data in the light of the propounded model emphasizes the

possibility to improve the morphology of the prepolymer by controlling the time-temperature profile upon cooling from the melt. Further evidence supporting this idea will be revealed in the next section.

The series of SSP at different reaction temperatures was also modeled, using the parameter values for the corresponding prepolymer ($DP_{n,0} = 56$) in Table 6.10. In other words, W_0 and w_c were taken from the fit of the 190°C data to make *a priori* predictions for the other temperatures. The simulation results, disclosed in Fig. 6.8.b, agree well with the data for $T = 115$, 145 and 170°C. The prediction for the highest temperature ($T = 205$°C) is excellent for the initial rate of polymerization, but underestimates the experimental data at longer times. More precisely, the model predicts that equilibrium is reached after $t \sim 10$ h whilst the experimental profile does not plateau within reaction time. However, an excellent fit can be achieved in this case if the no mass transfer assumption is relaxed, for an optimum water diffusivity of $D_{W,0} = 4.88 \cdot 10^{-14}$ m^2/s (the dashed curve in Fig. 6.8.b). This value is five orders of magnitude lower than the diffusion coefficient given by Eq. (6.55) – $D_{W,0} = 1.43 \cdot 10^{-9}$ m^2/s [35] – so this additional parameter is still consistent with polymer skinning. The successful description of the temperature dependence of Gaymans' SSP data by the solid-state model substantiates the postulate used to simulate the runs starting with different molar masses, namely that the reduction in rate as solid-state polymerization proceeds is indicative of water mass transfer limitations, not limited diffusion rates of end-groups.

6.4.4 Data of Blanchard *et al.*

In Section 1.3, a novel DuPont process for the manufacture of nylon-6 patented by Blanchard *et al.* in 1999 [56] has been presented, in which the product exiting the melt prepolymerization stage was subjected to a controlled time-temperature profile during solidification instead of the usual water quench. In this way, the subsequent postcondensation stage was improved by allowing the operation of the solid-phase polymerizer at higher temperatures with a feed of granules containing up to 6 % of caprolactam and cyclic oligomers. This led to favorable economics by decreasing the required residence time for solid-state polymerization. In addition, the expensive water extractor could be replaced by a flasher in which the extractable impurities were reduced from their equilibrium value (~ 11 %) to about 6 % by stripping or boiling them off from the prepolymer.

Blanchard and his colleagues ascribed the benefit of annealing the prepolymer to an increase of its softening temperature, in particular because the formation of the high-melting crystalline form (the α modification) was promoted by this treatment. This lessened particle agglomeration due to surface softening and consequently allowed for higher SSP operating temperatures. The effect of the thermal treatment on the crystallinity is not explicitly mentioned. Because some data obtained on small fixed-bed reactors (whose operation is not limited by T_s) are disclosed in the patent, it is instructive to examine them using the solid-state model.

The fixed-bed reactors consisted of glass tubes ($\phi = 3.12$ cm) immersed in a sand bath operating isothermally. A reactor was charged with $m = 20$ g of precursor granules and SSP was achieved by flowing nitrogen through the bed of particles ($u \sim 0.3$ cm/s). As these conditions are similar to the ones used by us in the experimental part of this

work, a differential regime can be safely assumed and the single particle model may therefore be applied.

Two series of polymerization data are represented in Figure 6.9. In a first run, a prepolymer that had *not* been subjected to the controlled temperature history (i.e. quenched) was reacted at $T = 210°C$ and DP_n values were reported after $t = 2$ and 4.6 h. Second, a single point at $t = 4.6$ h was also disclosed for an experiment at $T = 180°C$ on a prepolymer crystallized in controlled conditions (i.e. annealed). Other data reported by Blanchard were not considered since they fell out of the scope of the present model due to the use of sodium hypophosphite as a catalyst. A qualitative comparison of the two runs is not possible given that two parameters were varied at the same time (pretreatment and reaction temperature). This makes a comparison with the model particularly interesting.

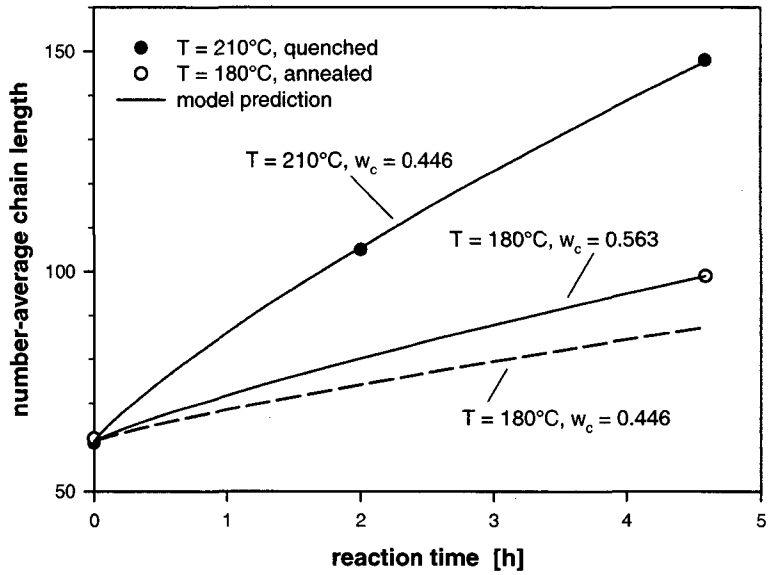

Figure 6.9 Comparison of model to data of Blanchard *et al.* [56] on the solid-state polymerization of a Du Pont nylon-6 prepolymer. Simulation results suggest that the operating advantages obtained with the novel particle-forming step disclosed in the Du Pont patent are related to an increased crystallinity

Simulation results in which the crystallinity was adjusted to fit the experimental data are also shown in Fig. 6.9 (with other conditions listed in Table 6.11). For the quenched sample, an excellent agreement between experiment and model prediction is observed for an optimized crystallinity of $w_c = 0.446$. This value is, within experimental accuracy, identical to the crystallinity of the prepolymer used in the present study ($w_c = 0.456$ – see Table 3.1), which is not unexpected since a water quench was applied in both cases. By contrast, a crystallinity value of $w_c = 0.563$ is required to describe the 210°C data, leading to the conclusion that crystallization occurred to a greater extent as a consequence of the controlled temperature history applied during the particle-forming step. To make a comparison possible, a simulation was performed at 180°C with the standard crystallinity value ($w_c = 0.446$). The result (dashed curve in Fig. 6.9) thus stresses the enhanced rate of polymer build-up that is obtained from the additional crystallization due to the annealing.

In conclusion, scrutinizing Blanchard's data by means of the developed model suggests that the advantage of this new DuPont process is not only related to a higher

softening temperature, but also lies in an increased rate of solid-state polymerization at a definite temperature due to an increased crystallinity.

Table 6.11 Parameters for simulation of Blanchard's SSP data

Parameter	Value [56]
Reaction temperature	T = 180°C (annealed) and 210°C (quenched)
Particle radius *	R = 1.5 mm
Initial number-average chain length †	$DP_{n,0}$ = 61
Initial caprolactam	$w_{C1,0}$ = 6.5 % (annealed) and 5.6 % (quenched)
Initial cyclic dimer	$w_{C2,0}$ = 0.6 %
Initial water	$w_{W,0}$ = 0 (assumption)
Gas phase concentrations	$c_{g,C1} = c_{g,C2} = c_{g,W} = 0$ (stripping)
Diffusion parameters	$D_{C1,0}$ and $D_{C2,0}$: see Section 6.5.3 ; $D_{W,0}$: see Eq. (6.55)

* Taken as the extruder radius at the flasher exit

† Monofunctional species were disregarded

6.5 Prediction of Fixed-Bed Experiments

We shall now examine the ability of the single particle model to handle our experimental data on the solid-state polymerization of commercial nylon-6 granules, obtained in the battery of fixed-bed reactors. Calculated and experimental polymerization profiles for the base case run are compared in Fig. 6.10, where the dashed curve represents the model prediction according to the basic assumptions (Section 6.2.1) for the reference set of parameters (Table 3.1). This is a truly predictive simulation since the only unknown parameters – the diffusivities of caprolactam and the cyclic dimer – were found to have no significant influence on the calculated DP_n values (and were consequently set to zero).

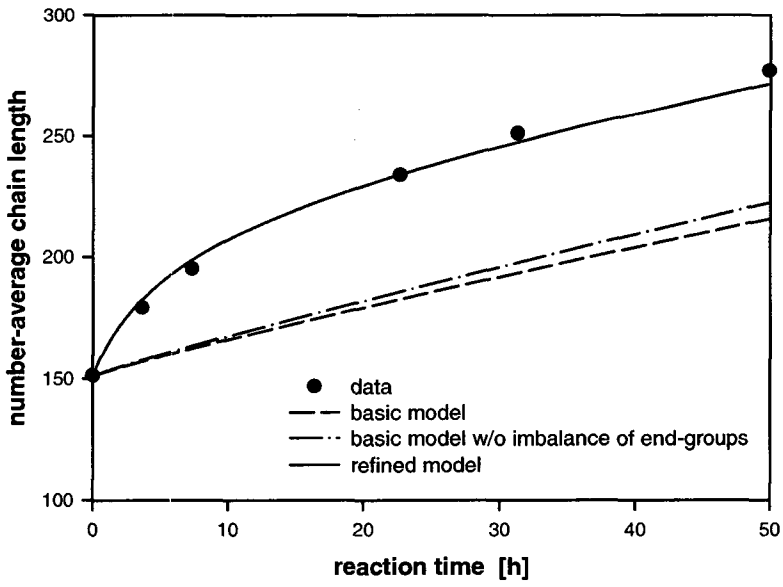

Figure 6.10 Model prediction of nylon-6 solid-state polymerization at 165°C in the fixed-bed reactors (base case run)

It appears from Fig. 6.10 that the basic solid-state model underestimates the rate of polymer build-up, particularly during the first hours of reaction. This cannot be explained by questioning one of the primary assumptions used (no gel effect, no convective resistance to volatilization, zero concentration of volatiles in the gas

phase), since this would lead to even smaller reaction rates. In addition, assuming no decarboxylation during the melt prepolymerization would not affect SSP very much. This can be seen by considering the relation between the maximal number-average chain length that can be achieved and the extent of decarboxylation (given without demonstration) :

$$DP_{n,max} = DP_{n,0}\left(\frac{2-\psi}{\psi}\right) \tag{6.88}$$

For the reference values of $DP_{n,0} = 151$ and $\psi = 0.0564$, Eq. (6.88) yields $DP_{n,max} = 5{,}200$, more than ten times the highest experimental DP_n under consideration. Therefore, decarboxylation in the VK column does not occur to such an extent that the resulting end-group imbalance should influence SSP. To stress this point, a simulation was performed with $\psi = 0$ (the dash-dot curve in Fig. 6.10) : the increase in polymerization compared to the base case calculation is indeed not significant.

In fact, the rate of chain building during SSP of nylon-6 is mainly controlled by the polycondensation kinetics, as discussed in Section 2.4, and the discrepancy in Fig. 6.10 should be investigated from this viewpoint. More precisely, we shall examine in the next section the possibility that the reactive functionalities are not uniformly distributed within the non-crystalline phase. This will require a more detailed picture of the effect of the semicrystalline structure on the solid-state polymerization, leading to an improved description of the experimental data (the solid curve in Fig. 6.10).

6.5.1 Refined Solid-State Assumptions

There are several potential reasons for the spatial distribution of end-groups throughout the amorphous phase to be inhomogeneous. Three cases are schematized in Figure 6.11 and discussed below. In all of these pictures, the local concentration of end-groups is postulated to vary from one amorphous region to another, leading to different local reaction rates. The average reaction rate will thus be different than in a homogenous system as a result of its non-linear dependence on the concentration ; precisely, an increased overall rate of solid-state polymerization is expected because the order of reaction is higher than one. In other words, this refined solid-state concept consists in assuming a second level of segregation in the nylon granule. The first level is the partition between crystalline and amorphous phases, which, given the exclusion of the reactive species from the crystallites, is a case of total segregation. The second level now assumes that the amorphous phase itself is partitioned, leading to a total segregation of the end-groups but to an instantaneous equilibration (micromixing) of the volatile by-products, because of the difference in diffusivity (see Section 2.4).

First, the crystallites may assemble into meso-scale superstructures that do not fill the entire space (Fig. 6.11.a). This situation is unlikely to happen in undrawn nylons crystallized under mild conditions, because spherulites usually grow to completion (i.e. until their coming into contact with each other) within minutes [57, 58]. In addition, it was shown in Chapter 5 that the granules of this study contained an insignificant amount of spherulites, the crystalline lamellae being mostly distributed at random throughout the amorphous matrix. Therefore, the partition of the

amorphous phase suggested in Fig. 6.11.a cannot explain our experimental results. However, this picture can hold for drawn PA6 fibers, in which the distinction between interlamellar and interfibrillar amorphous domains has been demonstrated [52, 53]. This assumption was successfully used in Section 6.4.2 to improve the model performance regarding Fakirov and Avramova's SSP data on oriented PA6 bristles.

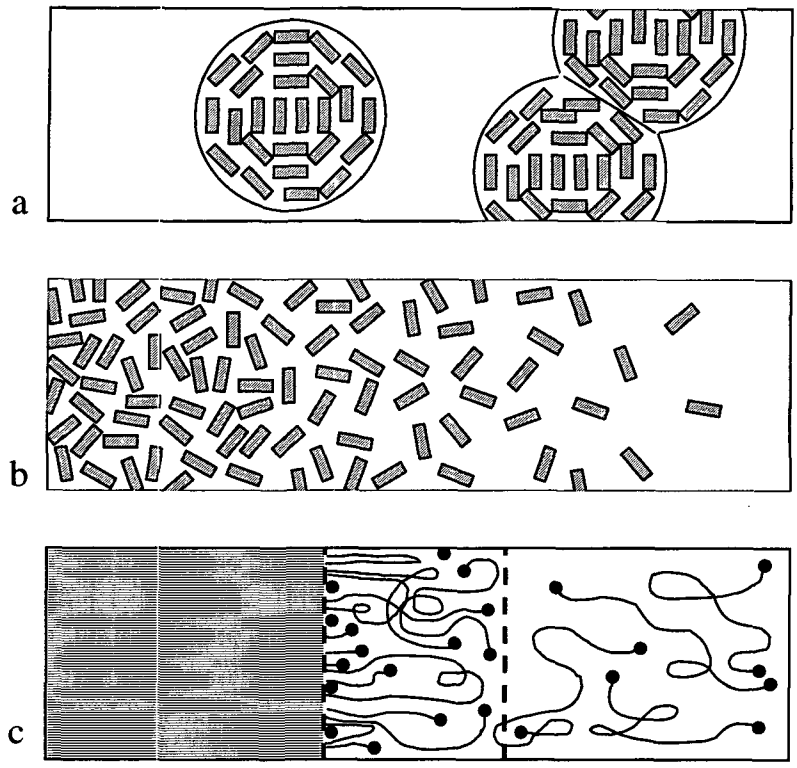

Figure 6.11 Different possibilities for a non-uniform effect of the crystalline structure on the concentration of reactive species in the amorphous phase. a) Crystalline superstructures ; b) A spatial crystallinity gradient ; c) A higher concentration of species in the vicinity of the basal surface

Second, a radial profile of crystallinity (Fig. 6.11.b) decreasing from the center to the surface of the particle may develop upon quenching the prepolymer from the melt, because of heat transfer during solidification. This is corroborated by Starkweather *et al.* [57], who observed that injection molded PA66 tensile bars were less crystalline on the surface than in the center. The effect of such a structural gradient on the course of SSP is illustrated in Figure 6.12, where a simulation for a linear crystallinity profile is compared to the reference run (uniform crystallinity) for the same overall value of $w_c = 0.456$. A higher rate of polymerization is indeed predicted in the former case (Fig. 6.12.a). The situation looks more complex for the caprolactam and cyclic dimer, due to the interplay between reaction and diffusion (Fig. 6.12.b). Given the difficulty to determine such a morphological feature, this idea was not investigated any further. Moreover, Albano *et al.* [59] recently performed calculations for PA66 plaques based on the dynamic crystallization kinetics and did not obtain a significant crystallinity profile for a cooling rate of 20 K/min.

Third, it is within possibility that the concentration of functionalities is higher near the crystalline surface than in the remainder of the amorphous phase, because of the time required for those end-groups rejected from the crystallites upon solidification to diffuse into the entire amorphous matrix. This would explain the high rates of SSP

observed during the first hours of reaction. It has been shown in Section 2.3.2 that the time scales for end-group diffusion through interchange reactions and forward polycondensation are similar when the diffusion length is equal to the characteristic distance between end-groups, d (see Fig. 2.17). However, taking half the interlamellar spacing ($l/2$) instead of d as the diffusion length in Eq. (2.27) leads to the conclusion that reaction is much faster than the diffusional homogenization of chain-ends throughout the amorphous phase (see the l/d calculation in Section 2.2.3). Therefore, the assumption that end-groups are segregated between a boundary layer in the vicinity of the crystalline lamellae and the bulk amorphous phase is plausible (Fig. 6.11.c).

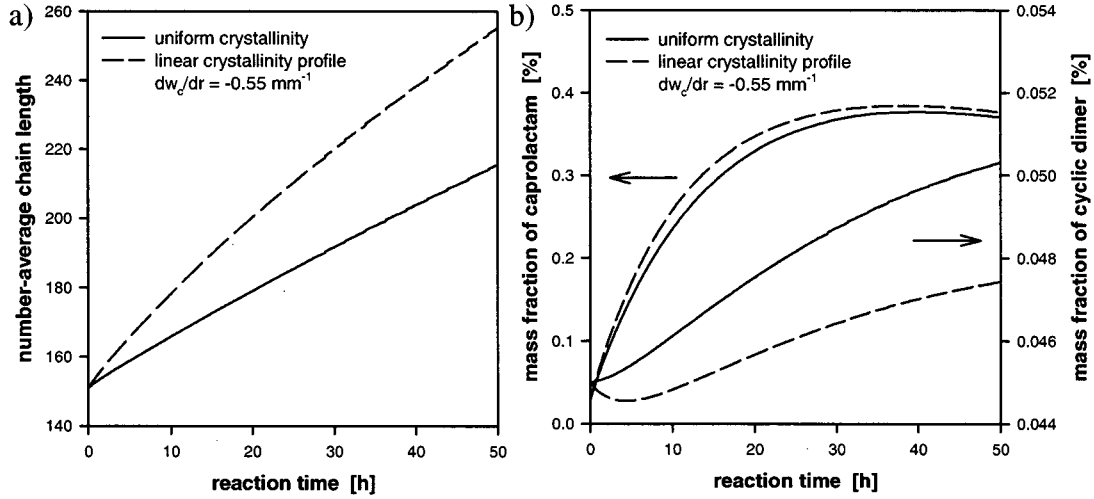

Figure 6.12 Effect of a spatial gradient of crystallinity on : a) Polymer build-up ; b) Volatile species. Simulations were performed using reference parameter values, except $\nu = 0$ (plane sheet)

Based on the simplified picture of the semicrystalline structure made of regularly alternating crystalline and amorphous zones, the initial concentration of chain-ends in the interphase (shown as pertaining to molecular cilia in Fig. 6.11.c), c_i, and in the bulk amorphous phase, c_a, are readily expressed as

$$c_i = c^* \left(\frac{l\,F}{2\sigma} \right) \tag{6.89}$$

$$c_a = c^* \left(\frac{l(1-F)}{l-2\sigma} \right) \tag{6.90}$$

where F and σ stand respectively for the initial fraction of end-groups present in the interphase and for the boundary layer thickness. The factor 2 appears because the concentration effect takes place on *both* basal planes of a crystallite (the contribution of the growth planes to the total surface of the lamella is negligible). After elimination of the concentration c^* and the interlamellar spacing l by means of Eq. (2.11) and (2.14), respectively, the following expressions are obtained :

$$c_i = c \left(\frac{F\,\Lambda\alpha_{200}\,(P(1-w_c)+w_c)}{2\sigma\,w_c} \right) \tag{6.91}$$

$$c_a = c\left(\frac{(1-F)\,\Lambda\alpha_{200}\,P(1-w_c)}{\Lambda\alpha_{200}\,P(1-w_c)-2\sigma\,w_c}\right) \tag{6.92}$$

The parameters involved in these equations are compiled in Table 6.12. The boundary layer thickness, σ, is conveniently approximated as the width of the rigid amorphous phase (see the three-phase model of semicrystalline polymers discussed in Section 2.2.1) for which a value for unoriented PA6, obtained by SANS, was recently disclosed in the literature [60]. The lateral size of the crystallite, $\Lambda\alpha_{200}$, has been determined by WAXD.

Table 6.12 Structural parameters of the refined solid-state model

Parameter	Symbol	Typical value	Source
Fraction of end-groups in the interphase	F	0.464	Data fit (see next section)
Ratio of crystal-to-amorphous densities	P	1.138	Pflüger [35]
Crystallinity	w_c	0.456	DSC measurement
Lateral size of crystallite	$\Lambda\alpha_{200}$	12 nm	WAXD measurement
Thickness of interphase	σ	0.62 nm	Murthy and Orts [60]

In summary, a refined solid-state model is postulated, in which reactive end-groups are partitioned between a region close to the crystalline lamellae and the remainder of the amorphous phase. According to this picture, which is again related to the non-equilibrium nature of the semicrystalline polymer, the partition coefficient F must be equal to the fraction of chain-ends in the molten polymer that are expelled upon crystallization, plus the fraction of ends initially present in the volume occupied by the interphase, that is,

$$F = w_c\left(1+\frac{2\,\sigma}{\Lambda\alpha_{200}}\right) \cong w_c \tag{6.93}$$

if the latter contribution is neglected. Given this physical meaning for F, no unknown parameter is introduced in the refined model and *a priori* predictions of polymerization profiles are still possible.

6.5.2 Simulation of Polymerization Profiles

The experimental time course of number-average chain length is well described by the refined solid-state model at all reaction temperatures (Figure 6.13). A considerable improvement of the model performance is thus achieved by implementing the refined solid-state assumption. In particular, both the initial curvature of the polymerization profile and the reaction rate at larger times are successfully modeled. The constant F was adjusted to fit all runs simultaneously, yielding an optimal value of $F = 0.464$. This is very close to the crystalline mass fraction ($w_c = 0.456$), and thus backs up the physical significance of F suggested in Eq. (6.93).

Next, the polymerizations with samples of different crystallinities were modeled assuming a different value of F for each simulation. Again, the model agrees well with the data (Figure 6.14.a). The best-fit value of F is represented as a function of w_c in Fig. 6.14.b. The correlation in Eq. (6.93) is remarkably substantiated inside the

limited crystallinity range under consideration, which adds credence to the propounded model.

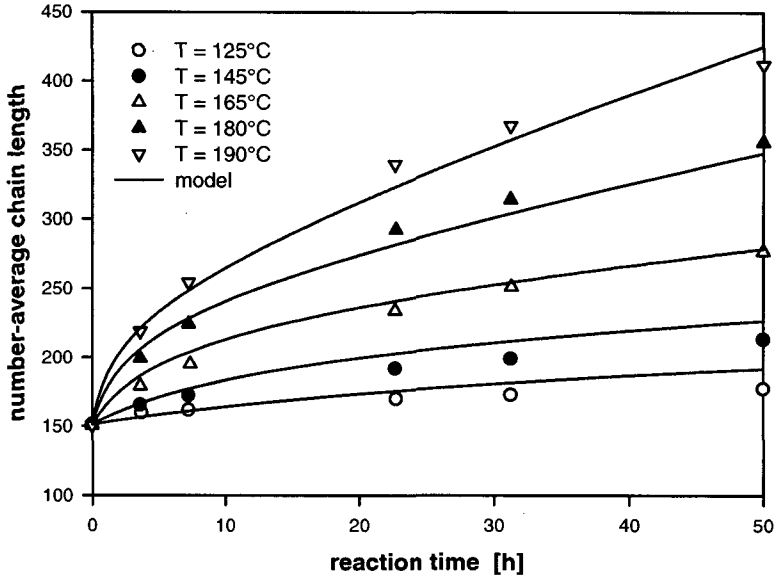

Figure 6.13 Comparison of polymerization profiles predicted by the refined solid-state model with experimental data from the battery of fixed-bed reactors. Simulations were performed with $F = 0.464$ as the best-fit value for all runs

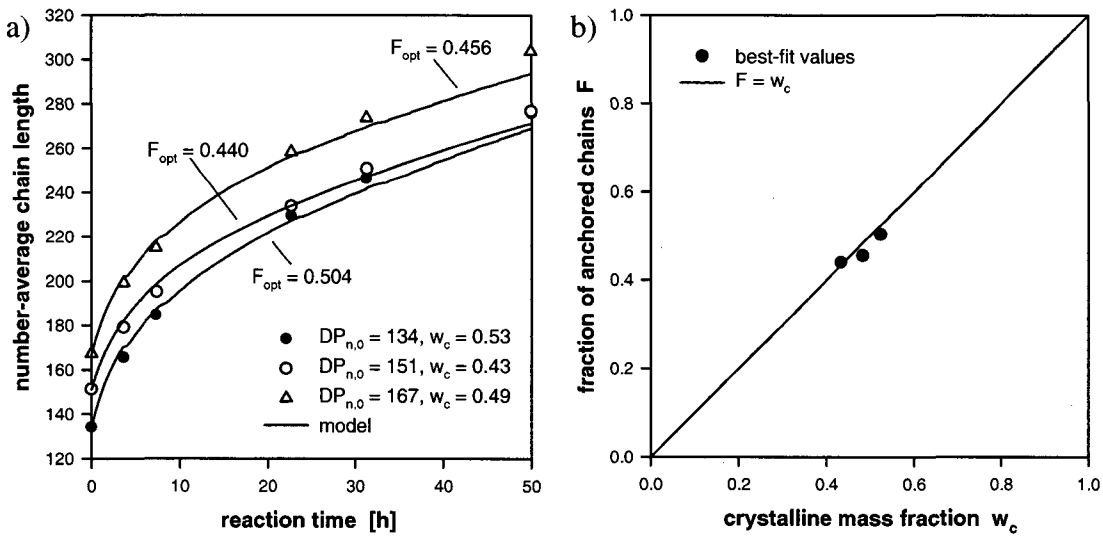

Figure 6.14 Effect of crystallinity on F. a) Simulation of experiments with different values of w_c ; b) Correlation between F and w_c

6.5.3 Simulation of Caprolactam and Cyclic Dimer Profiles

Simulation results for the spatial-average values of caprolactam and the cyclic dimer vs. time for different temperatures are displayed in Figure 6.15, using optimal values of the amorphous diffusivities, $D_{C1,0}$ and $D_{C2,0}$. The concentrations of C_1 and C_2 in the extracted polymer were assumed to be sufficiently low to avoid a free volume effect, if any, on the diffusion process. Therefore, $D_{C1,0}$ and $D_{C2,0}$ represent diffusivities in the limit of zero concentration and were taken to be constant during SSP. Experimental data points and calculated curves are in good agreement, both for

remonomerization (Fig. 6.15.a) and the formation of the cyclic dimer (Fig. 6.15.b). The reader is referred to Section 4.3 for a qualitative explanation of the data.

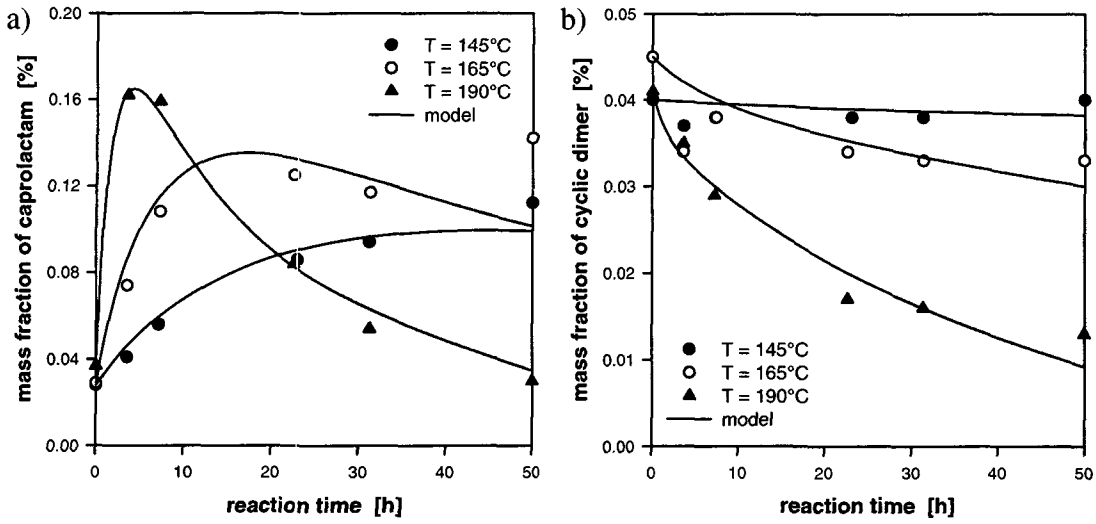

Figure 6.15 Modeling of volatile by-products at different reaction temperatures. a) Caprolactam time-profile ; b) Cyclic dimer time-profile

The optimized values of $D_{C1,0}$ and $D_{C2,0}$ both obey an Arrhenius relationship in the temperature range under consideration (125-190°C), as shown in Figure 6.16. The correlations in Fig. 6.16 bear out *a posteriori* the assumption of treating caprolactam and the cyclic dimer as volatile species. Though evident for C_1, this was not necessarily obvious for C_2 given its high melting point – T_m = 347°C [61].

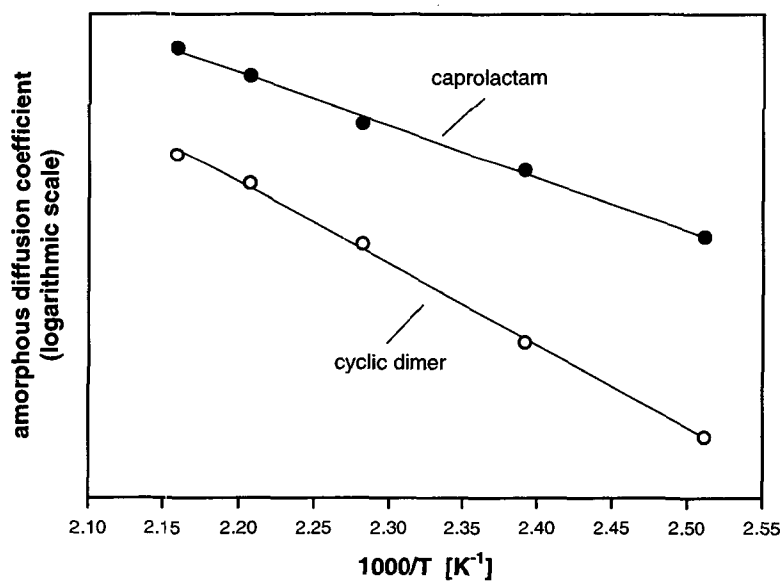

Figure 6.16 Arrhenius diagram for the diffusion coefficients of caprolactam and the cyclic dimer in the limit of zero concentration

The absence of any deviation from linearity in Fig. 6.16 indicates that the diffusion of volatiles is not limited by the availability of free volume. In other words, diffusion appears as a purely activation-controlled process in the temperature range investigated, which is not surprising since the lowest reaction temperature (125°C) is still much higher than the glass transition temperature (61°C). This allows

implementing the temperature dependence of the diffusion coefficients in the kinetic model without the need for estimates of the various parameters of the free volume theory. In addition, the relative order of the diffusion coefficients with regard to the different solutes ($D_{W,0} > D_{C1,0} > D_{C2,0}$), and to the activation energies ($E_{d,W} < E_{d,C1} < E_{d,C2}$), are consistent with their respective size ($M_W < M_{C1} < M_{C2}$).

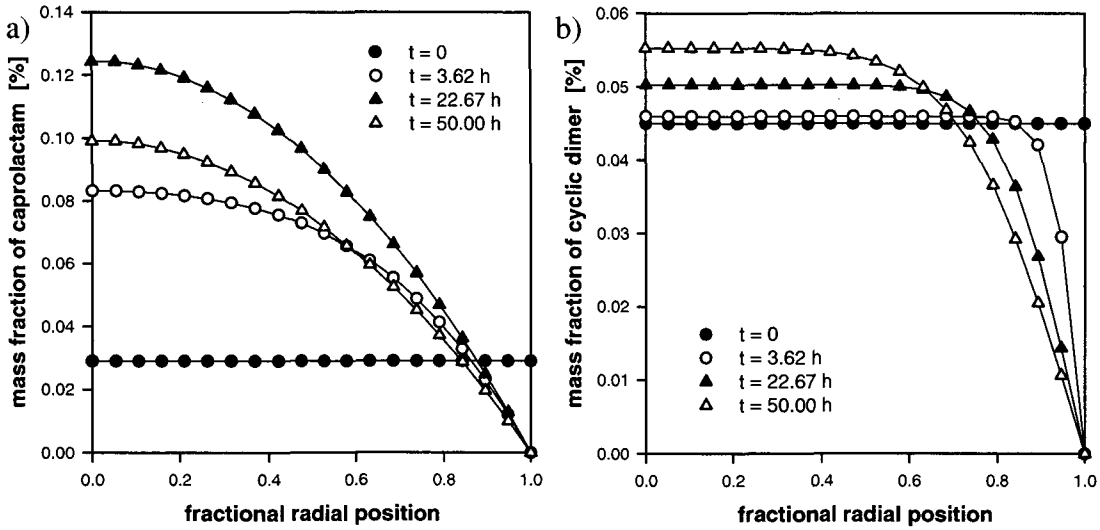

Figure 6.17 Radial concentration profiles for the by-products at different times for the reference run. a) Caprolactam ; b) Cyclic dimer

Using the diffusion coefficients derived above, radial concentration profiles inside the particle were calculated at the reference temperature of 165°C, for different reaction times up to 50 h. The results, disclosed in Figure 6.17, illustrate the interplay between reaction and diffusion. Caprolactam (Fig. 6.17.a) and the cyclic dimer (Fig. 6.17.b) build up in the interior of the polymer particle due to generation by the cyclization reaction, while macro-level diffusion leads to a decrease in concentration in the outer shell of the particle. This latter effect is more pronounced for the cyclic dimer because of its much smaller diffusivity. In fact, diffusion of C_2 is so slow that the concentration gradient penetrates only the outer fringes of the polymer particle within reaction time, whilst diffusion of C_1 takes place inside the entire particle quite early during the reaction. The number of finite-difference grid points have been increased from 10 to 20 to generate these profiles to account for the relatively sharp gradients of C_2 near $r = R$.

Finally, the time evolution of caprolactam and the cyclic dimer during the SSP experiment in which the fixed-bed reactors were fed with an unextracted prepolymer was also modeled, using the above optimal diffusion coefficients (i.e. tuned on the extracted runs). Experimental data points and calculated curves compare reasonably well, as shown in Figure 6.18 – the prediction is particularly good for the cyclic dimer. This supports the above conclusion that the diffusion of by-products is not limited by the scarcity of free volume. In case of such a limitation, the additional free volume provoked by the presence of large amounts of extractables would indeed lead to higher diffusivities. Consequently, the diffusion coefficients in the model are assumed to depend only on the temperature (Fig. 6.16 and Eq. 6.55) and on the crystallinity (Eq. 2.22), but neither on the concentration of small molecules, nor on the molar mass of the polymer.

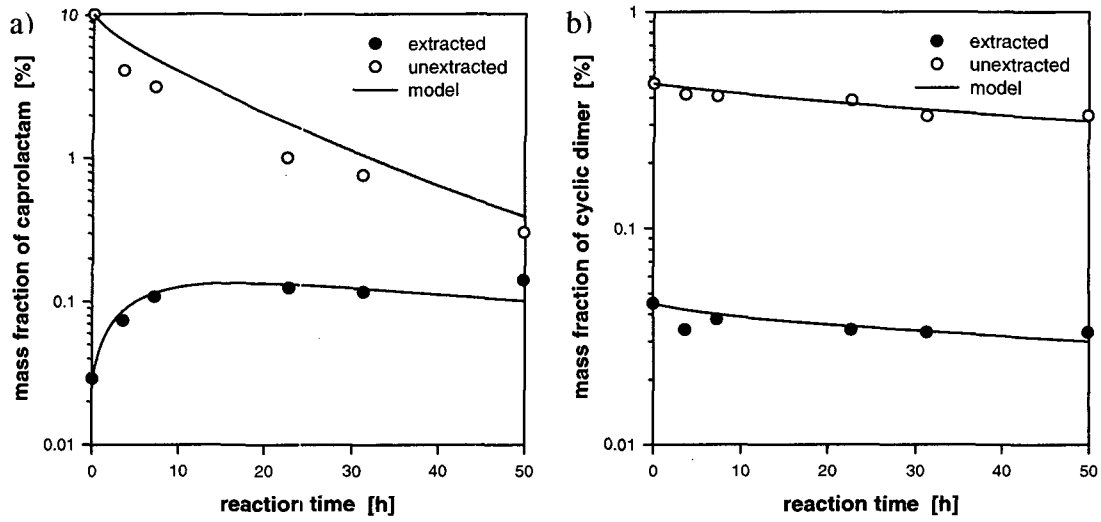

Figure 6.18 Model performance for solid-state polymerization of an unextracted polymer at 165°C. a) Caprolactam profile ; b) Cyclic dimer profile. The diffusivities from the fit of the extracted runs were used to simulate the unextracted runs

In summary, the single particle model has been shown to work and has been compared to a wide range of data, including both literature reports and our own set of experiments. This validated some core model assumptions and provided a closer insight into the influence of semicrystallinity on solid-state polymerization. In particular, the structural effects of the mechanical and thermal history on the polymerization were brought to the fore, although they are not necessarily easy to quantify. For the first time, accurate values of the diffusion coefficients of caprolactam and the cyclic dimer could be obtained, which is of the utmost importance regarding any realistic optimization or design strategy of an industrial nylon-6 solid-state reactor. In addition, the model is comprehensive and on a phenomenological basis, which allows *a priori* simulations. This is obviously a prerequisite for a rational scale-up. By contrast, the most recent model of nylon-6 solid-state polymerization [49] contains seven data-fitted parameters that are certainly poorly extrapolable.

6.6 References

[1] Kuhn W (1930). Über die Kinetik des Abbaues hochmolekularer Ketten. *Ber. Chem. Dtsch. Ges.*, 63, 1503.

[2] Schulz G.V. (1939). Über die Kinetik der Kettenpolymerisationen. V. Der Einfluss verschiedener Reaktionsarten auf die Polymolekularität. *Z. Phys. Chem.*, B43, 25.

[3] Flory P.J. (1936). Molecular size distribution in linear condensation polymers. *J. Am. Chem. Soc.*, 58, 1877.

[4] Flory P.J. (1946). Fundamental principles of condensation polymerization. *Chem. Rev.*, 39, 137.

[5] Flory P.J. (1953). Principles of polymer chemistry. Cornell University Press pub., Ithaca, New York.

[6] Laurence R.L., Galvan R. and Tirrel M.V. (1994). Mathematical modelling of polymerization kinetics. In : Polymer reaction engineering, McGreavy ed., Blackie pub., 87.

[7] Lowry G.G. (1970). Markov chains and Monte Carlo calculations in polymer science. Marcel Dekker pub., New York.

[8] Basedow A.M., Ebert K.H. and Ederer H.J (1978). Kinetic studies on the acid hydrolysis of dextran. *Macromol.*, 11, 774.

[9] Nattorp A., Graf M., Spühler C. and Renken A. (1999). Model for random hydrolysis and end degradation of linear polysaccharides: application to the thermal treatment of mannan in solution. *Ind. Eng. Chem. Res.*, 38, 2919.

[10] Gupta S.K., Naik C.D., Tandon P. and Kumar A. (1981). Simulation of molecular weight distribution and cyclic oligomer formation in the polymerization of nylon 6. *J. Appl. Polym. Sci.*, 26, 2153.

[11] Ray W.H. (1972). On the mathematical modeling of polymerization reactors. *J. Macromol. Sci. - Revs. Macromol. Chem.*, C8, 1

[12] Gupta S.K. and Kumar A. (1987). Reaction engineering of step growth polymerization. Plenum Press pub., New York.

[13] Tirrell M.V., Pearson G.H., Weiss R.A. and Laurence R.L. (1975). An analysis of caprolactam polymerization. *Pol. Eng. Sci.*, 15, 386.

[14] Gupta S.K., Kumar A. and Agrawal K.K. (1982). Simulation of three-stage nylon 6 reactors with intermediate mass transfer at finite rates. *J. Appl. Polym. Sci.*, 27, 3089.

[15] Miller N.C., Toffolo R.W., McAuley K.B. and McLellan P.J. (1996). Determining polymer chain length distributions using numerical inversion of Laplace transforms. *Polym. Reac. Eng.*, 4, 279.

[16] Zeman R. and Amundson N.R. (1963). Continuous models for polymerization. *AIChE J.*, 9, 297.

[17] Zeman R. and Amundson N.R. (1965). Continuous polymerization models. II. Batch reactor polymerization. *Chem. Eng. Sci.*, 20, 637.

[18] Ziff R.M. and McGrady E.D. (1986). Kinetics of polymer degradation. *Macromol.* 19, 2513.

[19] Tai K., Arai Y., Teranishi H. and Tagawa T. (1980). The kinetics of hydrolytic polymerization of ε-caprolactam. IV. Theoretical aspect of the molecular weight distribution. *J. Appl. Polym. Sci.*, 25, 1789.

[20] Gupta S.K. and Kumar A. (1983). Simulation of step growth polymerization. *Chem. Eng. Commun.*, 20, 1.

[21] Merrill E.W. (1996). Thermodynamic aspects of devolatilization of polymers. In : Polymer devolatilization, Albalak R.J. ed., Marcel Dekker pub., 13.

[22] Götz W. (1997). High molecular weight polyamides obtained from nitriles. *U.S. patent 5,596,070 to BASF.*

[23] Kruissink C.A., van der Want G.M. and Staverman A.J. (1958). On the mechanism of the polymerization of ε-caprolactam. I. The polymerization initiated by ε-aminocaproic acid. *J. Polym. Sci.*, 30, 67.

[24] Reimschuessel H.K. and Dege G.J. (1970). Polyamides: decarboxylation and desamination in nylon 6 equilibrium polymer. *J. Polym. Sci. : Part A-1*, 8, 3265.

[25] Dege G.J. and Reimschuessel H.K. (1973). Peroxidation of caprolactam and its effect on equilibrium polymerization of cyclic dimer. *J. Polym. Sci., Polym. Chem. Ed.*, 11, 873.

[26] Flory P.J. (1939). Kinetics of polyesterification : a study of the effects of molecular weight and viscosity on reaction rate. *J. Am. Chem. Soc.*, 61, 3334.

[27] Semlyen J.A. and Walker G.R. (1969). Equilibrium ring concentrations and the statistical conformations of polymer chains II - Macrocyclics in nylon 6. *Polymer*, 10, 597.

[28] Heikens D., Hermans P.H. and van der Want G.M. (1960). On the mechanism of the polymerization of ε-caprolactam. IV. Polymerization in the presence of water and either an amine or a carboxylic acid. *J. Polym. Sci.*, 44, 437.

[29] Tai K. and Tagawa T. (1983). Simulation of hydrolytic polymerization of ε-caprolactam in various reactors. A review on recent advances in reaction engineering of polymerization. *Ind. Eng. Chem. Prod. Res. Dev.*, 22, 192.

[30] Tai K., Teranishi H., Arai Y. and Tagawa T. (1979). The kinetics of hydrolytic polymerization of ε-caprolactam. *J. Appl. Polym. Sci.*, 24, 211.

[31] Tai K., Teranishi H., Arai Y. and Tagawa T. (1980). The kinetics of hydrolytic polymerization of ε-caprolactam. II. Determination of the kinetic and thermodynamic constants by least-squares curve fitting. *J. Appl. Polym. Sci.*, 25, 77.

[32] Mallon F.K. and Ray W.H. (1998). A comprehensive model for nylon melt equilibria and kinetics. *J. Appl. Polym. Sci.*, 69, 1213.

[33] Loo L.S., Cohen R.E. and Gleason K.K. (1998). Correlation times of motion of deuterium oxide in polyamide 6 rods. *Macromol.*, 31, 8907.

[34] Giori C. and Hayes B.T. (1970). Hydrolytic polymerization of caprolactam. I. Hydrolysis – polycondensation kinetics. *J. Polym. Sci. : Part A-1*, 8, 335.

[35] Pflüger R. (1975). Physical constants of poly(imino(1-oxohexamethylene) (polyamide 6) and poly(iminohexamethyleneiminoadipoyl) (polyamide 66). In : Polymer handbook, Brandrup J. and Immergut E.H. eds., Wiley pub.

[36] Secor R.M. (1969). The kinetics of condensation polymerization. *AIChE J.*, 15, 861.

[37] Knorr R.S. (1991). High tenacity nylon yarn. *U.S. patent 5,073,453 to Monsanto.*

[38] Srinivasan R., Almonacil C., Narayan S., Desai P. and Abhiraman A.S. (1998). Mechanism, kinetics and potential morphological consequences of solid-state polymerization. *Macromol.*, 31, 6813.

[39] Gupta A. and Gandhi K.S. (1984). In : Frontiers of chemical reaction engineering, Doraiswany L.K. and Mashelkar R.A. eds., Wiley Eastern pub., 667.

[40] Hindmarsh A.C. (1980). LSODE and LSODEI, two new initial value ordinary differential equation solvers. *ACM Signum* Newsletter, 15, 10.

[41] Steiner E., Rey T. and McCroskey M. (1990). SimuSolv Reference Guide. Dow Inc. pub., Midland, MI.

[42] Arai Y., Tai K., Teranishi H. and Tagawa T. (1981). Kinetics of hydrolytic polymerization of ε-caprolactam. III. Formation of cyclic dimer. *Polymer*, 22, 273.

[43] Mochizuki S. and Ito N. (1978). Optimal polymerization temperature profile for nylon-6 with low cyclic oligomers content. *Chem. Eng. Sci.*, 33, 1401.

[44] Ramagopal A., Kumar A. and Gupta S.K. (1983). Optimal temperature profiles for nylon 6 polymerization in plug-flow reactors. *J. Appl. Polym. Sci.*, 28, 2261.

[45] Gupta S.K., Damania B.S. and Kumar A. (1984). Optimization of nylon-6 reactors with end-point constraints. *J. Appl. Polym. Sci.*, 29, 2177.

[46] Cawthon T.M. and Smith E.C. (1960). Polymerization and depolymerization of nylon 6 above and below its melting point. *Polymer Preprints*, 1, 98.

[47] Zimmermann J. (1964). Equilibria in solid-phase polyamidation. *Polym. Letters*, 2, 955.

[48] Kaushik A. and Gupta S.K. (1992). A molecular model for solid-state polymerization of nylon-6. *J. Appl. Polym. Sci.*, 45, 507.

[49] Kulkarni M.R. and Gupta S.K. (1994). Molecular model for solid-state polymerization of nylon 6. II. An improved model. *J. Appl. Polym. Sci.*, 53, 85.

[50] Fakirov S. and Avramova N. (1982). Influence of thermal treatment, molecular weight and orientation on the mechanical properties of polyamide-6. *Acta Polymerica*, 33, 271.

[51] Gaymans R.J., Amirtharaj J. and Kamp H. (1982). Nylon 6 polymerization in the solid state. *J. Appl. Polym. Sci.*, 27, 2513.

[52] Murthy N.S. and Orts W.J. (1994). Hydration in semicrystalline polymers: small-angle neutron scattering studies of the effect of drawing in nylon-6 fibers. *J. Polym. Sci. Part B : Polym. Phys.*, 32, 2695.

[53] Hutchinson J.L., Murthy N.S. and Samulski E.T. (1996). Deuterium NMR studies of water in oriented nylon 6 fibers. *Macromol.*, 29, 5551.

[54] Mallon F.K. and Ray W.H. (1998). Modeling of solid-state polycondensation. I. Particle models. *J. Appl. Polym. Sci.*, 69, 1233.

[55] Mallon F.K. (1997). Solid state polycondensation : modelling and productivity enhancements. Thesis, University of Wisconsin-Madison.

[56] Blanchard E.N., Cohen J.D., Iwasyk J.M., Marks D.N., Stouffer J.M., Aslop A.W. and Lin C. (1999). Process for preparing polyamides. *World patent 99/10408 to DuPont.*

[57] Starkweather H.W., Moore G.E., Hansen J.E., Roder T.M. and Brooks R.E. (1956). Effect of crystallinity on the properties of nylons. *J. Polym. Sci.*, 21, 189.

[58] Schreiber S. and Philipps P.J. (1997). Crystallization of copolymers based on nylon 66. *Annu. Tech. Conf. – Soc. Plast. Eng.*, 55, 1872.

[59] Albano C., Sciamanna R., González R., Navarro O. and González E. (1999). Study and modelling of the nylon solidification process. Proceedings of the 2nd European Congress of Chemical Engineering, Montpellier, France.

[60] Murthy N.S. and Orts W.J. (1994). D_2O as a probe for studying the nanocrystalline regions in nylon 6 using small-angle neutron scattering. *Proc. ACS Div. Polym. Mater. Sci.: Sci. Eng.*, 71, 293.

[61] Hermans P.H. (1956). Constitution of the cyclic polyamides isolated from nylon 6 polymers. *Nature*, 177, 126.

7. Simulation of a Moving Packed-Bed Reactor

The solid-state polymerization model of Chapter 6 has been developed at the particle level, thus limiting its validity range to reactors with a uniform residence time distribution and inside which each nylon granule experiences the same environment at a given time. This holds for a differential reactor in which the polymer phase is processed discontinuously, as evidenced by the model performance regarding PA6 postcondensation performed at laboratory scale in fixed or fluidized-beds. However, the situation is more complicated for industrial reactors because some properties that only show up on a larger scale must be considered. For instance, axial concentration profiles will arise if the reactor operates in the integral mode, leading to a possible control by the vapor-liquid equilibrium.

In the following, we shall revisit the industrial moving packed-bed reactor presented in Chapter 1 based on a scale-up of the single particle framework. A dynamic reactor model will be formulated, which is suitable for analyzing start-up and grade transition operations as well as for steady-state design.

7.1 Scale-Up of the Single Particle Model

Although extensive modeling work on nylon-6 melt reactors has been published [1-4], there is none for PA6 solid-state reactors. In fact, the two modeling studies in the open literature about SSP in moving packed-beds deal with PET [5, 6]. A schematic of the moving packed-bed reactor is shown in Figure 7.1. The feed of prepolymer pellets enters the top and flows downward by gravity. Nitrogen is supplied at the bottom of the column and passes counter-currently through the reactor to sweep off the low molar mass by-products.

The basic assumptions of the reactor model are formulated as follows :

- The polymer phase is physically segregated. Solid-state polymerization taking place inside a nylon granule is described by the single particle model of Chapter 6.

- The polymer phase has a plug flow velocity profile. This assumption is reasonable providing care is taken that draw-off at the bottom of the vessel only promotes the vertical flow of the bed of granules, but does not cause mixing within the bed [7]. In addition, baffles may be used to homogenize the flow and ensure a uniform RTD [8].

- The gas phase has a plug flow velocity profile, given the empirical relation for the Péclet number in a fixed-bed :

$$Pe \approx \frac{L}{R} > 10^3 \tag{7.1}$$

where L stands for the reactor length and R for the radius of a polymer granule. This also implies that the porosity is uniform throughout the bed.

- The gas phase is isobaric and at constant volume. The pressure drop has indeed been found to be very low [9]. Thus, exact modeling of the pressure is not very valuable and has been omitted from this model.

- The reactor is adiabatic (no energy exchange with the surroundings). Further assumptions dealing with the energy balance are discussed below.

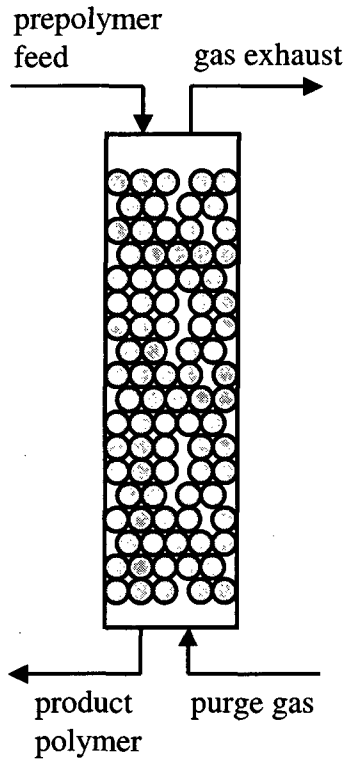

Figure 7.1 Schematic of a moving packed-bed reactor for solid-state polymerization

As the temperature of the entering polymer and purge gas need not be the same, an energy balance must be considered. For this purpose, we assume that there is no generation or consumption of heat inside the reactor. Indeed, it was seen in Section 2.4 that the production of heat by chemical reaction is insignificant ($\Delta T_{ad} \sim 0.5$ K). Next, the crystallinity is constant during SSP (Chapter 5), so the melting enthalpy needs not be taken into account. Note that this does not hold for PET, which undergoes secondary crystallization during SSP [10] ; consequently, a PET solid-state reactor is expected to heat as the polymer crystallizes. Third, the contribution of by-product volatilization is also disregarded, which appears reasonable for a feed consisting of extracted and dry granules.

To keep the analysis simple, the transport of heat is postulated to be purely convective (no axial dispersion). Furthermore, the section of the reactor is assumed to be well mixed thermally, given that heat transfer in a granule is very fast ($t_h \sim 20$ s, see

Section 2.4) compared to a residence time of several hours. This leads to the following expression for the energy balance on an infinitesimal volume element perpendicular to the tube axis,

$$\frac{\partial T}{\partial t} = \left(\frac{\partial T}{\partial z}\right) \frac{\rho_g c_{p,g} Q_g - \rho_a c_{p,p} Q_p}{AL\left(\varepsilon \rho_g c_{p,g} + (1-\varepsilon)\rho_a c_{p,p}\right)} \tag{7.2}$$

where ρ_g and $c_{p,g}$ stand respectively for the density and specific heat of the gas phase, Q_p is the polymer volumetric flow rate, and A is the tubular cross section. The spatial coordinate z is dimensionless and represents the fractional reactor length.

The population-balance equations for the species in the polymer phase are readily written as

$$\frac{\partial c_i^*}{\partial t} = \left(-\frac{1}{\tau_p}\right)\frac{\partial c_i^*}{\partial z} + R_i + D_i\left(\frac{\partial^2 c_i^*}{\partial r^2} + \frac{\nu}{r}\frac{\partial c_i^*}{\partial r}\right)$$

$$i = C_1, C_2, W, \zeta_1, \lambda_{\zeta,k} \qquad \zeta = P, Q, R, S \qquad k = 0, 1, 2 \tag{7.3}$$

where the diffusion term applies only for the volatile compounds (C_1, C_2 and W), and τ_p is the polymer residence time :

$$\tau_p = \frac{AL(1-\varepsilon)}{Q_p} \tag{7.4}$$

The balance on individual species in the gas phase is given by

$$\frac{\partial c_{g,i}}{\partial t} = \left(\frac{\vartheta}{\tau_g}\right)\frac{\partial c_{g,i}}{\partial z} - \frac{D_i S_v}{\varepsilon}\left(\frac{\partial c_i^*}{\partial r}\right)_{r=R} \qquad i = C_1, C_2, W \tag{7.5}$$

where τ_g is the gas residence time,

$$\tau_g = \frac{AL\varepsilon}{Q_g} \tag{7.6}$$

and S_v is the mass transfer surface area per reactor volume, expressed by

$$S_v = \frac{3(1-\varepsilon)}{R} \tag{7.7}$$

The parameter ϑ in Eq. (7.5) accounts for the flow pattern. For the standard counter-current configuration, $\vartheta = 1$. If the streams of polymer and purge gas flow co-currently, then $\vartheta = -1$.

The system of PDEs formed by Eqs. (7.2), (7.3), and (7.5) must be supplied with initial and boundary conditions. At the limits of the reactor, these are provided by the

composition of the feeds of prepolymer and purge gas. The surface concentration of volatiles in the polymer phase is fixed by Flory-Huggins VLE (Eq. 6.69). The initial conditions may be specified from a steady state operating point (simulation of a grade transition) or by setting all concentrations at their inlet values (simulation of reactor start-up). Both the particle radius r and the reactor axis z are discretized using the finite-different technique with 8 x 8 grid points. The resulting set of 1248 coupled ODEs is numerically solved using Gear's BDF-LSODE algorithm [11] in the SimuSolv integration package [12] to yield the time and spatial profiles of the different quantities of interest. Spatial-average values are then computed as indicated in Section 6.2.3. The computing time for a dynamic simulation was typically 10 hours on a Sun station.

7.2 Steady State Operation

It can be readily seen from Eq. (7.2) that the model predicts the reactor to be isothermal at steady state. Precisely, the stationary temperature takes the value of the inlet gas temperature T_g provided the following condition holds :

$$Q_g \rho_g c_{p,g} > Q_p \rho_a c_{p,p} \tag{7.8}$$

In words, the product of gas flow rate and its heat capacity must be larger than the corresponding quantities for the polymer. Otherwise, the gas heat capacity will not dominate the polymer and the gas will be cooled down to the entering polymer temperature.

An example of steady state calculation is disclosed in Figure 7.2, in which the influence of the nitrogen volumetric flow rate on the stationary remonomerization profile at 190°C has been investigated. Experimental data from the fixed-bed reactors are also represented for comparison, making use of the analogy between the plug-flow reactor and the batch reactor.

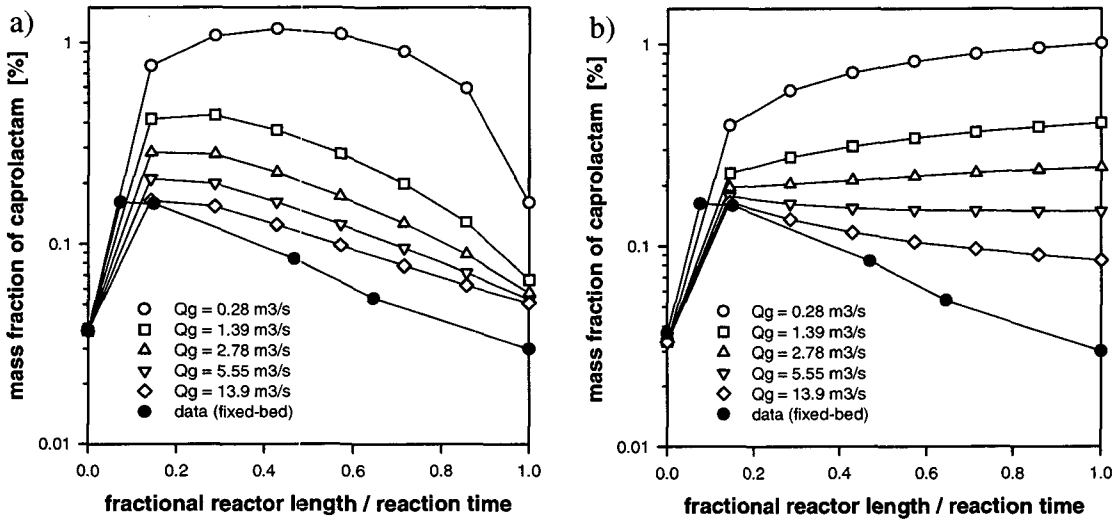

Figure 7.2 Influence of the nitrogen feed rate on the steady state remonomerization profile at 190°C – comparison with the batch results from the fixed-bed reactors. a) Counter-current configuration ; b) Co-current configuration

The gas flow rate is obviously a critical parameter to match any specification for the residual monomer in the output product. By contrast, the caprolactam content was found to be independent of the nitrogen velocity in the fixed-beds (Section 4.1). This stresses the difference between the differential and integral operating modes. The latter case applies for industrial packed-beds of several meters in height, in which the by-product molecules devolatilized from the polymer granules gradually increase the corresponding gas phase concentration along the reactor axis, up to the point where the VLE controls the overall process. A consequence is that the counter-current configuration (Fig. 7.2.a) is more suitable to decrease the outlet concentration of caprolactam than the co-current configuration (Fig. 7.2.b).

Evidently, the moving-packed bed reactor should reach a differential regime for very large values of the gas flow rate. The polymer residence time in the tubular reactor would then meet the batch reaction time identically. Indeed, Fig. 7.2 shows that the calculated steady state remonomerization profile approaches the experimental batch data for a high value of Q_g.

Remonomerization is predicted to take place essentially within the first 20 % of the total column length (Fig. 7.2.a). Therefore, a recycle loop of purge gas in the upper part of the solid-state reactor appears as an alternative design to minimize the outlet caprolactam with a lower consumption of nitrogen. This put emphasis on the reactor model as a potential tool for optimization studies.

7.3 Reactor Start-Up and On-Line Grade Transitions

This section is aimed at illustrating the model ability to simulate transient operations. For instance, the heating of the polymer bed during reactor start-up is displayed in Figure 7.3, representing calculated temperature profiles for different times (given as a fraction of the polymer residence time). A 10°C difference was taken between gas and polymer inlet temperatures. The isothermal steady state profile discussed in the previous section is reached after $t = \tau_p$, the residence time of the bed of granules.

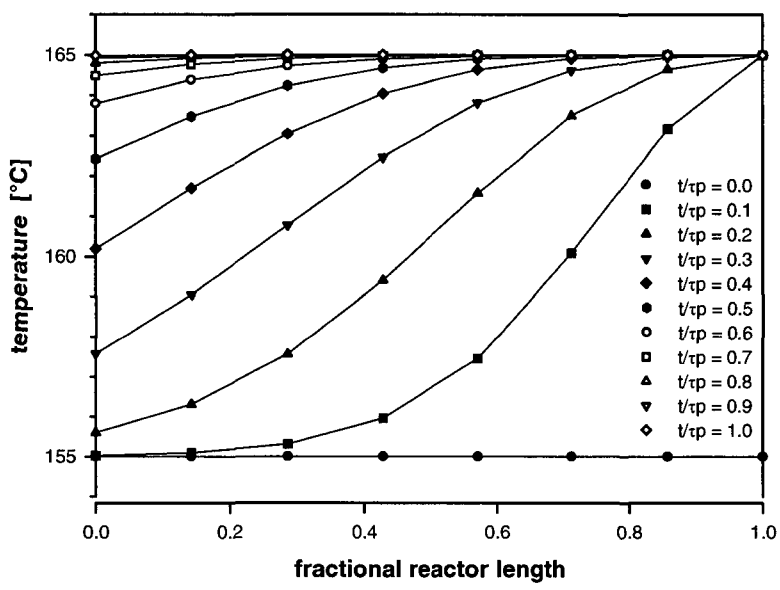

Figure 7.3 Temperature distribution during reactor start-up

The spatial distributions of degree of polymerization and caprolactam during reactor start-up are shown in Figure 7.4. Again, the calculated distributions approach a common curve after one residence time of the polymer bed, which corresponds to the stationary profile. Given the plug flow behavior of both phases, the steady state is indeed obtained after $t = \max(\tau_g, \tau_p) = \tau_p$, since the polymer residence time is typically 10^2 to 10^3 times longer than the residence time of the purge gas. The outlet caprolactam passes through a maximum very shortly after the reactor has been started (Fig. 7.4.b).

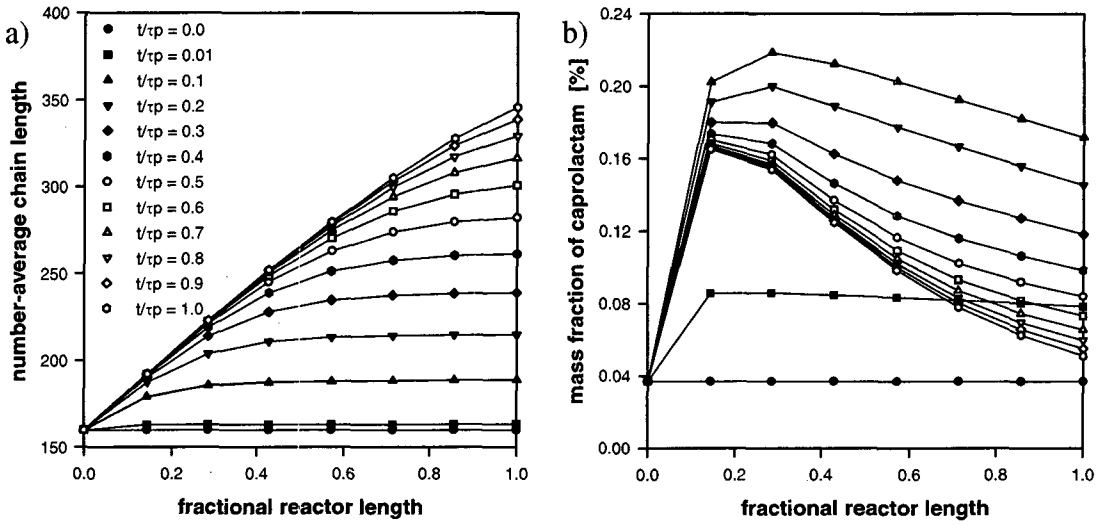

Figure 7.4 Development of axial profiles during reactor start-up. a) Number-average chain length ; b) Caprolactam. Simulations were performed using reference parameter values, except T = 190°C and $Q_g = 13.9\ m^3s^{-1}$

The model is also suitable to investigate the dynamic response to a perturbation from the steady state. This may be a fluctuation in the feed composition or a change of some operating condition used to effect an on-line grade transition or for regulation purposes. For instance, Figure 7.5 shows how changes in different control parameters affect the outlet number-average chain length and residual caprolactam.

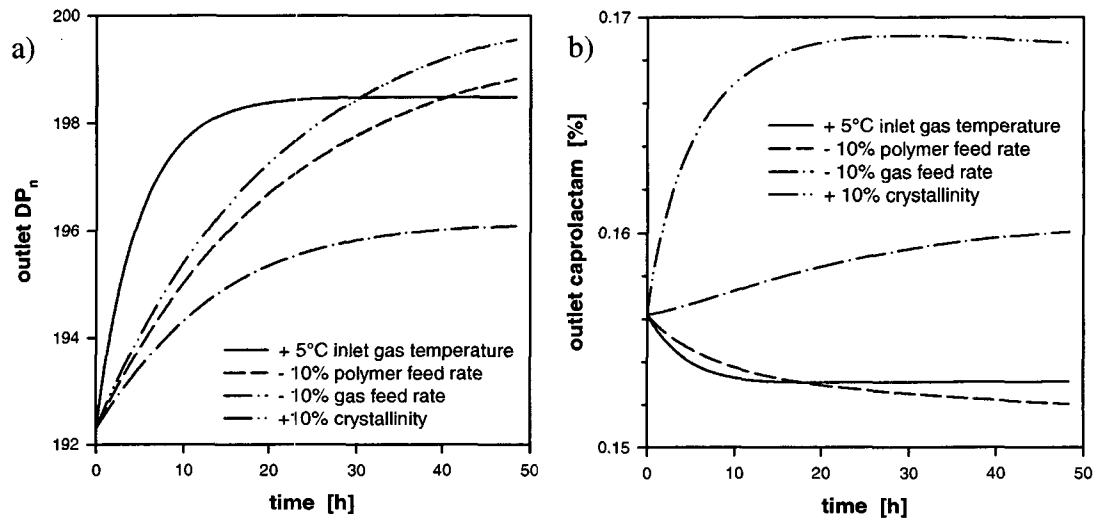

Figure 7.5 Dynamic response of outlet characteristics from several possible control variables. a) Number-average chain length ; b) Caprolactam

In summary, a dynamic model has been developed to describe the solid-state polymerization of nylon-6 in a continous moving-packed bed reactor, based on the phenomenological understanding of the process at the particle level. If needed, some of the assumptions that have been used to keep the analysis simple may be relaxed to simulate a specific reactor. For instance, an uneven flow of polymer pellets may be handled by introducing a dispersive term in the formulation of the population-balance equations. In addition, a non-isothermal steady state temperature profile may be modeled by considering the conductive dispersion of heat inside the polymer bed, or by taking into account the cooling due to the vaporizing condensate. However, all of these cases require introducing further model parameters.

The developed model may serve as a tool to address process optimization and reactor design issues. An application regarding reactor control would require diminishing significantly the computing time. Indeed, the time delays for simulation and polymer analysis are similar. For instance, Leffew *et al.* [13] mention a time of ten to twelve hours from the moment the polymer passes the point in the reactor where nitrogen is fed until a measure of the relative viscosity becomes available from the control laboratory.

7.4 References

[1] Gupta S.K. and Tjahjadi M. (1987). Simulation of an industrial nylon 6 tubular reactor. *J. Appl. Polym. Sci.*, 33, 933.

[2] Pal D. and Gupta S.K. (1989). Simulation of non-vaporizing tubular nylon 6 reactors with radial gradients : finite-difference computation. *Polymer*, 30, 1918.

[3] Jana A. and Gupta S.K. (1990). Nylon 6 polymerization in tubular reactors : orthogonal collocation results. *J. Polym. Eng.*, 9, 23.

[4] Hipp A.K. and Ray W.H. (1996). A dynamic model for condensation polymerization in tubular reactors. *Chem. Eng. Sci.*, 51, 281.

[5] Hagen R. (1995). Ein Reaktormodell für die Festphasenpolykondensation von Polyethylenterephthalat. *Chem.-Ing.-Tech.*, 67, 770.

[6] Mallon F.K. and Ray W.H. (1998). Modeling of solid-state polycondensation. II. Reactor design issues. *J. Appl. Polym. Sci.*, 69, 1775.

[7] Beaton D.H. (1974). Continuous, solid-phase polymerization of polyamide granules. *U.S. patent 3,821,171 to DuPont.*

[8] Tang Z.-L., Wang X.-Q., Hung N.-X. and Gerking L. (1999). Polyamide-6 polymerization and its melt flow in the VK tube reactor with optimized baffle structure. *Angew. Makromol. Chem.*, 266, 7.

[9] Pipper G. and Cordes C. (1989). Removal of caprolactam and oligomers thereof from nylon granules containing same. *U.S. patent 4,816,557 to BASF.*

[10] Chang T.M. (1970). Kinetics of thermally induced solid state polycondensation of poly(ethylene terephthalate). *Polym. Eng. Sci.*, 10, 364.

[11] Hindmarsh A.C. (1980). LSODE and LSODEI, two new initial value ordinary differential equation solvers. *ACM Signum* Newsletter, 15, 10.

[12] Steiner E., Rey T. and McCroskey M. (1990). SimuSolv Reference Guide. Dow Inc. pub., Midland, MI.

[13] Leffew K.W., Yerrapragada S.S. and Deshpande P.B. (1999). Modeling and optimization of a continuous solid-state polymerization process : a *six sigma* perspective. *Proceedings*, AIChE Spring Meeting, March 14-18, Houston TE, 49.

8. Conclusions and Outlook

In this work, an attempt was made to deal comprehensively with the complicated phenomenon of solid-state polymerization of nylon-6. The motivating force for modeling the kinetics of postcondensation on a phenomenological basis was both to gain a better understanding of the process and address reactor issues. As a result, the operation of continuous solid-phase polymerizers can be simulated for both their steady state and dynamic regimes. In the latter case, the model is a useful tool to handle reactor start-up and shutdown, account for possible fluctuations in the feed composition, and simulate on-line grade transitions.

A detailed reaction scheme was formulated to allow the prediction of numerous characteristics of the output product, such as viscosity, number-average molar mass, polydispersity index, imbalance of end-groups, humidity content, extent of remonomerization, and formation of the cyclic dimer. The developed model may therefore serves as a reliable tool for reactor design, optimization, and control. Indeed, the definition of any realistic objective function to find optimum conditions for the control variables should include several of the state variables cited above. Hence, the level of detail of the model makes it possible to address questions such as, for instance: What are the optimum operating conditions that bring the molar mass to a desired value within a minimum residence time, while keeping the concentration of the undesired cyclic species below a specified value ?

Solid-state polymerization was found to be a complex interplay between chemistry, transport phenomena, and structure of the solid polymer (Figure 8.1). Particularly, the semicrystalline morphology was shown to have a profound influence on the kinetics, equilibrium, and mass transfer in the solid phase.

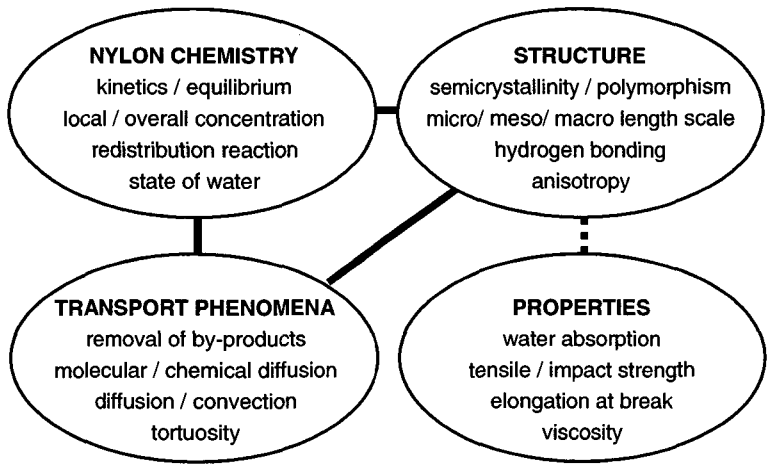

Figure 8.1 Solid-state polymerization as an interplay between chemistry, transport phenomena, and structure

In this study, we attempted to show that the implication of the micromorphology has been somewhat neglected so far, which contributed to a lack of fundamental understanding of solid-state polymerization. This is perhaps because concepts in polymer reaction engineering traditionally focus on the relation between reaction kinetics and transport phenomena, whereas the study of polymer structure is more the field of material science engineers, who seek to establish structure-properties relationships (the dashed line in Fig. 8.1). For instance, a striking observation is that the state of water in polyamides has been well documented for a long time, but that most polymer chemists dealing with the modeling of polymerization in the solid state lacked to take this information into account.

This offers new prospects to enhance postreactor operations for nylon-6. In particular, because the crystallinity was shown to have such a beneficial effect on the process, increasing the crystalline content in commercial pellets beyond the common value of about 50 % would result in higher reaction rates, a lower content of monomer, as well as the possibility to operate the reactor at a higher temperature without resin sticking. In this way, either the investment costs could be reduced or the productivity increased. In addition, a lower extent of remonomerization would decrease the required amount of purge gas.

Potential possibilities to increase the crystallinity lie in a better control of the cooling of the prepolymer after the melt polymerization stage. Routinely, the polymer strand exiting the VK column is simply quenched in a water bath. An improved morphology could be obtained by controlling the time-temperature profile during this solidification step. It must be emphasized that the overall crystallinity is not the single parameter of interest, but that other features such as the ratio of the two crystalline polymorphs, meso-scale structures like spherulites, the rigid amorphous phase, and the possible occurrence of a radial profile of crystallinity within the polymer chips are all expected to influence solid-state polymerization. There exists a need for further research in these areas.

Appendix A – List of Abbreviations

Abbreviation	Definition	Section where first used
CLD	Chain length distribution	2.1
DSC	Differential scanning calorimetry	1.3
FVT	Free volume theory	2.2
HMDA	Hexamethylene diamine	2.1
HPLC	High-performance liquid chromatography	3.3
NMR	Nuclear magnetic resonance	2.2
ODE	Ordinary differential equation	6.2
PAEKK	Poly(aryl ether ketone ketone)	2.1
PAi	Polyamide-*i*	1.3
PAij	Polyamide-*i,j*	1.3
PBT	Poly(butylene terephthalate)	1.3
PDE	Partial differential equation	6.2
PE	Polyethylene	1.1
PEN	Poly(ethylene naphthalate)	2.2
PET	Poly(ethylene terephthalate)	1.3
PID	Proportional integral differential	3.1
PLM	Polarized light microscopy	3.4
PMMA	Poly(methyl methacrylate)	2.3
POM	Poly(oxymethylene)	2.2
PP	Polypropylene	1.1
PPS	Poly(phenylene sulfide)	2.2
PS	Polystyrene	1.1
PTFE	Polytetrafluoroethylene	3.1
PVC	Poly(vinyl chloride)	1.1
RTD	Residence time distribution	2.3
SANS	Small-angle neutron scattering	2.2
SSP	Solid-state polymerization	1.3
TG	Thermogravimetry	3.3
VLE	Vapor-liquid equilibrium	2.2
WAXD	Wide-angle X-ray diffraction	2.2

Appendix B – List of Symbols

Symbol	S.I. unit	Definition or label	Section where first used
a	m	Axis parameter of crystalline unit cell	2.2
A	m^2	Tubular cross-section	7.1
A_i	-	Coefficient in Antoine equation for the pure vapor pressure	6.2
b	m	Axis parameter of crystalline unit cell	2.2
B_i	K	Coefficient in Antoine equation for the pure vapor pressure	6.2
c	m	Axis parameter of crystalline unit cell	2.2
c	mol m^{-3}	Overall concentration	2.2
c^*	mol m^{-3}	Local concentration	2.2
c_a	mol m^{-3}	Concentration in the bulk amorphous phase	6.5
c_b	mol m^{-3}	Effective bulk concentration	2.3
c_g	mol m^{-3}	Gas phase concentration	6.2
c_i	mol m^{-3}	Concentration in the interphase	6.5
c_m	mol m^{-3}	Effective concentration	2.3
$c_{p,g}$	J kg^{-1} K^{-1}	Specific heat at constant pressure of gas	7.1
$c_{p,p}$	J kg^{-1} K^{-1}	Specific heat at constant pressure of polymer	2.4
C_2^g	K	Polymer WLF parameter	2.2
C_i	K	Coefficient in Antoine equation for the pure vapor pressure	6.2
C_i	mol m^{-3}	Concentration of cyclic oligomer of length i	1.2
d	m	Characteristic distance between end-groups	2.2
D	m^2 s^{-1}	Diffusion coefficient	2.2
D_∞	m^2 s^{-1}	Diffusion coefficient at $T \rightarrow +\infty$	2.2
D_0	m^2 s^{-1}	Diffusion coefficient at $w_c = 0$	2.4
D_{eff}	m^2 s^{-1}	Effective diffusion coefficient	2.3
De	-	Deborah number for diffusion	2.2
DP_n	-	Number-average chain length	2.3
DP_v	-	Viscosity-average chain length	6.4
DP_w	-	Mass-average chain length	6.1
E_a	J mol^{-1}	Apparent activation energy	4.3

Symbol	S.I. unit	Definition or label	Section where first used
E_d	J mol^{-1}	Activation energy of diffusion	2.2
E_i^0	J mol^{-1}	Non-catalyzed activation energy of reaction i (i = 1, 2, 3, 4, 5)	6.2
E_i^c	J mol^{-1}	Catalyzed activation energy of reaction i (i = 1, 2, 3, 4, 5)	6.2
$f(x)$	m^{-1}	Frequency function of minimum end-group-to-end-group distance	2.3
F	-	Initial fraction of end-groups in the interphase	6.5
$G(s, t)$	mol m^{-3}	Generating function of the CLD	6.1
h	m	Bed height	3.2
k	s$^{-0.5}$	Non-autonomous rate constant	4.3
k_1	m^3 mol^{-1} s^{-1}	Forward ring opening rate constant	6.2
k_1'	s^{-1}	Reverse ring opening rate constant	6.2
k_2	m^3 mol^{-1} s^{-1}	Forward polycondensation rate constant	2.3
k_2'	m^3 mol^{-1} s^{-1}	Reverse polycondensation rate constant	2.3
$k_{2,0}$	m^3 mol^{-1} s^{-1}	Intrinsic forward polycondensation rate constant	2.3
$k_{2,e}$	m^3 mol^{-1} s^{-1}	Entangled forward polycondensation rate constant	2.3
k_3	m^3 mol^{-1} s^{-1}	Forward polyaddition rate constant	6.2
k_3'	s^{-1}	Reverse polyaddition rate constant	6.2
k_4	m^3 mol^{-1} s^{-1}	Forward cyclic dimer ring opening rate constant	6.2
k_4'	s^{-1}	Reverse cyclic dimer ring opening rate constant	6.2
k_5	m^3 mol^{-1} s^{-1}	Forward cyclic dimer polyaddition rate constant	6.2
k_5'	s^{-1}	Reverse cyclic dimer polyaddition rate constant	6.2
k_i^0	m^3 mol^{-1} s^{-1}	Non-catalyzed rate constant of reaction i (i = 1, 2, 3, 4, 5)	6.2
$k_{i,\infty}^0$	m^3 mol^{-1} s^{-1}	Non-catalyzed rate constant of reaction i at $T \rightarrow +\infty$	6.2
k_i^c	m^6 mol^{-2} s^{-1}	Catalyzed rate constant of reaction i (i = 1, 2, 3, 4, 5)	6.2
$k_{i,\infty}^c$	m^6 mol^{-2} s^{-1}	Catalyzed rate constant of reaction i at $T \rightarrow +\infty$	6.2
k_p	m^3 mol^{-1} s^{-1}	Propagation rate constant	2.3
k_r	m^3 mol^{-1} s^{-1}	Redistribution rate constant	2.3
k_t	m^3 mol^{-1} s^{-1}	Termination rate constant	2.3
K	-	Gel effect number	2.3
K_{12}	m^3 kg^{-1} K^{-1}	Polymer free volume parameter	2.2
K_1	m^3 mol^{-1}	Equilibrium constant for ring opening	2.2
K_2	-	Equilibrium constant for polycondensation	2.2

Symbol	S.I. unit	Definition or label	Section where first used
K_3	$m^3\ mol^{-1}$	Equilibrium constant for polyaddition	2.2
K_4	$m^3\ mol^{-1}$	Equilibrium constant for cyclic dimer ring opening	6.2
K_5	$m^3\ mol^{-1}$	Equilibrium constant for cyclic dimer polyaddition	6.2
K_1^*	$m^3\ mol^{-1}$	Apparent equilibrium constant for ring opening	2.2
K_2^*	-	Apparent equilibrium constant for polycondensation	2.2
K_3^*	$m^3\ mol^{-1}$	Apparent equilibrium constant for polyaddition	2.2
K_r	-	Equilibrium constant for redistribution	2.3
l	m	Lamellar spacing	2.2
L	m	Reactor length	7.1
L_c	m	Characteristic length scale	2.4
m	kg	Mass	6.4
M	$mol\ m^{-3}$	Concentration of monomer	6.1
$M_{1,c}$	$kg\ mol^{-1}$	Critical molar mass in Tirrell's model	2.3
$M_{2,c}$	$kg\ mol^{-1}$	Critical molar mass in Tirrell's model	2.3
M_i	$kg\ mol^{-1}$	Molar mass of species i	2.3
M_e	$kg\ mol^{-1}$	Molar mass between entanglements	2.3
M_n	$kg\ mol^{-1}$	Number-average molar mass	2.2
n	-	Order of reaction	2.2
N	-	Number of particles	2.3
N	-	Number of nodes in radial direction	6.2
N_{Av}	mol^{-1}	Avogadro number	2.2
O	-	Center of sphere	2.3
p	-	Conversion of functional groups	2.3
p	Pa	Pressure	2.2
p_i	Pa	Partial pressure of component i	6.2
p_i^0	Pa	Pure vapor pressure of component i	6.2
P	-	Ratio of crystalline-to-amorphous densities	2.2
PDI	-	Polydispersity index	6.1
Pe	-	Péclet number	7.1
P_i	$mol\ m^{-3}$	Concentration of bifunctional chains of length i	1.2
$P_{i,e}$	$mol\ m^{-3}$	Concentration of entangled bifunctional chains of length i	2.3
$P(i, t)$	$mol\ m^{-3}$	Continuous approximation of the CLD	6.1
Q_g	$m^3\ s^{-1}$	Volumetric flow rate of gas	3.1
Q_i	$mol\ m^{-3}$	Concentration of monofunctional acid chains of length i	6.2
Q_p	$m^3\ s^{-1}$	Volumetric flow rate of polymer	7.1
r	$mol\ m^3\ s^{-1}$	Reaction rate	2.4
r	m	Spatial coordinate of the polymer	6.2
R	$J\ mol^{-1}\ K^{-1}$	Gas constant	2.2
R	m	Polymer size	2.2

Symbol	S.I. unit	Definition or label	Section where first used
R_i	mol m^{-3}	Concentration of monofunctional amine chains of length i	6.2
R_i	mol m^{-3} s^{-1}	Chemical production rate of species i	6.2
s	-	Symmetry number	6.2
S	-	Ratio of solute-to-polymer densities	2.2
S_i	mol m^{-3}	Concentration of dead chains of length i	6.2
S_v	m^{-1}	Surface area per volume	7.1
t	s	Time	3.1
t_c	s	Characteristic time for crystallization	2.4
t_d	s	Characteristic time for diffusion	2.2
t_h	s	Characteristic time for heat transfer	2.4
t_r	s	Characteristic time for reaction	2.4
t_s	s	Drainage time of pure solvent	3.3
T	K	Temperature	2.2
T_{amb}	K	Ambient temperature	3.1
T_c	K	Maximal crystallization temperature	3.4
T_{cc}	K	Critical crystallization temperature	2.2
T_g	K	Glass transition temperature	2.2
T_m	K	Crystalline melting temperature	2.2
T_s	K	Softening temperature	3.4
v	-	Number of degrees of freedom	2.2
v_c	-	Volume fraction of crystalline phase	2.2
V	m^3	Volume	6.2
V_1^*	m^3 kg^{-1}	Solute specific critical free volume	2.2
V_2^*	m^3 kg^{-1}	Polymer specific critical free volume	2.2
V_{FH}	m^3 kg^{-1}	Specific hole free volume	2.2
w	-	Overall mass fraction	3.2
w^*	-	Local mass fraction	6.2
w_c	-	Mass fraction of crystalline phase	2.2
$w_{c,f}$	-	Mass fraction of crystalline phase inside the fibrils	6.4
w_f	-	Fibrillar mass fraction	6.4
w_s	-	Mass fraction of solute	2.2
W	mol m^{-3}	Concentration of water	1.2
x	m	Minimum end-group-to-end-group distance	2.3
x_d	m	Distance to bulk	2.3
x_m	m	Critical reaction distance for polycondensation	2.3
X	m	Pseudo-parameter in equation for $f(x)$	2.3
z	-	Fractional reactor length	7.1
$Z(z, t)$	mol m^{-3}	Z-transform of the CLD	6.1
α	m^{-3}	Proportionality factor	2.3
α	m^2 s^{-1}	Thermal diffusivity	2.4
β	-	Angle parameter of crystalline unit cell	2.2
β	-	Chain immobilization factor	2.2

Symbol	S.I. unit	Definition or label	Section where first used
χ_i	-	Flory-Huggins interaction parameter of component *i*	6.2
δ	m	Critical reaction distance for redistribution	2.3
$\Delta 2\theta_\alpha$	-	Index of crystal density	3.4
ΔH_1	J mol^{-1}	Enthalpy of ring opening	6.2
ΔH_2	J mol^{-1}	Enthalpy of polycondensation	2.4
ΔH_3	J mol^{-1}	Enthalpy of polyaddition	6.2
ΔH_4	J mol^{-1}	Enthalpy of cyclic dimer ring opening	6.2
ΔH_5	J mol^{-1}	Enthalpy of cyclic dimer polyaddition	6.2
ΔH_m	J kg^{-1}	Enthalpy of melting	3.4
ΔH_m^0	J kg^{-1}	Enthalpy of melting of a wholly crystalline sample	3.4
Δr	m	Radial increment	6.2
ΔS_1	J mol^{-1} K^{-1}	Entropy of ring opening	6.2
ΔS_2	J mol^{-1} K^{-1}	Entropy of polycondensation	6.2
ΔS_3	J mol^{-1} K^{-1}	Entropy of polyaddition	6.2
ΔS_4	J mol^{-1} K^{-1}	Entropy of cyclic dimer ring opening	6.2
ΔS_5	J mol^{-1} K^{-1}	Entropy of cyclic dimer polyaddition	6.2
ΔT	K	Extent of supercooling	3.4
ΔT_{ad}	K	Adiabatic temperature rise	2.4
ΔV	m^3	Volume element	2.3
ε	-	Porosity	3.1
ϕ	m	Reactor inner diameter	3.1
γ	-	Overlap factor	2.2
Γ	-	Euler gamma function	2.3
η_{kin}	-	Kinetic effectiveness factor	2.2
φ	-	Number of phases	2.2
ϑ	-	Flux condition flag	7.1
κ	-	Number of components	2.2
λ	m	Wavelength	3.4
λ_a	W m^{-1} K^{-1}	Thermal conductivity of amorphous phase	2.4
$\lambda_{\zeta,k}$	mol m^{-3}	*k*th unnormalized moment of the CLD for the ζ species ($\zeta = P, Q, R, S$)	6.1
λ_m	s	Mean relaxation time of polymer	2.2
$\Lambda\alpha_{200}$	m	Lateral size of α-crystallite	2.2
μ	kg m^{-1} s^{-1}	Dynamic viscosity	3.3
μ_{rel}	-	Relative viscosity	3.2
μ_s	kg m^{-1} s^{-1}	Dynamic viscosity of pure solvent	3.3
ν	-	Polymer geometrical factor	6.2
π	-	Pi = 3.141592654...	2.3
ρ	m^{-3}	Density of particles	2.3
ρ_a	kg m^{-3}	Density of amorphous phase	2.2
ρ_c	kg m^{-3}	Density of crystalline phase	2.2
ρ_g	kg m^{-3}	Density of gas phase	7.1

Symbol	S.I. unit	Definition or label	Section where first used
ρ_s	kg m^{-3}	Density of solute	2.2
σ	m	Thickness of boundary layer	6.5
σ	(var.)	Standard deviation	3.2
σ^2	(var.)	Variance	6.1
τ	-	Tortuosity ratio	2.2
τ_g	s	Residence time of gas phase	7.1
τ_p	s	Residence time of polymer phase	7.1
ξ	-	Ratio of solute-to-polymer jumping units	2.2
ψ	-	Extent of decarboxylation	6.2
2θ	-	Scattering angle	3.4

Christian Spühler
born February 8, 1972
Swiss citizen

Education

1987-1990	Secondary education : Gymnase de Burier, La Tour-de-Peilz → Maturité, type mathematics-sciences ; chemistry prize
1990-1996	Swiss Federal Institute of Technology, Lausanne → Diploma in chemical engineering
1999	→ Federal expert in radioprotection

Experience

1996-2000	Swiss Federal Institute of Technology, Lausanne → Doctoral thesis at the Institute of Chemical Engineering in collaboration with BASF Inc., Ludwigshafen. *Kinetic Studies and Modeling of Nylon-6 Solid-State Polycondensation.* → Assistant to Prof. Renken for the course *Chemical Reaction Engineering*, and to Dr. Meyer for the course *Organic and Polymer Chemistry.* → Supervision of laboratory work of undergraduate students.
1995-1996	→ Diploma work (5 months) in collaboration with Hoechst Inc., Frankfurt a. M. *Kinetic Studies on the Formation of Sorbic Acid by Depolymerization of a Polyester.*
1992	CIBA-GEIGY Monthey, training course (2 months) → *Set-up of analytical HPLC procedures with diode-array detection, training of a lab assistant.*

Languages

French (mother tongue), English, German

Publications

Spühler C., Zimmerer W., and Renken A. (1998). *Microgravimetric Determination of Polycondensation Kinetics.* DECHEMA Monographs, 134, Wiley-VCH Pub., 587-595.

Nattorp A., Graf M., Spühler C., and Renken A. (1999). *Model for Random Hydrolysis and End Degradation of Linear Polysaccharides: Application to the Thermal Treatment of Mannan in Solution.* Ind. Eng. Chem. Res., 38 (8), 2919-2926.